University of Alberta

Library Release Form

Name of Author: Adrian D. Audet

Title of Thesis: Closed Loop Control of HCCI using Camshaft Phasing and Dual Fuels

Degree: Master of Science

Year this Degree Granted: 2008

Adrian D. Audet

University of Alberta

Closed Loop Control of HCCI using Camshaft Phasing and Dual Fuels

by

Adrian D. Audet

A thesis submitted to the Faculty of Graduate Studies and Research in partial fulfillment of the requirements for the degree of Master of Science.

Department of Mechanical Engineering

Edmonton, Alberta

Fall 2008

University of Alberta

Faculty of Graduate Studies and Research

The undersigned certify that they have read, and recommend to the Faculty of Graduate Studies and Research for acceptance, a thesis entitled Closed Loop Control of HCCI using Camshaft Phasing and Dual Fuels submitted by Adrian D. Audet in partial fulfillment of the requirements for the degree of Master of Science.

Dr. C.R. (Bob) Koch

Dr. M. D. Checkel

Dr. A. Lynch

Dr. F. Fahimi

Abstract

Feedback control of a Homogeneous Charge Compression Ignition (HCCI) internal combustion engine through the aid of camshaft phasing and dual fuels is discussed in this dissertation. Control is achieved by modulating the effective compression ratio inside the combustion chamber and by varying the ratio of the input fuels; iso-octane and n-heptane. Varying the ratio of these two fuels changes the fuel octane number of the mixture, effecting the timing of combustion. Increasing the effective compression ratio increases the temperature inside the combustion chamber, advancing combustion. Proportional Integral (PI) control is implemented for the single-input single-output control problems. System identification is also applied to the engine in order to derive dynamic models between the inputs and outputs of the engine. These identified black box models are then used in the design of model based controllers. The performance of all control algorithms is validated experimentally and tested for the disturbance rejection characteristics.

Table of Contents

1 Introduction **1**

1.1 Motivation 1

1.2 Problem Statement 2

1.3 Thesis Organization 2

1.4 Thesis Contributions 3

2 Background & Theory **5**

2.1 HCCI Fundamentals 5

2.1.1 HCCI Combustion Cycle 5

2.1.2 Speed-Load Range 8

2.1.3 Ignition Timing 11

2.1.4 Fuel Octane Control 16

2.1.5 Valve Timing Effects on HCCI 16

2.2 Feedback Control and System Identification Fundamentals 21

2.3 HCCI Physics 23

2.4 Control Oriented Modeling and System Identification of HCCI 25

2.5 Control of HCCI 26

2.5.1 Introduction 26

2.5.2 Physical Model Based Controllers 26

2.5.3 Empirically-Derived Model Based Controllers 28

2.5.4 Non-Model Based Control 31
2.5.5 Summary 32

3 Experimental Setup **33**

3.1 Experimental Setup 33
3.1.1 Short Block Assembly 33
3.1.2 Cylinder Head 35
3.1.3 Camshaft Phasing 35
3.1.4 Intake and Exhaust System 38
3.1.5 Fuel System 38
3.1.6 Dynamometer 41
3.1.7 Sensors 41
3.1.8 Data Acquisition and Control System 42
3.2 Testing Conditions 47
3.2.1 Stable Engine Operation 48
3.3 Measurement Calibrations 51

4 PI Control **53**

4.1 Combustion Timing Control Using IVC Timing 53
4.1.1 Plant 54
4.1.2 Controller 57
4.1.3 Results 59
4.2 Combustion Timing Control Using Fuel Octane Changes 67
4.2.1 Plant 68
4.2.2 Controller 71
4.2.3 Results 72
4.3 PI Control Discussion 80
4.4 Controller Load Rejection Performance 82

4.4.1 Engine Limits . . . 83
4.4.2 Actuator Limits . . . 84
4.4.3 Efficiency . . . 85
4.4.4 Discussion . . . 89
4.5 Summary . . . 96

5 SYSID and MBC **98**
5.1 System Identification . . . 98
5.1.1 Experiment Design . . . 98
5.1.2 Analysis . . . 106
5.1.3 Discussion . . . 123
5.2 Model-Derived Control of HCCI . . . 131
5.2.1 Design and Implementation . . . 131
5.2.2 Experimental Feedforward Results . . . 139
5.3 Summary . . . 146

6 Conclusion **148**
6.1 Conclusions . . . 148
6.2 Future Work . . . 150

Bibliography **151**

A Experimental Data Summary **162**
A.1 Repeatability Analysis . . . 162
A.2 Description of Data Logs . . . 168
A.3 Data for Chapter 2 . . . 175
A.4 Data for Chapter 3 . . . 177
A.5 Data for Chapter 4 . . . 181
A.6 Data for Chapter 5 . . . 207

B Camshaft Phaser Control System **213**

B.1 Description of the System Hardware 213

B.1.1 Vane-type Camshaft Phasers 213

B.1.2 Physical Camshaft System 216

B.1.3 Oil System 217

B.1.4 Electrical System 217

B.2 Software and Control Loop Definition 219

B.3 Open Loop and Closed Loop Results 220

C Mercedes E550 Cylinder Head **223**

C.1 Head Modifications 223

C.2 Valve Lift Profile 224

C.3 Combustion Chamber Volume 225

C.4 Combustion Chamber Geometry 226

C.5 Valve Discharge Coefficients 226

C.5.1 Measurement Apparatus 227

C.5.2 Results 229

D Experimental Setup and Calibrations **231**

D.1 Programs Used 231

D.2 Injector Flow Rate Calibration 231

D.3 Oil and Coolant Temperature Control 234

D.4 Pressure Sensor 235

D.5 Emission Bench 238

D.6 dSPACE CA50 calibration 241

D.7 CAS Time Delay 242

D.8 Load Cell Calibration 243

D.9 Pressure Transducer Calibrations 243

D.10 Laminar Air Flow Calibration 247

E Feedforward Controller Design **248**

E.1 IVC Feedforward Controller 248

E.2 Fuel Octane Feedforward Controller 251

E.3 Simulink Models 252

List of Tables

2.1 Survey of HCCI control 32

3.1 Engine specifications 35
3.2 Valve phasers characteristics 37
3.3 Engine testing conditions 48

4.1 Sensitivity and linearity of CA50 to IVC timing 57
4.2 IVC timing controller PI gains 59
4.3 Sensitivity and linearity of CA50 to fuel octane 70
4.4 Properties of iso-Octane and n-Heptane 72
4.5 Fuel octane controller PI gains 72
4.6 Variance of PI controllers 82
4.7 Summary of Gains 82
4.8 Controller gains values used for all the injected fuel energy sweeps. . . 83

5.1 Conditions for system identification tests 100
5.2 Stability of engine parameters during system identification tests. . . . 101
5.3 Mean Values for IVC input 106
5.4 Mean Values for fuel octane input 107
5.5 Mean Values for injected fuel energy input 107
5.6 Mean Values for engine speed input 107
5.7 Scaling values 107

5.8 Estimated time delays, nk, of input signals 109
5.9 Fit % of ARAMX models 113
5.10 Fit % of Box-Jenkins models 113
5.11 Linearity test with IVC timing input 120
5.12 Linearity test with fuel octane input 120
5.13 Identified ARMAX transfer functions for actuators 122
5.14 Identified ARMAX transfer functions for disturbances 122
5.15 Average ARMAX models used in feedforward design 134
5.16 Feedforward controllers 135
5.17 Feedforward controller variance 141

A.1 Repeatability of engine conditions 164
A.2 Uncertainty of measured engine parameters 165
A.3 Table of repeated $SYSID2$ Models 168
A.4 Parameter Descriptions - 1 170
A.5 Parameter Descriptions - 2 171
A.6 Parameter Descriptions - 3 172
A.7 Parameter Descriptions - 4 173
A.8 Parameter Descriptions - 5 174
A.9 Chapter 2 Data 176
A.10 Knock Intensity Calibration for Chapter 3 178
A.11 Chapter 3 data 179
A.12 Experimental BasePoints for Chapter 3 180
A.13 IVC timing sweeps - 1 182
A.14 IVC timing sweeps - 2 183
A.15 Fuel octane sweeps - 1 184
A.16 Fuel octane sweeps - 2 185

A.17 IVC step inputs 186
A.18 Fuel octane step inputs 187
A.19 Injected fuel energy disturbance - IVC control 188
A.20 Engine speed disturbance - IVC control 189
A.21 Injected fuel energy disturbance - fuel octane control 190
A.22 Injected fuel energy disturbance - fuel octane control 191
A.23 Load range sweep at BasePoint1 - IVC control 192
A.24 Load range sweep at BasePoint2 - IVC control 193
A.25 Load range sweep at BasePoint3 - IVC control 194
A.26 Load range sweep at BasePoint4 - IVC control 195
A.27 Load range sweep at BasePoint5 - IVC control 196
A.28 Load range sweep at BasePoint1 - fuel octane control 197
A.29 Load range sweep at BasePoint2 - fuel octane control 198
A.30 Load range sweep at BasePoint3 - fuel octane control 199
A.31 Load range sweep at BasePoint4 - fuel octane control 200
A.32 Load range sweep at BasePoint5 - fuel octane control 201
A.33 Load range sweep at BasePoint1 - no control 202
A.34 Load range sweep at BasePoint2 - no control 203
A.35 Load range sweep at BasePoint3 - no control 204
A.36 Load range sweep at BasePoint4 - no control 205
A.37 Load range sweep at BasePoint5 - no control 206
A.38 System identification data points. 208
A.39 System identification data points - linearity test. 209
A.40 Injected fuel energy disturbance - various controllers 210
A.41 Engine speed disturbance - various controllers 211
A.42 Injected fuel energy disturbance - various controllers 212

C.1 Combustion chamber volume 226

D.1 Programs used 231

D.2 Injection calibration data 233

D.3 Injector calibration coefficients 234

D.4 Emissions Bench 241

List of Figures

2.1 4-Stroke combustion process for SI, CI and HCCI engines. 7
2.2 Pressure trace of HCCI and SI cycles 7
2.3 P-V diagram of HCCI and SI cycles 8
2.4 Speed-Load range of typical automobile and HCCI 9
2.5 HCCI cyclic variation 10
2.6 HCCI engine knock 11
2.7 HCCI pressure trace and motoring trace 13
2.8 Mass fraction burned curve of HCCI 14
2.9 Effective compression ratio for different IVC timing 18
2.10 End of compression temperature for different IVC timing 18
2.11 Negative valve overlap pressure trace 20
2.12 Internal Exhaust Gas Recirculation (iEGR) 20
2.13 Feedback control schematic 22
2.14 Feedforward control schematic 22

3.1 Short block assembly of engine 34
3.2 Crankshaft adapter assembly 36
3.3 Long block assembly 36
3.4 Camshaft phaser controller 37
3.5 Intake valve timing dynamics 38
3.6 Exhaust valve timing dynamics 38

3.7 Intake and exhaust system 39
3.8 Fuel system schematic 40
3.9 Injector flow rate calibration 40
3.10 Dynamometer setup 41
3.11 ADAPT DAC system 43
3.12 CAS system 44
3.13 dSPACE MicroAutoBox system 46
3.14 Timing of the MicroAutobox ECU 46
3.15 Knock limit calibration. 51
3.16 Effect of SOC on the CA50 calculation 52

4.1 HCCI engine plant model 53
4.2 IVC controller schematic 54
4.3 Steady state response for IVC changes 56
4.4 Normalized steady state response for IVC changes 56
4.5 Step response of CA50 to an IVC change 57
4.6 Implemented IVC controller 58
4.7 BasePoint1: Load changes for IVC controller 61
4.8 BasePoint2: Load changes for IVC controller 62
4.9 BasePoint3: Load changes for IVC controller 62
4.10 BasePoint4: Load changes for IVC controller 63
4.11 BasePoint5: Load changes for IVC controller 63
4.12 BasePoint1: Load changes for IVC controller 2 64
4.13 BasePoint3: Load changes for IVC controller 2 64
4.14 BasePoint1: Speed changes for IVC controller 65
4.15 BasePoint2: Speed changes for IVC controller 65
4.16 BasePoint3: Speed changes for IVC controller 66

4.17 BasePoint4: Speed changes for IVC controller 66
4.18 BasePoint5: Speed changes for IVC controller 67
4.19 Fuel octane controller schematic 68
4.20 Steady state response for fuel octane changes 69
4.21 Normalized Steady state response for fuel octane changes 70
4.22 Step response of CA50 for fuel octane change 71
4.23 Implemented fuel octane controller schematic 72
4.24 BasePoint1: Load changes for fuel octane controller 74
4.25 BasePoint2: Load changes for fuel octane controller 74
4.26 BasePoint3: Load changes for fuel octane controller 75
4.27 BasePoint4: Load changes for fuel octane controller 75
4.28 BasePoint5: Load changes for fuel octane controller 76
4.29 BasePoint1: Load changes for fuel octane controller 2 76
4.30 BasePoint3: Load changes for fuel octane controller 2 77
4.31 BasePoint1: Speed changes for fuel octane controller 77
4.32 BasePoint2: Speed changes for fuel octane controller 78
4.33 BasePoint3: Speed changes for fuel octane controller 78
4.34 BasePoint4: Speed changes for fuel octane controller 79
4.35 BasePoint5: Speed changes for fuel octane controller 79
4.36 Schematic of controllers for load rejection performance 83
4.37 Load sweep schematic 84
4.38 Indicated Efficiency for load sweep at BasePoint1 86
4.39 Indicated Efficiency for load sweep at BasePoint2 87
4.40 Indicated Efficiency for load sweep at BasePoint3 87
4.41 Indicated Efficiency for load sweep at BasePoint4 88
4.42 Indicated Efficiency for load sweep at BasePoint5 88
4.43 Excess Oxygen in exhaust for load sweep at BasePoint3 92

4.44 CA50 vs. Engine efficiency 93
4.45 Hydrocarbon emission for load sweep at BasePoint3 93
4.46 Carbon Monoxide emissions for load sweep at BasePoint3 94
4.47 COV of engine load, $IMEP$, for load sweep at BasePoint3 94
4.48 Knock intensity for load sweep at BasePoint3 95
4.49 Burn duration for load sweep at BasePoint3 95

5.1 Experimental data of $SYSID2_{IVC}$ 102
5.2 Engine stability at $SYSID2_{IVC}$ 102
5.3 Experimental data of $SYSID2_{ON}$ 103
5.4 Engine stability at $SYSID2_{ON}$ 103
5.5 Experimental data of $SYSID2_{E}$ 104
5.6 Engine stability at $SYSID2_{E}$ 104
5.7 Experimental data of $SYSID2_{RPM}$ 105
5.8 Engine stability at $SYSID2_{RPM}$ 105
5.9 Model validation of $SYSID_{IVC}$ 111
5.10 Model validation of $SYSID_{ON}$ 111
5.11 Model validation of $SYSID_{E}$ 112
5.12 Model validation of $SYSID_{RPM}$ 112
5.13 Residual analysis of $SYSID2_{IVC}$ 115
5.14 Spectral analysis of residuals $SYSID2_{IVC}$ 116
5.15 Residual analysis of $SYSID2_{ON}$ 116
5.16 Spectral analysis of residuals $SYSID_{ON}$ 117
5.17 Residual analysis of $SYSID2_{E}$ 117
5.18 Residual analysis of $SYSID2_{E}$ 118
5.19 Spectral analysis of residuals $SYSID2_{E}$ 118
5.20 Residual analysis of $SYSID2_{RPM}$ 119

5.21 Spectral analysis of residuals $SYSID2_{RPM}$ 119
5.22 Linearity test with IVC timing input 121
5.23 Linearity test with fuel octane input 121
5.24 Step response all IVC timing models 124
5.25 Bode plot of all IVC timing models 124
5.26 Step response all fuel octane models 126
5.27 Bode plot of all fuel octane models 126
5.28 Step response all injected fuel energy models 128
5.29 Bode plot of all injected fuel energy models 128
5.30 Step response all engine speed models 129
5.31 Bode plot of all engine speed models 129
5.32 Schematic of feedforward controller 132
5.33 Pole-Zero map of IVC timing plant model 135
5.34 Pole-Zero map of fuel octane plant model 136
5.35 Pole-Zero map of injected fuel energy plant model 137
5.36 Pole-Zero map of engine speed plant model 138
5.37 Simulation of feedforward controller using IVC timing 138
5.38 Simulation of feedforward controller using fuel octane number 139
5.39 Schematic of implemented feedforward scheme 139
5.40 Engine load disturbance - various controllers 142
5.41 Engine speed disturbance - various controllers 143
5.42 Multiple disturbances - various controllers 145
5.43 Schematic of SYSID tests 147

A.1 Repeatability of IVC timing sweep 164
A.2 Repeated SYSID2 test for IVC timing 166
A.3 Repeated SYSID2 test for fuel octane 166

A.4 Repeated SYSID2 test for fuel energy 167
A.5 Repeated SYSID2 test for engine speed 167

B.1 Camshaft phaser oil system 213
B.2 Simulated camshaft phaser response 216
B.3 Timing chain setup 217
B.4 Electrical setup of camshaft phaser controller 219
B.5 Camshaft phaser calculation 219
B.6 Open loop phaser characteristics 221
B.7 Intake closed loop step response 221
B.8 Exhaust closed loop step response 222

C.1 Cylinder head modification 223
C.2 Valve lift profiles 225
C.3 Exhaust forward discharge coefficients 229
C.4 Exhaust reverse discharge coefficients 230

D.1 iso-Octane injector calibration 233
D.2 n-Heptane injector calibration 234
D.3 Oil system 235
D.4 Coolant system 235
D.5 In-cylinder pressure sensor 237
D.6 Piezo-electric pressure transducer calibration 238
D.7 Piezo-electric pressure transducer calibration results 238
D.8 CA50 calibration between dSPACE and CAS 241
D.9 Determination of CAS calculation delay 242
D.10 Load cell calibration 243
D.11 Absolute intake pressure calibration 243

D.12 Relative intake pressure calibration 244
D.13 Exhaust pressure calibration 244
D.14 Iso-Octane pressure calibration 245
D.15 N-Heptane pressure calibration 245
D.16 Oil pressure calibration 246
D.17 Air flow meter pressure calibration 246
D.18 Air flow meter calibration 247

E.1 Simulation of feedforward controller using IVC timing 253
E.2 Simulation of feedforward controller using fuel octane number 254

Nomenclature

Acronyms

aTDC	after Top Dead Center
BD	Burn Duration
bTDC	before Top Dead Center
CA10	Crank Angle of 10% mass fraction burned [deg]
CA50	Crank Angle of 50% mass fraction burned [deg]
CA90	Crank Angle of 90% mass fraction burned [deg]
CFD	Computation Fluid Dynamics
CI	Compression Ignition
CR	Compression Ratio
EGR	Exhaust Gas Recirculation
eEGR	external Exhaust Gas Recirculation
EVC	Exhaust Valve Closing
FTM	Fast Thermal Management

GDI	Gasoline Direct Injection
HCCI	Homogeneous Charge Compression Ignition
HTR	High Temperature Reaction
iEGR	internal Exhaust Gas Recirculation
IMEP	Indicated Mean Effective Pressure
IVC	Intake Valve Closing
IVO	Intake Valve Opening
LTR	Low Temperature Reaction
LQG	Linear Quadratic Gaussian
LQR	Linear Quadratic Regulator
MFB	Mass Fraction Burned
MIMO	Multi Input Multi Output
MPC	Model Predictive Control
NEDC	New European Drive Cycle
NO_x	Oxides of Nitrogen
NVO	Negative Valve Overlap
ON	Octane Number
PRBS	Pseudo Random Binary Sequence

PRF	Primary Reference Fuel
PI	Proportional Integral
PID	Proportional Integral Derivative
SI	Spark Ignition
SISO	Single Input Single Output
VVA	Variable Valve Actuation
VVT	Variable Valve Timing

Symbols

θ	Crankshaft angle [deg]
γ	Specific heat ratio c_p/c_v [-]
λ	Gravimetric air to fuel ratio [-]
k	Controller gain [-]
m	mass [kg]
P	In-cylinder pressure [kPa]
Q	Heat Transfer [J]
r	Residual mass fraction [-]
R	Gas Constant $[\frac{J}{kgK}]$
t	Time [s]
T	Temperature [k]
V	In-cylinder volume $[m^3]$

Subscripts

eff	Effective value
exh	Of the exhaust leaving the engine
fresh air	Of the fresh air entering the engine
fuel	Of the fuel into the engine
iso-Octane	Of the iso-Octane fuel
IVC	At the instant of IVC
max	Maximum during the closed cycle
n-Heptane	Of the n-Heptane fuel
netR	Net release in cycle
tdc	At the instant of TDC
tr	Of the trapped mass

Chapter 1

Introduction

1.1 Motivation for the Research

Two of the largest issues in the modern world are the diminishing supply of fossil fuels and global climate change caused by greenhouse gasses. Automobiles are one of the largest consumers of fossil fuels [Department of Energy, 2007], and subsequently one of the largest producers of carbon dioxide (which is a greenhouse gas), indicating that automobiles are the cause of two of the largest problems we face today. This makes technologies to improve the efficiency of internal combustion engines currently a very important topic. The problem is not as simple as efficiency, however; other automobile emissions are tightly regulated, and steadily become more regulated [Zhao, 2007b]. Particulate Matter (PM), Oxides of Nitrogen (NO_x), unburned HydroCarbons (uHC) and Carbon Monoxide (CO) are the main pollutant emissions from automobiles, and technologies that reduce these emissions are more important now than they have ever been in the past [Stone, 1999]. NO_x emissions are attributed to the formation of acid rain [R.Turns, 2000]. PM, CO and uHC emissions are all attributed to various health hazards and environmental damage [Heywood, 1988]. A technology is needed that not only increases the efficiency of the automobile, but decreases its pollutant emissions as well.

When looking at the entire vehicle life cycle some alternative methods of automobile propulsion, such as fuel cells and electric cars, currently are not attractive alternatives to Internal Combustion (IC) engines [Atkins and Koch, 2003]. More improvement is needed for these technologies to become widespread. Short term to medium term solutions are needed that decrease both fuel consumption and pollutant emissions of IC engines. Homogeneous Charge Compression Ignition (HCCI) is an alternative mode of combustion that can meet these requirements. This technology can be feasibly implemented in current automotive engines; it does not require a new fueling infrastructure and it will not decrease the vehicle's performance. The start of combustion of HCCI cannot be directly controlled like it can be in conventional engine modes such as Spark Ignition (SI) or Compression Ignition (CI). Although HCCI boasts many benefits, problems such as the ones discussed in this thesis currently limit wide scale implementation into automobiles.

1.2 Problem Statement

The primary goal of this research is to evaluate the potential of camshaft phasing and dual fuel injection for the control of HCCI combustion timing. The control methods are evaluated for their ability to reject system disturbances, such as engine load and speed changes. These controllers are also evaluated on their load range of operation. Techniques of system identification are used to obtain black-box models of the system, and these models are also used for controller design.

1.3 Thesis Organization

This thesis is organized into 6 chapters. Chapter 2 begins with an introduction to HCCI which discusses the benefits it has over other combustion modes. The problem of combustion timing control is then stated in this chapter, which is followed by

an introduction to feedback control. The chapter concludes with a short literary review on HCCI and on the applications of control to HCCI. Chapter 3 describes the experimental setup used in this study. The test conditions and testing procedure are also outlined in this chapter. The application of Proportional Integral (PI) control to the combustion timing of an HCCI engine is displayed in Chapter 4. This chapter also shows the operational load range for the controllers. To obtain a better control performance, a mathematical model of the plant is used, and the identification of this model from experiential data is discussed in Chapter 5. The identified models are then used in a feedforward control scheme. Chapter 6 summarizes the major results and provides recommendations for further research.

1.4 Thesis Contributions

The major contributions of this research are summarized below:

- Configured and programmed the control system for the hydraulic camshaft phasers, as well as the system for the implementation of dual fuels. This system allows the research group to continue with HCCI control research.
- Designed and constructed a single cylinder engine barrel that has an adjustable compression ratio and will adapt the cylinder head equipped with electronic VVT. This will be very beneficial to any further HCCI control research the group does.
- Implemented a feedback control system that regulates HCCI combustion timing using a calculated value of combustion timing from an in-cylinder pressure sensor. This system is novel to our research group, and the implementation of this system will provide a tool for later graduate students.
- Used system identification techniques to find process models, which are then

used in feedforward control design. This further validates research that has shown that linear control techniques can be successfully applied to the HCCI control problem.

Chapter 2

Background

HCCI engine fundamentals that are pertinent to this thesis are introduced in this chapter. The HCCI combustion timing control problem is then described and the control solution outlined. A literature review of HCCI and the control of HCCI concludes this chapter.

2.1 HCCI Fundamentals

2.1.1 HCCI Combustion Cycle

The basic 4-stoke combustion process for HCCI, Spark Ignition (SI), and a Diesel or Compression Ignition (CI) engines is shown in Figure 2.1. The figure shows that HCCI exhibits characteristics from both CI and SI engine cycles. HCCI is operated at wide open throttle similar to a diesel engine. However, in a SI engine the air-fuel charge is premixed so that no particulate emissions are formed. These particulate emissions are a result of the diffusion flame seen in CI engines [R.Turns, 2000]. In this thesis a comparison between a base SI engine and HCCI is performed. Cylinder pressure and Pressure-Volume (P-V) plots for HCCI and SI combustion events are shown in Figures 2.2 and 2.3 respectively, all test points noted in figures are tabulated in more detail in Appendix A. In this figure it is evident that the combustion process

of HCCI occurs much more quickly than that of SI combustion. For a spark ignition engine the flame takes a finite amount of time to travel from the spark plug to the rest of the combustion chamber, whereas for a HCCI engine the mixture autoignites at multiple locations, so the flame front travels much shorter distances before all the fuel is burnt. This results in a much faster combustion for HCCI engines than for SI engines. The P-V diagram shows the considerable pumping losses for the SI engine, while they are minimal for the HCCI engine. These pumping losses are a principle reason why SI engines have a low thermal efficiency when operating at part load [Stone, 1999].

Another benefit of the HCCI combustion process is the low production of nitrous oxides emissions (NO_x), which is a main contributor to acid rain and photochemical smog [R.Turns, 2000]. Emission regulations in both north America and Europe are decreasing the allowable NO_x emissions from combustion engines, so the reduction of these emissions is very important [Zhao, 2007b]. During SI combustion the fuel-air mixture is ignited by a spark, and as the mixture burns from the spark kernel the combustion products are continually compressed which causes an increase in the temperature. When the mixture is completely burned the temperature of the combustion products at the spark location can be well over the NO_x formation temperature of 1800K [R.Turns, 2000]. HCCI combustion is generally rapid enough that the elevated temperature of the combustion products does not occur, and it also operates in the presence of diluents such as excess air or residual gases, so the peak combustion temperature is kept below 1800K and little to no NO_x is formed [Zhao, 2007b].

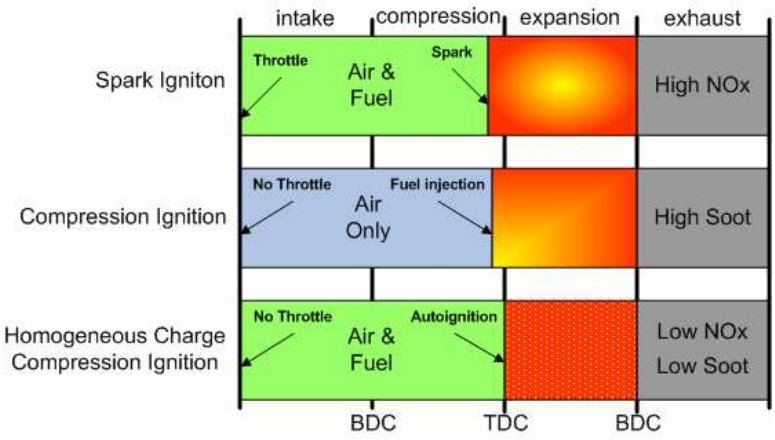

Figure 2.1: 4-Stroke combustion process for SI, CI and HCCI engines.

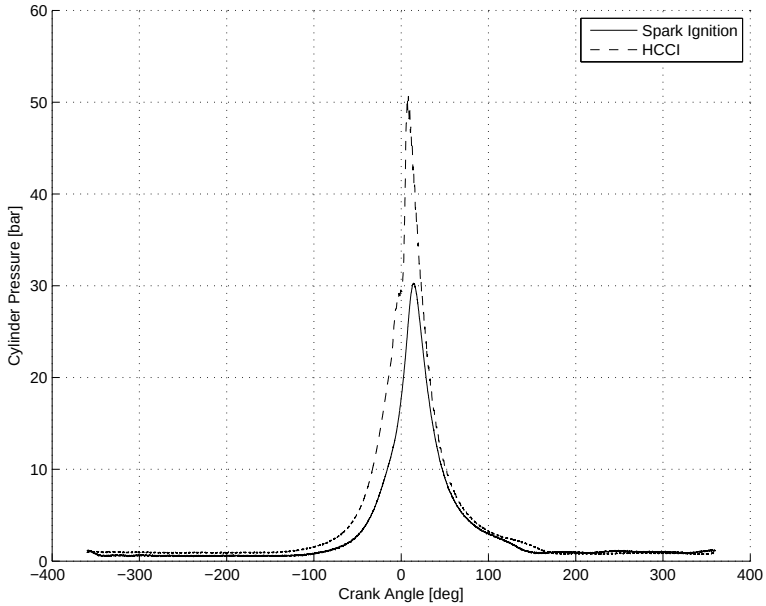

Figure 2.2: SI and HCCI cylinder pressure - 4.2bar IMEP and 1000RPM. (SI1 and HCCI1 test points)

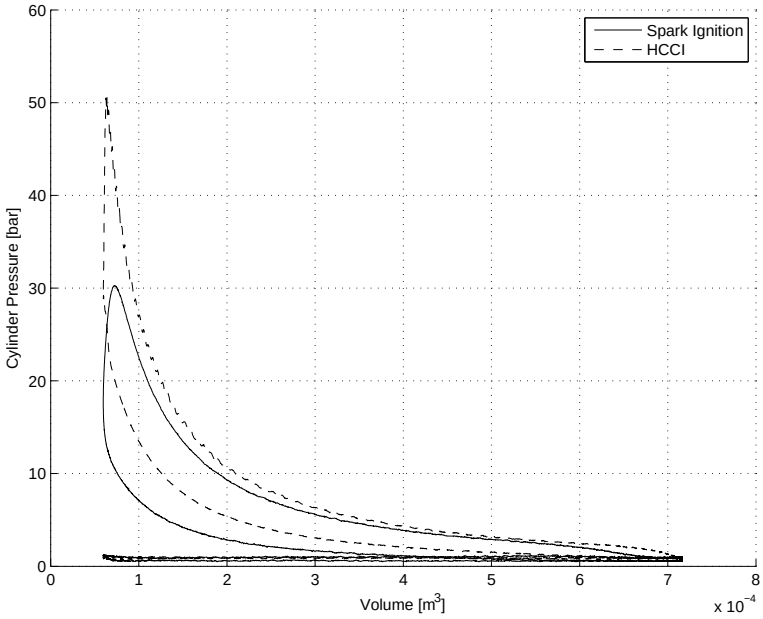

Figure 2.3: Pressure-Volume diagram for SI and HCCI combustion cycles - 4.2bar IMEP and 1000RPM. (SI1 and HCCI1 test points)

2.1.2 Speed-Load Range

Automobiles typically operate in certain engine speed-load ranges. An example of an economy car's speed load range is shown in Figure 2.4 [Santoso et al., 2005]. Also shown in this figure is the HCCI speed-load for a typical spark ignition HCCI engine which does not achieve the high-speed, high-power ranges needed for an automotive application. Although expanding the speed-load range of HCCI is the subject of intense research [Olsson et al., 2004,Milovanovic et al., 2005,Hyvonen et al., 2003] HCCI is still a part load concept which must be coupled with either SI of CI combustion.

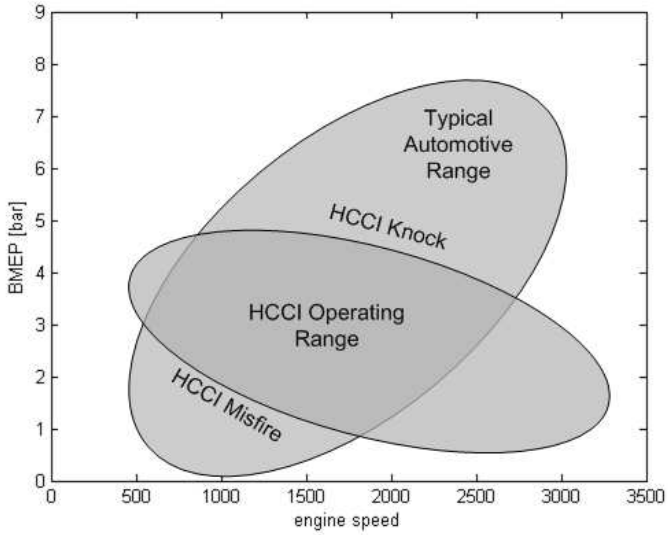

Figure 2.4: Typical speed load range of an automobile as well as the typical speed load range for a HCCI engine.

The HCCI speed-load range is limited by two major combustion modes: increased cyclic variation and engine knock. The first condition appears on the low load, or high engine speed limits of the HCCI speed-load range. Cyclic variation of the engine load leads to poor driveability of the automobile, and it also precedes the onset of engine misfire which leads to high engine emissions and low efficiency [Stone, 1999]. An example of HCCI combustion with high cyclic variation is shown in Figure 2.5. This plot shows 50 consecutive engine cycles where the Indicated Mean Effective Pressure (IMEP) of each engine cycle is calculated and this value is seen to vary substantially from cycle to cycle.

High load HCCI is limited by engine knock. For SI engines knock is described as the auto-ignition of air-fuel mixture before the spark [Heywood, 1988]. This creates large pressure gradients inside the chamber which oscillate at waves in ceratin modes which result in audible knocking or pinging sounds [Draper, 1933]. Damage to the engine occurs from knock due to increased heat transfer to the cylinder walls and increased forces to the engine components. There is also a decrease in efficiency from

the increased heat transfer. In HCCI engines knock is the onset of vibration modes inside the cylinder which have the similar effects as knock in SI engines [Sheppard et al., 2002, Vressner et al., 2003]. An increased heat release rate will increase the chance of knock in HCCI [Zhao, 2007c]. Cylinder pressure traces for HCCI cycles under knocking and non-knocking conditions are seen in Figure 2.6. The rapid pressure oscillations present are undesirable and correspond to the knocking mode of the engine.

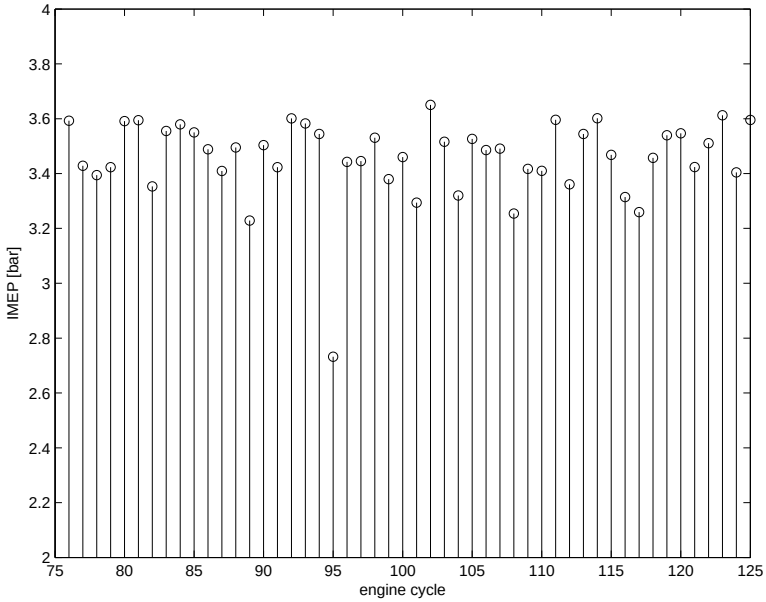

Figure 2.5: Consecutive IMEP values showing the cyclic variation of HCCI. (HCCI2 test point)

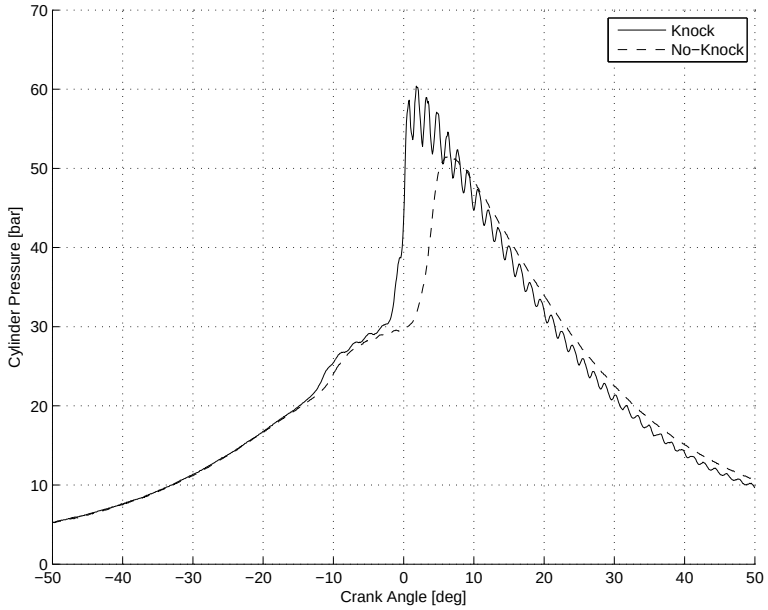

Figure 2.6: Pressure traces with no knock and harmful engine knock present. (HCCI3 and HCCI4 test points)

2.1.3 Ignition Timing

The cylinder pressure for a typical HCCI combustion event is plotted in Figure 2.7. Also seen in this figure is the cylinder pressure for a motored cycle; no fuel is injected. The effect of the combustion process on the cylinder pressure is evident from this figure. There are many ways in which the combustion event can be described. The maximum cylinder pressure, P_{max}, and maximum cylinder pressure rise rate $\frac{\delta P}{\delta \theta}_{max}$ are important parameters because of structural limitations on the engine components [Taylor, 1977]. Pressures that are too large can cause engine parts to fail. Timing of the combustion process is also important, and there are many different ways that the timing of HCCI can be calculated. By taking three time derivatives of a low-pass filtered pressure trace a threshold value can be used to determine the timing of the start of combustion [Checkel and Dale, 1986]. This method must be tuned for each engine and for the specific operating conditions. The most commonly used method to determine combustion timing is done by calculating the heat release and

using this as a basis [Tunestal and Johansson, 2007]. Another common method is the Rassweiler-Withrow method [Rassweiler and Withrow, 1938].

For this work the CA50 calculation is done using the heat release method as outlined in [Heywood, 1988]. The net heat released, δQ_{netR}, is the difference between the measured pressure trace and the pressure trace that would have occurred during polytropic compression:

$$\delta Q_{netR} = \frac{\gamma}{\gamma - 1} p dV + \frac{1}{\gamma - 1} V dp \tag{2.1}$$

γ is the ratio of specific heats and a value of 1.33 is used for this analysis [Heywood, 1988]. The cylinder pressure, p, is measured. The volume of the combustion chamber, V, is a known value using the crank-slider mechanism [Heywood, 1988]. Mass fraction burned, MFB_θ, is the cumulative heat released to a certain crank angle, θ, divided by the total heat released:

$$MFB_\theta = \frac{\sum_{\theta=0}^{\theta=\theta} \delta Q_{netR}}{\sum_{\theta=0}^{\theta=b} \delta Q_{netR}} \tag{2.2}$$

The mass fraction burned and net heat release rate for a HCCI combustion event is shown in Figure 2.8. From the mass fraction burned curve the crank angle timing of when certain percentages of fuel have burned can be calculated. The Crank Angle at 50% mass fraction fuel burned (CA50) is commonly used to describe the combustion timing of HCCI whereas CA10 sometimes denotes the start of combustion [Zhao, 2007c]. For this study CA50 is the only metric used to describe combustion timing and the time for CA20 to CA80 describes the burn duration of HCCI. Typically the CA50 value is between -2 °and 15 °after Top Dead Center (aTDC) for the engine in this study.

From the heat release rate in Figure 2.8 it is evident that for this fuel there are two

stages of combustion. The first stage is termed the Low Temperature Reaction (LTR) and the second stage is termed the High Temperature Reaction (HTR) [Kalghatgi, 2007]. Two stage reactions are common in paraffins, but some paraffins like n-Heptane will exhibit this low temperature reaction much more than iso-Octane [Kalghatgi, 2007].

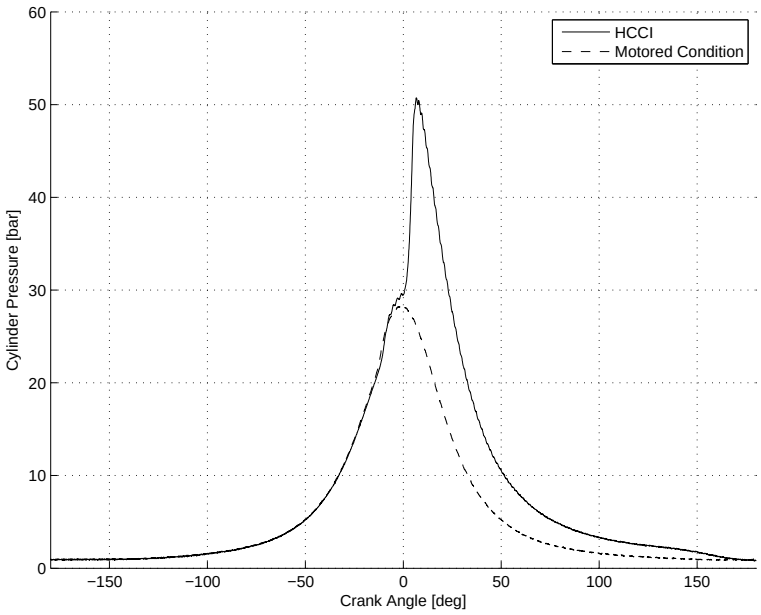

Figure 2.7: Cylinder pressure for a HCCI combustion event and a motoring pressure trace. (HCCI5 and MOT1 test points)

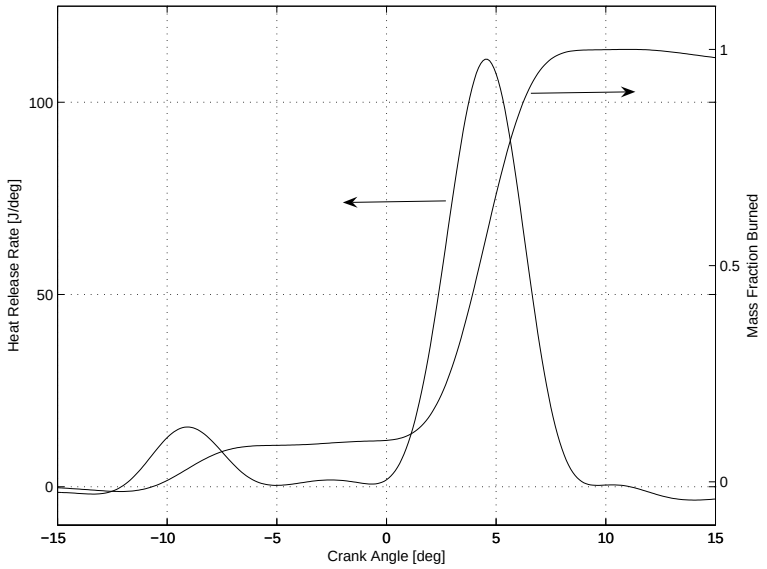

Figure 2.8: Mass fraction burned and heat release rate curves for a HCCI combustion event. (1^{st} engine cycle of HCCI1 test point)

Unlike SI engines that use a spark to initiate combustion, or CI engines which use the injection timing of the fuel, HCCI combustion timing is driven by chemical kinetics. The initiation of combustion is caused by a combination of many factors including initial temperature, initial pressure, compression ratio, internal and external Exhaust Gas Recirculation (EGR), and fuel composition [Atkins and Koch, 2005, Swan et al., 2007].

HCCI combustion timing changes with both engine speed and injected fuel quantity, but for successful automotive applications both speed and load must be free to change during operation. Other engine parameters need to be changed to compensate for changes in engine speed and load to maintain a suitable combustion timing. The start of combustion for HCCI is dictated by many engine parameters, so in order to control the start of combustion the relative effects of the engine parameters need to be understood.

Increasing the injected fuel quantity (decreasing λ) and engine compression ratio will both advance combustion timing. Changing the fuel energy not only changes the

combustion timing, but it dictates the load as well, so this parameter will be difficult to use to control the combustion timing. Changes in the compression ratio require substantial changes to the mechanical structure of the engine.

Increased external EGR retards the combustion timing yet this EGR has multiple effects on the HCCI combustion process [Atkins, 2004]. While the dilution and specific heat capacity effect is more prominent for external EGR, the charge heating effect is stronger for internal EGR and results in combustion timing advance. Both internal and external EGR have also been shown to be suitable methods for control of HCCI combustion timing [Agrell et al., 2003a].

Increasing the initial temperature and pressure will advance the combustion timing. [Shahbakhti et al., 2007c] shows the HCCI ignition can be predicted using a model developed by [Livengood and Wu, 1955] and analysis shows that temperature has a strong effect on combustion timing, so this parameter could be a suitable control for combustion timing [Shahbakhti et al., 2007b]. However, the temperature of the intake manifold cannot be changed very quickly without engine modifications. Alternatively, the end of compression temperature can be quickly changed by modifying the intake valve timing [Tunestal and Johansson, 2007].

The fuel composition has a very strong effect on the timing of HCCI ignition. Numerous studies have investigated the effects of different fuels on HCCI engines [Atkins, 2004, Atkins and Koch, 2005, Olsson et al., 2001]. While for some cases fuel octane number of actual fuels does not correlate well with combustion timing, [Atkins, 2004], it has been shown by other researchers that the blending ratio of iso-Octane and n-Heptane does correlate well with ignition timing [Olsson et al., 2001]. By implementing two fuel systems or by using reformer system the ratio of the fuels into the engine ignition timing can be quickly changed [Olsson et al., 2001].

The actuator requirements in HCCI combustion control are specific and fast response is very important to maintain low ignition timing variations in HCCI [Tunestal

and Johansson, 2007]. It is important that the timing can be changed without sacrificing control of the engine load. Since the technology will be implemented in a mass production setting there is also the need for it to be simple and cost effective. This array of requirements have resulted in researchers implementing a variety of methods in search of the *best* way to control HCCI. Some of these methods are outlined below.

2.1.4 Fuel Octane Control

The composition of the fuel being combusted has a primary effect on the start of combustion. Straight chained paraffins like n-Heptane autoignite more easily than paraffins such as iso-Octane, which has stronger bonded hydrogen atoms [Heywood, 1988]. These two fuel determine the scale by which the autoignition quality of all other fuels are based on. By blending volumes of iso-Octane, $V_{iso-Octane}$, and n-Heptane, $V_{n-Heptane}$, the Octane Number (ON) of the fuel going into the engine can be controlled:

$$ON = \frac{V_{iso-Octane}}{V_{iso-Octane} + V_{n-Heptane}} \tag{2.3}$$

This strategy of HCCI combustion timing control uses two port injection fuel systems, one with each of the aforementioned fuels. The volume of each injected fuel can be estimated by the injector pulse width. Using this strategy there is almost immediate control of the fuel octane number going into the engine, limited only by the fuel dynamics of the intake system. The use of this technology is one of the issues explored in this thesis.

2.1.5 Valve Timing Effects on HCCI

The gas flow through an internal combustion engine is controlled by the intake and exhaust valves. The flow is very complex and is effected by many factors including: valve timing, valve profiles, intake system geometry, exhaust system geometry [Hey-

wood, 1988]. Optimal valve timing strategies exist for different operating conditions in SI, CI and HCCI engines; some points require more internal EGR while some conditions require advanced timing of valves to achieve optimal volumetric efficiencies. Since changes in valve timing will effect air flow through the engine, engine components, termed Variable Valve Timing (VVT) [Stone, 1999], have been developed that can modify valve timing during engine operation.

Valve phasing is a common VVT strategy which allows the valve profile to shift relative to the timing of the crankshaft. The is very helpful for control of HCCI since the Intake Valve Closing (IVC) timing can be modified. As shown by [Tunestal and Johansson, 2007], changing the IVC timing will change the effective compression ratio, CR_{eff}, of the engine, defined as:

$$CR_{eff} = \frac{V_{tdc}}{V_{tdc} + V_{IVC}} \tag{2.4}$$

The change in effective compression ratio as a function of IVC timing is shown in Figure 2.9. This effective compression ratio change will alter the temperature at the end of the compression stroke, which will advance or retard combustion timing. The end of compression temperature based on isentropic compression as a function of valve timing is shown in Figure 2.10. This analysis assumes the air inside the cylinder behaves as a ideal gas and that the temperature and pressure inside the cylinder is the same as the intake manifold when the intake valve closes.

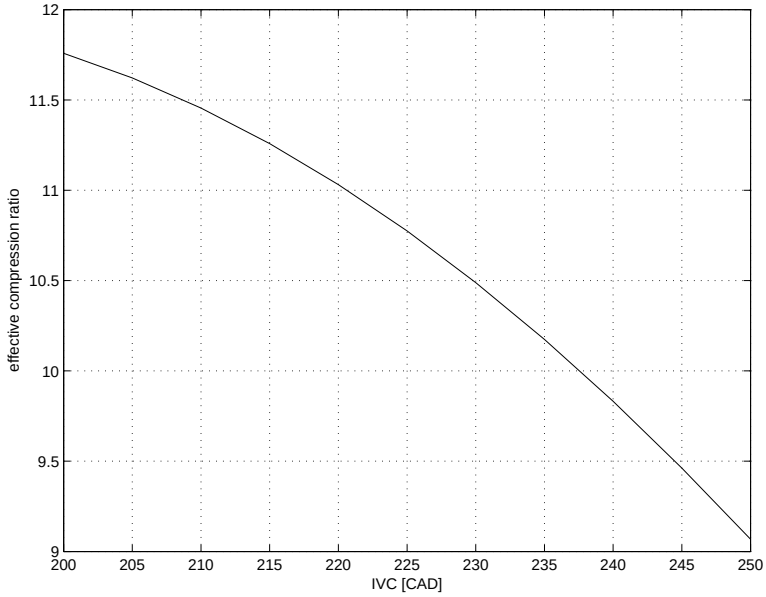

Figure 2.9: Effective compression ratio as a function of the IVC timing.

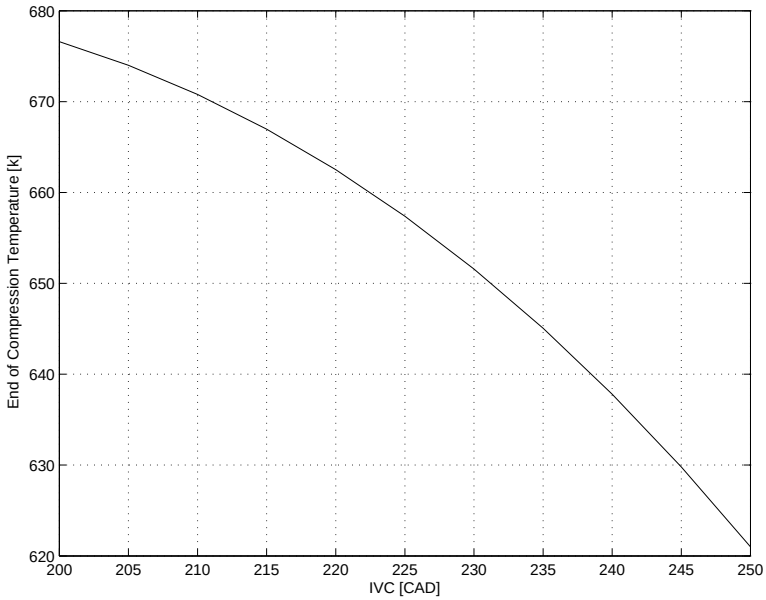

Figure 2.10: End of compression temperature for different IVC timing

Negative Valve Overlap (NVO) is a common method used in HCCI to trap hot EGR [Zhao, 2007a]. Typical SI timing values for Exhaust Valve Close (EVC) are around 10 °aTDC in order to ensure all exhaust is evacuated from the cylinder, but by closing the valves before TDC hot residuals are retained. This EGR promotes

HCCI combustion and is necessary for many operating conditions [Lavy et al., 2000]. The pressure trace for large NVO and small NVO can be seen in Figure 2.11. This figure shows the compression and expansion of the trapped exhaust. For typical NVO strategies the EVC and IVO timings are symmetric around TDC to minimize pumping losses [Zhao, 2007a], but this strategy was not employed for this study due to restrictions in the camshaft phasing apparatus.

A value of the mass of retained residual, m_{tr}, can be calculated using the pressure at EVC, P_{evc}, the temperature of exhaust, T_{exh}, the volume at EVC, V_{evc}, and the molar mass of the exhaust, R:

$$m_{tr} = \frac{P_{evc}V_{evc}}{RT_{exh}} \tag{2.5}$$

The mass fraction of residual, r, assuming no external EGR, is then calculated using the mass flow rate of the fresh air, $m_{freshair}$, and the flow rate of the injected fuel, m_{fuel}:

$$r = \frac{m_{tr}}{m_{tr} + m_{freshair} + m_{fuel}} \tag{2.6}$$

Calculated mass fraction of residual for a sweep of the exhaust valve timing is shown in Figure 2.12. Here it is seen that the internal residual can be changed by as much as 14% with a 23 °change in EVC timing.

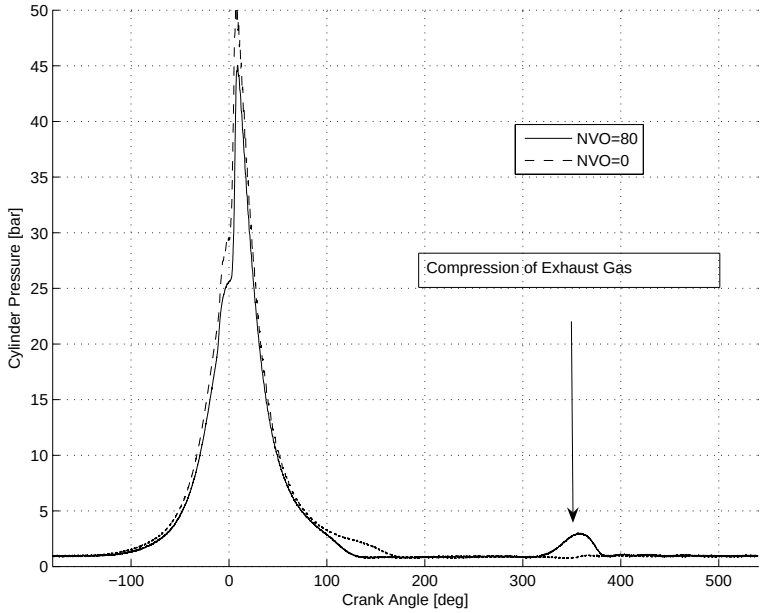

Figure 2.11: Pressure trace for two different valve timing strategies: with and without NVO. (HCCI1 and HCCI6 test points)

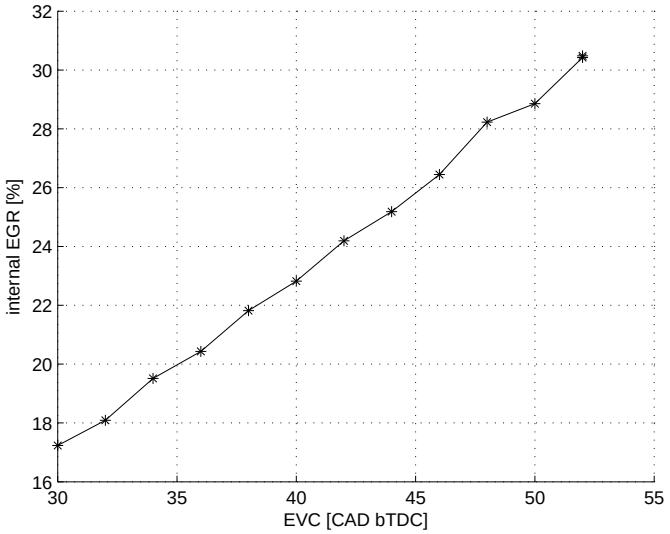

Figure 2.12: Calculated internal EGR mass fraction as function of EVC. (IEGR test points)

2.2 Feedback Control and System Identification Fundamentals

While the use of feedback control is centuries old [Mayr, 1970], the widespread commercial use of control for automotive applications can be attributed to the breakthrough of computer control [Kiencke and Nielsen, 2000]. Currently feedback control is necessary for the operation of many vehicle systems, such as ABS, proper function of the catalytic converter, cruise control, and idle speed control. This study investigates the use of digital feedback control applied to HCCI combustion timing, so a brief introduction to digital feedback control is given.

The structure of a feedback control scheme is shown in Figure 2.13. For feedback control a measurement of the plant output is compared with the desired value of the plant output and the difference is called the error. A controller adjusts the input to the plant according to the value of the error. Proportional Integral Derivative (PID) control is one of the most widely used forms of feedback controllers [Johnson and Moradi, 2005]. In digital PID control a combination of the error, the integral of the error, and the derivative of the error from a sampled system are calculated at some rate. The control output is generated once per sample and output as a continuous signal through a zero order hold:

$$u(t) = K_c \left[e_k + \frac{T_s}{T_i} \sum_{i=0}^{t} e_i + \frac{T_D}{T_s}(e_k - e_{k-1}) \right] \tag{2.7}$$

Most implementations of PID controllers implement elements such as integrator anti-windup and anti-derivative kick but these are not used in this thesis.

Feedforward control does not act on the error term like feedback control, but often uses a mathematical model of the plant and adjusts the control input in response to measured disturbances or changes in the set point [Levine, 1996]. Feedforward is commonly used in automotive applications to maintain steady engine speed [Levine, 1996]. The benefit of feedforward control is that output error does not have to occur

before the plant input is changed. The input is changed according to the anticipated output given by a model of the system. A diagram of a system with feedforward control can be seen in Figure 2.14. To implement feedforward control it is necessary to have a mathematical model of the plant that can be run in real-time which is sometimes very difficult to attain. Often feedback control is implemented in conjunction with feedforward control. The feedback attenuates plant-model mismatch, and unmeasured disturbances.

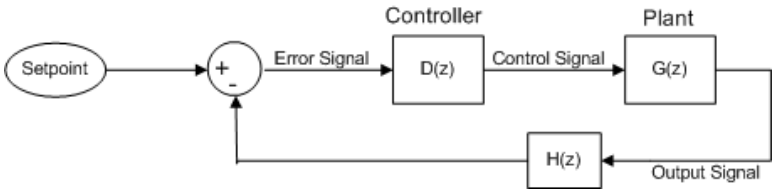

Figure 2.13: Schematic of a typical feedback control scheme.

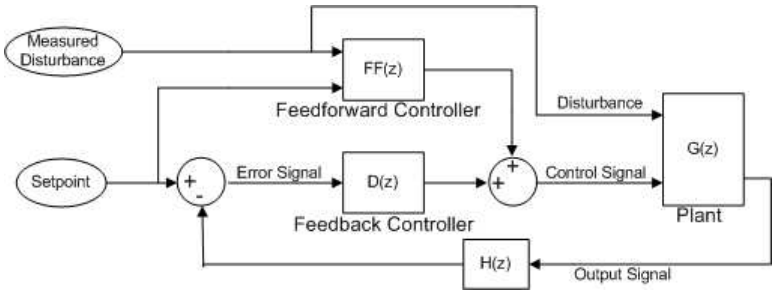

Figure 2.14: Schematic of a typical feedforward control scheme.

For some systems it is nearly impossible to derive mathematical models, or the models are too complex to be used for controller design. Lower order models must mimic the dynamics of interest with sufficient accuracy for the operating range in question. One standard technique identifying mathematical models from experimental data is called system identification [Ljung, 1987]. An overview of the procedure identifying a model from experimental data is: first design an experiment that can produce useable data, this usually involves constructing an input signal that will excite all the model properties that are to identified. Next the data is collected, the

data must be a suitable length and have a high signal to noise ratio. Thirdly, for parametric system identification a mathematical form for the model is chosen, as well as the fit criterion. The model is then numerically calculated. The last step is to validate this model and evaluate the fit criteria. Iteration is usually required to obtain the simplest model that still captures the dynamics of interest. This procedure is used in many fields of science and engineering, and numerical tools have been built to aid in system identification [mat, 2006].

2.3 HCCI Physics

An early example of HCCI is accredited to Onishi *et al.* with their work on Active Thermo-Atmosphere Combustion (ATAC) [Onishi et al., 1979]. In this study they showed the efficiency gains and emissions reduction for HCCI in a two-stroke engine. Najt and Foster investigated controlled auto-ignition in a four stroke engine [Najt and Foster, 1983]. They denote the combustion process Compression Ignited Homogeneous Charge (CIHI), and show that the auto-ignition timing is governed by the chemical kinetics of the hydrocarbon-air mixture.

With fuel efficiency and emissions regulations a top concern research into HCCI has been very active for the past ten years [Zhao, 2007b]. Using optical access to combustion chambers the HCCI process has been viewed and studied [Hildingsson et al., 2005]. Many models have been created that allow researchers to see the underlying physics that drive HCCI [Kirchen et al., 2007, Kongsereeparp and Checkel, 2008]. Numerous experimental parameter studies have been performed to find the range of stable combustion [Atkins, 2004]. HCCI to SI transitions have also been studied since HCCI will most likely be implemented as a part load concept [Santoso et al., 2005].

One main problem with HCCI is the limited load range of stable operation. Re-

search into the expansion of the load range has been performed by researchers using increased manifold pressure [Olsson et al., 2004]. This research has shown that increases in the manifold pressure will cause an increase in the high load range of HCCI. Research into the cyclic variations at the misfire limit of HCCI have also been performed extensively [Shahbakhti et al., 2007a]. The mechanisms causing engine misfire and cyclic variation have been investigated experimentally and the effects of various parameters have been studied.

Due to consumer demand for *cleaner* cars as well as government regulations on emissions the HCCI technology is being developed for commercial automobiles by companies such as General Motors and Daimler AG. Although research done by these corporations has not been published, numerous articles have noted their goals of producing vehicles that will incorporate HCCI into the engine technology [Motors, 2007, AG, 2007].

Extensive modeling of HCCI combustion has been performed [Westbrook et al., 2002, Kusakak et al., 2002, Kongsereeparp and Checkel, 2007, Kirchen et al., 2007]. One primary variable of interest is the timing of HCCI. Modeling of HCCI is done for different reasons; large computationally intensive models are developed to aid in understanding the physics behind the combustion process while simpler and faster models are developed for the purpose of HCCI control. Large models incorporate chemical kinetics of the reactions, and can contain hundreds of chemical reactions [Westbrook et al., 2002]. These reactions are then coupled with thermodynamics models of the combustion chamber, either multi-zone or single zone. Models that couple with Computational Fluid Dynamics (CFD) code have also been developed to attempt to model the in-cylinder turbulence [Kusakak et al., 2002]. These models have been used to understand and quantify the effects of parameter variation that would be difficult or impossible to perform in an experimental engine. While the usefulness of these models cannot be undervalued, their application to control design

is somewhat limited.

2.4 Control Oriented Modeling and System Identification of HCCI

Numerous researchers have developed control models that are capable of running within the time constraints of an HCCI engine; control oriented models. The bulk of these models are physics-based models while some of them are created from experimental data using system identification procedures. As noted in [Tunestal and Johansson, 2007] physics based models to predict autoignition can be grouped into three main categories; the knock integral model, the integrated Arrhenius rate threshold model, and the Shell autoignition model. [Shahbakhti et al., 2007c] shows work done using the knock integral model, but this work was not applied to an experimental engine. In [Shaver et al., 2006b] the Arrhenius rate threshold model was developed and applied online for control purposes. The Shell autoignition model was also developed but it was found to be too computationally demanding for realtime applications [Bengtsson, 2004].

Experimentally derived models have also been shown as suitable ways of determining models for control purposes. Sensitivity estimation has been done and has been shown to work well [Olsson et al., 2001]. This method does not identify any dynamics of the system since the work is done on stationary engine data. System identification methods have also been applied to the HCCI combustion [Pfeiffer et al., 2004]. In this work multi-input multi-output state-space models were identified and later used for LQR and MPC control schemes.

2.5 Control of HCCI

2.5.1 Introduction

For practical implementation of HCCI it is necessary to have some form of feedback control to regulate the combustion timing [Tunestal and Johansson, 2007]. In HCCI there is no means of directly controlling the combustion timing, which is strongly influenced by coolant temperature, air temperature, engine speed and engine load. The experimental work done on feedback control of HCCI combustion timing is summarized in this section. Since there are many methods of control design, the many works are separated into physical model based control, experimentally derived model based control, and manually tuned controllers and these are further sub-categorized by the research groups.

2.5.2 Physical Model Based Controllers

2.5.2.1 Scania

Closed loop combustion control of HCCI using PID controllers and model based controllers is described in [Agrell et al., 2003b, Agrell et al., 2003a, Agrell et al., 2005a, Agrell et al., 2005b]. Using a Active Valve Train (AVT) hydraulic valve timing system mounted on a one-cylinder test engine they simultaneously adjusted both the Intake Valve Close (IVC) point as well as the amount of Negative Valve Overlap (NVO). In their initial paper they simulated both the HCCI engine cycle and their controllers for CA50 [Agrell et al., 2003b]. These engine simulations are then verified by experiential data. They then used a combination of IVC timing and the amount of NVO to control CA50 [Agrell et al., 2003a]. This control was done with PID controllers; where a criterion is used to switch between either controlling IVC timing or amount of NVO. In further work, a model based control system was incorporated [Agrell et al., 2005a].

Model based control was added to improve the transient performance of the controller, as the earlier PID controllers were shown to be relatively slow. In order to further improve the control performance an in-cylinder state estimator was added [Agrell et al., 2005b] where λ estimation was derived using the ideal gas law while neglecting gas dynamics in the intake and exhaust.

In these works successful control of CA50 was shown using combinations of IVC timing and the amount of NVO. Disturbance rejection was tested under load and speed transients. Tracking performance of these controllers was not quantified with variance statistics, but the figures show 2° changes in the CA50 when speed and load transients are applied [Agrell et al., 2005b].

2.5.2.2 University of Michigan

The development of a physical model for nonlinear control of HCCI were given in [Chiang and Stefanopoulou, 2007, Chiang et al., 2007]. They used a simplified nonlinear feedback controller to regulate the CA50 during load transients [Chiang et al., 2007]. The controller performance was tested offline using a more detailed model that incorporated gas dynamics, heat transfer, combustion and cycle-to-cycle variation. While these models were calibrated using real engine data, the controller was never tested on an engine. Control was done by modifying the lift of a secondary exhaust valve opening to control the internal EGR.

2.5.2.3 Stanford University

A MIMO controller was used to decouple the control of combustion timing and peak cylinder pressure in [Shaver et al., 2005]. A slower combustion timing controller was implemented with the IVC as the actuator, while a cycle-to-cycle controller modulated the peak pressure using EVC timing to change inducted gas composition. The development of an engine model for HCCI that was used to formulate a H_2 controller was

given in [Shaver et al., 2006a]. This controller was then validated experimentally and they noted the control strategy was quite effective. The model inputs were trapped residuals and effective compression ratio, which were both controlled by VVA. The model outputs were combustion timing and the maximum cylinder pressure.

In [Shaver et al., 2006a] the controller was tested for step and sinusoidal changes in the work output. They do not quantify the variance of combustion timing.

2.5.2.4 Robert Bosch GmbH

Both data driven and physics based models were used to design controllers to track load, while regulating the pressure rise and CA50 [Kulzer et al., 2007]. Direct injection and VVA were both used as actuators in this system. Feedforward control was implemented, using steady state maps and a physical based model. Mode switching was also incorporated in the controller which switches from Gasoline Direct Inject (GDI) spark mode to the HCCI mode. The engine was run through the European NEDC drive cycle to show its practicality.

2.5.3 Empirically-Derived Model Based Controllers

2.5.3.1 Lund University

The use of system identification to design model based controllers and the implementation of these controllers on various engine test setups is described in [Olsson et al., 2001, Bengtsson et al., 2004, Strandh et al., 2005, Bengtsson et al., 2006c, Bengtsson et al., 2006b, Bengtsson et al., 2006a, Bengtsson et al., 2007, Pfeiffer et al., 2004].

Their first work on HCCI control implemented combustion timing control and load control using the ratio of n-heptane and iso-octane with two injectors used for each cylinder [Olsson et al., 2001]. PID controllers, with low-pass filters on the derivative and feed-forward terms, were then tested experimentally. The gain of the combustion

timing controller was gain scheduled. It was derived to be a function of engine speed, intake temperature, mass of fuel, octane and CA50. The IMEP controller was set to be slower than the timing controller, so that it did not drastically effect the combustion timing. In this work they noted that the system preformed well, but they reported problems in estimating the sensitivity of the timing and this effected the performance of the timing controller. Errors of more than 5 °are observed during speed and load ramps.

In their next work a model based (LQG) controller was developed using system identification techniques [Bengtsson et al., 2004]. Variations in octane were still used to control the timing, but an ion sensor was also used a feedback sensor for CA50 as well as the pressure sensor. The model based LQG controller was shown to perform slightly better than the manually tuned PID controller. In another study, system identification was used to identify a model between the mechanical compression ratio and CA50 [Bengtsson et al., 2006b]. A Saab variable compression ratio engine was used for the tests. For this study they successfully implemented an LQG controller capable of disturbance rejection and reference tracking. Both of these studies plot the performance of the combustion timing controller during speed and load transients. Minimal errors in the combustion timing were observed.

Fast Thermal Management (FTM) was used in yet another study to control the CA50 timing [Haraldsson et al., 2004]. Here control was done with a manually tuned PID loop. The time constant was found to be 8 engine cycles, which they note as being relatively slow. They also noted that gain scheduling the controller would benefit performance during load ramps. Large errors, around 2 °, in the combustion timing were observed during speed and low changes.

Variable Valve Actuation (VVA) was used for timing control of HCCI [Strandh et al., 2005]. The VVA system used a lost motion system, whereby the intake valve can be hydraulically closed ahead of the cam curve. System identification techniques

were used to derive a SISO model between a linearized value of the IVC timing and CA50. This model was then used in the design of LQG controller as well as a MPC controller. A non-model based PID controller was also implemented in this study for comparison purposes. All three controllers were found to be satisfactory. It was also observed that if only IVC is used to control CA50, it cannot be done over the entire HCCI operating range.

The group at Lund University then demonstrated that MIMO models can be identified to a reasonable accuracy, and these models can be used in the design of an MPC controller to achieve cycle-to-cycle control [Bengtsson et al., 2006c]. Like the previous studies this controller used VVA to change combustion timing. Engine load was controlled using MPC while minimizing the fuel consumption and emissions, and also satisfying a constraint on maximum pressure rise. To minimize fuel economy the weighted CA50 set point was set to TDC, but was constrained by maximum pressure rise, in order to avoid harmful engine knock. Their next work also used a MIMO MPC controller designed with system identification, but here fuel octane was used as the input to control CA50 [Bengtsson et al., 2006b]. Both these papers reported that using MIMO system identification can produce a useable MPC controllers. A further study provides a direct comparison between the MPC controllers using variable octane and VVA [Bengtsson et al., 2006a]. Variable octane provided better control of CA50 at high loads than VVA since VVA had the effect of reducing the volumetric efficiency which reduced the high load capability. However, using VVA provided a faster response in CA50 since the variable octane strategy has slower dynamics associated with fuel transport and evaporation. Their most recent work provided a summary of most of their work done in the area of HCCI control; they examine potential future HCCI control strategies [Bengtsson et al., 2007]. They suggested more detailed physical based control models are needed and it was also indicated that cycle to cycle control of trapped residuals would be very beneficial.

2.5.4 Non-Model Based Control

2.5.4.1 Keio University

By modulating the fraction of external residuals, as well as the temperature of the intake air/resiudal mixture a PI controller for HCCI was implemented [Tetsuo Ohmura and Iida, 2006]. They used a combination of two PI controllers, a slow one for IMEP, and a faster one for CA50. This engine was fueled with Dimethyl Ether and used four different camshaft profiles to change the amount of exhaust re-breathing.

2.5.4.2 MIT

HCCI was controlled in [Matthews et al., 2005] using open and closed loop controllers for load set point tracking of HCCI. The control variable was engine load in IMEP and to control this the fuel input, IVC and EVO were varied on hydraulic VVT engine. The engine was first statically mapped, where the timing was set at the point for maximum torque. Using the static map the open loop controller was then implemented. To compensate for error in the static map feedback was added, which was an integrator term. These controllers were verified experimentally, and the closed loop controller was found to track inputs in load more easily than the open loop controller. The controller showed lower coefficient of variation (COV) for the IMEP than that of open loop load control, 3.2% and 2.6% respectively.

2.5.4.3 University of California - Berkeley

[Souder et al., 2004] has shown that microphones can be used a feedback signals for combustion timing control. An exhaust back pressure valve was used to regulate the amount of residuals, which were used to effect the combustion timing.

2.5.5 Summary

Each different research group has approached the HCCI combustion timing problems in different ways. Table 2.1 is a summary of the different controllers and methods of actuation seen in these previous studies.

Table 2.1: Summary of the previous work done in feedback control for HCCI combustion timing.

Affiliation	Method of Actuation	Controller	Notes
University of Michigan	Lift adjustment of 2nd Exhaust opening	nonlinear observer-based control	Control is not tested experimentally
Scania	IVC and NVO	Non-linear compensation CA50 controller with engine state correction (λ)	Tested experimentally.
Robert Bosch GmbH	Direct injection and VVA	Feed-forward control using steady-state maps and physical based models	Tested experimentally over an entire drive cycle.
Stanford University	IVC and NVO	Physical based 2-input 2-output linear controller	Tested experimentally.
Lund University	Fast Thermal Management	Manually tuned PID to control CA50	Noted slow response compared to other methods of control
Lund University	Variable Octane	MPC controller designed with system identification	Tested Experimentally
Lund University	IVC	MPC controller designed with system identification	Tested Experimentally
Keio University	IVC and exhaust profile	Manually tuned PID	Tested Experimentally
University of California	Exhaust back pressure valve	Manually tuned PID	Used a microphone for feedback signal
Massachusetts Institute of Technology	IVC and EVO	static open loop map with integrator feedback term	Tested experimentally

Chapter 3

Experimental Setup, Testing Procedure & Data Analysis

This chapter first describes the experimental setup used in this study. The testing procedure and operation limits are then described, and the chapter concludes with a brief discussion of the sensor calibrations.

3.1 Experimental Setup

3.1.1 Short Block Assembly

The short block assembly for the one-cylinder test engine can be seen in Figure 3.1. This is a custom made system designed as part of the work performed in this thesis. Table 3.1 shows some specifications of the engine. The system required extensive modification to incorporate the camshaft phasing cylinder head that is used in this study. The engine block is a *Ricardo Hydra Mark III* and the crankshaft is also from the same manufacturer. The connecting rod bearing is ground down for the custom connecting rod made by *Carrillo Industries*. Also, a new piston is designed and custom made by *Diamond Pistons*. The piston is specified to give a high compression ratio while still having adequate valve clearance. Valve clearance allowed the flexibility to drastically modify the valve timing which is required for this study. The rough

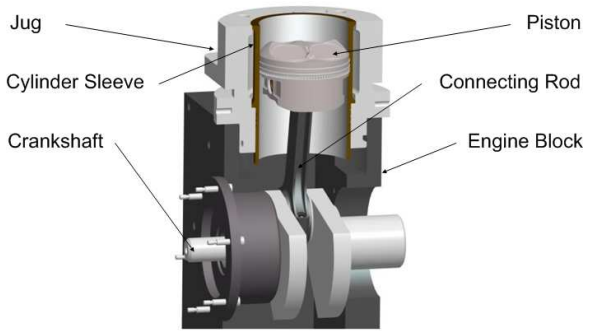

Figure 3.1: Overview of the short block assembly of the engine.

shape of the piston is not optimal for reduction of unburned hydrocarbons due to the large amount of crevices [Heywood, 1988].

The cylinder jug is designed to house the wet cylinder sleeve, which is custom made from *Darton International Inc.*, and bolted to both the cylinder head and the engine block. The whole system has an adjustable compression ratio by turning a large ring on the jug which raises and lowers the head relative to the block, which changes the clearance volume of the engine. When adjusting the compression ratio of the engine it is necessary to adjust the timing chain. For this study the mechanical compression ratio is kept at a constant value of 12:1.

The crankshaft bolts to the dynamometer through a splined shaft and and two flexible couplings. This allows the entire engine assembly to vibrate separately from the dynamometer test cell. Since the weights of the piston and connecting rod are changed for this experiment the crankshaft was professionally re-balanced to minimize the engine vibrations.

Table 3.1: Specifications of the one-cylinder test engine

Bore	97mm
Stroke	88.9mm
Displacement	653cc
Connecting Rod Length	159mm
Compression Ratio	12:1 (adjustable)
Number of Valves	4
Valve lift	9.3mm

3.1.2 Cylinder Head

The engine uses a cylinder head from a 2007 E550 Mercedes (donated to this project by Daimler AG) [e55, 2007]. This cylinder head is chosen since it is a four-valve per cylinder engine with independent camshaft phasing for both intake and exhaust camshafts. The cylinder head is manufactured for an eight cylinder engine, so as part of this thesis it is slightly modified for the one cylinder research engine, see the Appendix C for a description. The head is fitted with an in-cylinder pressure transducer, which will be discussed later. Before assembly into the dynamometer cell some necessary measurements were taken from the head, such as: chamber volume, valve size, valve lift and profiles, and discharge coefficients in both forward and reverse directions. The details of these measurements can be seen in the Appendix C. To assemble this head to the engine an adapter shaft for the end of the crank is manufactured to turn the timing chain. A schematic of this assembly is shown in Figure 3.2. All the necessary cooling and oiling lines are also plumbed for proper valve operation. The assembled cylinder head can be seen in Figure 3.3.

3.1.3 Camshaft Phasing

The cylinder head used in this study has built in camshaft phasers. In production Mercedes E550 engines these phasers are controlled by the engine's Electronic Control Unit (ECU) but for this research custom controllers are designed and built. For this

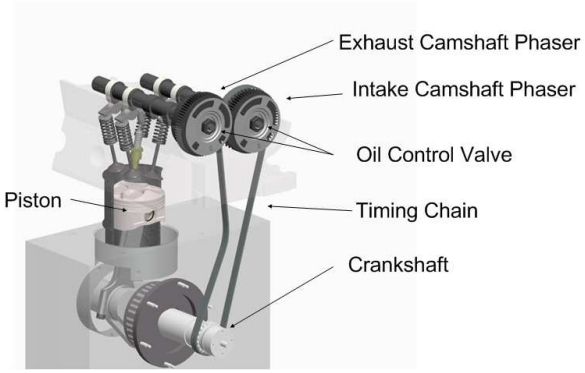

Figure 3.2: Crankshaft adapter assembly

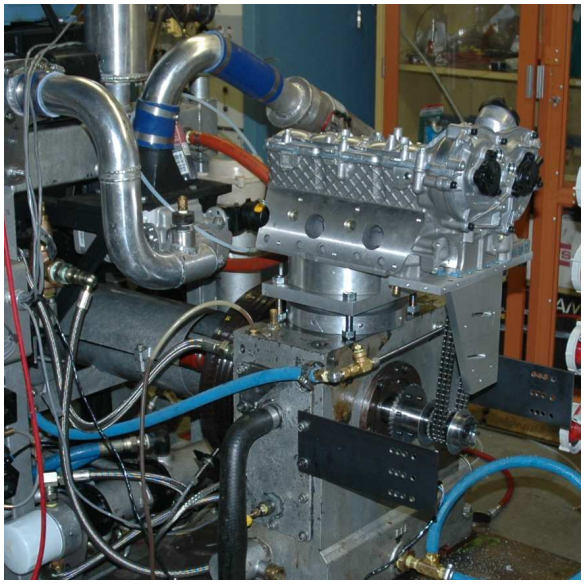

Figure 3.3: Overview of the long block assembly of the engine.

study phasers are controlled using the dSPACE MicroAutoBox, and the details of this controller can be seen in the Appendix B. A schematic of the controller is shown in Figure 3.4. The PI controller runs at a 1kHz sample rate and the gains are manually tuned.

The timing adjustment of 40° can individually be set for both the intake and exhaust valves. The timings used in this study can be seen in Table 3.2. The change in valve timing is not instantaneous due to the dynamics of the system. Figures 3.5 and 3.6 show the transient response of both the intake and exhaust valve phasers. The phaser dynamics are time based, so as the engine speed is increased it will take more engine cycles to complete the same timing change.

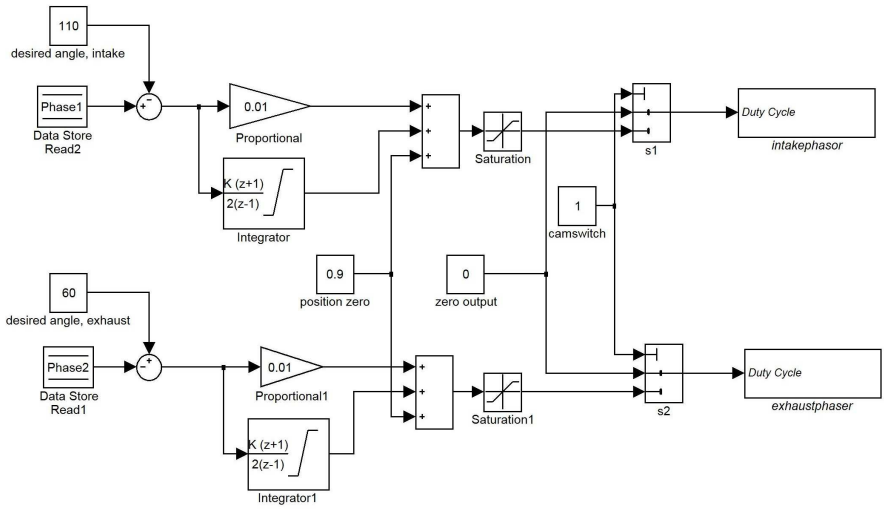

Figure 3.4: Schematic of the camshaft phaser controller. A PI controller is used to adjust the duty cycle of a solenoid valve.

Table 3.2: Timing and response of intake and exhaust valves.

	Timing Range	Transient Response [CAD/s]
Intake	202-242 aTDC	130
Exhaust	13-53 bTDC	130

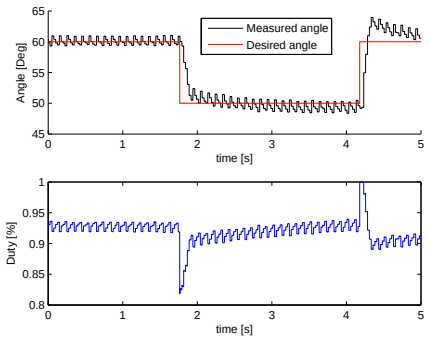

Figure 3.5: Transient response of the intake camshaft timing at an engine speed of $1200RPM$. (test point $IVC1$)

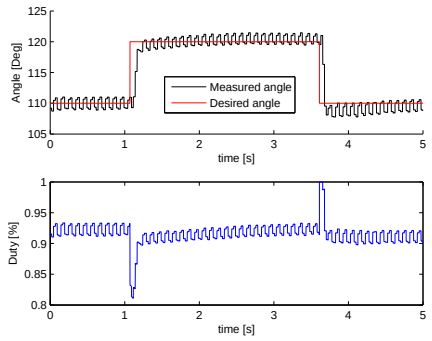

Figure 3.6: Transient response of the exhaust camshaft timing for and engine speed of $1200RPM$. (test point $EVC1$)

3.1.4 Intake and Exhaust System

A schematic of the intake and exhaust systems can be seen in Figure 3.7 showing the main components as well as the temperature and pressure measurements points. The air heater is placed upstream of the injectors, but after the electrically driven supercharger. The intake air pulsations are damped with a large barrel before the laminar air flow meter. Intake temperature and pressure readings are taken upstream of the injectors and downstream of the air heater. The exhaust is plumbed from the engine to the exhaust fan and out of the building. The emissions samples, exhaust pressure, exhaust temperature, and λ measurements were taken within 10cm of the exhaust port.

3.1.5 Fuel System

The fuel system schematic can be seen in Figure 3.8. The fuel is injected into the intake air directly onto the intake valves, at TDC. Both the iso-Octane and n-Heptane injectors are placed at the same distance from the intake valves. These two independent fuel systems are installed on this engine so that blending of iso-Octane and

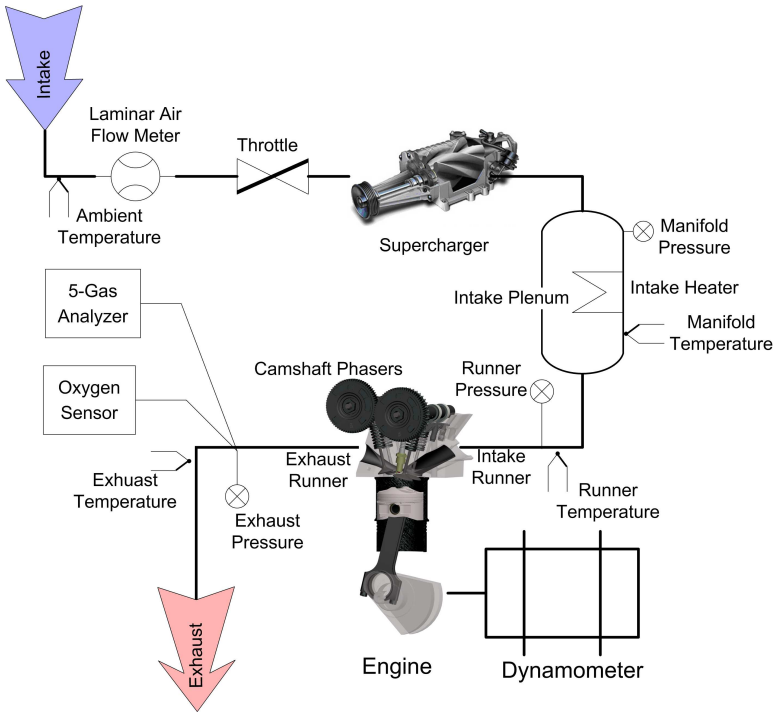

Figure 3.7: Schematic of the intake and exhaust system for the experimental setup.

n-Heptane can be done on a real time basis. The fuel systems are typical of a SI production engine in a modern automobile. There is a fuel regulator that maintains 3bar fuel pressure relative to the manifold. Both fuel systems are calibrated to determine the injector flow rates. This is done so that the mass flow rate of both fuels can be estimated. Calibration is done with a *Pierburg PLU 4000* fuel mass flow meter and the details of this calibration can be seen in the Appendix D. Figure 3.9 shows the calibration for both the iso-octane and n-heptane fuel systems. Using this calibration the real-time fuel octane number is controlled.

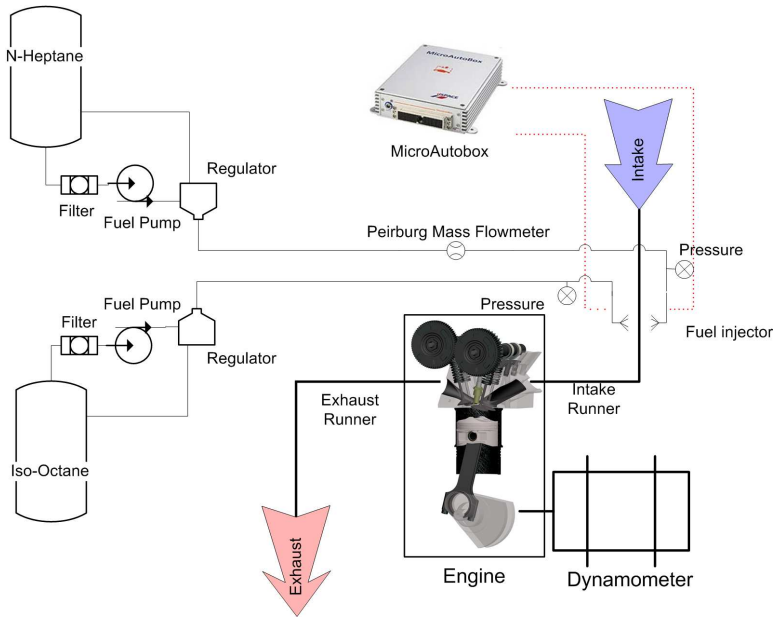

Figure 3.8: Schematic of the fuel system for the experiential setup. Two separate fuel systems are incorporated so that the fuel octane number can be controller in real time.

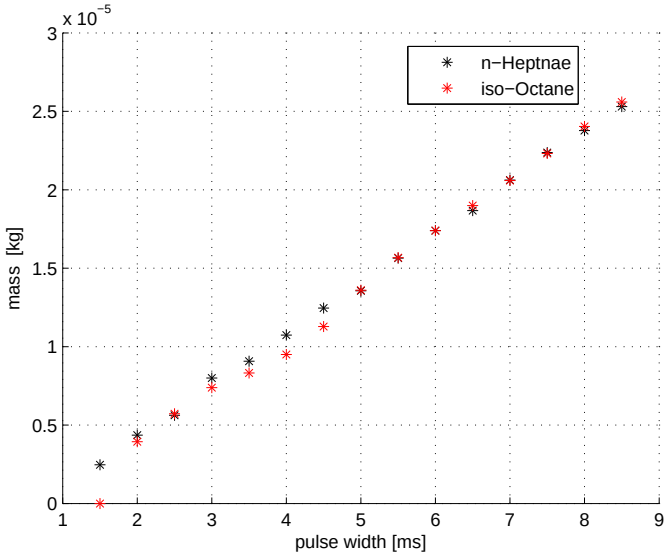

Figure 3.9: Calibration of the injector flow rate as a function of pulse width.

3.1.6 Dynamometer

To control the power output of the engine as well as motor the engine a 37kW DC electric motor is used. This is controlled with a *Eurotherm Drives 590+* drive controller that is used to regulate the engine speed or torque. The torque absorbed by the electric motor is measured with a *Interface Inc. SSM-A-J-200N* load cell. A picture of the this assembly is seen in Figure 3.10.

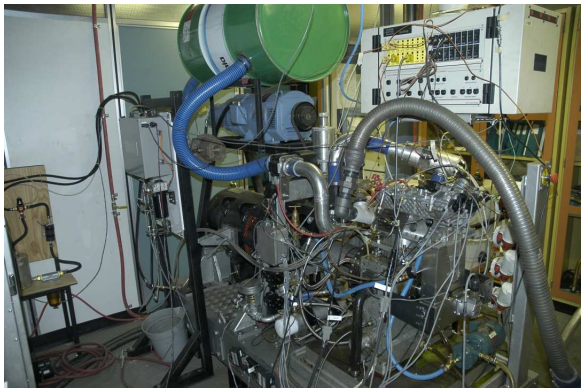

Figure 3.10: Picture of the entire experiential setup.

3.1.7 Sensors

A detailed table of the sensors used in this study is found in the Appendix A. The sampling systems for both the J-Type and K-Type thermocouples have built in reference junctions so no ice-baths are required. These signals are sampled at 10 Hz since they have relatively slow response to transients. For pressure measurements various diaphragm pressure transducers are used. These sensors have different sampling rates depending on the application. These sensors are calibrated frequently and the calibrations can be seen in the Appendix D. To measure the in-cylinder pressure a *Kistler 6043A60* piezoelectric pressure transducer is used. This sensor is water cooled to prevent thermal drift and sampled every tenth of crank angle degree using the CAS system and *BEI Industries XH25D-SS-3600-T2-ABZC-7272-SM18* shaft encoder. Since this sensor measures pressure differential there is substantial drift in

the absolute valve of pressure over time, so the signal is pegged to the absolute value of the intake manifold every engine cycle when the intake valve is open. Air flow is measured with a *Cussons Technology P7200/108* laminar airflow meter, and the calibration for this can be seen in the Appendix D. An *ECM AFRecorder 1200* wide-band oxygen sensor is used for fast measurement of the engine λ ratio. The exhaust emission are also measured with a five gas analyzer system [Atkins, 2004]. The O_2, CO_2, CO, uHC, and NO_x concentration of the dry exhaust gas are measured with this system. These measurement devices required constant calibration using calibration gases, and the details of the calibration and the operation of this system can be seen in Appendix D. Engine vibrations are measured with a production grade knock sensor, Bosch *Model 261 230 120*. The barometric pressure is measured with a standard mercury barometer.

3.1.8 Data Acquisition and Control System

To record all the sensor data and control the various systems three interfaces are used. These are the A&D ADAPT, A&D Baseline CAS and dSPACE MicroAutoBox.

3.1.8.1 ADAPT System

The A&D ADAPT system used in this experimental setup is a hardware and software system that is designed for conducting engine/dynamometer tests [A&D Technologies, 2003]. A schematic of the ADAPT system can be seen in Figure 3.11. The data logging for this system is time based and sampled at 10Hz, so it is not triggered to sample at certain points in the engine cycle. This system is responsible for controlling the dynamometer and also runs the oil and coolant systems which have internal PID control loops. All temperature and pressure signals, except for in-cylinder pressure signal, are recorded by this system. The temperature and pressure of the intake system are also controlled through this interface.

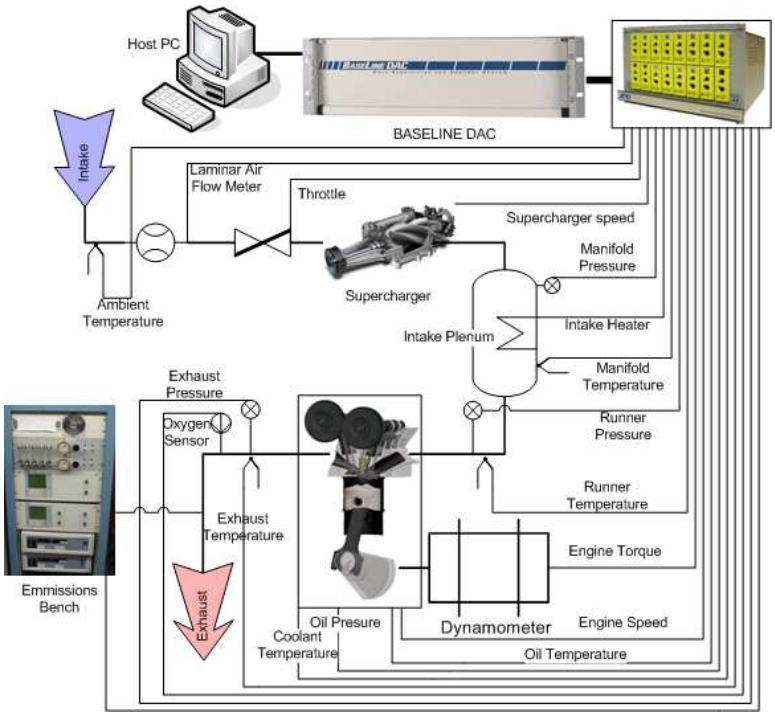

Figure 3.11: Schematic of the ADAPT control and data acquisition computer.

3.1.8.2 CAS System

The A&D Baseline CAS is a hardware and software system designed for real-time analysis and data acquisition of internal combustion engines [A&D Technologies, 2001]. It is responsible for recording the in-cylinder pressure transducer as well as the knock sensor of the engine. The schematic of this system can be seen in Figure 3.12. The sampling of these two signals is event based, with the computer set to sample every tenth of a crank angle degree. The system also performs common calculations on the recorded pressure and knock traces; such as IMEP and CA50 for the pressure trace and knock intensity for the knock trace. These calculations are done online. The system is configured so that an analog output voltage is proportional to certain metrics computed. This allows feedback using CA50 as a measured output which is updated at the gas exchange TDC every engine cycle. There is a two combustion event sampling delay in the output of metrics such as CA50, as shown in Appendix D.

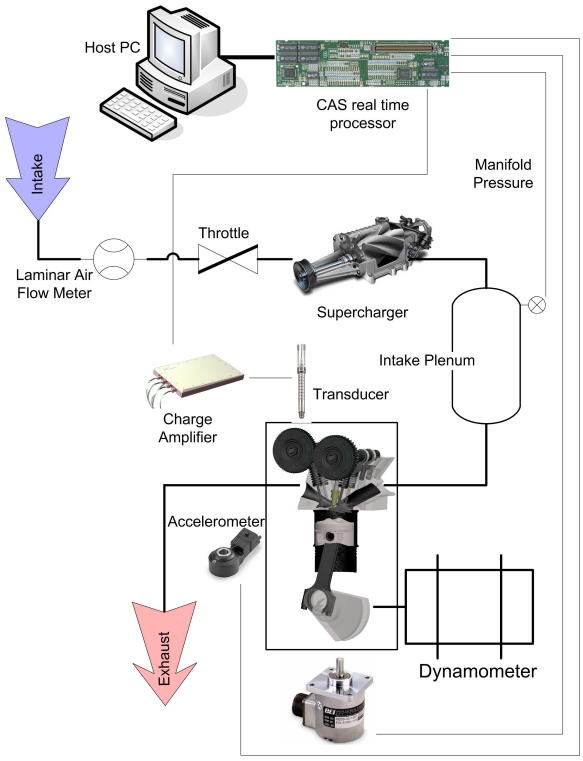

Figure 3.12: Schematic of the Combustion Analysis System (CAS).

3.1.8.3 dSPACE System

The dSPACE MicroAutoBox is a rapid prototyping system designed to be used as a automotive ECU [dSPACE GmbH, 2004]. Control of the fuel injectors, spark timing, and camshaft phasing is done with a dSPACE MicroAutobox 1401. The programming of this system is done using MatLab Simulink's Real Time Workshop using S-Functions supplied by dSPACE. The Simulink program is listed in the Appendix D. The inputs and outputs of this system require conditioning to be used on the engine and this is done with a set of custom electronics based on designs by Hitachi [Borg, 2003]. A schematic of this system can be seen in Figure 3.13. A 36-1 toothed wheel determines the crank angle for this system, while one pulse per camshaft rotation determines the location on the engine cycle. Simulink blocks provided by dSPACE are used to program fuel injection and spark outputs. The solenoid actuators for

the phasers use PWM inputs. Figure 3.14 shows the input and outputs signals for this system. From this figure the timing of the controller calculation is seen. The CA50 timing is calculated by the CAS which then updates the analog output that corresponds to the CA50 value. This update is done at the gas exchange TDC, which is almost a full 1050 °after CA50 has occurred. The interrupt to start the injector calculations, and run the event the based controller, occurs 75 °before TDC. This allows enough time for the computation for the fuel pulse widths which happen at TDC on the closed intake valves. The calculated fuel changes will not be seen until the next engine cycle, and the dSPACE system will not measure these changes until two cycles after that.

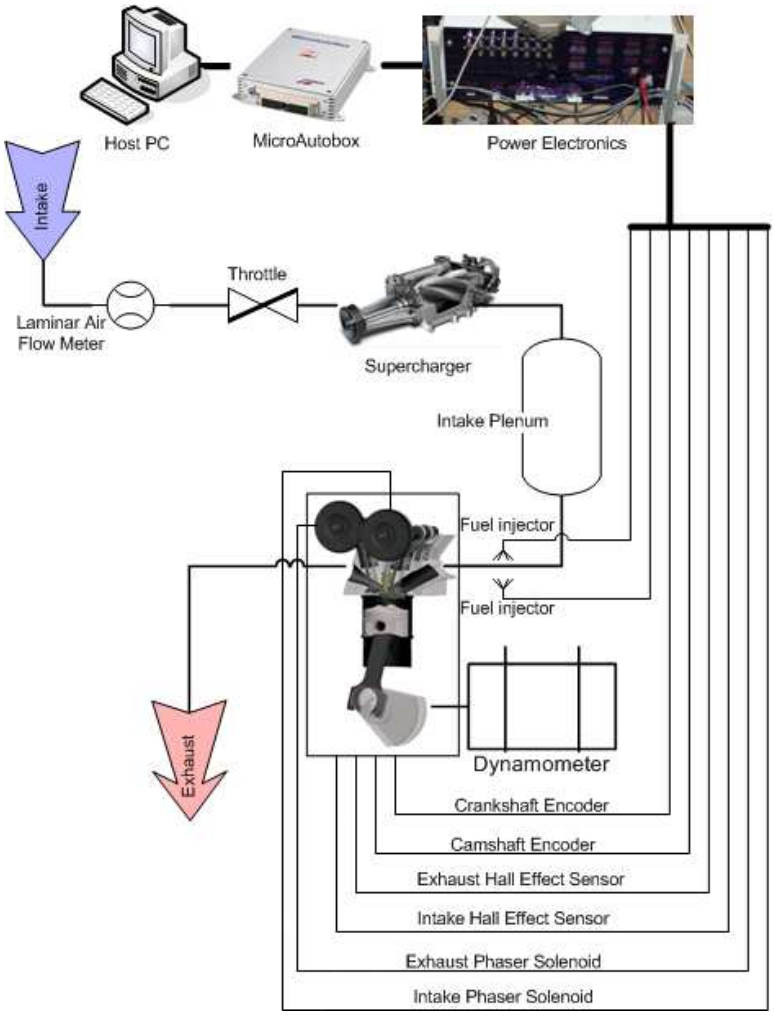

Figure 3.13: Schematic of the MicroAutobox ECU and the various elements under its control.

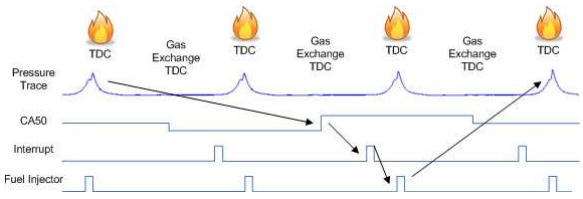

Figure 3.14: Timing of the MicroAutobox ECU signals.

3.2 Testing Conditions

Three different types of test are performed for this study; steady state tests, transient tests, and system identification tests. Steady state tests are performed at constant engine conditions so that accurate values of specific emissions, and efficiencies can be computed. The transient tests are performed to design the controllers, as well as test the controller performance. System identification tests are performed to identify control models for the HCCI engine, and are taken for a much longer duration (3000 cycles) than both the transient and steady state tests. The sample rates for these three different tests are the same, except that for the long system identification tests the pressure trace is not logged. The CAS computer has a finite amount of memory available, so it is limited to logging 500 consecutive pressure traces. For long duration tests only IMEP, knock intensity, and CA50 values are logged (without 0.1 °cylinder pressure) for up to 30000 cycles.

For all the test conditions the coolant and oil temperature are held to constant values. This is done with a feedback control loop that is outlined in the Appendix D. The coolant is set to 70 °C and the oil is set to 60 °C. During all tests the temperatures do not deviate by more than 2 °C from their set mean value. For this study experiments are done at five different engine conditions, these points are listed in Table 3.3. These different conditions are chosen to find the effects of both engine speed and intake conditions on the control methods of combustion timing. The first three points in this table are conditions at 1000RPM with different intake conditions. Each of these three points has a different intake pressure and temperature. These two parameters have been shown to have a large effect on HCCI combustion timing, especially the intake temperature [Shahbakhti et al., 2007b], so they are expected to have an effect on the combustion timing controller implemented in this study. On this engine the intake pressure and intake temperature are coupled together with the

efficiency of the supercharger, since no intercooler is used, so when the pressure is increased the temperature is increased. The controller for this study are set up to update every engine cycle, so when the engine speed is changed the sample rate of the controller is changed. The last two points in Table 3.3 are at a higher engine speed so the effect of changing the sample rate of the controller, and plant, can be found. During these tests all other engine conditions are held constant, such as coolant temperature, oil temperature and pressure, exhaust valve timing, and fuel pressure.

Table 3.3: Description of five different engine conditions that all the subsequent tests are preformed. (test points $BP1$, $BP2$, $BP3$, $BP4$, and $BP5$)

Description	Engine Speed [RPM]	Injected Energy [kj]	fuel octane number	IVC Timing [°aTDC]	Manifold Press. [kPa]	Manifold Temp. [°C]
BasePoint1	1000	0.718	10	230	110	60
BasePoint2	1000	0.718	28	230	125	80
BasePoint3	1000	0.718	43	230	140	105
BasePoint4	1250	0.718	11	230	125	80
BasePoint5	1500	0.718	6	230	125	80

3.2.1 Stable Engine Operation

The range of stable HCCI load is between the misfire limit on the low load side and the knock limit on the high load side. These two phenomenons are quantified so that only stable data is used in the analysis.

3.2.1.1 Misfire Limit

Engine misfire, where the fuel air mixture fails to ignite, is encountered at the low load operating region of HCCI. Before and during misfire high cyclic variation of engine burn parameter are encountered [Heywood, 1988]. One cycle will produce a strong reaction while the next cycle may not ignite at all. This results in very *rough* running

engine (large torque variations) which is undesirable. CO and uHC emissions will be higher when an engine is running at a misfire condition [Heywood, 1988]. To quantify the amount of misfire, or the smoothness of the engine operation, the coefficient of variation of IMEP is used:

$$COV_{IMEP} = \frac{standard \;\; deviation(IMEP)}{mean(IMEP)} \tag{3.1}$$

This value is calculated for 300 engine cycles. The typical range for this metric is around 2% for most of the data in this study. When operated at high value of COV_{IEMP} the HCCI combustion usually becomes more and more unstable, an effect that is explained by the cylinder walls cooling down. A heuristically chosen limit of 5% was found to work quite well as the limit of misfire. At values above this the HCCI will almost always degrade into a stall, or zero power output condition.

3.2.1.2 Knock Limit

The knock limit is seen on the high load side of the HCCI operating range. Knock is the phenomenon where large pressure oscillations exist inside the combustion chambers. These oscillations generally lead to Noise, Vibration, and Harshness (NVH) as well as efficiency loss and increased emissions [Heywood, 1988]. The frequency of these oscillations can be predicated using the solution to the 3-D wave equation for a right cylinder [Draper, 1933]. Multiple modes of vibration exist for this shape, and the frequency of these modes is a function of the bore of the cylinder and the speed of sound in the chamber:

$$f_{m,n} = \frac{C \cdot \rho_{m,n}}{\pi \cdot B} \tag{3.2}$$

Where:

$f_{m,n}$ = specific vibration frequency mode $[Hz]$

C = local speed of sound $[\frac{m}{s}]$

$\rho_{m,n}$ = vibration mode factor [-]

B = cylinder bore $[m]$

m = circumferential mode number [-]

n = radial mode number [-]

Where the speed of sound in the combustion chamber is:

$$C = \sqrt{kRT} \tag{3.3}$$

Where:

C = local speed of sound $[\frac{m}{s}]$

k = ratio of specific heats [-]

T = temperature $[K]$

R = ideal gas constant $[\frac{kJ}{kgK}]$

For most HCCI knocking conditions the main mode of vibration is at the first mode [Eng, 2002]. The methods to quantify the knock intensity of HCCI are usually based on the knowledge of the frequency of oscillation which of this engine is approximately $5440Hz$. A widely used method for quantifying knock seen on the pressure trace is done by computing the Root Mean Squared (RMS) value of a bandpass filtered pressure trace [Borg et al., 2006]. The pressure trace is first filtered to allow only the information between $5kHz$ and $20kHz$. The RMS value of the this signal is then computed:

$$P_{rms} = \left(\frac{1}{N}[\hat{p} \cdot \hat{p}]\right)^{1/2} \tag{3.4}$$

For this study the P_{RMS} is used as then measure of knock in the combustion chamber. The unacceptable knock limit is based on a correlation with knock heard

by the engine operator, which is shown in Figure 3.15. The unacceptable value of engine knock is chosen to be $P_{rms} = 0.06bar$, at values above this aggressive knock is audible.

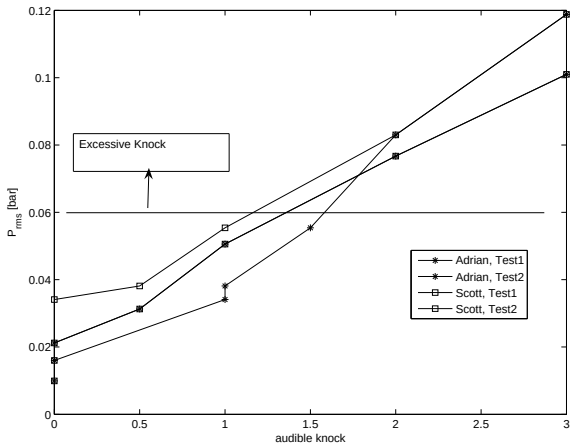

Figure 3.15: Operator audible knock correlated to cylinder pressure P_{rms}. (test points KI)

3.3 Measurement Calibrations

The experimental setup used in the is study is fully calibrated for all the data taken, and the detailed calibration records can be seen in Appendix D.

The equipment requiring the most frequent calibration is the emissions sample system. While the measurements of the systems are rarely off by large magnitudes the drift of the measurement is apparent from one calibration to the next.

A new piezo-electric pressure transducer is used in this study, and the entire system is tested with a dead weight calibrator before any data is taken. It is found that the sensor has the same sensitivity as the factory calibrator had determined.

All other transducers such as diaphragm pressure sensors, load cells, and wide-band O_2 sensors are calibrated multiple times.

The method that CAS computes CA50 is based on the heat release analysis. The system allows an input so that the user dictate when the heat release analysis begins

on the pressure trace, so for spark ignition engines this would be around the timing of the spark event. For HCCI there is no knowledge of the start of combustion previous to the heat release analysis, so the analysis is programmed to begin at 20 ° before TDC every time. An off line analysis of the pressure trace is done to see the effect this parameter has on the computed CA50 and is shown in Figure 3.16. Here it is seen that as the start of combustion is varied the difference on CA50 is less than 0.5 ° confirming that a fixed start of combustion can be used. Once the CA50 value is computed by CAS it is converted to an analog signal, sent to the dSPACE MicroAutoBox, where it is reinterpreted as a CA50 timing value. The error between the two signals has a standard deviation of 0.034 ° validating the CA50 in dSPACE.

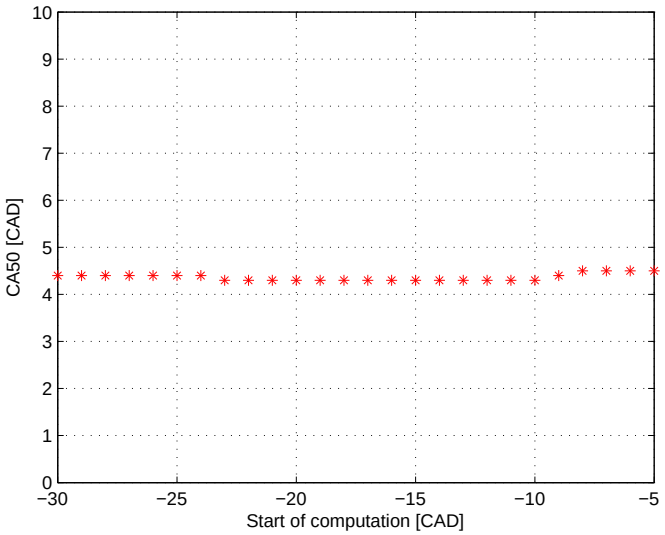

Figure 3.16: The effect of changing the start of calculation on the computed CA50 value.

Chapter 4

PI Control

The results of controlling combustion timing using the fuel octane and IVC timing with PI controllers is outlined in this chapter. Both transient results and tests over varying conditions are presented and discussed. A block diagram of the plant is shown in Figure 4.1.

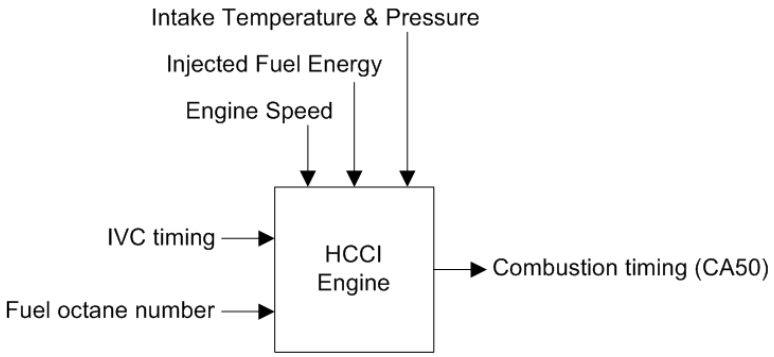

Figure 4.1: Schematic of HCCI engine and the input, outputs, and disturbances.

4.1 Combustion Timing Control Using IVC Timing

It has been shown by other researchers that the combustion timing of HCCI can be adequately controlled by modifying the Intake Valve Close (IVC) timing [Agrell et al., 2005b, Bengtsson et al., 2006a]. Adjustments in the IVC timing change the effective compression ratio of the engine, which effects the end of compression temperature.

Increasing the temperature advances the combustion timing of HCCI. This section outlines the results of implementing a manually tuned PI controller for HCCI ignition timing using the IVC timing as the actuator. A block diagram of the control system is shown in Figure 4.2 which is single input single output since all variables including octane number are held constant.

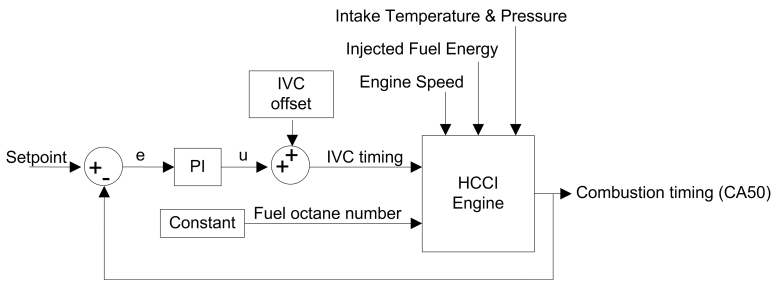

Figure 4.2: Schematic of the controller for CA50 using IVC timing.

4.1.1 Plant

Changing the IVC timing changes the effective compression ratio of the engine. The timing range for IVC in this study is between 202 and 242 ° aTDC. Changing IVC timing to a later value results in a lower effective compression ratio for timing after Bottom Dead Center (BDC). Had the timing range been before BDC of the engine, a later IVC timing would result in a higher effective compression ratio, but this is never used here. The effective compression ratio is calculated by taking the clearance volume and dividing it by the volume at the IVC point:

$$CR_{eff} = \frac{V_{tdc}}{V_{tdc} + V_{IVC}} \tag{4.1}$$

The effective compression ratio for the valve timing range in this study is shown in Figure 2.9. The steady state response of the HCCI combustion timing to changes in the IVC timing is plotted in Figure 4.3. IVC timing sweeps are performed at five different engine conditions and this figure shows the different trends found at the 5

different base points. The data from this plot is normalized by subtracting the mean values of the entire sweep from both IVC timing and CA50 which is shown in Figure 4.4. Linear fits are applied to the data and the R^2 value of linear best fits are in Table 4.1. Also shown in the table is the estimated slope from the linear fit. All the coefficients of determination found are above 0.9 and the slopes, or sensitivities, are similar in magnitude. No distinct trend is seen for the different slopes at the five different engine conditions.

It is apparent that the sensitivity of HCCI combustion timing to changes in the IVC timing does not change drastically between the 5 different engine conditions. For BasePoint2, BasePoint4 and BasePoint5 the only difference is the engine speed. From the figure it is seen that the sensitivity does not appear to change as the engine speed is increased to 1500RPM, from the initial value of 1000RPM. The sensitivity of the HCCI combustion timing to changes in the IVC timing appears to be independent of the engine speed and manifold temperature and pressure for the range studied here. The high R^2 values of the linear fit indicate that the nonlinearity between the IVC timing and CA50 is minimal.

The step response of the CA50 to IVC is seen in Figure 4.5. There is a two cycle delay between the change in measured IVC timing and the HCCI combustion timing.

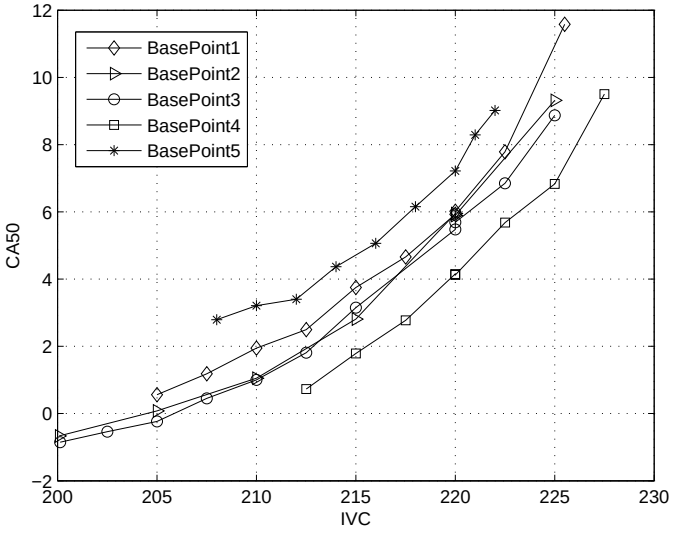

Figure 4.3: Steady state response of CA50 to changes in the IVC timing. (test points $BP1_{IVCss}$, $BP2_{IVCss}$, $BP3_{IVCss}$, $BP4_{IVCss}$, and $BP5_{IVCss}$)

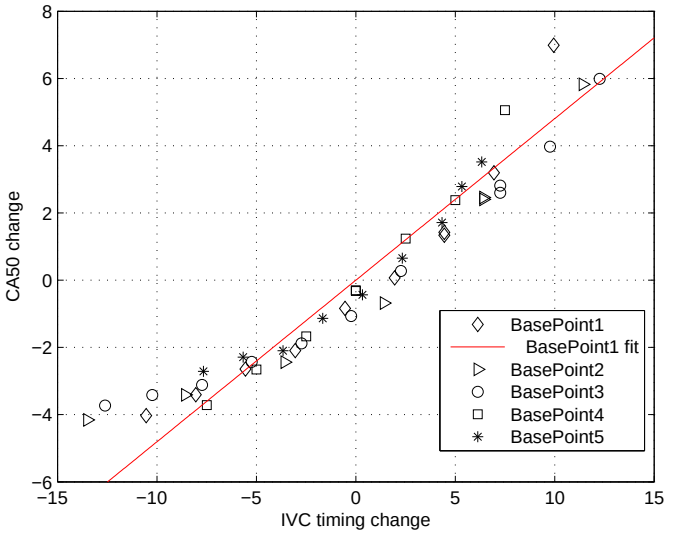

Figure 4.4: Normalized steady state response of CA50 to changes in the IVC timing. Linear best fit lines are applied to the data to quantify how linear the trends are. (test points $BP1_{IVCss}$, $BP2_{IVCss}$, $BP3_{IVCss}$, $BP4_{IVCss}$, and $BP5_{IVCss}$)

Table 4.1: Sensitivity and linearity of CA50 to IVC timing. (test points $BP1_{IVCss}$, $BP2_{IVCss}$, $BP3_{IVCss}$, $BP4_{IVCss}$, and $BP5_{IVCss}$)

Operating Point	sensitivity $\frac{^oCA50}{^oIVC}$	R^2
BasePoint1	0.48	0.91
BasePoint2	0.39	0.93
BasePoint3	0.39	0.95
BasePoint4	0.39	0.97
BasePoint5	0.45	0.95

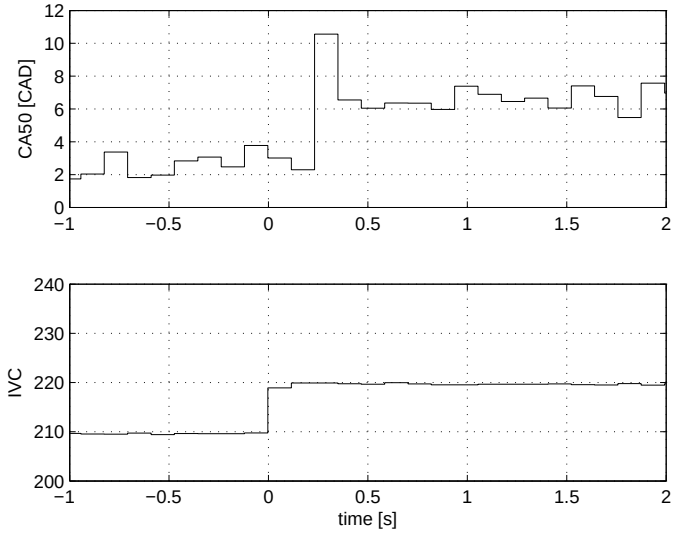

Figure 4.5: Step response of CA50 to a change in the IVC timing. (test point $BP1_{IVCstep}$)

4.1.2 Controller

The CA50 value is computed by the CAS computer using the heat release method, as discussed in Chapter 3. This value is output to the MicroAutobox via an analog signal at every engine cycle. The controller is event based, so it updates once every engine cycle. The Simulink model of the implemented controller can be seen in Figure 4.6. Making the controller event based fixes the controller sampling rate to the speed of the engine. Hence, as the engine speeds up the controller updates faster. This is done because most of the engine dynamics involved are assumed to be mainly event

based and not time based.

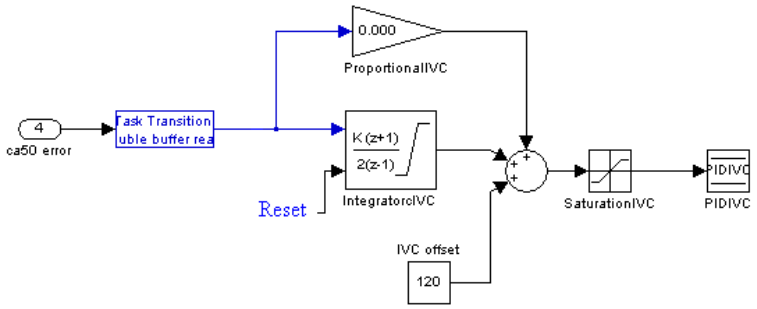

Figure 4.6: Simulink model of the controller for CA50 using IVC. The model is located in an interrupt based subsystem which is triggered once per engine cycle.

When Ziegler-Nichols tuning of the PI controller using open loop step response curve is implemented into a digital controller, the results are unstable controllers [Franklin et al., 1998]. Instead of using this method, for this study all the PI controller tuning is done manually. To tune the controller, the proportional term is first increased until near instability is observed. The gain is then decreased to half and the integral term is then increased until satisfactory performance is observed. The controller gains for the IVC timing controller can be seen in Table 4.2. The controller is implemented as:

$$u_k = k_p e_k + k_i \sum_{i=0}^{k} e_i + u_{FF_k} \tag{4.2}$$

Where e_k is the difference between the setpoint and actual CA50 value as shown in Figure 4.2. u_{FF_k} is a constant controller offset that is controller by the operator. A zero order hold converts the sampled output to a continuous signal. No derivative action of the controller is used due to signal noise.

Table 4.2: Controller gains for the controller using IVC timing on the engine.

Operating Point	k_P	k_i
BasePoint1	0.6	0.15
BasePoint2	0.6	0.2
BasePoint3	0.6	0.1
BasePoint4	0.8	0.2
BasePoint5	0.9	0.2

4.1.3 Results

The performance of the controller is tested for its regulatory control of combustion timing (CA50). Since essentially constant combustion timing for all conditions is needed, the tracking performance of the controller is not tested i.e. the controller is there to reject disturbances. Small variations of CA50 as a function of engine operating conditions are needed to maximize thermal efficiency [Lupul, 2008] but this optimization problem is not investigated here. For all tests in Table 4.2, with the exception of BasePoint5, the set point for CA50 is 5 °aTDC.

Large disturbances of HCCI combustion timing are changes in engine load and engine speed. Changes in other engine conditions, such as coolant temperature, manifold temperature, and manifold pressure will also modify HCCI combustion, but these parameters change relatively slowly compared to engine speed and load in normal engine operation. The controller performance when injected fuel energy is changed by 50J in subsequent engine cycles is seen in Figures 4.7, 4.8, 4.9, 4.10, and 4.11. For all these tests, the nominal amount of injected fuel is 718J, so a 50J step corresponds to a change of 7%. For these tests, the injected fuel energy is manually stepped 50J every 50 engine cycles. The steps are performed in both directions. It is seen that the controllers converge to the correct desired steady state CA50 value after an initial transient. In all cases the controller is required to make large adjustments to the IVC input of 5–10 °, illustrating that control is necessary for HCCI operation. The largest

adjustments are required for the controllers at BasePoint1 (BP1). Large combustion timing deviations are seen for the controller at BasePoint1, the CA50 becomes as late as 10 °aTDC. Late timing values cause increased values of CO and uHC emissions, so this is very undesirable. These late combustion events coincide with the step decrements in the injected fuel energy. It is thus advantageous to preemptively change the IVC timing as the fuel is decreased so that these late combustion timings can be avoided using feedforward control, see Chapter 5.

The purpose of increasing the injected fuel energy is to increase the power output of the engine. An increased power output is not seen in all cases. The knock intensity, injected fuel energy and indicated power for BasePoint1 and BasePoint3 are shown in Figures 4.12 and 4.13. For BasePoint1 the indicated engine power does not increase substantially as 50J more energy is injected, whereas it does for BasePoint3. The knock intensity for BasePoint3, Figure 4.13, does not increase as more fuel is injected, it remains below 6kPa for the entire test, which is noted earlier as the threshold for strong engine knock. This is not the case for BasePoint1, where the knock intensity is seen to increase above 10kPa when more fuel is injected. The knock phenomenon is causing a decrease in the efficiency resulting in a lower power output. As noted in [Heywood, 1988] increased knock intensity will increase the in-cylinder heat transfer, decreasing the amount of work produced during the cycle and lowering the efficiency.

The controller performance when the engine speed is stepped 100RPM is plotted in Figures 4.14, 4.15, 4.16, 4.17 and 4.18. As noted by [Zhao, 2007c] HCCI combustion timing is a time based process, so as the engine speed is increased and all other parameters are constant, the combustion timing will retard. To advance the HCCI combustion reaction some engine parameter must be used to compensate the decreased time available for the reactions to occur. As shown in this figure increasing the effective compression ratio through IVC timing will speed up the reactions, advancing the combustion timing to a more suitable value. No engine misfires are

present in any of these transients, yet there are a substantial number of early and late combustion events. It appears there is no difference between the disturbance rejection for BasePoint1, BasePoint2 and BasePoint3. BasePoint5 shows substantial cyclic variations in CA50 timing value. These variations are prominent in open loop operation without the controller. These variations reduce the effectiveness of the control of CA50 due to moderate to low controller gain values.

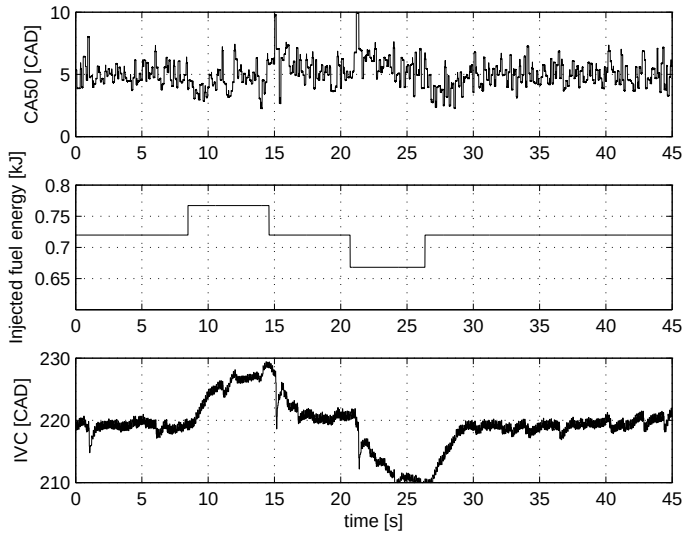

Figure 4.7: Fuel energy disturbance rejection performance IVC timing control. (test point $BP1_{IVCtransient1}$)

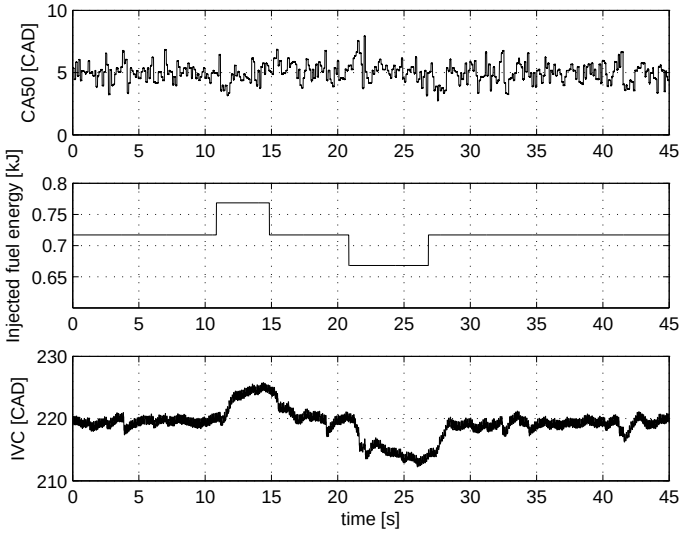

Figure 4.8: Fuel energy disturbance rejection performance IVC timing control. (test point $BP2_{IVCtransient1}$)

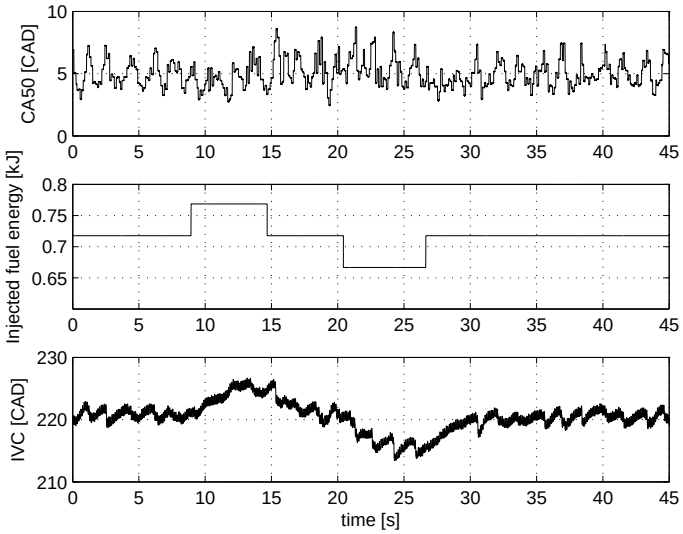

Figure 4.9: Fuel energy disturbance rejection performance IVC timing control. (test point $BP3_{IVCtransient1}$)

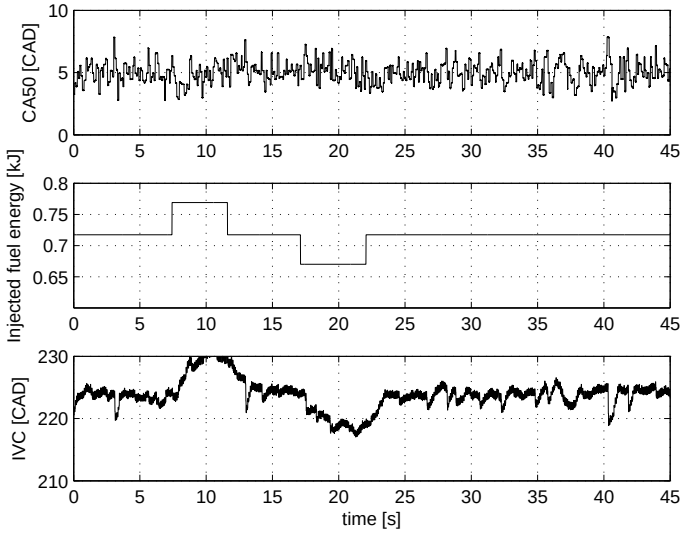

Figure 4.10: Fuel energy disturbance rejection performance IVC timing control. (test point $BP4_{IVCtransient1}$

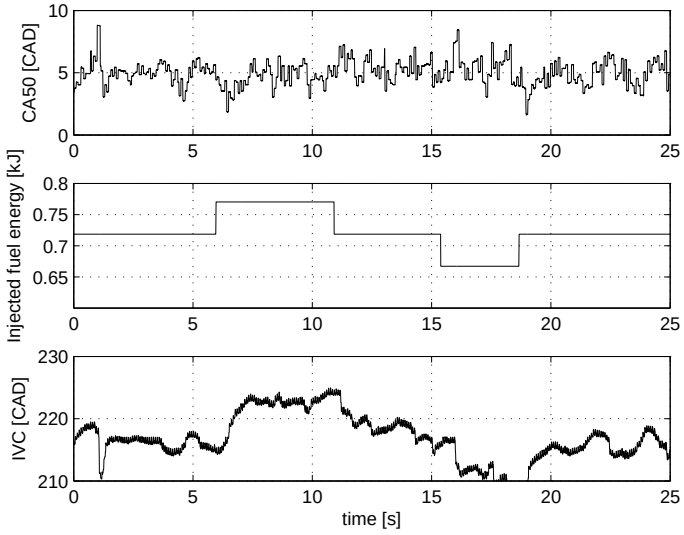

Figure 4.11: Fuel energy disturbance rejection performance IVC timing control. (test point $BP5_{IVCtransient1}$)

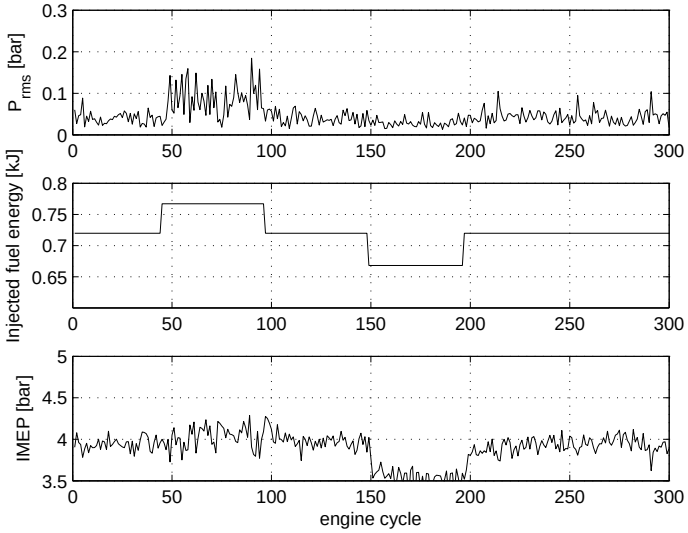

Figure 4.12: Knock intensity (P_{rms}) changes and indicated power (IMEP) for step changes in fuel energy at a constant combustion timing via IVC timing control. (test point $BP1_{IVCtransient1}$)

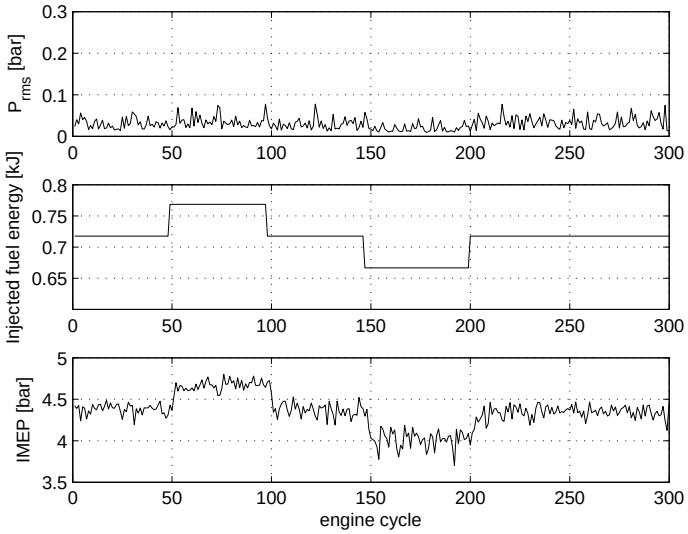

Figure 4.13: Knock intensity (P_{rms}) changes and indicated power (IMEP) for step changes in fuel energy at a constant combustion timing via IVC timing control. (test point $BP3_{IVCtransient1}$)

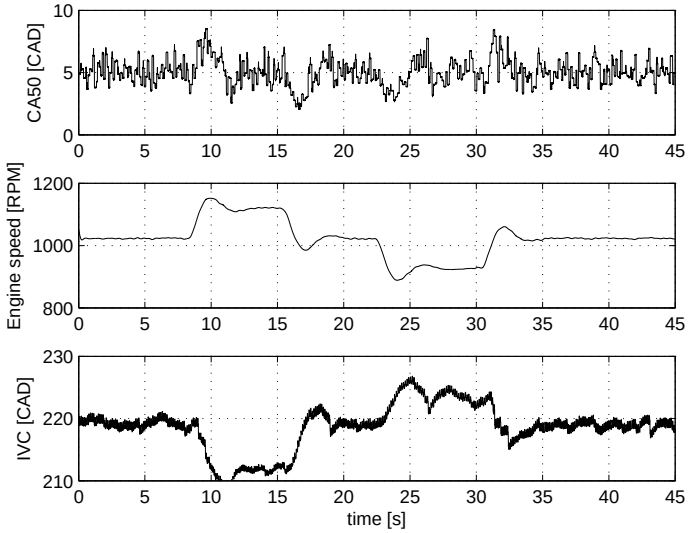

Figure 4.14: Engine speed disturbance rejection performance using IVC timing control. (test point $BP1_{IVCtransient2}$)

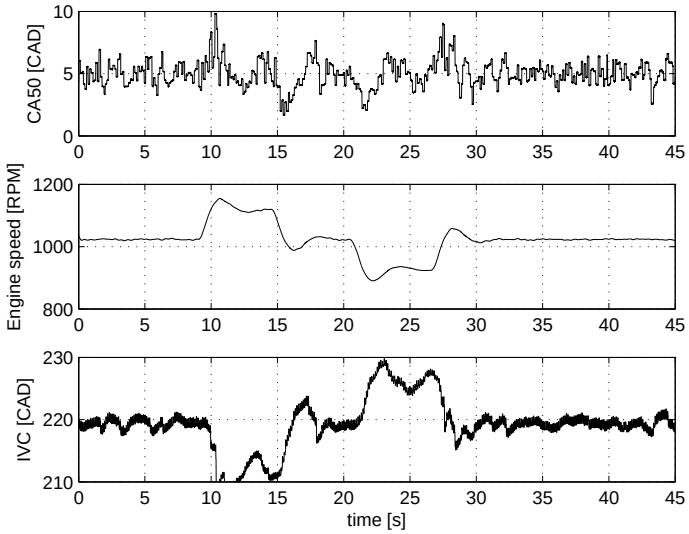

Figure 4.15: Engine speed disturbance rejection performance using IVC timing control. (test point $BP2_{IVCtransient2}$)

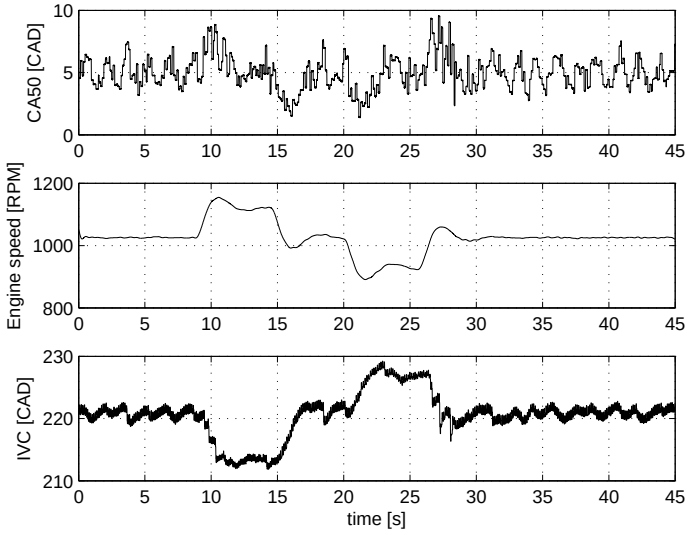

Figure 4.16: Engine speed disturbance rejection performance using IVC timing control. (test point $BP3_{IVCtransient2}$)

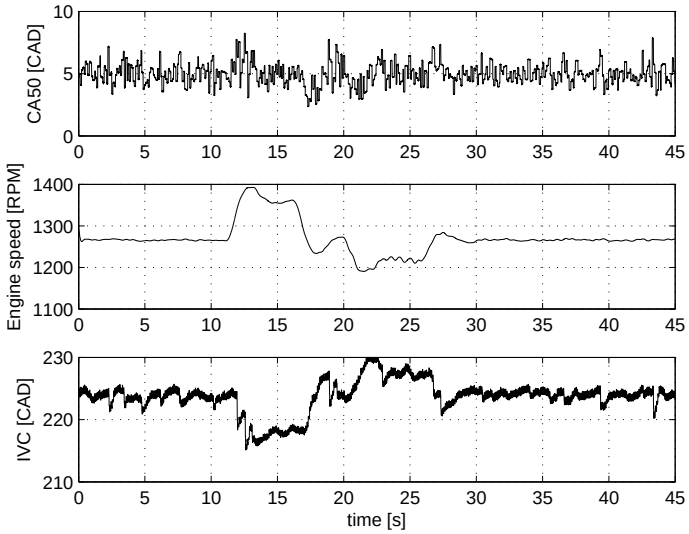

Figure 4.17: Engine speed disturbance rejection performance using IVC timing control. (test point $BP4_{IVCtransient2}$)

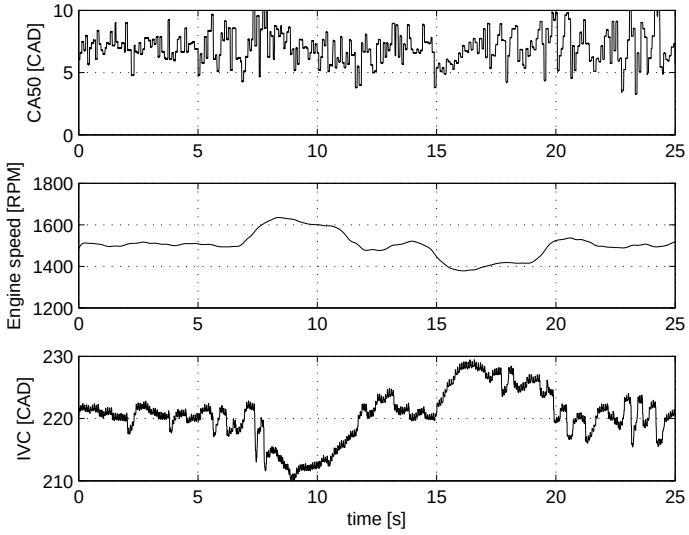

Figure 4.18: Engine speed disturbance rejection performance using IVC timing control. (test point $BP5_{IVCtransient2}$)

4.2 Combustion Timing Control Using Fuel Octane Changes

HCCI combustion timing is not only dependant on the temperature and pressure conditions of the compression stroke, but also on the chemistry of the fuel being used [Kalghatgi, 2007]. Different fuels will auto ignite differently, so by taking two fuels and blending then in real time the combustion timing can be changed, as shown by [Olsson et al., 2001]. The following section describes the performance of a PI controller that regulates HCCI combustion timing using the blending ratio of iso-Octane and n-Heptane. A block diagram of the control system is shown in Figure 4.19 which is single input single output control since all variables including IVC timing are held constant.

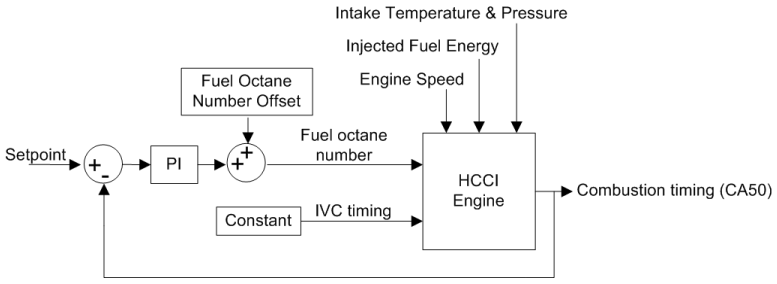

Figure 4.19: Schematic of the controller for CA50 using fuel octane.

4.2.1 Plant

Iso-Octane and n-Heptane are the two base fuels used to define the RON and MON octane ratings for practical fuels. The volumetric ratio of a iso-Octane and n-Heptane is termed the fuel octane, so a 70% iso-Octane mixture has a fuel octane of 70. A retardation in the combustion timing is expected with an increase in fuel octane.

The changes in HCCI combustion timing associated with changes in fuel octane are shown in Figure 4.20 for all 5 engine conditions. For these tests all other parameters are held constant including the injected fuel energy based on the lower heating value of the fuels. This figure shows that there is trend between the volumetric ratio of the injected fuels and the combustion timing for all engine conditions. The data from this figure is normalized in Figure 4.21 and linear best fits are applied. The data is normalized by removing the mean values of fuel octane and CA50 for each sweep. The R^2 values are shown in Table 4.3 along with the slope of each linear curve fit. In this table the calculated slopes, or sensitivities, of CA50 to the fuel octane appears very similar for all the different engine conditions, but the actual fuel octane to achieve a similar combustion timing is much different for each operating condition, as seen in Figure 4.20. The coefficient of determination of the linear fits are all above 0.9 indicating a strong correlation. This strong correlation of the linear fit indicates that there is a linear trend between the fuel octane and CA50 timing.

The open loop step response of the system is seen in Figure 4.22. A step in fuel

octane from fourteen to four is input into the engine and the advance in CA50 is measured. From this figure it can be seen that there is at least a three cycle time delay for the system, this includes the calculation time of the CAS computer, which is noted in Appendix D as two engine cycles, as well as the time delay of the fuel dynamics.

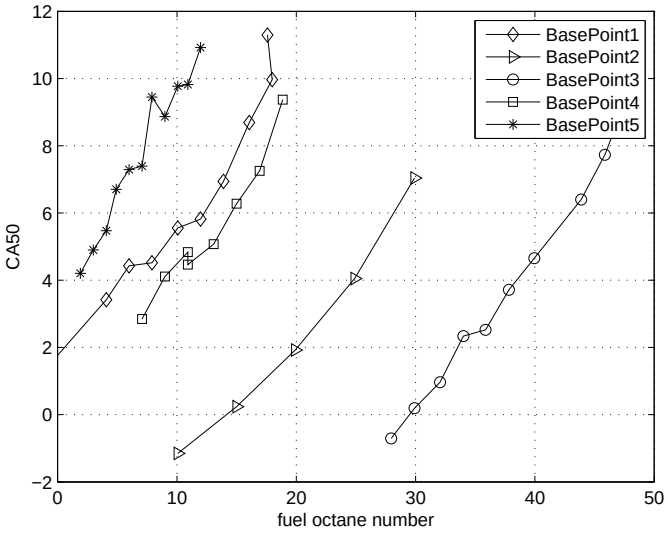

Figure 4.20: Steady state response of engine for different octanes. (test points $BP1_{ONss}$, $BP2_{ONss}$, $BP3_{ONss}$, $BP4_{ONss}$, and $BP5_{ONss}$)

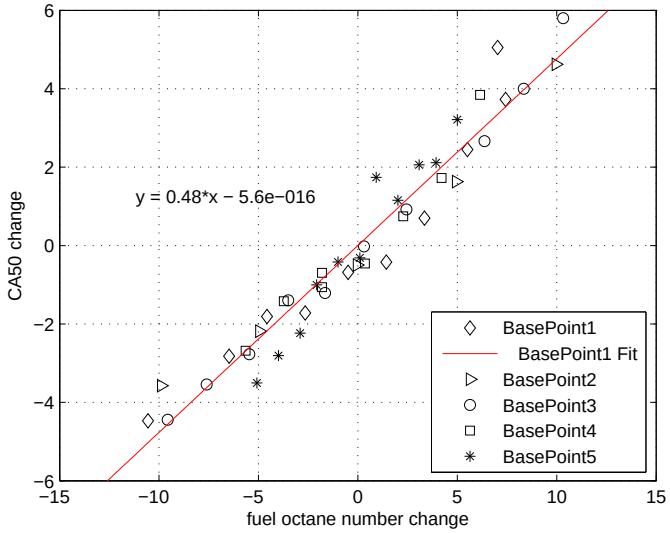

Figure 4.21: Normalized steady state response of engine for different octanes. Linear fits are applied to the data to quantify how linear each relationship, see Table 4.3. (test points $BP1_{ONss}$, $BP2_{ONss}$, $BP3_{ONss}$, $BP4_{ONss}$, and $BP5_{ONss}$)

Table 4.3: Sensitivity and linearity of CA50 to fuel octane number. (test points $BP1_{ONss}$, $BP2_{ONss}$, $BP3_{ONss}$, $BP4_{ONss}$, and $BP5_{ONss}$)

Operating Point	sensitivity $\frac{^oCA50}{ON}$	R^2
BasePoint1	0.48	0.93
BasePoint2	0.41	0.98
BasePoint3	0.49	0.99
BasePoint4	0.50	0.95
BasePoint5	0.66	0.96

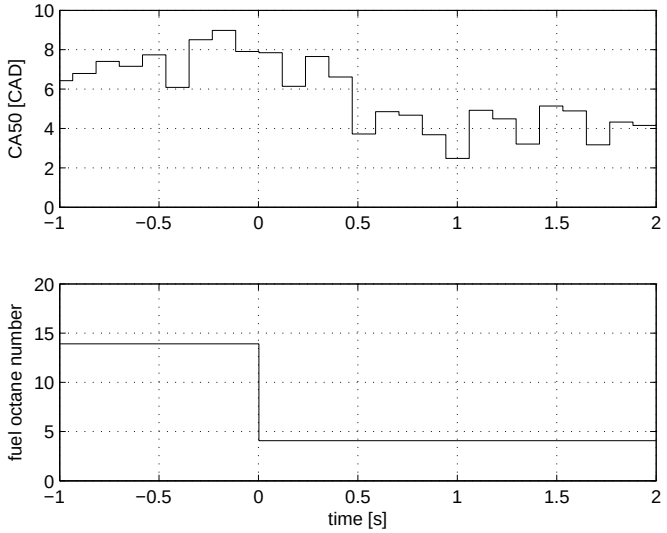

Figure 4.22: Engine timing response (CA50) to a step change (14-4) in the octane. (test point $BP1_{ONstep}$)

4.2.2 Controller

By utilizing the two fuel systems installed on the engine, as well as the injector pulse width to flow rate calibration, the fuel octane of the fuel going into the engine can be controlled. This is done while maintaining a constant injected fuel energy based on the density and lower heating values of the separate fuels, values seen in Table 4.2.2. The resolution of the fuel octane changes is 0.25. As these adjustments can be made on a cycle to cycle basis, the wall-wetting dynamics decrease the speed in which the engine can be influenced. These adjustments are done with the MicroAutobox. A schematic of the control structure can be seen in Figure 4.23. Similar to the IVC timing controller this controller is sample based, it updates once every engine cycle.

Table 4.4: Properties of iso-Octane and n-Heptane used in the controller. Values from [R.Turns, 2000].

fuel	Lower Heating Value $[\frac{kJ}{g}]$	density $[\frac{g}{m^3}]$
iso-Octane	44.8	703
n-Heptane	44.9	684

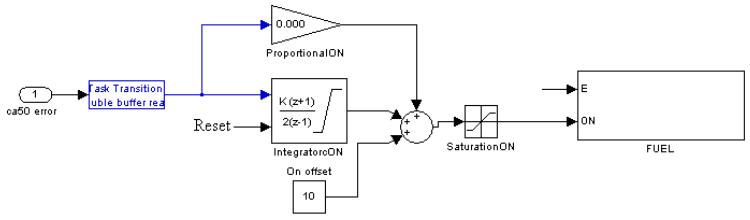

Figure 4.23: Simulink diagram of the implemented controller for CA50 using fuel octane.

The controller is tuned in a similar manner to the combustion timing controller using IVC timing. The tuning values can be seen in Table 4.5. The controller has the form as Equation 4.2.

Table 4.5: Implemented controller gains for the controller using fuel octane.

Operating Point	k_P	k_i
BasePoint1	0.27	0.1
BasePoint2	1.5	0.3
BasePoint3	1.5	0.2
BasePoint4	1.6	0.3
BasePoint5	1	0.3

4.2.3 Results

The controller is tested for its ability to reject disturbances of both load and engine speed. The controller's ability to compensate for a 50J change in injected fuel energy is shown in Figures 4.24, 4.25, 4.26, 4.27 and 4.28 for the 5 different engine conditions. In all cases the controller is able to compensate for the change in engine load. In Figure

4.24 the controller saturates at 0 fuel octane number, so a larger decrease in fuel energy would result in steady state error. Integrator anti-windup is not implemented. For Figures 4.24, 4.25, 4.26, and 4.28 there is a substantial transient error in the combustion timing, in some cases it retards as late as 10 °aTDC. This late combustion timing causes undesirable emissions as discussed earlier.

The knock intensity, injected fuel energy and indicated power for BasePoint1 and BasePoint3 are shown in Figure 4.29 and 4.30. It is seen that as the injected fuel energy is increased for BasePoint1 the knock intensity substantially increases. The indicated power does not increase with this extra fuel energy, indicating a lower thermal efficiency. The lower efficiency results from the same mechanism noted earlier; as the knock intensity increases the in-cylinder heat transfer increases which results in a lower thermal efficiency. The situation is different for BasePoint3, for the added energy the knock intensity maintains a lower level throughout the test, and there is a substantial increase in indicated power when extra fuel is added.

The controller performance when the engine speed is stepped 100RPM is plotted in Figures 4.31, 4.32, 4.33, 4.34 and 4.35. For these tests the speed set point is manually stepped every 50 engine cycles, and the effect of the dynamometer controller is apparent in the figures. The engine dynamometer has a PID controller to track the desired speed. The largest errors for all five engine conditions are seen in Figure 4.31. These errors appear to decrease for BasePoint2, and BasePoint3 as a result of the increased manifold temperatures and pressures at these conditions. Controller saturation can also be seen in Figures 4.31 and 4.35.

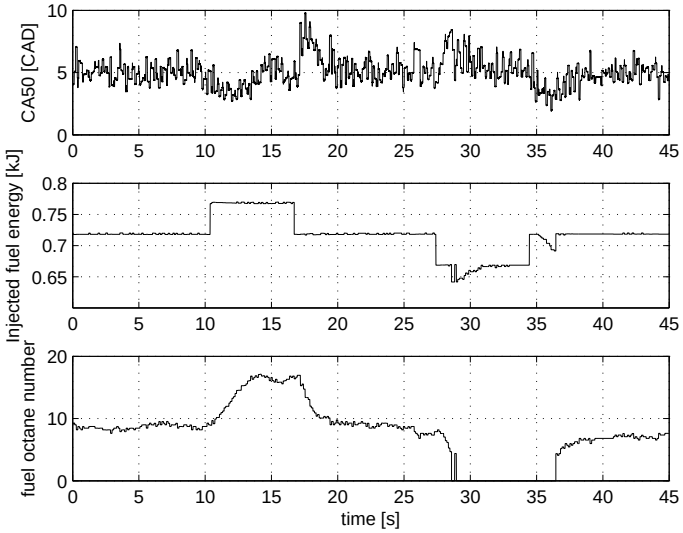

Figure 4.24: Fuel energy disturbance rejection performance using fuel octane control (test point $BP1_{ONtransient1}$)

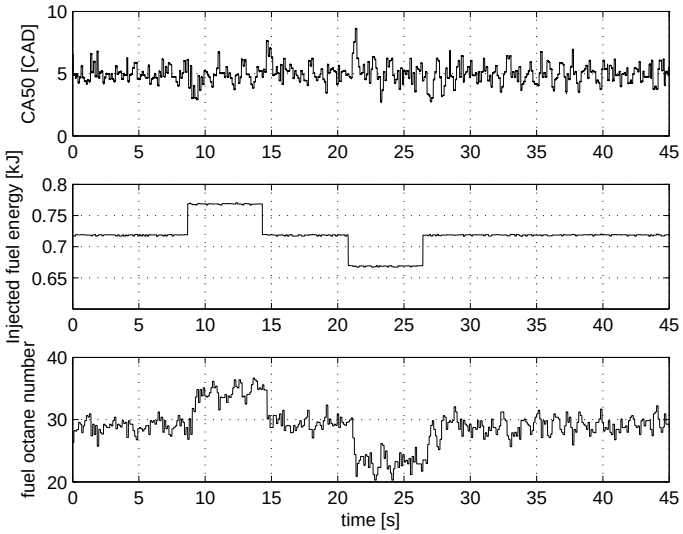

Figure 4.25: Fuel energy disturbance rejection performance using fuel octane control (test point $BP2_{ONtransient1}$)

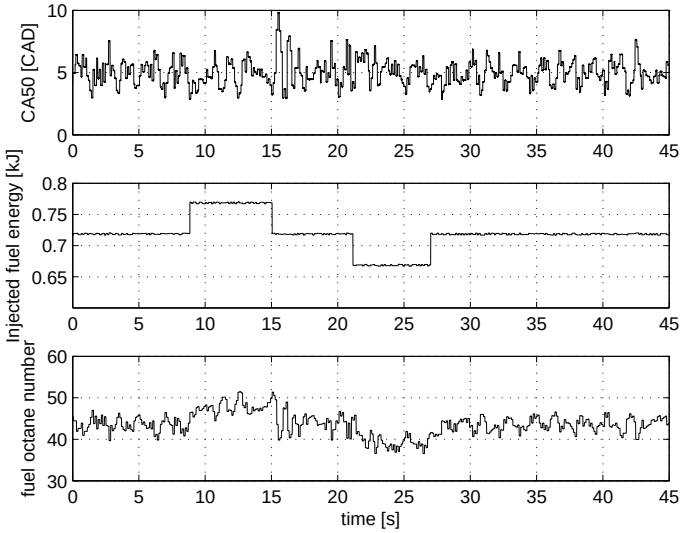

Figure 4.26: Fuel energy disturbance rejection performance using fuel octane control (test point $BP3_{ONtransient1}$)

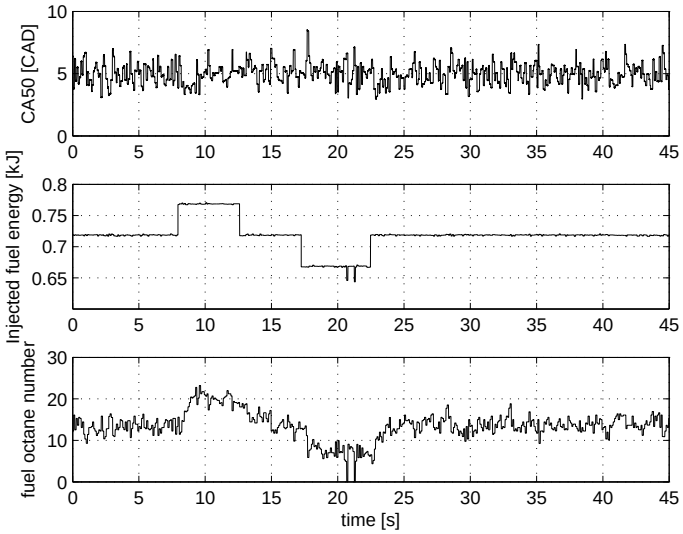

Figure 4.27: Fuel energy disturbance rejection performance using fuel octane control (test point $BP4_{ONtransient1}$)

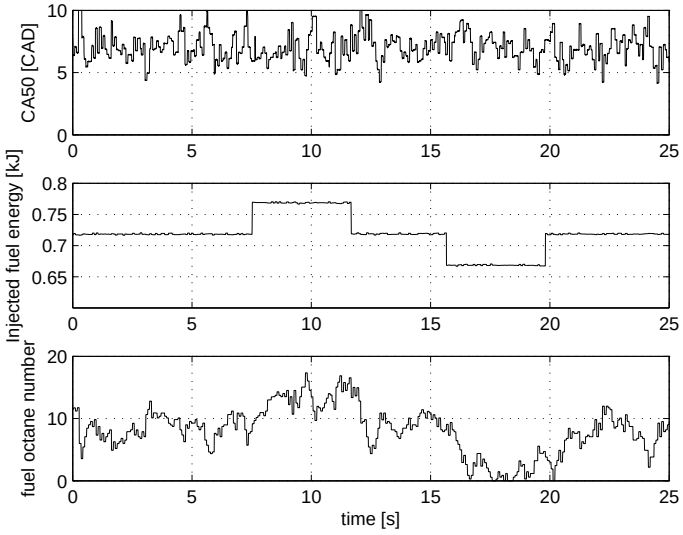

Figure 4.28: Fuel energy disturbance rejection performance using fuel octane control (test point $BP5_{ONtransient1}$)

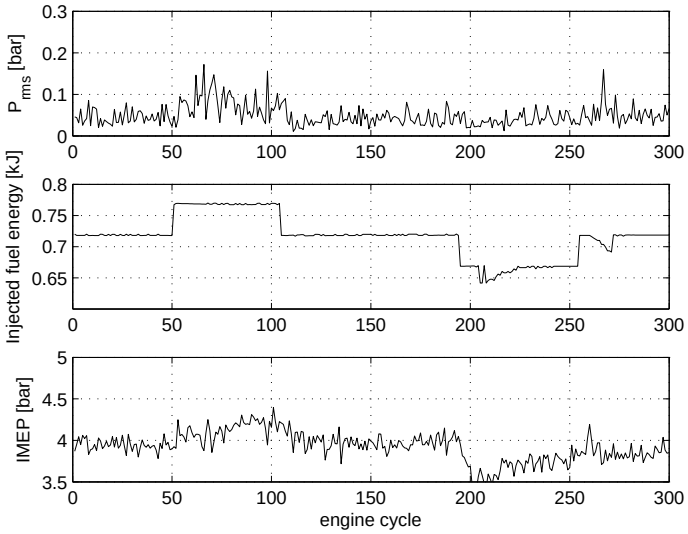

Figure 4.29: Knock intensity (P_{rms}) changes and indicated power (IMEP) for step changes in fuel energy at a constant combustion timing via fuel octane control. (test point $BP1_{ONtransient1}$)

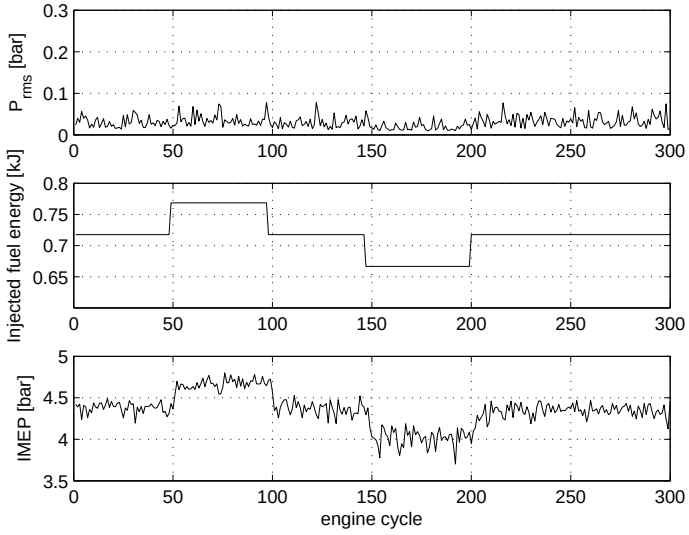

Figure 4.30: Knock intensity (P_{rms}) changes and indicated power (IMEP) for step changes in fuel energy at a constant combustion timing via fuel octane control. (test point $BP3_{ONtransient1}$)

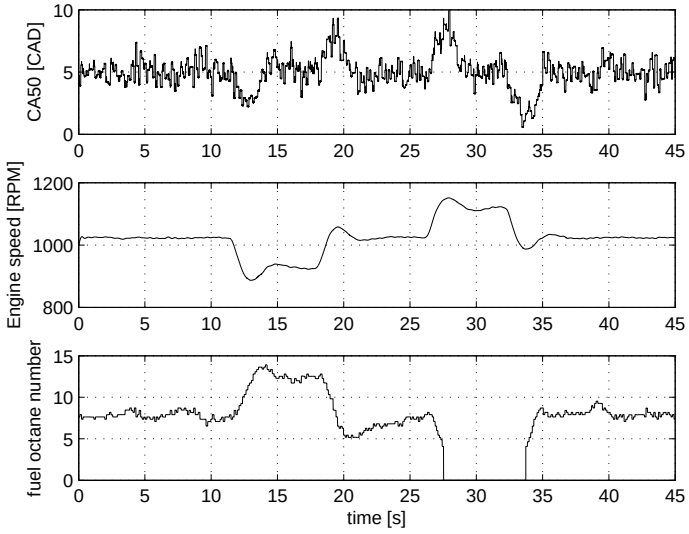

Figure 4.31: Engine speed disturbance rejection performance using fuel octane control. (test point $BP1_{ONtransient2}$)

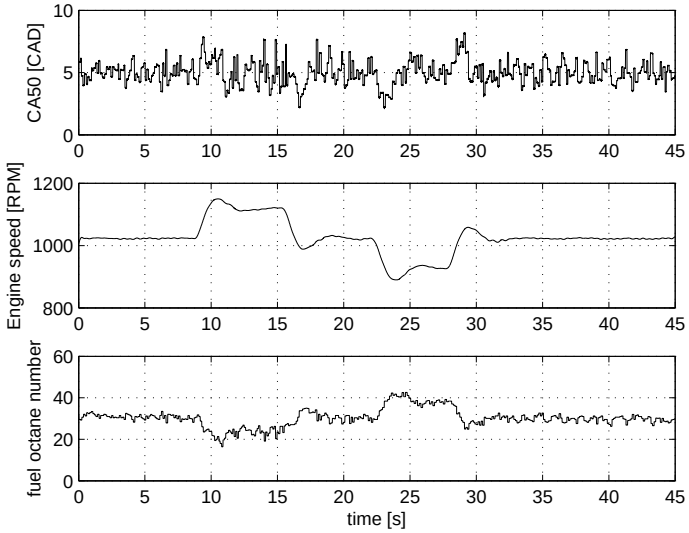

Figure 4.32: Engine speed disturbance rejection performance using fuel octane control. (test point $BP2_{ONtransient2}$)

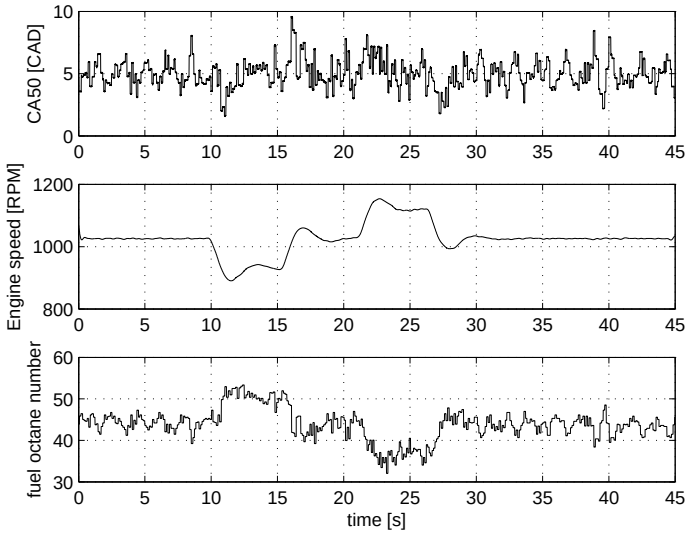

Figure 4.33: Engine speed disturbance rejection performance using fuel octane control. (test point $BP3_{ONtransient2}$)

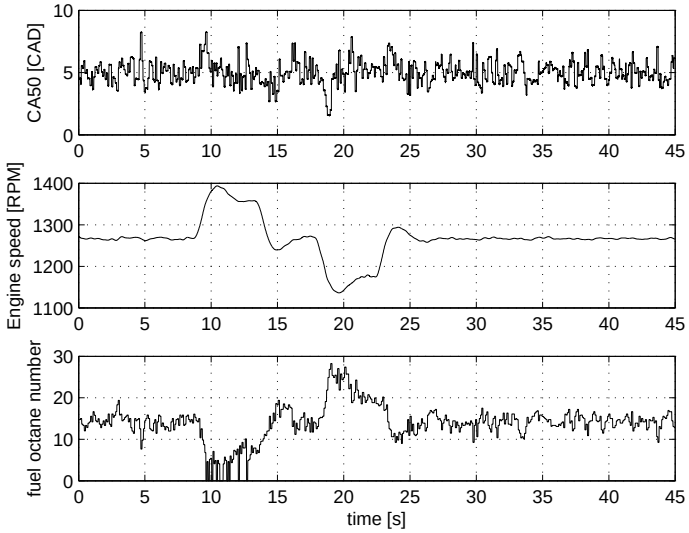

Figure 4.34: Engine speed disturbance rejection performance using fuel octane control. (test point $BP4_{ONtransient2}$)

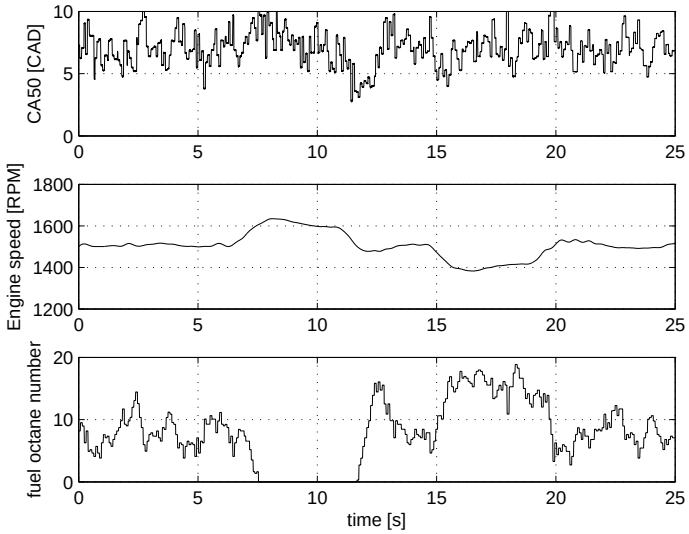

Figure 4.35: Engine speed disturbance rejection performance using fuel octane control. (test point $BP5_{ONtransient2}$)

4.3 PI Control Discussion

The implementation of the two different HCCI combustion timing controllers at the five different engine conditions required manually tuning the proportional and integral values of the controller. A summary of the gains can be seen in Table 4.7. The resulting tuning values at the different engine conditions are found to be very similar. The controller using IVC timing as the input has gain values that are nearly identical. This indicates that the dynamics between the IVC timing and the HCCI combustion timing are not drastically changing between the test conditions used in this study. With the exception of BasePoint1, the gains for the controller using the fuel octane number are also very similar, indicating similar dynamics between the engine conditions. The results of the steady state sensitivity tests, Figure 4.3 and 4.20, also show that the sensitivities between the different actuators and the HCCI combustion timing do not drastically change between the different engine conditions. This is further verified when linear fits are applied to these steady state tests. The estimated sensitivities are all very similar, and all the fits have a strong correlation.

It is observed that for the engine conditions with lower dilution, BasePoint1, the knock phenomenon decreases engine efficiency when extra fuel is added (Figures 4.12 and 4.29). The problem is seen for both controllers. For the engine conditions with high dilution, the knock phenomenon was not observed and an appropriate amount of engine load was produced with added fuel, Figures 4.13 and 4.30. It is important that adequate levels of dilution are maintained to avoid the onset of engine knock, as it leads to lower engine efficiency as well as engine damage. If it is impossible for the dilution to be increased, the engine should be switched from HCCI mode to spark ignition as the knock limit has been reached. The implementation of cylinder knock measurements could be used to constrain the combustion, as done by [Bengtsson et al., 2006c] in which a maximum pressure rise rate condition was always met by the

controller.

For most of the disturbances initial error in the HCCI combustion timing is apparent before the controller is able to regulate the timing back to 5 °aTDC. While some error is unavoidable it is important to mitigate this error so that engine misfire, as well as short term knock is avoided. Both of the situations lead to lower efficiency as well as higher pollutant emissions. This error can be decreased by increasing the controller gains but this also increases the oscillation of the response. It is seen that there is a delay, denoted θ, in the system which poses a fundamental limitation for the bandwidth of the controller, which will be limited to less than $1/\theta$ [Skogestad and Postlethwaite, 2005]. Some disturbances are difficult to measure. However, in this case measurements of some of the large disturbances are possible since these disturbances are engine inputs. A feedforward controller can possibly be used to compensate for measured disturbances before errors are present in the output.

The variance of the combustion timing is computed for the regulatory control tests. This is done so that the performance of the different controllers can be compared. The computed values can be seen in Table 4.6. The variance of the combustion timing is usually larger for the disturbances in engine speed than that of injected fuel energy, which is mainly a function of the chosen disturbance step size. The disturbances for engine speed is 100RPM while disturbance for injected fuel energy is 50J. For some test conditions, BasePoint3 and BasePoint4, the variance of CA50 is lower when fuel octane number is used to control the combustion timing. However for BasePoint1 and BasePoint5 the variance is lower when IVC timing is used to control CA50. It appears that both controllers have similar abilities in rejecting these system disturbances. In all cases in Table 4.6 the variance is higher when no compensation scheme is used - no control.

Table 4.6: Calculated variance of combustion timing (CA50) for the two regulatory combustion timing controllers for disturbances of injected fuel energy, E, and engine speed, ω.

Actuator	No Control		fuel octane		IVC timing	
Disturbance	E	ω	E	ω	E	ω
BasePoint1	3.18	7.47	1.54	2.07	1.37	1.32
BasePoint2	2.56	6.99	0.69	1.06	0.62	1.35
BasePoint3	2.81	6.01	1.12	1.39	1.35	2.07
BasePoint4	2.21	2.64	0.76	1.08	0.79	0.96
BasePoint5	4.40	4.18	1.32	2.04	1.02	1.82

Table 4.7: Summary of gains used with IVC timing control and fuel octane control. Average gains are also shown.

	fuel octane		IVC timing	
Operating Point	k_P	k_i	k_P	k_i
BasePoint1	0.27	0.1	0.6	0.15
BasePoint2	1.5	0.3	0.6	0.2
BasePoint3	1.5	0.2	0.6	0.1
BasePoint4	1.6	0.3	0.8	0.2
BasePoint5	1	0.3	0.9	0.2
Average	1.2	0.24	0.7	0.2

4.4 Controller Load Rejection Performance

In the previous section fuel octane and IVC timing are used to control the combustion timing. Five different base engine conditions are tested under load and RPM disturbances and PI controllers are tuned for each case. In this section the average gain values of the five different proportional integral controllers from the previous section are used to test the load range of each controller at the different engine operating conditions. The tuning values used are given in Table 4.8. At each of the five engine operating points described in Table 3.3 the injected fuel energy is varied while controlling the combustion timing using the averaged gain values. The injected fuel energy is changed from the misfire limit of combustion to the knock limit of com-

Table 4.8: Controller gains values used for all the injected fuel energy sweeps.

	Proportional Gain	Integral Gain
IVC Timing Controller	0.7	0.15
Fuel octane Controller	1.2	0.24

bustion. For each engine condition three injected fuel energy sweeps are performed; one with IVC timing controlling the combustion timing, one with fuel octane number controlling combustion timing, and one with no control on the combustion timing. A schematic of the controllers is seen in Figure 4.36. During the sweeps all the other engine parameters, such as intake temperature and pressure, are maintained. Data are recorded when the engine has reached a steady state, and during all these tests the exhaust emissions are sampled.

For all the tests in this section the timing set point for CA50 is 5 °aTDC. For accurate comparison of results a consistent value of the CA50 setpoint is needed.

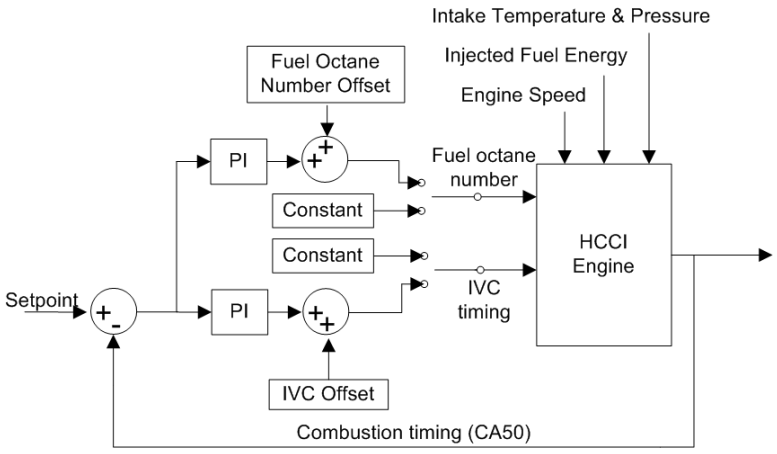

Figure 4.36: Schematic of the controller for load rejection performance

4.4.1 Engine Limits

For all the cases the engine load changed from the knock limit of the engine to the lean limit of the engine (as defined in Chapter 3). As noted in [Lupul, 2008], high load stable HCCI is limited by the knock limit. The increased heat release rate increases

the knock intensity, which eventually leads to lower efficiency and engine damage. Low load HCCI is limited by the increased cyclic variation and eventually misfire where no reaction occurs. All five engine conditions in Table 3.3 lie somewhere in between these two limits of combustion, and by increasing or decreasing the amount of injected fuel energy the limits of combustion can be realized, as shown in Figure 4.37.

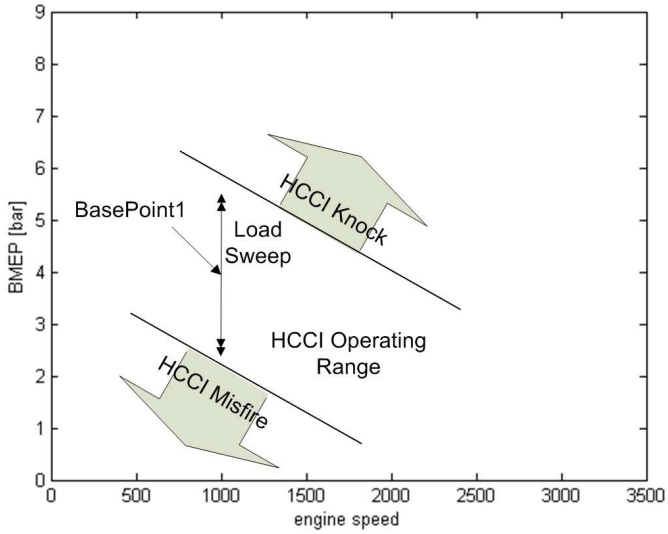

Figure 4.37: Load sweep schematic

4.4.2 Actuator Limits

Each actuator has physical limits of their range of operation. The IVC timing can only be modified a total of 40 °(200 °- 240 °aTDC) and the fuel octane can only be changed from 0 to 100. For all the engine conditions in Table 3.3 the IVC timing at its center point of 220 °aTDC, so the range of the actuator is optimized. However, for some of the conditions in this table, the fuel octane begins at relatively low values, the lowest being 6 for BasePoint5. The controller using fuel octane at this engine condition will quickly become saturated at 0 if the engine conditions change.

At the lower saturation limit of the fuel octane controller, the injector pulse width

for the iso-Octane injector is at or very near zero. Because of this, an error in the injected fuel quantity and fuel octane number can occur. This is (see the injector calibration plots) due to the non-linearity between the fuel injector pulse width and the injected amount of fuel at these very low pulse widths. This non-linearity is not compensated by the controller algorithm, so there is an error between the desired and actual amount of fuel going into the engine. This causes error in the efficiency calculation which is based on the estimated fuel going into the engine. These errors are only prominent at very low fuel octanes of less than 3.

4.4.3 Efficiency

The indicated efficiency is calculated using the measured IMEP and the estimated value of injected fuel energy. The amount of fuel energy is estimated using the calibration of the fuel injectors as discussed in Appendix D. IMEP is measured with the in-cylinder pressure transducer. The swept volume is a known geometric property of the engine. The indicated efficiency is calculated via:

$$\eta_i = \frac{IMEP * V_{swept}}{E_{injectedfuel}}$$

This efficiency does not take into account the work done by the supercharger or the intake air heater, but this will not affect the comparisons done here.

Figures 4.38, 4.39, 4.40, 4.41, and 4.42 show the indicted efficiency as it varies through the engine load sweep for the five different engine conditions. Shown in these plots is: open loop where no timing control is used (CA50 varies as the load is changed); fuel octane to control the combustion timing to 5 °aTDC; and IVC timing to control the combustion timing to 5 °aTDC.

By utilizing control methods to maintain the CA50 at 5 °aTDC the range of peak efficiency is widened in all cases. For the open loop control case, the load range is

much smaller than the range when using either IVC timing or fuel octane to control the combustion timing. The efficiency is not constant even though the CA50 timing is regulated with either IVC timing or the fuel octane. Also, at each engine condition the maximum efficiency achieved is different.

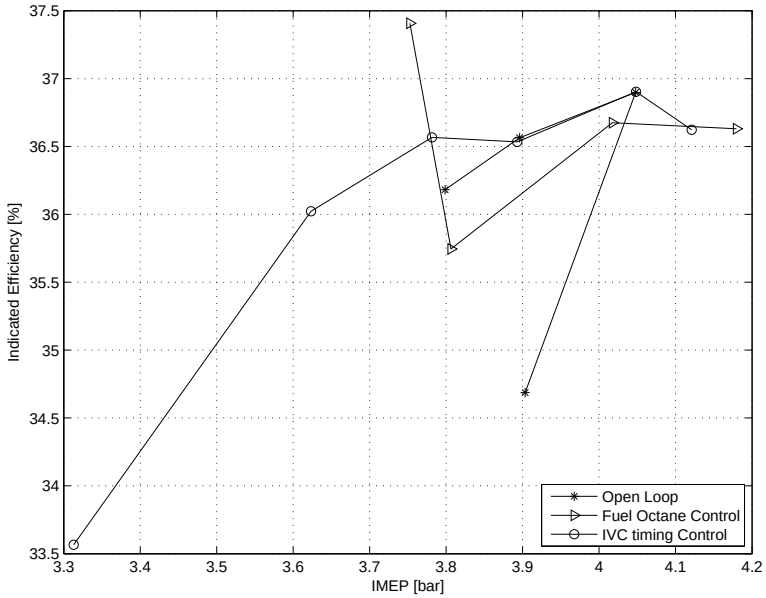

Figure 4.38: Indicated efficiency for the load range sweep for open loop, fuel octane control and IVC control for BasePoint1.(tests $BP1_{OLloadsweep}$, $BP1_{ONloadsweep}$ $BP1_{IVCloadsweep}$)

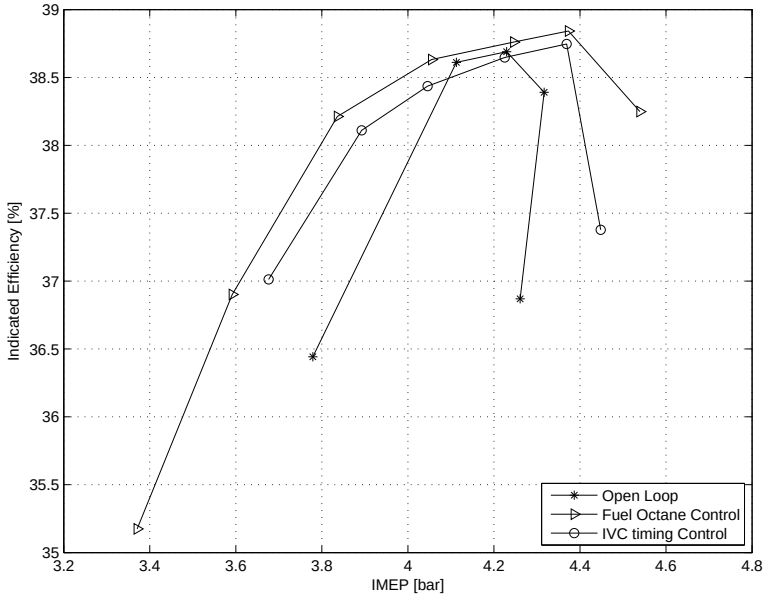

Figure 4.39: Indicated efficiency for the load range sweep for open loop, fuel octane control and IVC control for BasePoint2.(tests $BP2_{OLloadsweep}$, $BP2_{ONloadsweep}$ $BP2_{IVCloadsweep}$)

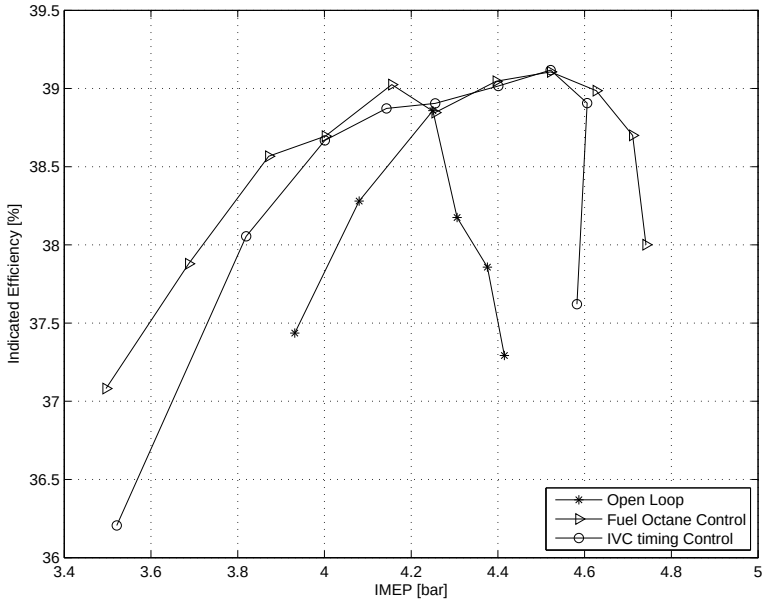

Figure 4.40: Indicated efficiency for the load range sweep for open loop, fuel octane control and IVC control for BasePoint3.(tests $BP3_{OLloadsweep}$, $BP3_{ONloadsweep}$ $BP3_{IVCloadsweep}$)

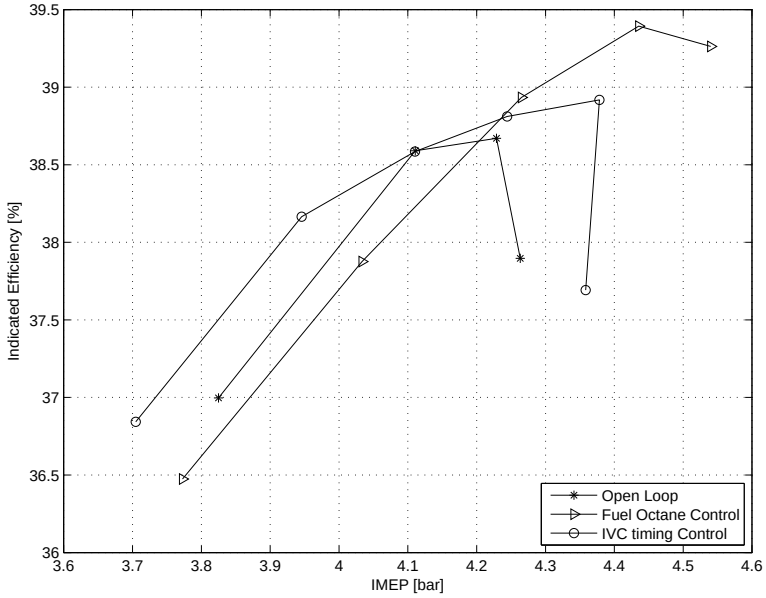

Figure 4.41: Indicated efficiency for the load range sweep for open loop, fuel octane control and IVC control for BasePoint4.(tests $BP4_{OLloadsweep}$, $BP4_{ONloadsweep}$ $BP4_{IVCloadsweep}$)

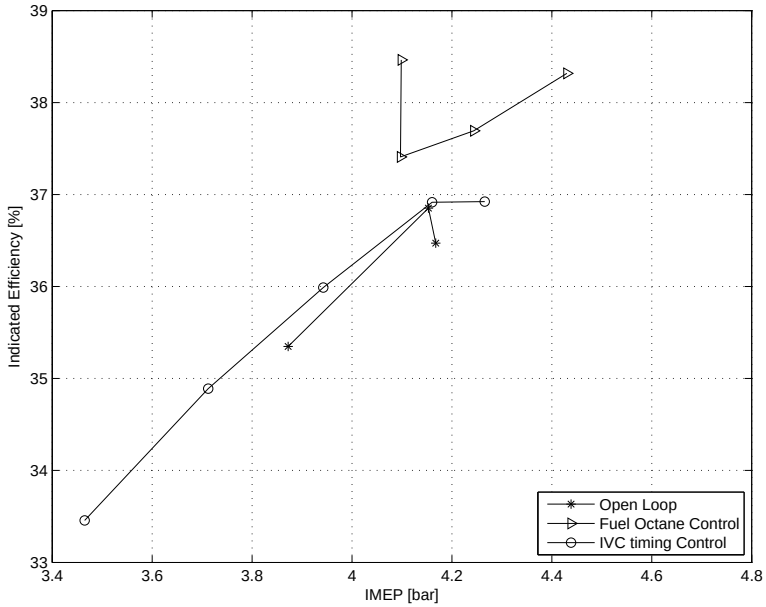

Figure 4.42: Indicated efficiency for the load range sweep for open loop, fuel octane control and IVC control for BasePoint5.(tests $BP5_{OLloadsweep}$, $BP5_{ONloadsweep}$ $BP5_{IVCloadsweep}$)

4.4.4 Discussion

At each engine condition there is a finite range of each actuator. It is initially expected that the range of actuation of the IVC timing controller would be limited by the phaser itself, since it can only adjust 40 °. However, this is not experimentally observed as none of the five test points required this actuator to saturate at it's mechanical limits for the disturbances tested.

When using IVC timing control the low load limits for all the injected fuel energy sweeps set by are cyclic variation. The coefficient of variation of the IMEP eventually reaches the limit of 5%. In order to regulate the combustion timing when the injected fuel energy is decreased, thereby retarding the CA50, the effective compression ratio is increased by the controller. This increases the end of compression temperature which advances combustion timing, counteracting the effect of decreased injected fuel energy. To increase the effective compression ratio the intake valve is closed earlier, which traps more intake air than a later value. This increases the dilution of the premixed charge, which is already increased by injecting less fuel. The cyclic variation of combustion has been noted to be strongly driven by the dilution of the premixed charge [Shahbakhti et al., 2007a].

Using IVC timing control, the high load side of the load sweep is limited by knock. At higher loads the effective compression ratio is decreased to counteract the advance in combustion caused by the added fuel. The decrease in effective compression ratio also decreases the amount of dilution because the intake valve is closed later in the cycle. This decreases the combustion duration which eventually leads to excessive engine knock.

Contrary to the IVC timing controller, the controller using fuel octane became saturated in many cases, Figures 4.38 and 4.42 in particular. When the controller became saturated at the lowest possible fuel octane of 0, non-linearities of the actuator

are also observed. Figures 4.39, 4.40 and 4.41 show the best example of the load range of this actuator. This controller could have been better utilized by choosing better base point conditions for each load sweep.

Other than saturation, the limits of this controller are similar to those of both the open loop load sweep and the load sweep using IVC timing to regulate combustion timing. High load is limited by excessive engine knock, and low load is limited by high cyclic variation of combustion. Figure 4.39 and 4.40 show that the range of the fuel octane controller to be much wider that the IVC timing controller. This can be attributed to that fact the IVC timing controller affects the dilution of the intake charge, having negative effects on combustion stability and knock. Whereas the fuel octane controller does not change the dilution, but merely the autoignition properties of the fuel. This effect can be seen in Figure 4.43 where the excess oxygen in the exhaust is plotted as a function of the injected fuel energy for the test points at BasePoint3. For the open loop and fuel octane control sweeps there is a similar trend between the load and the excess oxygen. For the IVC timing control sweep the slope of this trend is much steeper, which is due to the dilution effect of changing the intake valve timing.

For the cases where no combustion timing control is utilized, there is a peak of efficiency, which corresponds to a CA50 value around 5 °aTDC, and as the load is lowered or raised, the efficiency drops. The efficiency as a function of the CA50 timing for the open loop case is shown in Figure 4.44 for the 5 different engine conditions. Here the peak efficiency as a function of the combustion timing is seen. One reason for the decrease in efficiency is the change in the combustion timing. For SI engines, there exists a timing value that corresponds to a maximum efficiency, or Maximum Brake Torque (MBT) timing [Heywood, 1988]. This timing is a tradeoff between the compression work performed on the igniting charge and the expansion work performed on the piston. As the combustion event becomes earlier it takes

more power to drive the piston to TDC, but if the combustion event is too late the peak combustion pressure occurs too late in the cycle and expansion work is reduced. Although there is no MBT spark timing for HCCI these same principles apply to the HCCI combustion event; a best CA50 timing value exists that maximizes output torque.

By maintaining the combustion timing at a certain values, the engine efficiency should be maximized at different load values. It is seen in Figures 4.38, 4.39, 4.40, 4.41, and 4.42 that the efficiency is not constant when CA50 was maintained at 5 °. This indicates that the optimum timing value changes as the load changes, that the peak efficiency changes as the load changes, or that both things happen.

The brake specific unburned hydrocarbons, brake specific carbon monoxide emissions, load stability, and knock intensity are plotted as a function of engine load in Figure 4.45, 4.46, 4.47 and 4.48, for the test points at BasePoint3. The unburned hydrocarbons and carbon monoxide emissions continually increase as the engine load is decreased for the three different control methods. Both of these emissions represent losses in combustion efficiency [Heywood, 1988]. The carbon monoxide should be reacted with more oxygen to produce carbon dioxide, releasing more energy. Unreacted fuel also represents unutilized energy. The combustion efficiency will have an effect on the overall indicated efficiency of the engine, so these results indicate that peak indicated efficiency is changing during the load sweep, decreasing as the load is decreasing. Figure 4.48 shows the knock intensity through the load sweep. A similar trend is seen for each control method, that the knock intensity increases as the load is increased. As noted in [Heywood, 1988] increased engine knock will increase the heat transfer from the combustion gases to the cylinder walls. When more heat is transferred to the cylinder walls less energy goes to the piston in the form of work. Therefore, an increase in the knock intensity represents a decrease in the efficiency of the engine. Figure 4.48 indicates that the efficiency of the engine will decrease as

the load of the engine is increased because of the increase in the knock intensity.

The optimum timing for CA50 also changes during the load sweep. The burn duration for the load sweep at BasePoint3 is seen in Figure 4.49. For SI engines a different burn duration will move the optimum spark timing [Stone, 1999], and as this changes, the optimum timing of CA50 also changes. Because of cylinder heat transfer, and the optimum balance of compression and of expansion work, the optimum value of CA50 will change as the burn duration changes. In this figure the burn duration increases as the load is decreased for all three different load cases. The trends seen in Figures 4.38, 4.39, 4.40, 4.41, and 4.42 are caused by the change in maximum efficiency at each load, as well as the difference in optimum CA50 value at each engine load. An evaluation of the effect of CA50 on the engine efficiency could be used to further optimize the engine.

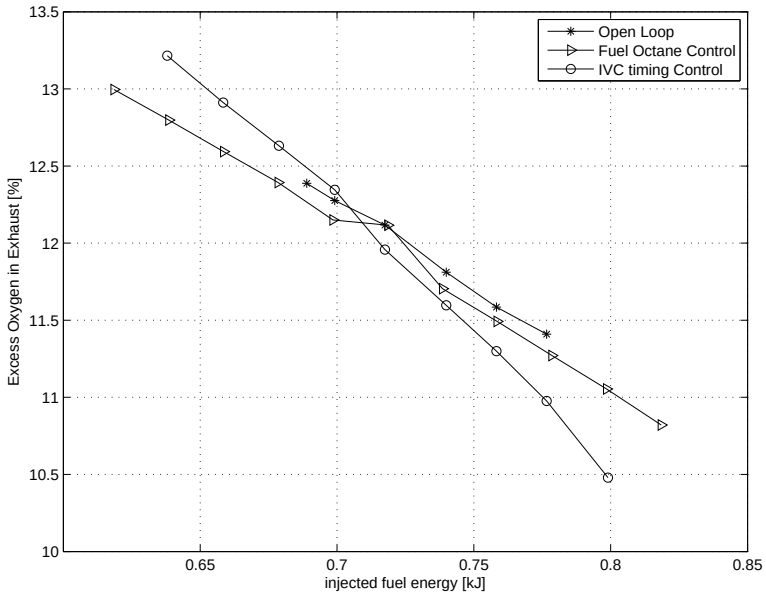

Figure 4.43: Exhaust oxygen percent for load range sweep for open loop, fuel octane control, and IVC control. (tests $BP3_{OLloadsweep}$, $BP3_{ONloadsweep}$ and $BP3_{IVCloadsweep}$)

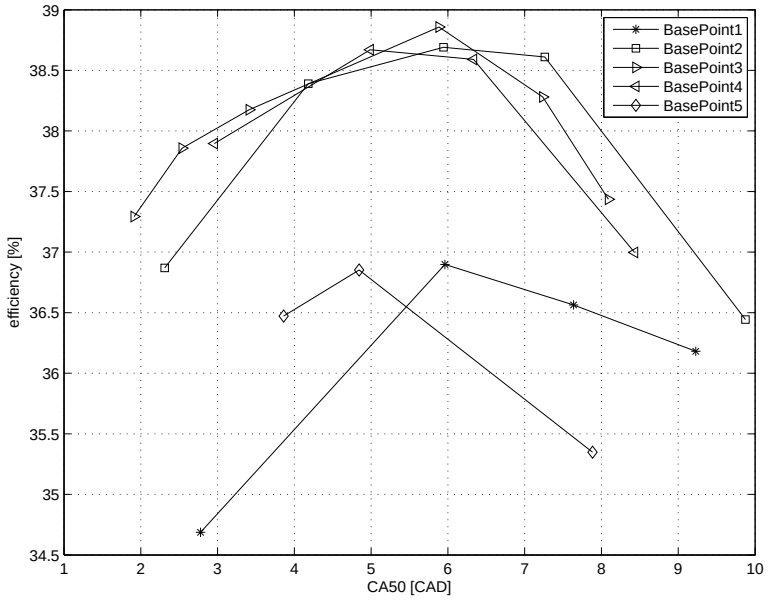

Figure 4.44: Engine efficiency as a function of CA50 for open loop. (tests $BP1_{OLloadsweep}$, $BP2_{OLloadsweep}$, $BP3_{OLloadsweep}$, $BP4_{OLloadsweep}$, and $BP5_{OLloadsweep}$)

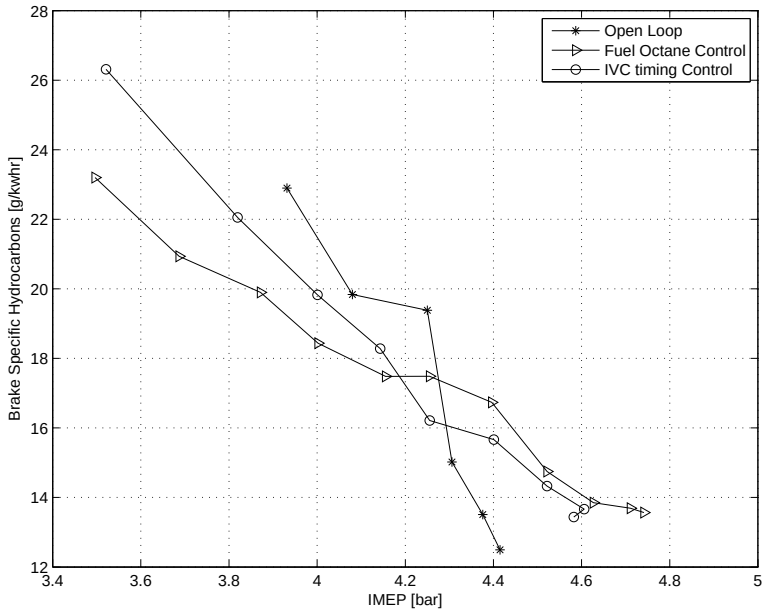

Figure 4.45: Specific hydrocarbon emissions for load range sweep for open loop, fuel octane control, and IVC control. (tests $BP3_{OLloadsweep}$, $BP3_{ONloadsweep}$ and $BP3_{IVCloadsweep}$)

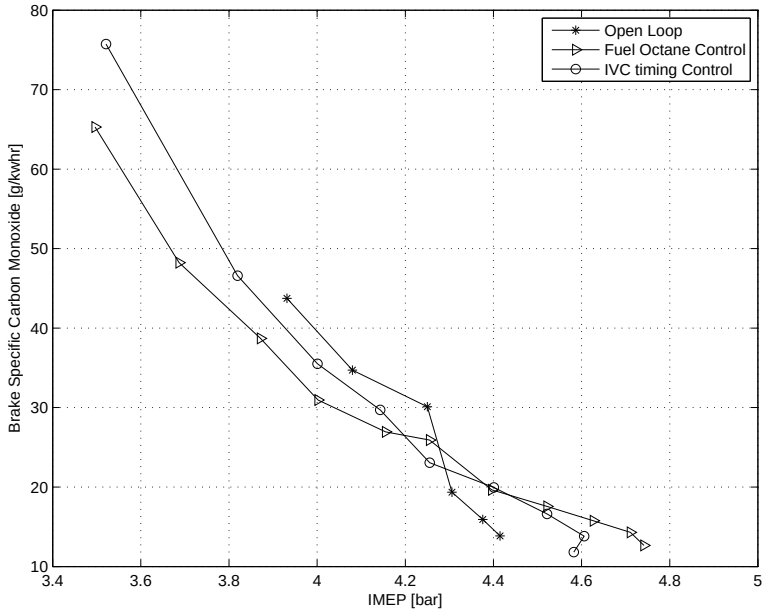

Figure 4.46: Calculated specific emissions, CO, for load range sweep for open loop, fuel octane control, and IVC control. (tests $BP3_{OLloadsweep}$, $BP3_{ONloadsweep}$ and $BP3_{IVCloadsweep}$)

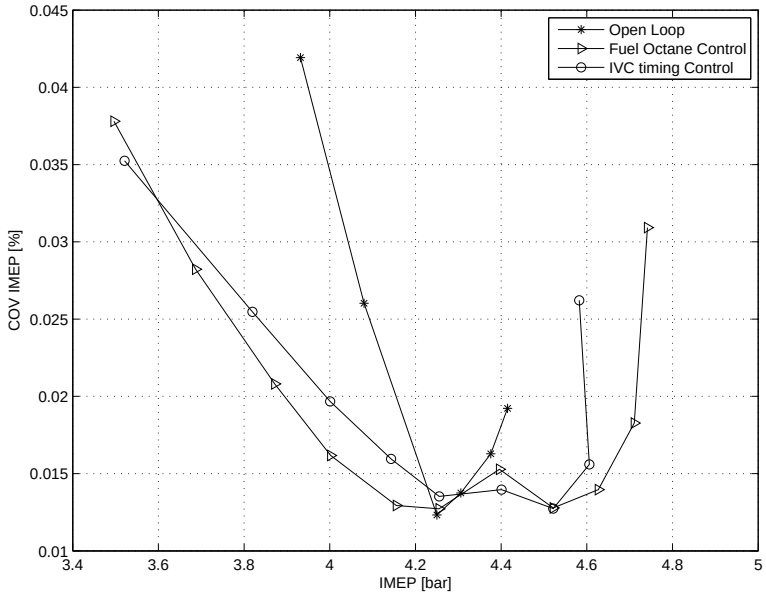

Figure 4.47: Coefficient of variation of engine load for load range sweep for open loop, fuel octane control, and IVC control. (tests $BP3_{OLloadsweep}$, $BP3_{ONloadsweep}$ and $BP3_{IVCloadsweep}$)

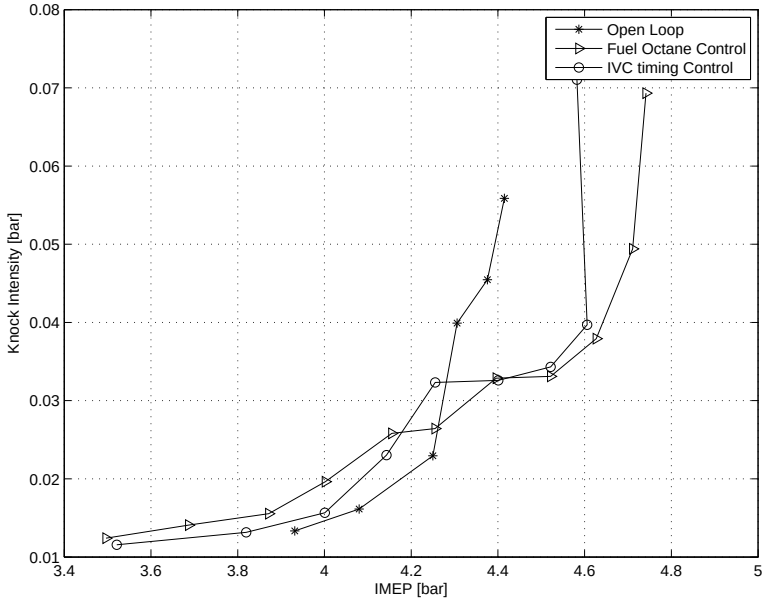

Figure 4.48: Knock intensity for load range sweep for open loop, fuel octane control, and IVC control. (tests $BP3_{OLloadsweep}$, $BP3_{ONloadsweep}$ and $BP3_{IVCloadsweep}$)

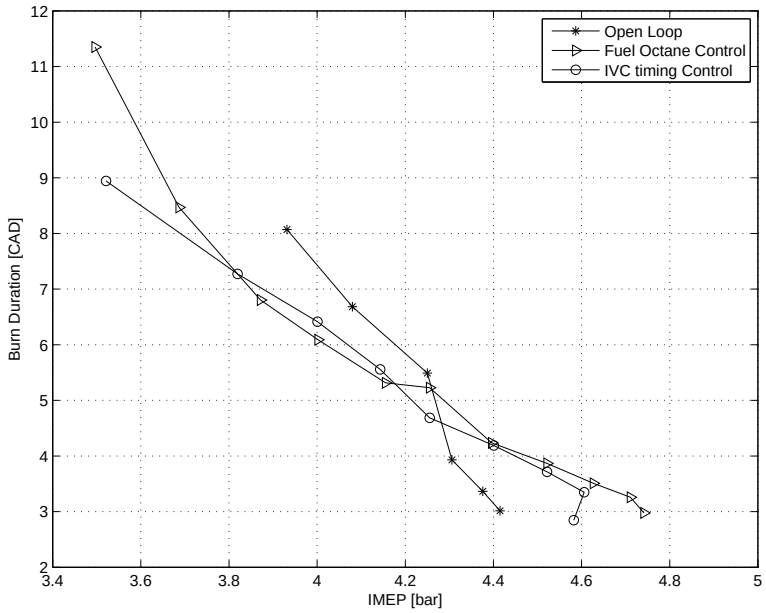

Figure 4.49: Burn duration for load range sweep for open loop, fuel octane control, and IVC control. (tests $BP3_{OLloadsweep}$, $BP3_{ONloadsweep}$ and $BP3_{IVCloadsweep}$)

4.5 Summary

Two PI controllers, one using IVC timing and the other using fuel octane, are implemented to regulate the CA50 timing. The controllers are manually tuned at five different engine conditions, and the gain values are found to be very similar at the different conditions. The controllers are tested for their disturbance rejection, and are found to perform much better than when no compensation is used. No substantial difference between the two controllers is observed.

Control of CA50 using IVC timing or fuel octane provides an almost 5 fold increase in load range variation compared to the case where no adjustment are done to compensate the change in timing resulting from the changes in injected fuel energy. Control is essential because of the very limited load range of efficient and stable open loop HCCI operation. At all five test conditions the open loop load range is only 0.4 bar while for BasePoint3 using fuel octane combustion timing control the range is over 0.9 bar IMEP.

Control using fuel octane provides the largest range of stable and efficient HCCI operation. There are conditions where the fuel octane controller became saturated, but this is primarily a function of the conditions chosen for the analysis, and similar results can be constructed for the IVC timing controller. By modulating the fuel octane only the chemical properties of the fuel are changed, whereas using IVC timing to change the effective compression ratio also affects the dilution of the mixture thereby lowering the range of operation.

For all the control methods and all test conditions, similar trends are observed in the brake specific emissions of CO and uHC's. The values are seen to continually increase as the load is decreased, or as the dilution is increased. The coefficient of variation of IMEP increases in a similar way, and eventually limits the low load range of HCCI. The knock intensity is seen to increase as the load is increased, or dilution

is decreased, and excessive knock limits the high load side at each test condition.

It is noted that a constant setpoint for the CA50 timing for all engine speeds and loads may not be the optimal solution. The desired CA50 may be a function of the engine load. Burn duration is seen to change as a function of the engine load, which has an effect on the optimal CA50 timing value.

Chapter 5

System Identification and Model Based Control

To design model based combustion timing controllers mathematical models of the engine are needed. This chapter outlines the identification of black-box models using system identification algorithms. In the first section, the experimental method used for system identification is outlined and details of the engine operating conditions are discussed. The algorithm for system identification, model structure choice, and model validation is presented in the next section. This section also includes residual analysis of the identified models. Then, the identified models at the five different engine operating conditions are listed and discussed. Finally, the models derived are used in a model based feedforward compensation.

5.1 System Identification

5.1.1 Experiment Design

It is important that the experiment is fully thought out so that the data generated are sufficiently informative [Ljung, 1987]. For this study system identification tests are performed at each engine of the conditions outlined in Table 3.3. This table shows three points at 1000RPM each with different intake temperature and pressures and two more points at engine speeds of 1250 and 1500RPM. The three tests at

1000RPM have different manifold pressures of 110kPa, 125kPa, and 140kPa. The two other tests have a manifold pressure of 125kPa. At each condition four different tests are performed: for each test either IVC timing, fuel octane, injected fuel energy or engine speed is excited. During the tests all other engine parameters are held constant.

A PRBS signal is used to excite the engine inputs (with the exception of engine speed). The bandwidth is specified so that the minimum signal width is 8 engine cycles. This number is chosen due to the limitations of the intake phaser. The mean values and ranges for each identification test are different for each test point. These values are changed so that the resulting changes in the CA50 value are inside the stable range of combustion (to avoid misfire or knock regions of combustion) but the steps are as large as possible to maximize the signal to noise ratio. The input levels for each test point are given in Table 5.1.

System identification techniques need a set of input-output data that is at least ten times longer than the slowest time constant and sampled at least twice as fast as the fastest time constant (preferably ten times) [Vernhaegen and Verdult, 2007]. The combustion timing information is event based, so the sample rate is fixed at the speed of the engine, but the length of the data can be specified. For these experiments very long data signals are taken so that the results are as reliable as possible, and so that the data set is always at least ten times longer than the slowest pertinent time constant. The tests are recorded for 3000 cycles.

Table 5.1: Engine conditions for system identification tests. SYSID1 corresponds to the conditions at BasePoint1.

Description	Engine Speed [RPM]	fuel octane	injected fuel energy [kJ]	IVC timing [CAD]	Manifold Press. [kPa]	Manifold Temp. [°C]
SYSID1	850 to 1050	0 to 17	0.65 to 0.76	205 to 222	110	60
SYSID2	850 to 1050	15 to 33	0.69 to 0.79	205 to 222	125	80
SYSID3	850 to 1050	25 to 45	0.66 to 0.78	200 to 222	140	100
SYSID4	1150 to 1350	0 to 20	0.68 to 0.75	214 to 225	125	80
SYSID5	1350 to 1550	0 to 10	0.69 to 0.75	211 to 223	125	80

The measured input/output data for the tests of SYSID2 can be seen in Figures 5.1, 5.3, 5.5, and 5.7 for individual inputs of IVC timing, fuel octane, injected fuel energy and engine speed excitations. Each of these separate experiments is approximately 6 minutes of recorded data, so maintaining all the other engine parameters constant for the duration of the experiment is very difficult. The oil, coolant and intake manifold temperature and intake manifold pressure should be constant for each of these tests but are plotted in Figures 5.2, 5.4, 5.6 and 5.8 to document the variation of these parameters during the test. Generally these engine parameters are regulated quite closely by the external control loops. However, it can bee seen in these figures that the coolant temperature cycles by 4 °C as the controller maintains it at 70 °C. When the engine speed is excited, Figure 5.8, the intake manifold pressure fluctuates. This is because the speed of the supercharger is kept at a constant value, rather than being regulated relative to the engine speed.

The variations of these parameters are shown in Table 5.2. Sensitivities of the combustion timing to some of these parameters can be found in [Shahbakhti et al.,

2007b] and [Shahbakhti and Koch, 2008], however, the sensitivity of combustion timing to oil temperature is not presented since oil temperature has nearly zero effect on the combustion timing at normal operating conditions. Using these sensitivities and measured error standard deviations the expected standard deviation in combustion timing is approximately 0.2 °. The changes in the combustion timing caused by the input excitation are around 10 °, so the error cause by the other engine parameters (intake temperature, pressure, and coolant temperature) are much smaller than the changes caused by the excited input.

Table 5.2: Standard deviation of engine parameter during system identification tests. (test points $SYSID2_{IVC}$, $SYSID2_{ON}$, $SYSID2_{E}$, and $SYSID2_{RPM}$)

Test Point	Coolant Temp. [°C]	Oil Temp. [°C]	Intake Temp. [°c]	Intake Pres. [kPa]
$SYSID2_{IVC}$	1.3	0.2	0.4	0.8
$SYSID2_{ON}$	1.1	0.2	0.2	0.8
$SYSID2_{E}$	1.2	0.3	0.3	0.8
$SYSID2_{RPM}$	1.3	0.2	0.7	0.9

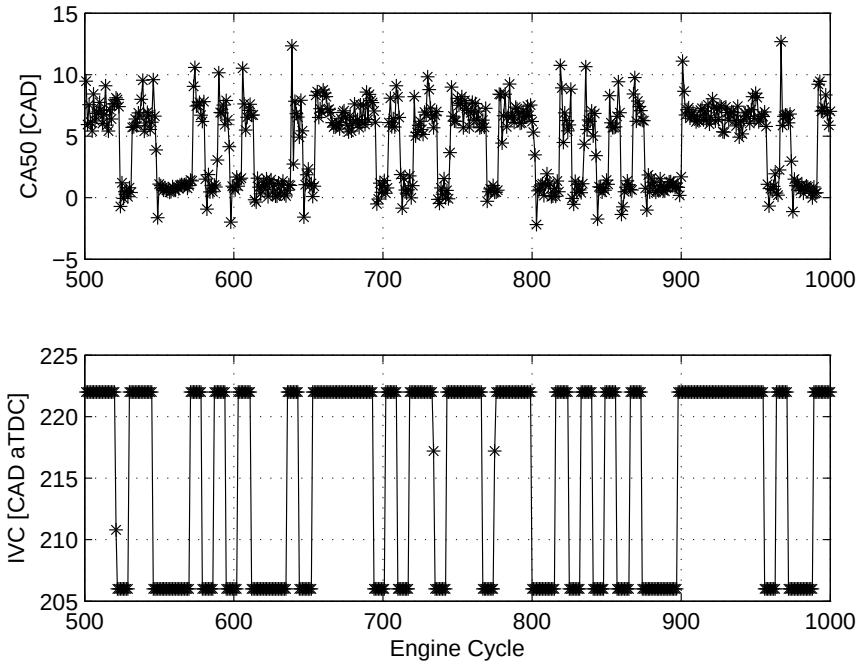

Figure 5.1: Experimental results of the system identification test with the IVC timing excited between 206 °and 222 °aTDC. (test $SYSID2_{IVC}$)

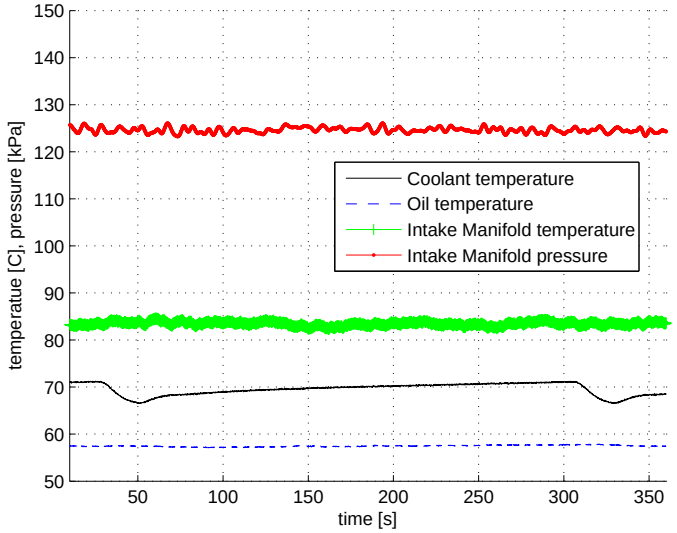

Figure 5.2: Stability of coolant temperature, oil temperature, intake manifold temperature and intake manifold pressure for the $SYSID2_{IVC}$

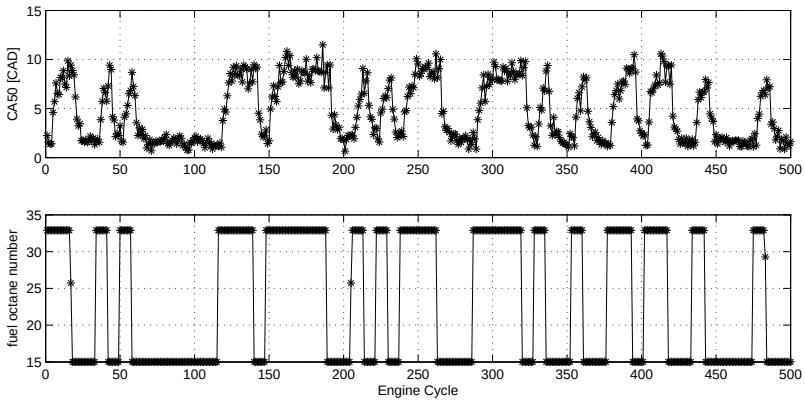

Figure 5.3: Experimental results of the system identification test with the fuel octane excited between 15 and 33. (test $SYSID2_{ON}$)

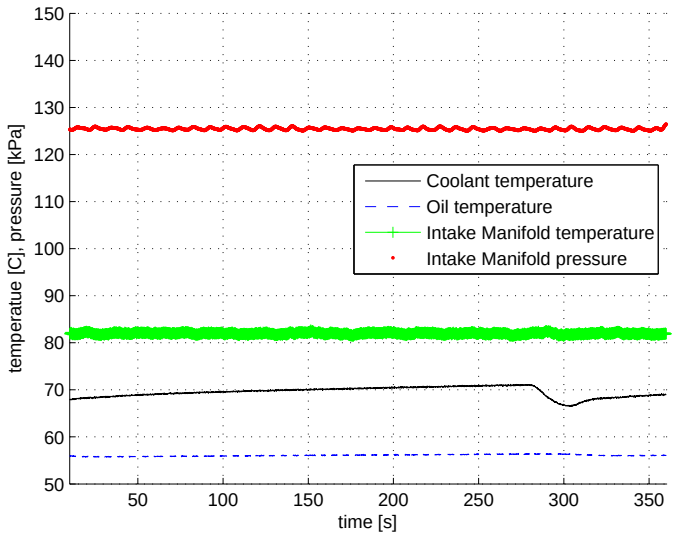

Figure 5.4: Stability of coolant temperature, oil temperature, intake manifold temperature and intake manifold pressure for the $SYSID2_{ON}$

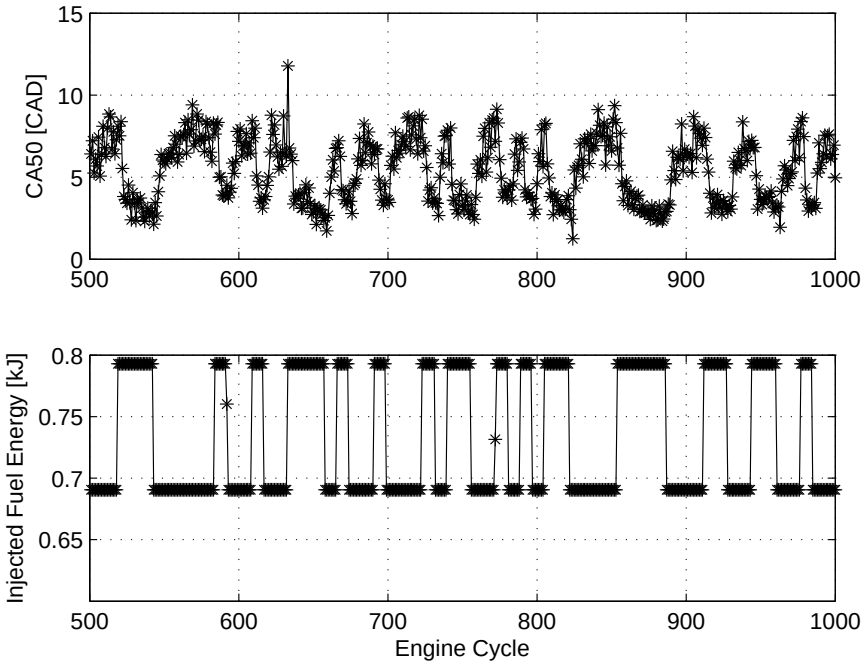

Figure 5.5: Experimental results of the system identification test with the injected fuel energy excited between 690J and 790J. (test $SYSID2_E$)

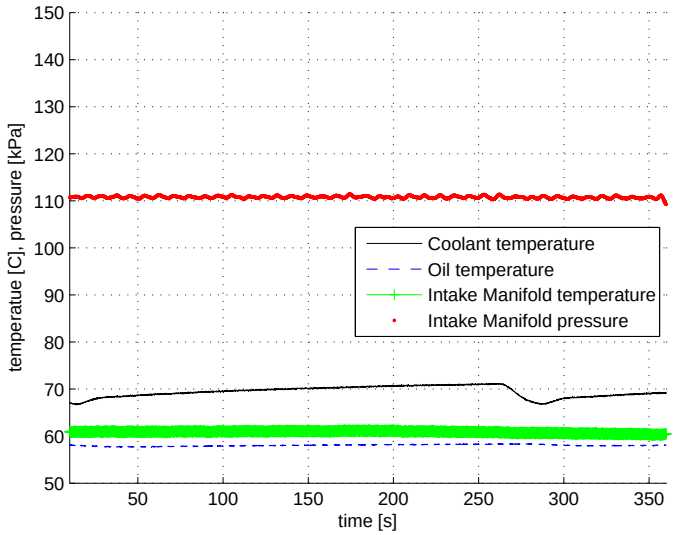

Figure 5.6: Stability of coolant temperature, oil temperature, intake manifold temperature and intake manifold pressure for the $SYSID2_E$

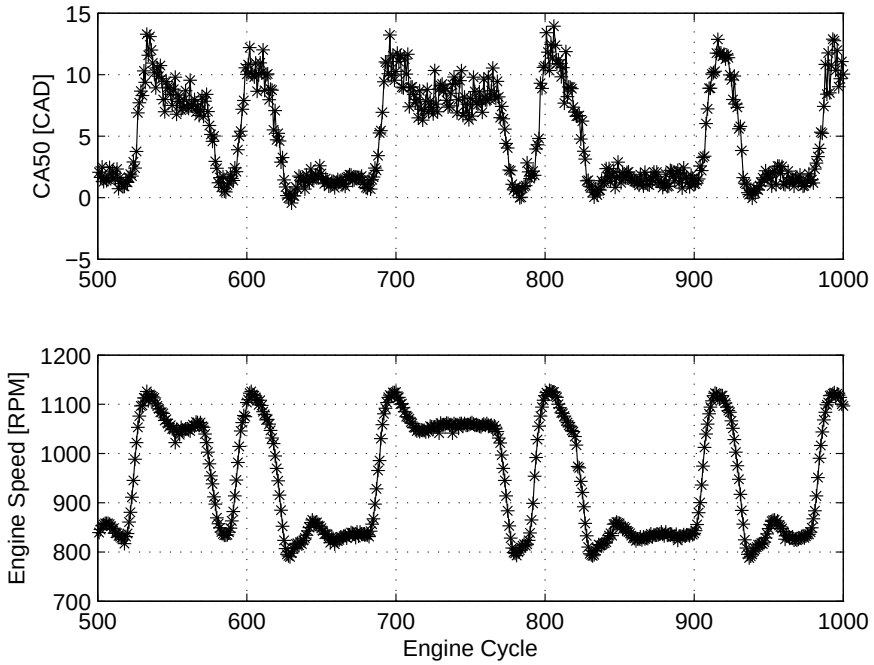

Figure 5.7: Experimental results of the system identification test with the engine speed excited between 850 and 1050RPM. (test $SYSID2_{RPM}$)

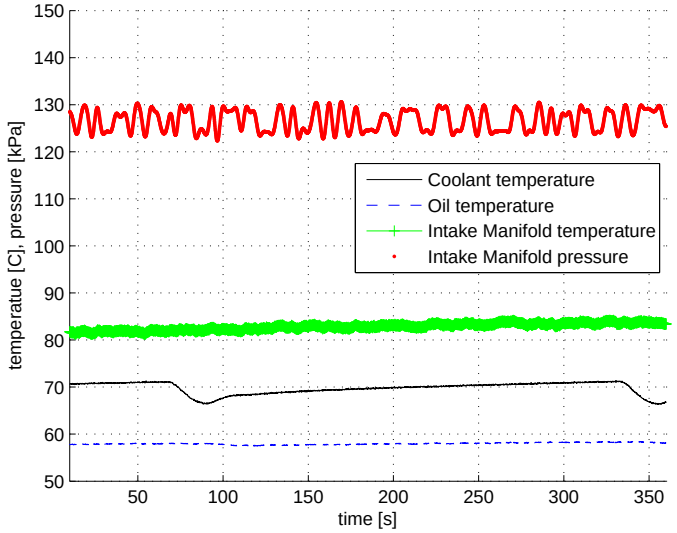

Figure 5.8: Stability of coolant temperature, oil temperature, intake manifold temperature and intake manifold pressure for the $SYSID2_{RPM}$

5.1.2 Analysis

Both the input and output data have non-zero means so the data is de-trended before system identification techniques are applied [Ljung, 1987]. The mean values used to detrend the data are shown in Table 5.3, 5.5, 5.4, and 5.6 for the identification test with IVC timing, fuel octane, injected fuel energy, and engine speed. Each data set is split into two sections so that the same data set that is used to derive the model is not used to validate it as well [Vernhaegen and Verdult, 2007]. The first two thirds of the data set (2000 engine cycles) is used to identify the model while the last one third is used for the model validation (1000 engine cycles). The input data is also prescaled before analysis is done. The scaling is performed so that the model unit step response has a steady state gain of approximately 1. This is done so that all the model parameters are of similar magnitude. The input data is scaled by the same coefficient for all of the five different engine conditions; this way the models obtained from the different conditions can be accurately compared. The scaling values are shown in Table 5.7.

Table 5.3: Mean values used to detrend the data for system identification with IVC timing as the excited input

Test Point	BasePoint1	BasePoint2	BasePoint3	BasePoint4	BasePoint5
Input Mean, IVC timing [°aTDC]	214	215	212	210	217
Output Mean, CA50 [°CAD]	4.9	4.4	3.3	5.8	5.7

Table 5.4: Mean values used to detrend the data for system identification with fuel octane as the excited input

Test Point	BasePoint1	BasePoint2	BasePoint3	BasePoint4	BasePoint5
Input Mean, fuel octane number [ON]	7.9	24.1	34.5	9.7	5.0
Output Mean, CA50 [°CAD]	5.3	4.8	3.1	4.8	5.6

Table 5.5: Mean values used to detrend the data for system identification with injected fuel energy as the excited input

Test Point	BasePoint1	BasePoint2	BasePoint3	BasePoint4	BasePoint5
Input Mean, injected fuel energy [kJ]	0.709	0.740	0.718	0.715	0.717
Output Mean, CA50 [°CAD]	7.5	4.8	5.9	5.5	7.2

Table 5.6: Mean values used to detrend the data for system identification with engine speed as the excited input

Test Point	BasePoint1	BasePoint2	BasePoint3	BasePoint4	BasePoint5
Input Mean, engine speed [RPM]	973	966	970	1262	1477
Output Mean, CA50 [°CAD]	5.7	5.2	4.7	5.5	6.5

Table 5.7: Scaling values used on the system identification data. The same scaling value is used for all five different engine conditions.

	IVC	fuel octane number	injected fuel energy	engine speed
Scaling Value	0.38	0.38	0.03	-50

For this study ARMAX models:

$$\begin{aligned} A(q)y(t) &= B(q)u(t-nk) + C(q)e(t) \qquad (5.1) \\ where: & \\ A(q) &= 1 + a_1 q^{-1} + \cdots\cdots + a_{na} q^{-na} \\ B(q) &= b_1 + b_2 q^{-1} + \cdots\cdots + b_{nb} q^{-nb+1} \\ C(q) &= 1 + c_1 q^{-1} + \cdots\cdots + c_{nc} q^{-nc} \end{aligned}$$

and Box-Jenkins models:

$$\begin{aligned} y(t) &= \frac{B(q)}{F(q)} u(t-nk) + \frac{C(q)}{D(q)} e(t) \qquad (5.2) \\ where: & \\ B(q) &= b_1 + b_2 q^{-1} + \cdots\cdots + b_{nb} q^{-nb+1} \\ C(q) &= 1 + c_1 q^{-1} + \cdots\cdots + c_{nc} q^{-nc} \\ D(q) &= 1 + c_1 q^{-1} + \cdots\cdots + c_{nc} q^{-nc} \\ F(q) &= 1 + c_1 q^{-1} + \cdots\cdots + c_{nc} q^{-nc} \end{aligned}$$

are identified. q^{-1} is the backshift operator. Box-Jenkins models are structured so that the disturbance model is independent from the process model, whereas with an ARMAX model it is assumed that the process and disturbance have a common denominator. These two treatments of the disturbance models are done since the noise model is expected to play a significant role in correctly identifying the system dynamics.

To correctly identify the model it is essential to estimate the pure time delay between each input and output [Ljung, 1987]. To do this a family of ARX models with different delays (0 to 20) are compared. The model resulting in the lowest sum

of squared prediction errors is the integer delay. Table 5.8 shows the estimated delays for the different tests described in Table 5.1. These delays are the number of samples, or engine cycles, it takes for the input to affect the output. This delay includes the delay inherent in computing the combustion timing from the pressure trace, as well as the communication between the CAS system which computes the combustion timing and the MicroAutoBox where this data is recorded. A single delay value is used in the model identification for the five different engine conditions, and the value used is also shown in this table.

Table 5.8: Estimate delays for system identification tests.

Test Number	IVC	fuel octane number	injected fuel energy	engine speed
SYSID1	2	3	3	2
SYSID2	2	3	3	0
SYSID3	2	3	2	0
SYSID4	2	3	3	1
SYSID5	3	2	3	1
Value Used	2	3	3	1

Using the estimated delay, both the ARMAX and Box-Jenkins models are estimated using Equation 5.1 and 5.2 respectively. Details of the methods are in [Ljung, 1987] and the methods are programmed in MATLAB System Identification toolbox [mat, 2006]. Once the models are created they are then validated against the one third of data that was not used in the model creation. To validate the model, the output of CA50 is compared to the measured output of CA50. Figures 5.9, 5.10, 5.11 and 5.12 show the measured output of CA50, Box-Jenkins output of CA50 and ARMAX output of CA50 for the test case SYSID2. The figures correspond to excitations of IVC timing, fuel octane, injected fuel energy and engine speed respectively for Figures 5.9, 5.10, 5.11 and 5.12 respectively. A measurement of the fit of each model is also given in these figures. The measurements of these models are low due

to the large cyclic variations in the CA50 signal; for steady state cases, the standard deviation of CA50 is around 0.7 °. The fit measurements for the other models at the different test conditions can be seen in Table 5.9 and 5.10 for the ARMAX and Box-Jenkins models respectively. While most of the model fits are between 50 and 75% at high engine speeds the fits become lower, the lowest being 34%. The decrease in model accuracy is attributed to the increased variation in combustion at these higher engine speeds. It should also be noted that the lowest fit occurs for the test where injected fuel energy is the input. The size of this output signal is smaller compared to the other outputs, resulting in the lowest signal to noise ratio. Changes in the injected fuel energy reach the limits of combustion (knock and misfire) quicker than changes in other engine inputs, so smaller variations of CA50 are achievable using injected fuel energy. No substantial difference is seen between the fits of the ARMAX and Box-Jenkins models, so all subsequent discussion is with ARMAX models.

Using an assembly of all the test data four extra models are created. This is done to evaluate how well one model can predict the HCCI dynamics at multiple different engine conditions. To create this model the input/output data for the five engine conditions are used in the derivation of ARMAX and Box-Jenkins models. Instead of only using one data set for the creation of the process models, the models are created using five data sets. The resulting model is the best approximation of the dynamics of all five engine conditions. The fit of these models is also shown in the last row of Table 5.9 and 5.10.

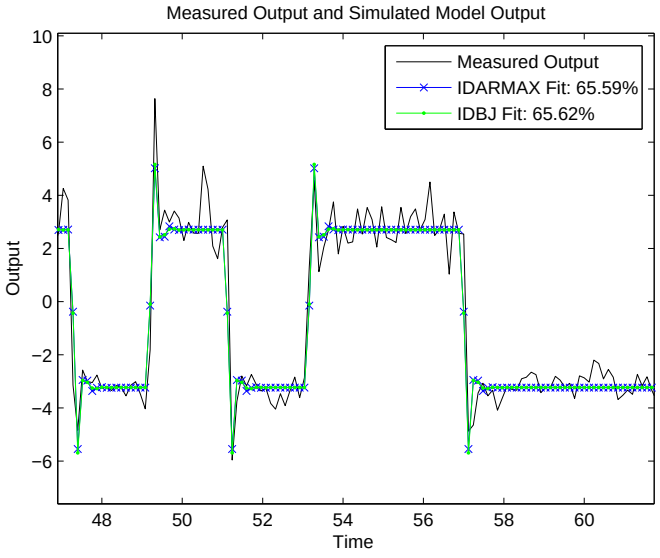

Figure 5.9: Comparison between experimental data and model outputs of ARMAX and Box-Jenkins models for BasePoint2 with IVC timing as the model input. The models were identified from a different data set than the comparison.

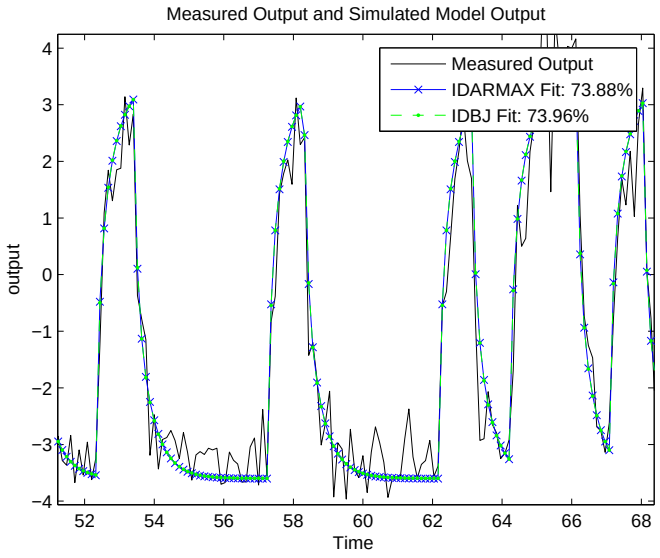

Figure 5.10: Comparison between experimental data and model outputs of ARMAX and Box-Jenkins models for BasePoint2 with fuel octane number as the model input. The models were identified from a different data set than the comparison.

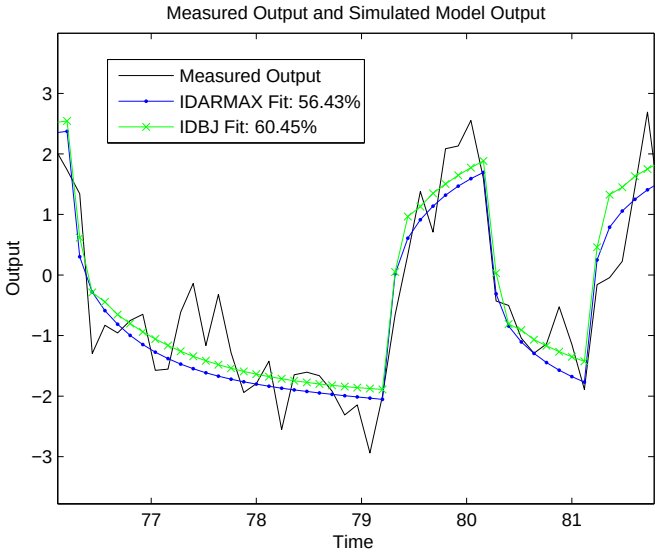

Figure 5.11: Comparison between experimental data and model outputs of ARMAX and Box-Jenkins models for BasePoint2 with injected fuel energy as the model input. The models were identified from a different data set than the comparison.

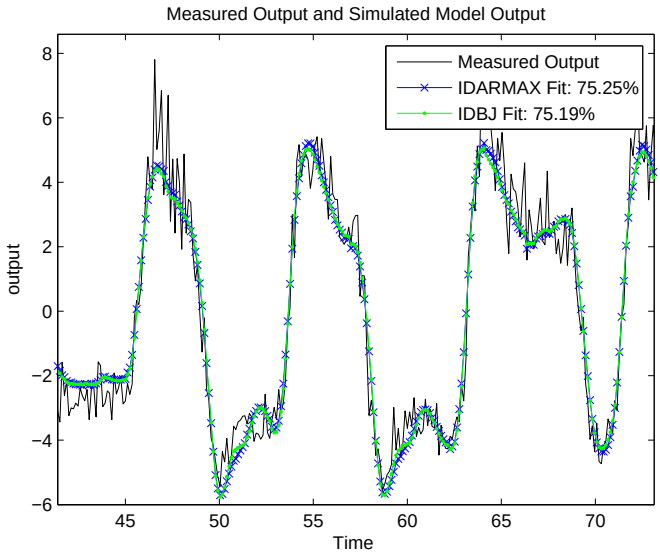

Figure 5.12: Comparison between experimental data and model outputs of ARMAX and Box-Jenkins models for BasePoint2 with engine speed as the model input. The models were identified from a different data set than the comparison.

Table 5.9: Calculated fit of ARMAX models for the 5 different test conditions and 4 different inputs

	Fit %			
Test Number	IVC	fuel octane number	injected fuel energy	engine speed
SYSID1	58	65	50	67
SYSID2	66	74	50	73
SYSID3	60	71	60	68
SYSID4	59	65	41	73
SYSID5	59	43	34	63
Combined Model	56	44	34	57

Table 5.10: Calculated fit of Box-Jenkins models for the 5 different test conditions and 4 different inputs

	Fit %			
Test Number	IVC	fuel octane number	injected fuel energy	engine speed
SYSID1	59	65	43	69
SYSID2	66	74	60	74
SYSID3	62	71	60	69
SYSID4	60	65	38	73
SYSID5	59	43	34	63
Combined Model	56	44	34	58

Residual analysis is performed to investigate how well each model approximates the data. Residuals are the difference between the model output and measured output, and these residuals are analyzed in two ways. Firstly, an autocorrelation of the residuals is calculated and the correlation of the input data and the residuals is then computed. This test indicates whether more output from the input exists than is explained by the current process model. Second, an error model is constructed and the spectrum of this is shown as the final model performance criterion. This also shows whether there is still a significant relationship between the input and the data output. These tests are outlined in [Ljung, 1987] and are already coded in MatLab [mat,

2006].

Residual analysis is shown only for the ARMAX models, but very similar results are seen for the Box-Jenkins models. Figures 5.13, 5.15, 5.17 and 5.20 show the autocorrelation of residual and correlation of the residual and input data for the four different system identification tests done at BasePoint3. For these figures the IVC timing, fuel octane number, injected fuel energy and engine speed are excited respectively. The top half of each figure shows the autocorrelation of the residuals, while the bottom half shows the cross correlation. For all these figures it is seen that the value of the autocorrelation lies within the 99% confident region. Any large values of the autocorrelation indicate a pattern in the residuals, and since the system identification assumes white noise the residuals are expected to be uncorrelated as well. In Figure 5.13 the value of the cross correlation function lies outside the confidence region centered around a lag of 18 engine cycles. Increments in the model order did not improve these results. No substantial deviations outside the confidence region are seen in Figure 5.15 for the cross correlation between fuel octane number and the model residuals. There is a region between 1 and 5 cycles that lies outside the confidence region for the cross correlation between injected fuel energy and the model residuals, Figure 5.17. This indicates some relationship has been missed, and there is an expected relationship for this area of the model. Different model structures and sizes were tried in order to eliminate this problem. It is seen that a 9th order model does not improve the residual correlation, Figure 5.18, when compared to the 2nd order model but improves the fit to 58% from 50%. The lower order models are used. As mentioned earlier the magnitude of input for injected fuel energy is limited by knock and misfire much more than the other signals, resulting in a lower signal to noise ratio. All the values of the cross correlation between engine speed and residuals lie within the confidence region indicating adequate model performance.

The Bode plots for the error models are shown in Figures 5.14, 5.16, 5.19, and 5.21

the dotted lines in the figures correspond to the confidence regions of three standard deviation. These error models are determined from the plant input residuals between process model and actual output and estimated using spectral analysis [Ljung, 1987]. Seen in the Bode plot are both the frequency response and the phase lag. Estimation of an error model helps determine if low frequency dynamics exists between the plant and the error residuals. If there is significant spectral content in the low frequency range of the model this indicates that there are dynamics that are not modeled. For a model that captures the dynamics the spectrum is expected to increase to at the higher end on spectrum up to the Nyquist frequency because the noise will be a high frequency. The Bode plot for the error model from IVC timing input and residuals for BasePoint3 conditions is seen in Figure 5.14, 5.16, 5.19 and 5.21. All these plots show low amplitude response in the range of approximately $2\frac{rad}{s}$.

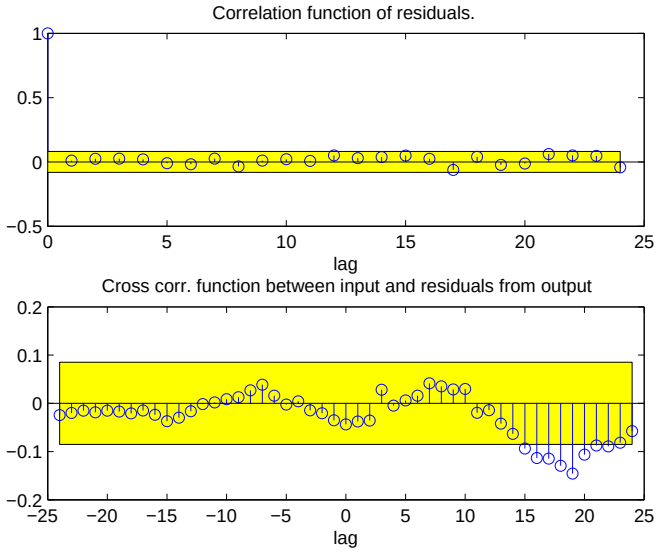

Figure 5.13: Residual analysis of ARMAX model obtained from $SYSID2_{IVC}$. The cross correlation is shown with the shaded region being the 99% confidence interval (top). The correlation of the residuals with the input data is shown along with the 99% confidence interval (bottom)

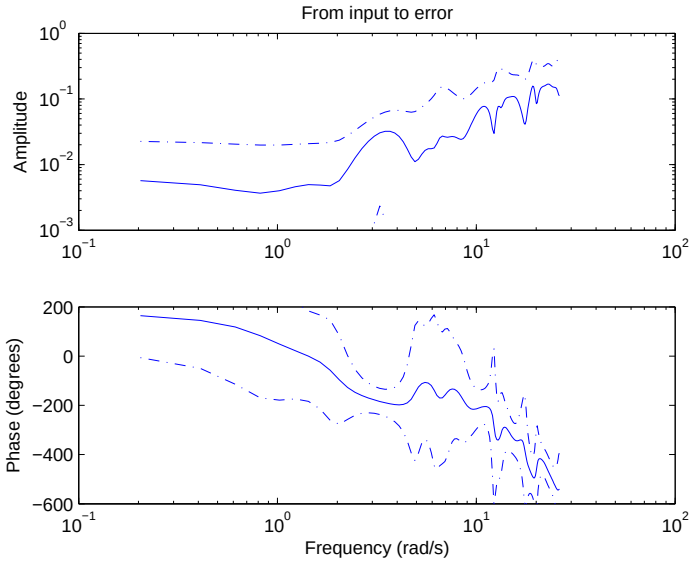

Figure 5.14: Bode plot of the relationship between the model input and the residuals between the model and the experimental data from $SYSID2_{IVC}$. The magnitude plot is shown (top) with the phase plot (bottom), and frequency is shown in radians per second. The data is plotted up to the Nyquist frequency.

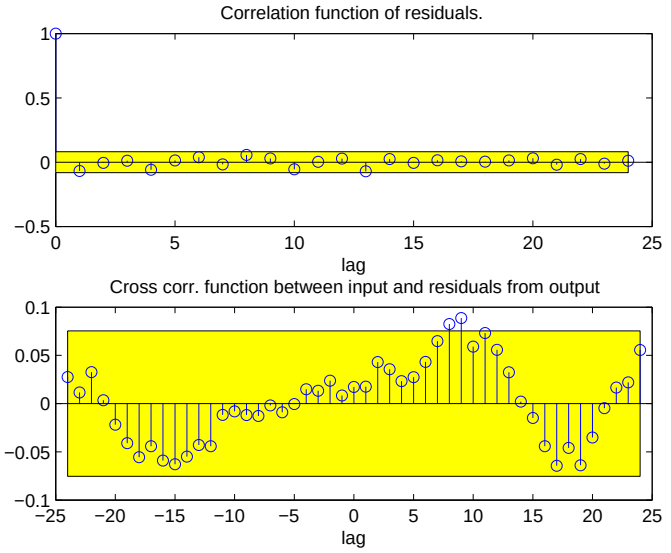

Figure 5.15: Residual analysis of ARMAX model obtained from $SYSID2_{ON}$. The cross correlation is shown with the shaded region being the 99% confidence interval (top). The correlation of the residuals with the input data is shown along with the 99% confidence interval (bottom)

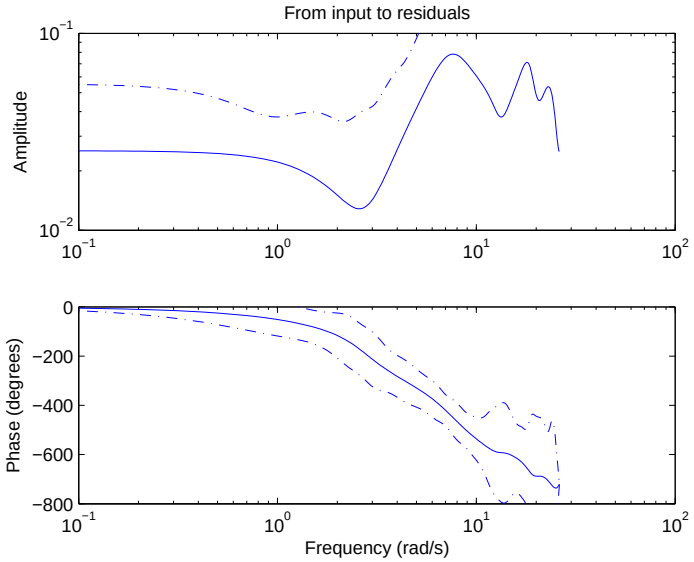

Figure 5.16: Bode plot of the relationship between the model input and the residuals between the model and the experimental data from $SYSID2_{ON}$. The magnitude plot is shown (top) with the phase plot (bottom), and frequency is shown in radians per second. The data is plotted up to the Nyquist frequency.

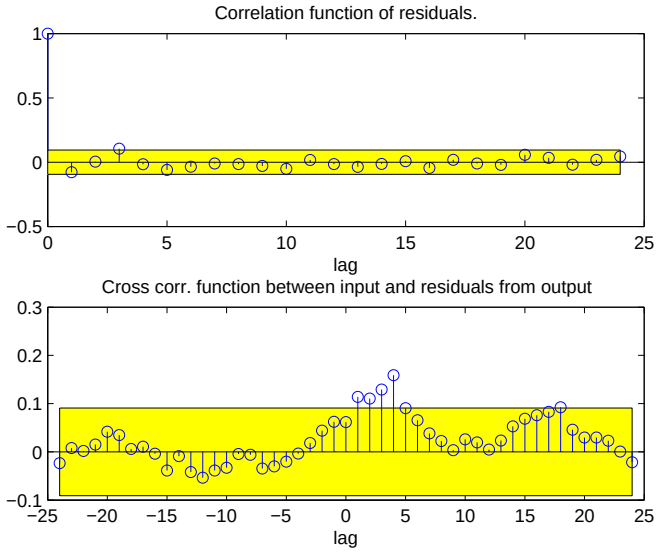

Figure 5.17: Residual analysis of 2nd order ARMAX model obtained from $SYSID2_E$. The cross correlation is shown with the shaded region being the 99% confidence interval (top). The correlation of the residuals with the input data is shown along with the 99% confidence interval (bottom)

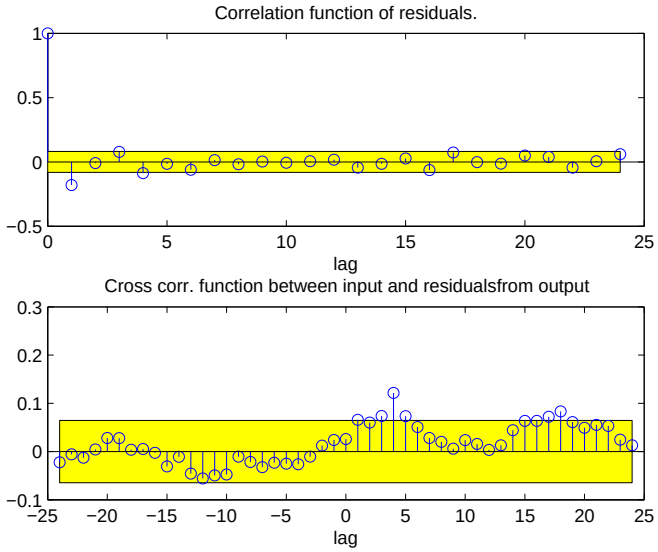

Figure 5.18: Residual analysis of 9th order ARMAX model obtained from $SYSID2_E$. The cross correlation is shown with the shaded region being the 99% confidence interval (top). The correlation of the residuals with the input data is shown along with the 99% confidence interval (bottom)

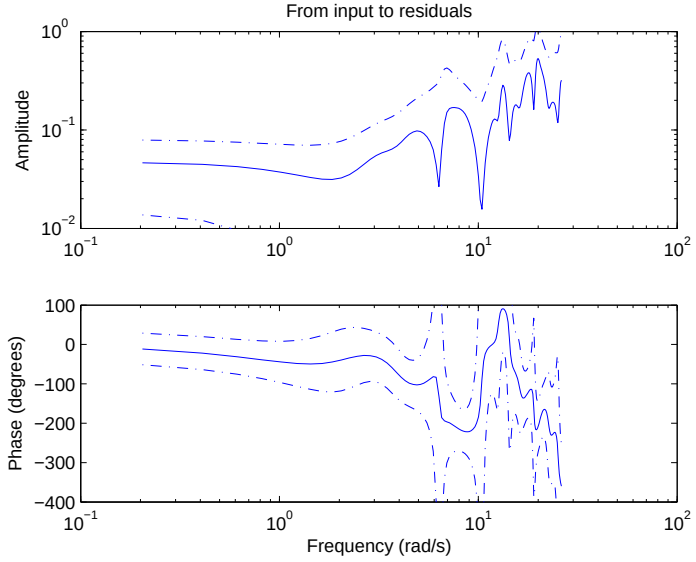

Figure 5.19: Bode plot of the relationship between the model input and the residuals between the model and the experimental data from $SYSID2_E$. The magnitude plot is shown (top) with the phase plot (bottom), and frequency is shown in radians per second. The data is plotted up to the Nyquist frequency.

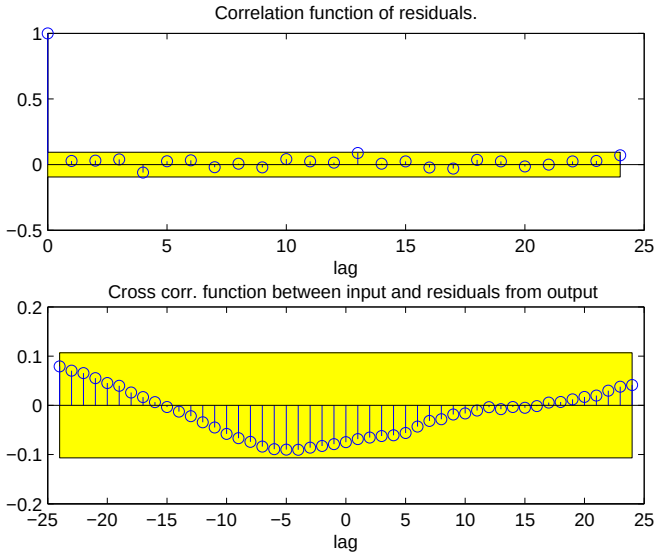

Figure 5.20: Residual analysis of ARMAX model obtained from $SYSID2_{RPM}$. The cross correlation is shown with the shaded region being the 99% confidence interval (top). The correlation of the residuals with the input data is shown along with the 99% confidence interval (bottom)

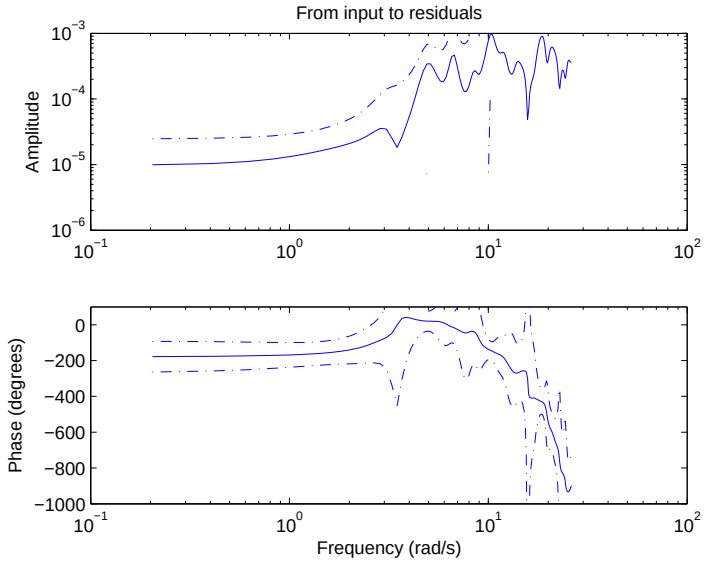

Figure 5.21: Bode plot of the relationship between the model input and the residuals between the model and the experimental data from $SYSID2_{RPM}$. The magnitude plot is shown (top) with the phase plot (bottom), and frequency is shown in radians per second. The data is plotted up to the Nyquist frequency.

In Section 4.1 non-linearity between the changes in the IVC timing and fuel octane

with the resulting CA50 value was discussed. Since the system identification method used assumes a linear system the identification is performed for BasePoint2 conditions for 3 different levels of IVC timing and fuel octane input. ARMAX models for this data are identified. The different identified models are seen in Table 5.11 and 5.12. To demonstrate the difference in the identified models at different conditions the step responses of these models can be seen in Figures 5.22 and 5.23 for the different input levels of IVC timing and fuel octane. In Figure 5.22 the step response for the models from the different levels are all very similar. This indicates that the non-linearity observed earlier between the IVC timing and combustion timing is not significant for this range of conditions. The step responses seen in Figure 5.23 are also similar, indicating weak non-linearity.

Table 5.11: Identified ARMAX model from experiments using different levels of input excitation for the IVC timing. The similar models indicate that the non-linearity was insignificant. (test points $SYSID2_{IVCs}$,$SYSID2_{IVCm}$, and $SYSID2_{IVCl}$)

Excitation Level [°aTDC]	ARMAX Model
210-218	$\frac{0.2041(z+1.828)}{(z+0.06227)(z^2+0.3125z+0.1398)}$
208-220	$\frac{0.20624(z+1.927)}{(z+0.1435)(z^2+0.2724z+0.1536)}$
206-222	$\frac{0.19303(z+2.066)}{(z+0.0954)(z^2+0.2975z+0.156)}$

Table 5.12: Identified ARMAX model from experiments using different levels of input excitation for the fuel octane. The similar models indicate that the non-linearity was insignificant. (test points $SYSID2_{ONs}$,$SYSID2_{ONm}$, and $SYSID2_{ONl}$)

Excitation Level [fuel octane]	ARMAX Model
23-27	$\frac{0.47125(z-0.1217)}{z^2(z-0.6371)(z+0.2084)}$
20-30	$\frac{0.50083(z-0.6547)}{z^2(z-0.7926)(z-0.2606)}$
15-33	$\frac{0.45296(z-0.6037)}{z^2(z-0.7671)(z-0.2602)}$

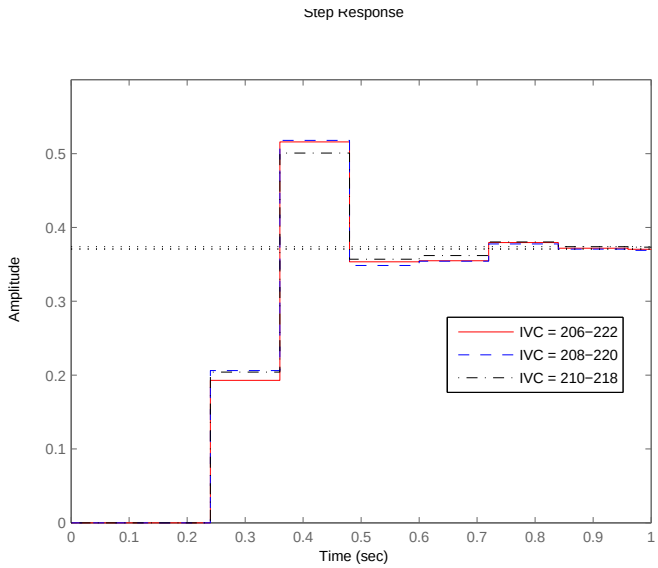

Figure 5.22: Step response of model obtained from experimental data with different excitation levels of the IVC timing. Similar step responses indicated there are not any prominent non-linearities. (test points $SYSID2_{IVCs}$,$SYSID2_{IVCm}$, and $SYSID2_{IVCl}$)

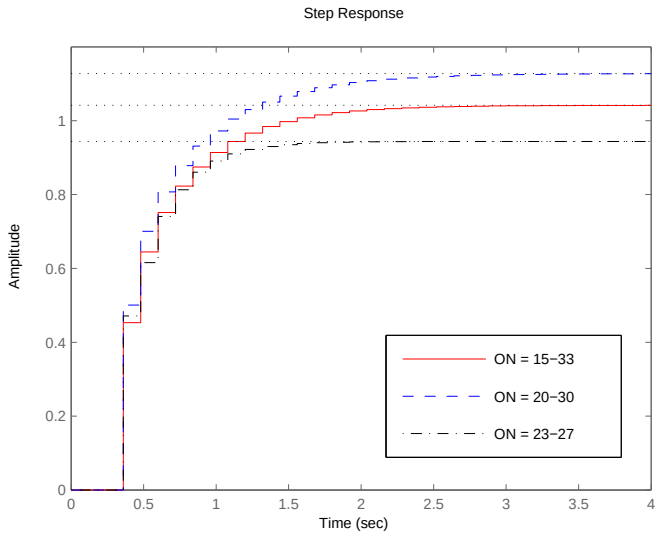

Figure 5.23: Step response of model obtained from experimental data with different excitation levels of the fuel octane. Similar step responses indicated there are not any prominent non-linearities. (test points $SYSID2_{ONs}$,$SYSID2_{ONm}$, and $SYSID2_{ONl}$)

Discrete transfer functions of the final models can be seen in Table 5.13 and 5.14.

This table includes all the models from the five different engine operating conditions. Also included in the table is the averaged model that uses data from all five different operating conditions. The order for the average models is different in some cases that the order for the individual models.

To determine the repeatability of the model obtained, the procedure is repeated for the models identified at the BasePoint2 condition; these are the $SYSID2_{IVC}$, $SYSID2_{ON}$, $SYSID2_{E}$, and $SYSID2_{RPM}$ models. Data is taken on an entirely different day from the original data set, and it is found that the identified model fit values and step responses are quite similar, with the exception of the models for $SYSID2_{E}$. Details of this analysis can be seen in Appendix A.

Table 5.13: Calculated ARMAX models for the different system identification tests for the two actuators.

Test Number	IVC	fuel octane number
SYSID1	$\frac{0.6216(z+1.66)(z-0.4031)}{z^2(z+0.2086)(z-0.1488)}$	$\frac{0.4701(z-0.3157)}{z^2(z-0.728)(z+0.3217)}$
SYSID2	$\frac{0.5098(z+2.101)(z-0.2921)}{z^2(z^2+0.1337z+0.0149)}$	$\frac{0.4639(z-0.5369)}{z^2(z-0.7521)(z-0.1726)}$
SYSID3	$\frac{0.2219(z+3.432)(z-0.4549)}{z^2(z-0.402)(z+0.1352)}$	$\frac{0.4902(z-0.6213)}{z^2(z-0.7179)(z-0.3499)}$
SYSID4	$\frac{0.6715(z+1.803)(z-0.3025)}{z^2(z^2+0.03023z+0.1205)}$	$\frac{0.4431(z-0.6336)}{z^2(z-0.8323)(z+0.0144)}$
SYSID5	$\frac{0.2660(z+4.1)(z-0.6349)}{z^2(z-0.4692)(z+0.06633)}$	$\frac{0.4798(z-0.6393)}{z^2(z-0.8267)(z+0.05826)}$
Average Model	$\frac{0.3918(z+2.476)}{z(z^2+0.3149z+0.171)}$	$\frac{0.4643(z-0.4584)}{z^2(z-0.7403)(z+0.002405)}$

Table 5.14: Calculated ARMAX models for the different system identification tests for the two disturbances.

Test Number	injected fuel energy	engine speed
SYSID1	$\frac{0.61209(z-0.8191)}{z^2(z-0.9185)(z+0.003341)}$	$\frac{0.7577z}{(z-0.3936)(z+0.289)}$
SYSID2	$\frac{0.43198(z-0.8512)}{z^2(z-0.9206)(z-0.2137)}$	$\frac{0.7403z}{(z-0.4909)(z+0.3891)}$
SYSID3	$\frac{0.6173(z-0.8975)}{z^2(z-0.936)(z-0.1879)}$	$\frac{0.6989z}{(z-0.4824)(z+0.3752)}$
SYSID4	$\frac{0.49637(z-0.8223)}{z^2(z-0.9217)(z+0.002564)}$	$\frac{0.6936z}{(z-0.4097)(z+0.2074)}$
SYSID5	$\frac{0.46233(z-0.9255)}{z^2(z-0.9702)(z-0.2546)}$	$\frac{0.5239z}{(z-0.4824)(z+0.2192)}$
Average Model	$\frac{0.5623(z-0.8763)}{z^2(z-0.9366)(z-0.1072)}$	$\frac{0.6571z}{(z-0.4873)(z+0.339)}$

5.1.3 Discussion

The step response of the identified models for the relationship between IVC timing and CA50 is shown in Figure 5.24. In this figure a step response is shown for each model from the five different conditions, as well as the average model. As noted earlier the data is scaled so that a unit step input produces an output on the order of one. The data from each test is scaled by the same constant, so if the models have identical steady state gain it would be seen here. It can be seen in the figure that this is not the case. The model from BasePoint3 conditions has the lowest gain and the model from BasePoint4 has the highest gain. This error in gain is a result of both modeling error and that the relationship between IVC timing and CA50 changes slightly for each operating condition. However, it is a very encouraging result that the steady state gain value for different operating points are not different by less than 20%. The dynamic characteristics of the different models appear very similar, they all have a certain amount of overshoot. For all the models, the peak response is seen on the third engine cycle and all the oscillations are damped by the sixth engine cycle. The bode plots of the identified models between IVC timing and CA50 are shown in Figure 5.25.

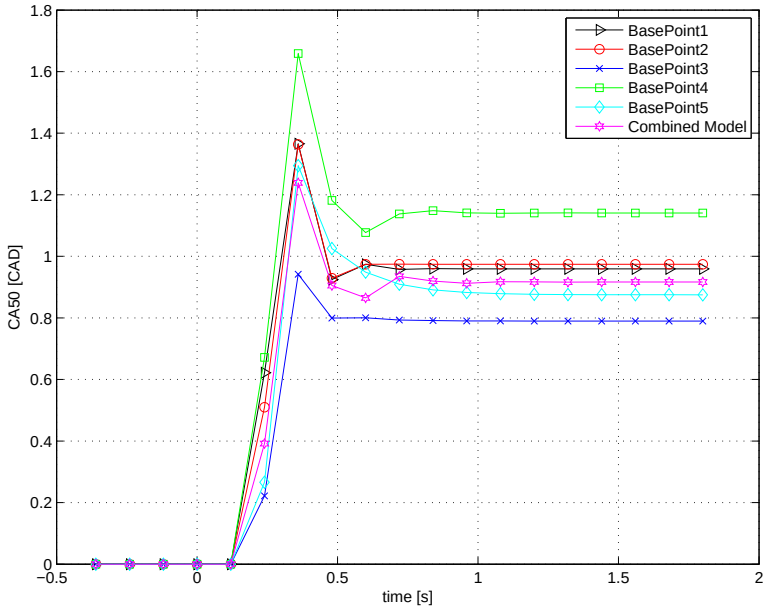

Figure 5.24: Step response of the 5 models identified between the IVC timing and CA50.

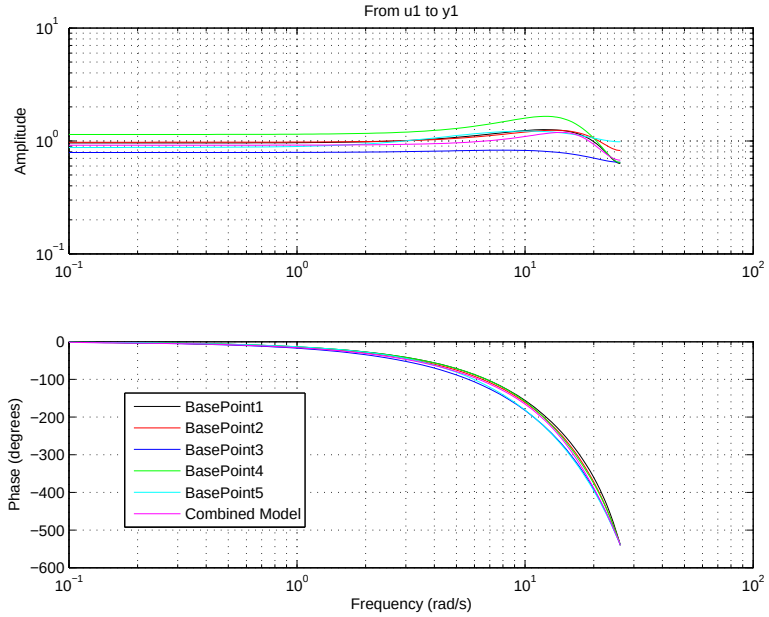

Figure 5.25: Bode plot of the 5 models identified between the IVC timing and CA50.

The step response of the identified models for the relationship between fuel octane and CA50 is shown in Figure 5.26. In this figure a step response is shown for each model from the five different conditions, as well as the average model. The data sets

for these models are scaled by the same value, so that a unity gain is achieved. The five different models all exhibit similar steady state gain values even though they are obtained from different test conditions, and with substantially different mean values for fuel octane. These gain values lie closer together than the steady state gain values between IVC timing and CA50. The derivation of the transfer function between the injectors and the actual fuel delivered to the cylinder is shown in [Kiencke and Nielsen, 2000]. Here it is seen that because of wall wetting inside the intake system a first order system will exist that slows the delivery of fuel to the cylinder. The results of Figure 5.26 are also first order, verifying that the correct dynamics have been identified.

All the models have similar time constants of around 2 engine cycles, which corresponds to 0.24 seconds at 1000RPM. The time response of the models does not appear to change drastically as the engine speed is increased, indicating that most of the dynamics are cycle based and not time based.

A larger pure time delay exists between the fuel octane and CA50 than the IVC timing and CA50. For the IVC timing models a two cycle time delay exists, yet for the fuel octane model a three cycle delay exists. Faster control can be obtained by using the IVC timing to control when compared to fuel octane. This can be partially explained by the wall wetting dynamics that will slow the effect of changing the fuel octane number, whereas changes in the IVC timing are not hindered by this dynamic.

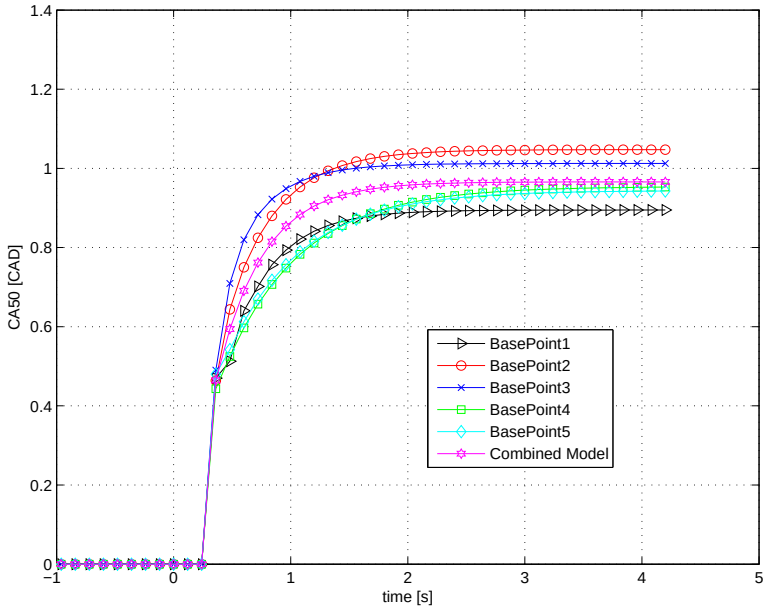

Figure 5.26: The step response of the 5 models identified between the fuel octane and CA50.

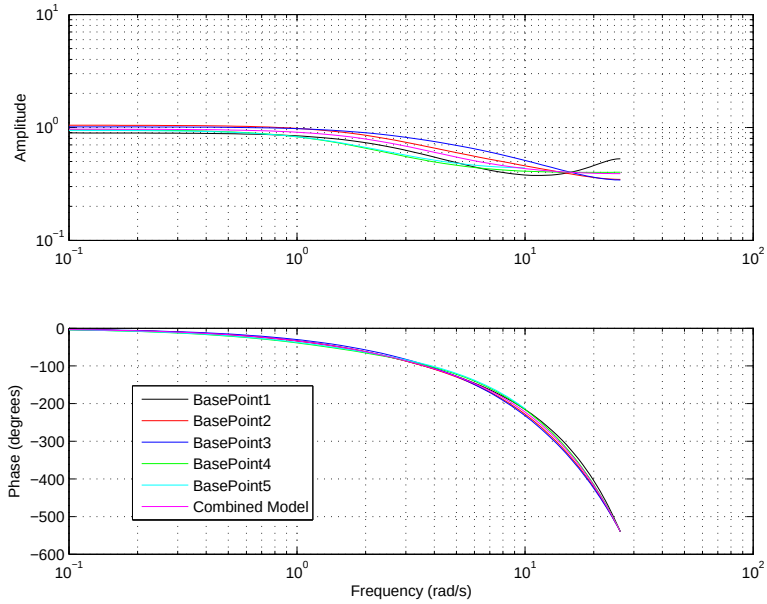

Figure 5.27: The bode plot of the 5 models identified between the fuel octane and CA50.

The step response of the identified models for the relationship between injected fuel energy and CA50 is shown in Figure 5.28. The identified models at the different

operating point all appear to have different steady state gains. There does not appear to be any correlation between the intake pressure and temperature to the steady state gain, BasePoint1 BasePoint2 and BasePoint3. The steady state gain does appear to increase with engine speed, BasePoint2 BasePoint4 and BasePoint5. However, it is important to note the fits of some of these models are below 50% so this trend is an attribute of the noise. The appearance of these models is very similar to that of Figure 5.28, a first order plus pure time delay system. However, the time constants of these systems are much larger on average than the time constants of the fuel octane and CA50 system. Both these systems are coupled with the fuel wall wetting dynamics, and that dynamic should not change. Another first order dynamic must be present that is making the models between injected fuel energy and CA50 different. As noted in [Chang et al., 2007] the cylinder wall temperature has a strong effect on the HCCI combustion, and subsequently the CA50 value. A different steady state value of the cylinder wall temperature exists at different engine conditions, especially different engine loads. During load changes the wall temperature tries to reach a steady value which [Chang et al., 2007] notes takes up to 60-100 seconds. This long dynamic could be affecting the identified model between the injected fuel energy and CA50. The load is constant for all the other models, so this dynamic will not have a large effect on the other identified models.

The pure time delay between injected fuel energy and CA50 is identical to the model of fuel octane number and CA50. This is expected since both methods use the fuel injection system.

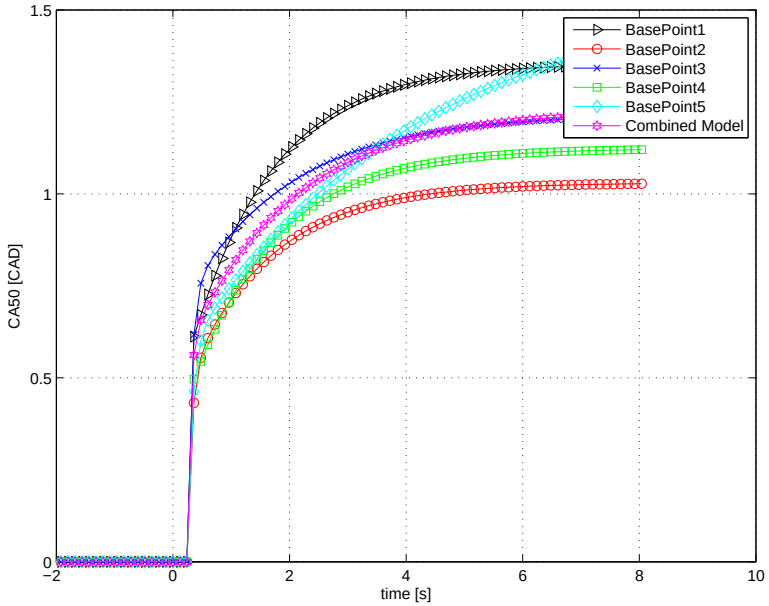

Figure 5.28: The step response of the 5 models identified between the injected fuel energy and CA50.

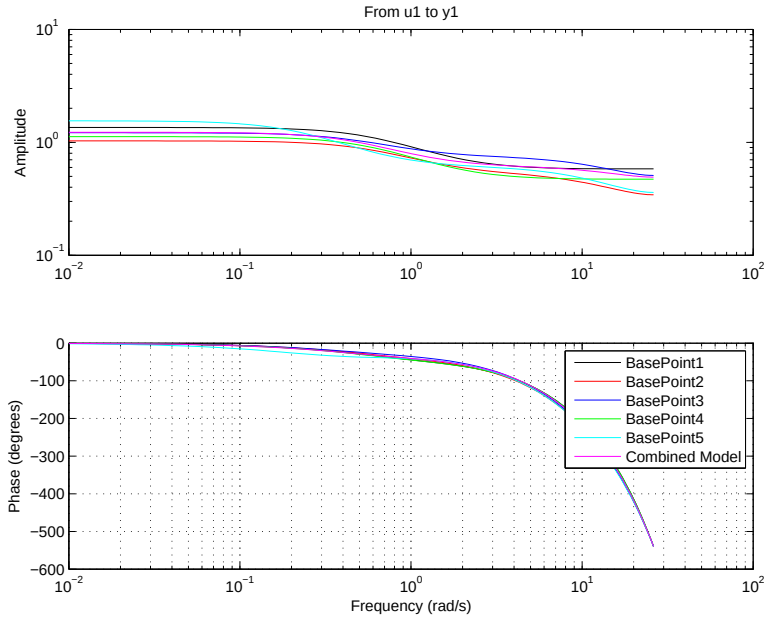

Figure 5.29: The bode plot of the 5 models identified between the injected fuel energy and CA50.

The step response of the identified models for the relationship between engine speed and CA50 is shown in Figure 5.30. There is not substantial difference in the

steady state gain between the different engine conditions. The dynamic appearance of these models also looks very similar.

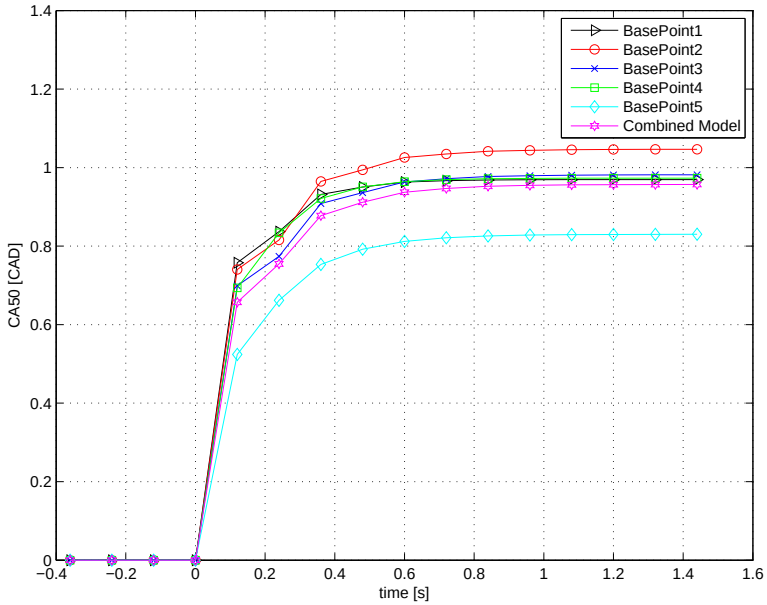

Figure 5.30: The step response of the 5 models identified between the engine speed and CA50.

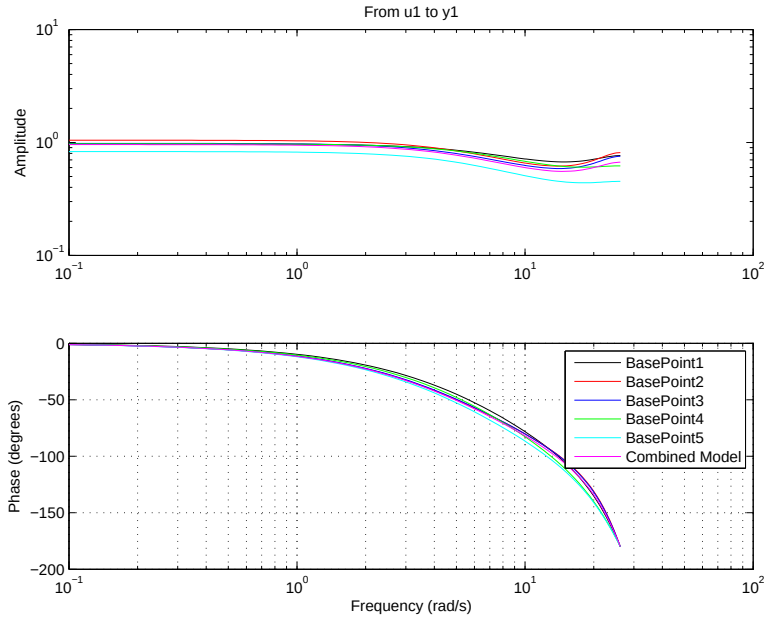

Figure 5.31: The bode plot of the 5 models identified between the engine speed and CA50.

The combined models are seen to approximate the dynamic relationships quite well at each engine condition. These models are created from a combination of test data from all five engine conditions, and the fits of these models are seen to be very good. This technique worked well because the dynamics and sensitivity of the system do not substantially change between the different engine conditions in this study.

5.2 Model-Derived Control of HCCI

In the previous section four single input single output models are identified for the four engine inputs: IVC timing, fuel octane, injected fuel energy, and engine speed. These models are obtained using input/output data for five different test conditions and seen to capture the dynamics of each individual input/output relationship. Here these identified process models are inverted and then implemented in feedforward controllers. To implement the feedforward controllers simple integral feedback control is also needed. The results of the controllers are then shown with a discussion and comparison to basic PI control.

5.2.1 Design and Implementation

Feedforward controllers (often in combination with feedback or adaptive control) are commonly used in automotive application since they provide ways to eliminate unacceptable errors of plant output [Levine, 1996]. Most vehicles use a feedforward component for idle speed control and λ control [Kiencke and Nielsen, 2000]. The goal of this feedforward controller is to minimize error caused by measured disturbances. Analysis done using a PI feedback controller shows that substantial error can be caused by step changes in engine speed and injected fuel energy and this can lead to very late combustion and misfire as well as early combustion and engine knock. Changes in injected fuel energy and engine speed are disturbances which are known. Using the models obtained from system identification, feedforward controllers are designed to attenuate changes in engine speed and injected fuel energy individually. A schematic of the controller is shown in Figure 5.32.

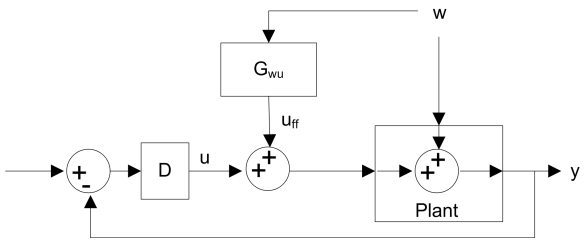

Figure 5.32: Schematic of a general feedforward controller where u is the controller output, y is the plant output, and w is the measured disturbance.

The goal of the controller is to maintain a constant plant output, y, (that is to regulate the combustion timing). The plant output for this figure is given by:

$$y = G_{wy}w + G_{uy}G_{wu}w + G_{uy}u \tag{5.3}$$

This assumes that the plant models are linear time invariant systems. The plant output, y, is a combination of the measured disturbance, w, and the controller input, u. A controller, G_{wu}, is used to attenuate measured disturbance and it is desired that the output stays constant for disturbance inputs, w. For this case it can be assumed that the plant output should stay at zero, then:

$$G_{uy} = -\frac{G_{wy}}{G_{uy}} = -G_{wy}G_{uy}^{-1} \tag{5.4}$$

G_{wy} corresponds to the identified model between the disturbance, either injected fuel energy or engine speed, and combustion timing. G_{uy} corresponds to the identified model between the actuator, either IVC timing or fuel octane number, which needs to be inverted. Using the identified models, feedforward controllers are designed and Table 5.2.1 shows the identified transfer functions. These transfer function are the result of system identification performed on data sets from all five engine conditions. It is seen in the previous section that these average models approximate the dynamics quite well for all five engine conditions. To decrease the number of controller tested

feedforward controllers are not made from the individual models from each of the basepoints.

In Table 5.2.1 the model for IVC timing is non-invertible due to zero's outside the unit circle. To invert this plant the zero is mapped inside the unit circle and the gain is adjusted so that the plant has the same steady state value, similar to the methods in obtaining invertible plants for Internal Model Control (IMC) [Garcia and Morari, 1982]. This is a non-unique method of inverting a non-minimum phase system, but provides a repeatable method to proceed with the controller design. The pure time delays of the identified models when present cause non-casual controllers. These pure time delays of the final controller is removed so that the controller is causal. Details of this procedure are given in Appendix E. For example, the model between IVC timing and CA50 is:

$$G_{IVC->CA50} = 0.392z^{-2}\frac{(1+2.474z^{-1})}{(1+0.31z^{-1}+0.171^{z-2})} \tag{5.5}$$

The non-minimum phase zero is moved inside the unit circle, and the gain adjusted so that the model becomes:

$$G^{*}_{IVC->CA50} = 0.9703z^{-2}\frac{1+0.404z^{-1}}{1+.31z^{-1}+0.171z^{-2}} \tag{5.6}$$

Following Equation 5.4, a feedforward controller of the measured injected fuel energy disturbance is designed as:

$$FF_{E->IVC} = -\frac{G_{E->CA50}}{G^{*}_{IVC->CA50}} \tag{5.7}$$

$$= z^{-1}0.579\frac{(1-0.8772z^{-1})(1+.31z^{-1}+0.171z^{-2})}{(1-0.9328z^{-1})(1-0.1072z^{-1})(1+1.404z^{-1})} \tag{5.8}$$

$$\tag{5.9}$$

The four controllers which result from each of the two disturbances (engine speed and injected fuel energy) being rejected by two inputs (IVC timing and fuel octane number) are listed in Table 5.16, and details given in Appendix E.

The response of these controller are initially tested in simulation to verify the response and stability as an unstable controller could damage the engine. The feedforward simulated disturbance rejection to step inputs using IVC timing and fuel octane are shown in Figures 5.37 and 5.38 respectively. For each of these figures first a step input of engine speed and then a step in injected fuel energy is given. Due to the causality of the model inversion, an initial error is present for all disturbances with the exception of the injected fuel energy disturbance for feedforward controller using fuel octane number. All the controllers quickly compensate for the disturbance so that the steady state value of the combustion timing is the desired value. The Simulink models for these simulations are found in the Appendix E.

A schematic of the actual implementation of the controller on the engine is seen in Figure 5.39. This differs from the ideal case as an integrator term on the feedback loop is added to compensate unmeasured disturbances such as intake temperature changes and unmodeled dynamics. For all cases, the gain of the integrator is set to 0.1 which is lower than the values used in the PI controllers since here the control is designed to reject slowly varying changes.

Table 5.15: Calculated ARMAX models from data of all five of the engine base points. The transfer functions are between the specified input and CA50.

IVC	fuel octane	injected fuel energy	engine speed
$\frac{0.3918(z+2.476)}{z(z^2+0.3149z+0.171)}$	$\frac{0.4643(z-0.4584)}{z^2(z-0.7403)(z+0.002405)}$	$\frac{0.5623(z-0.8763)}{z^2(z-0.9366)(z-0.1072)}$	$\frac{0.6571z}{(z-0.4873)(z+0.339)}$

Table 5.16: Feedforward controller designed from the identified models.

control method	engine speed disturbance	injected fuel energy disturbance
IVC timing control	$-\frac{0.6788z^3+0.2138z^2+0.1161z^1}{z^3+0.257z^2-0.2249z^1-0.06683}$	$-\frac{0.5806z^3-0.3264z^2-0.06116z-0.0871}{z^4-0.635z^3-0.3212z^2+0.0405z^1}$
fuel octane control	$-\frac{0.657z^3-0.485z^2-0.001z}{0.464z^3-0.282z^2-0.045z+0.035}$	$-\frac{0.562z^3-0.908z^2+0.363z+0.001}{0.464z^3-0.697z^2+0.269z-0.021}$

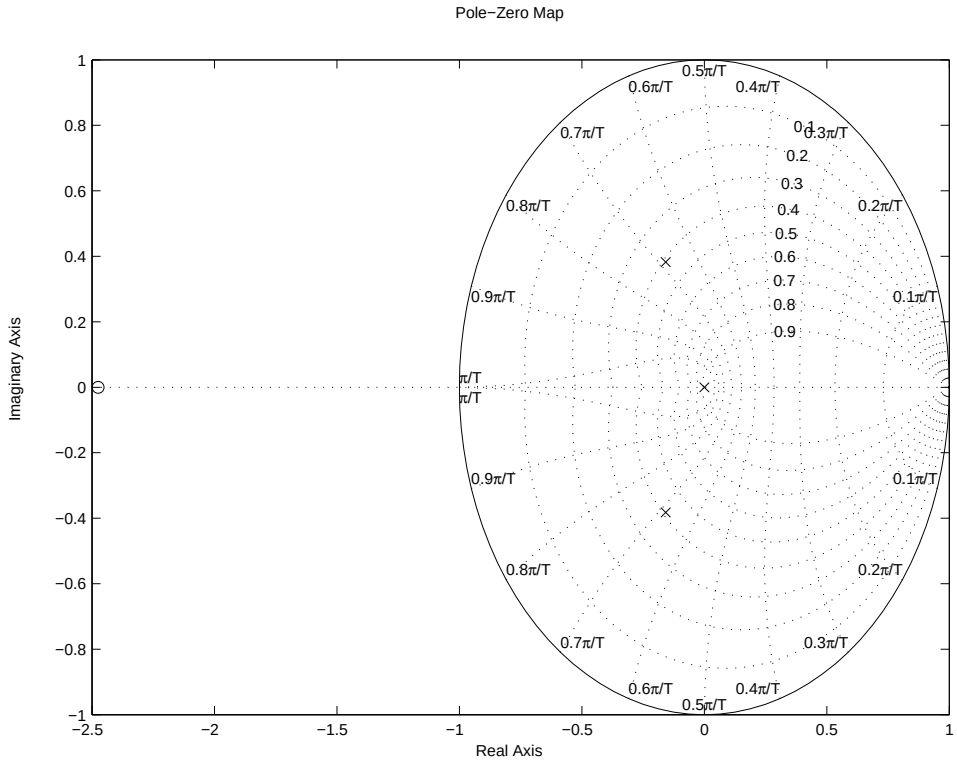

Figure 5.33: Pole-Zero map of IVC timing plant model

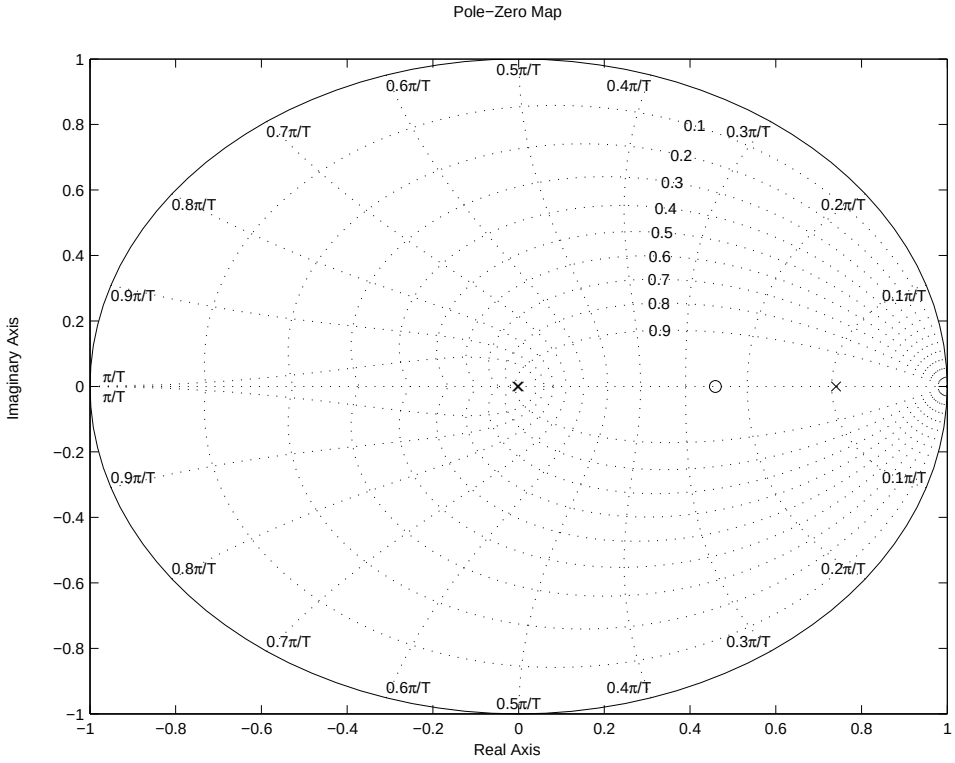

Figure 5.34: Pole-Zero map of fuel octane plant model

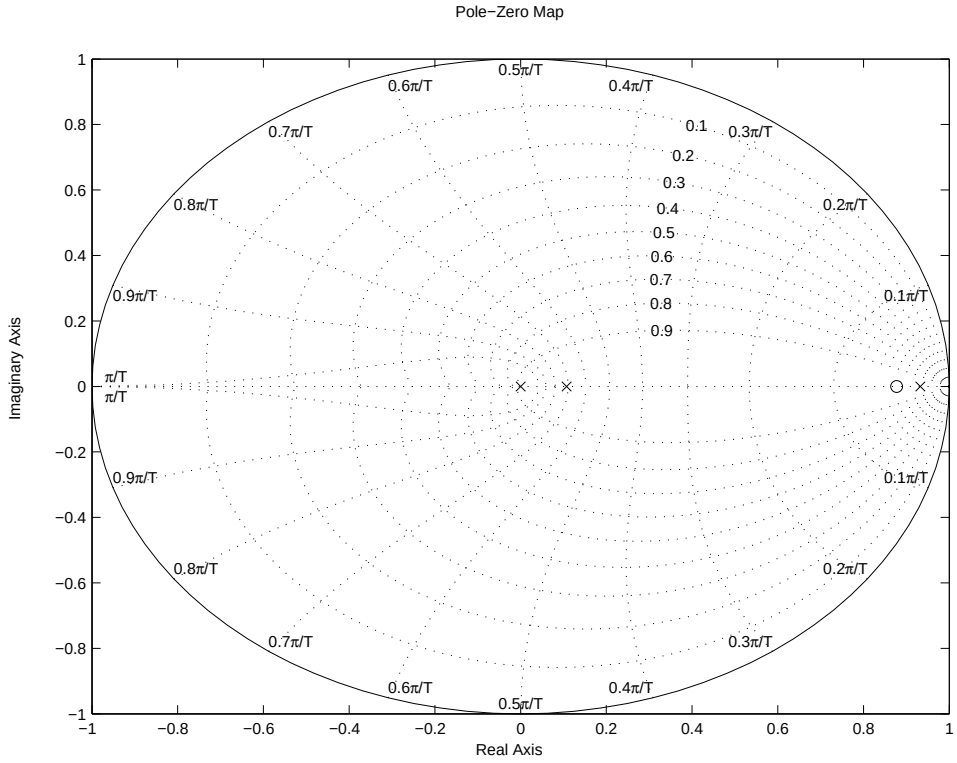

Figure 5.35: Pole-Zero map of injected fuel energy plant model

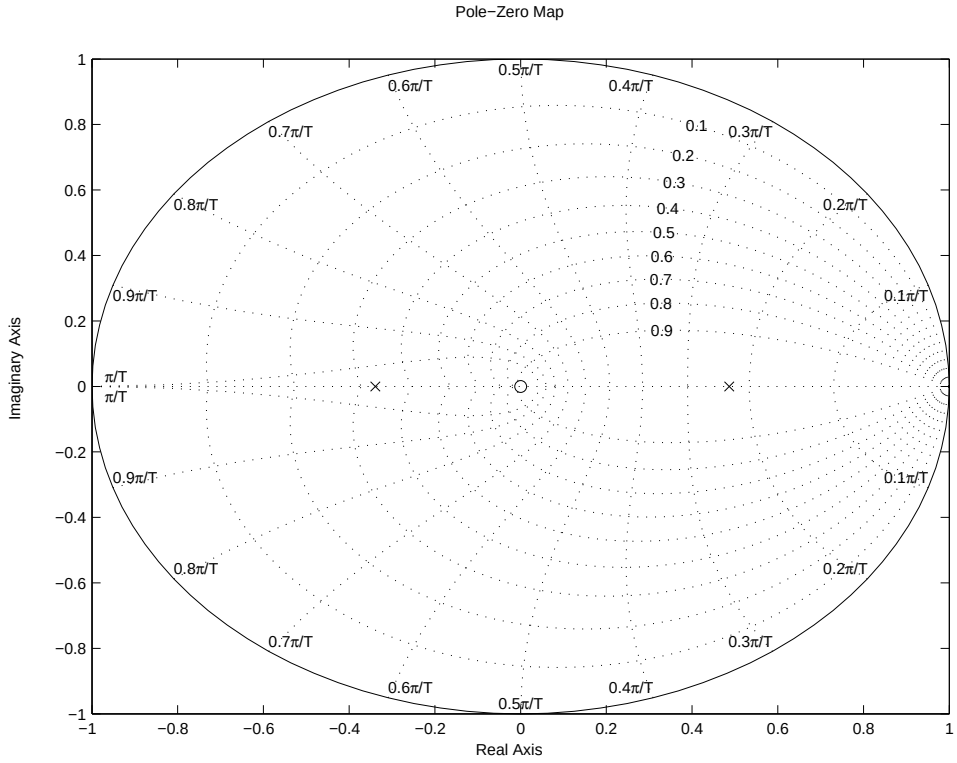

Figure 5.36: Pole-Zero map of engine speed plant model

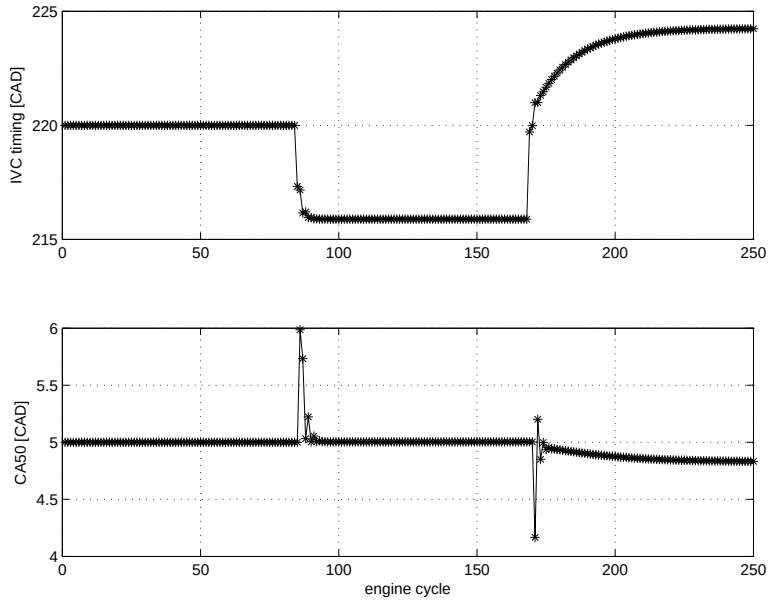

Figure 5.37: Simulation of the feedforward controller using IVC timing to regulate the combustion timing. A 100 RPM step is simulated at step 86 and a 0.05kJ step in fuel is simulated at cycle 170.

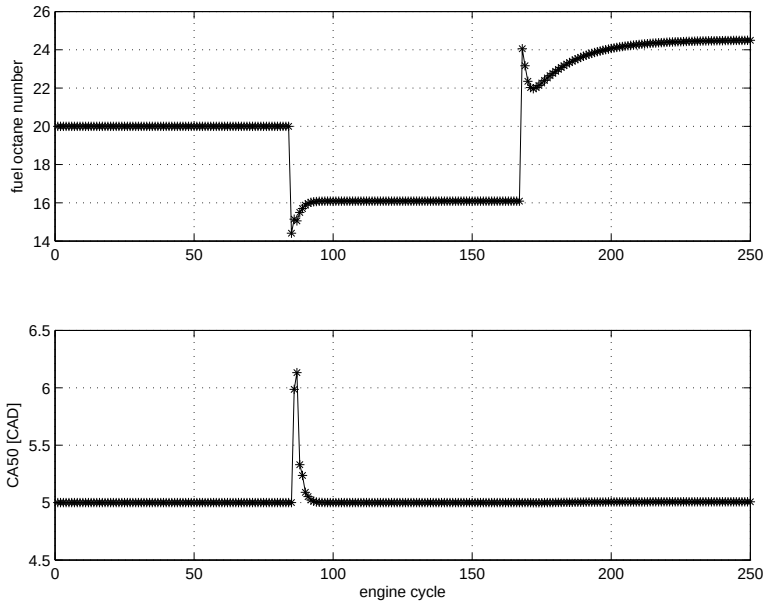

Figure 5.38: Simulation of the feedforward controller using the fuel octane number to regulate the combustion timing. A 100 RPM step is simulated at step 86 and a 0.05kJ step in fuel is simulated at cycle 170.

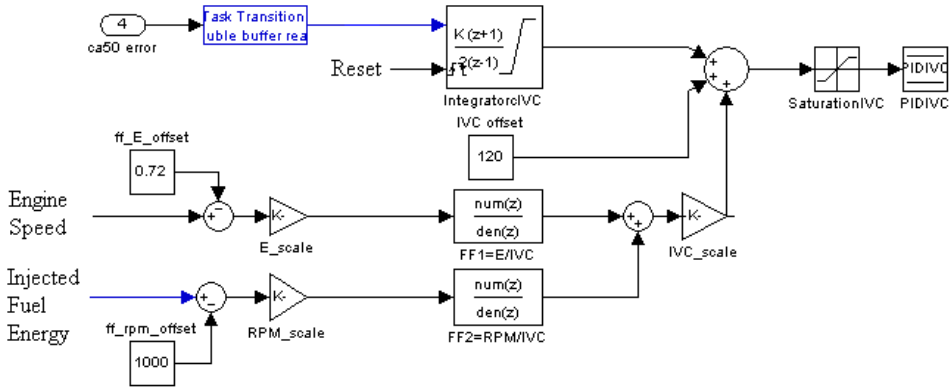

Figure 5.39: Schematic of implemented feedforward scheme. An integrator feedback term is added to handle the unmeasured disturbances.

5.2.2 Experimental Feedforward Results

The controllers are implemented and tested at all five engine conditions outlined in Table 3.3. The controller performance in rejecting measured disturbances of both injected fuel energy and engine speed is documented by examining the deviation of

combustion timing (CA50). The same disturbances are input that were used previously in Chapter 4. For the step tests of injected fuel energy, steps are timed as follows: at 100 cycles a 50J step occurs with a 50 cycle duration, and at 200 cycles a -50J step occurs with a 50 cycle duration. All the pulses are identical at each condition and for each controller. Due to software limitations, a timed step in engine speed cannot be easily performed, so this pulse is done manually. Similar lengths of steps are attempted to that of injected fuel energy, with the size of the step being 100RPM.

To quantify the ability of the feedforward controller to regulate the combustion timing the variance of the CA50 timing is calculated for each test case. This measure is used in other studies to quantify controller performance [Strandh et al., 2005] as the variance provides a good measure of the scatter of a data set around its mean [Montgomery and Runger, 2003]. All the calculated variances are listed in Table 5.17 for all the test conditions and controllers. As seen in the table, there is an improvement in the variance of combustion timing in all cases when using the feedforward control scheme. As noted earlier in Table 4.6, the performance of the control using either input of IVC timing or fuel octane is similar.

The measured CA50 values for the tests done at BasePoint2 engine conditions are shown in Figures 5.40 and 5.41 for disturbances in injected fuel energy and engine speed respectively. These plots show the results when using the four different methods of control and when using no control methods at all. In both plots, the deviations of the combustion timing are very apparent for the case when no control is used. In the case where PI control is used, the initial timing deviations can also been seen. In these cases the steps are not large enough to incur engine misfire. However the deviations are quite large in some cases. For the cases where feedforward is used it can be seen that there are no initial deviations from the setpoint, or they are at least not as prominent as the case where only PI control is used. In all the feedback control

cases, there is no steady state error in the combustion timing that can be seen in the case where no control is used. When using feedforward control it is essential to add a slow integral feedback term to eliminate steady state error caused by model mismatch and other slow disturbances such as coolant temperature and intake temperature.

Table 5.17: Variance of different controllers at the five different engine conditions subject to either a load disturbance of 0.05kJ of injected fuel energy or a speed disturbance of 100RPM.

	CA50 variance $[CAD^2]$				
Condition	No Control	PI_{IVC}	PI_{ON}	FF_{IVC}	FF_{ON}
BasePoint1, load disturbance	3.18	0.90	0.92	0.86	0.70
BasePoint1, speed disturbance	7.47	1.92	1.84	1.17	1.30
BasePoint2, load disturbance	2.56	0.81	0.65	0.66	0.49
BasePoint2, speed disturbance	6.99	1.72	1.30	0.84	0.63
BasePoint3, load disturbance	2.81	1.35	2.10	0.91	1.08
BasePoint3, speed disturbance	6.01	1.70	1.90	1.10	1.00
BasePoint4, load disturbance	2.21	1.01	0.79	0.80	0.60
BasePoint4, speed disturbance	2.64	1.48	1.15	1.00	0.70
BasePoint5, load disturbance	4.40	1.16	1.18	0.89	0.99
BasePoint5, speed disturbance	4.18	1.68	1.90	0.94	1.48

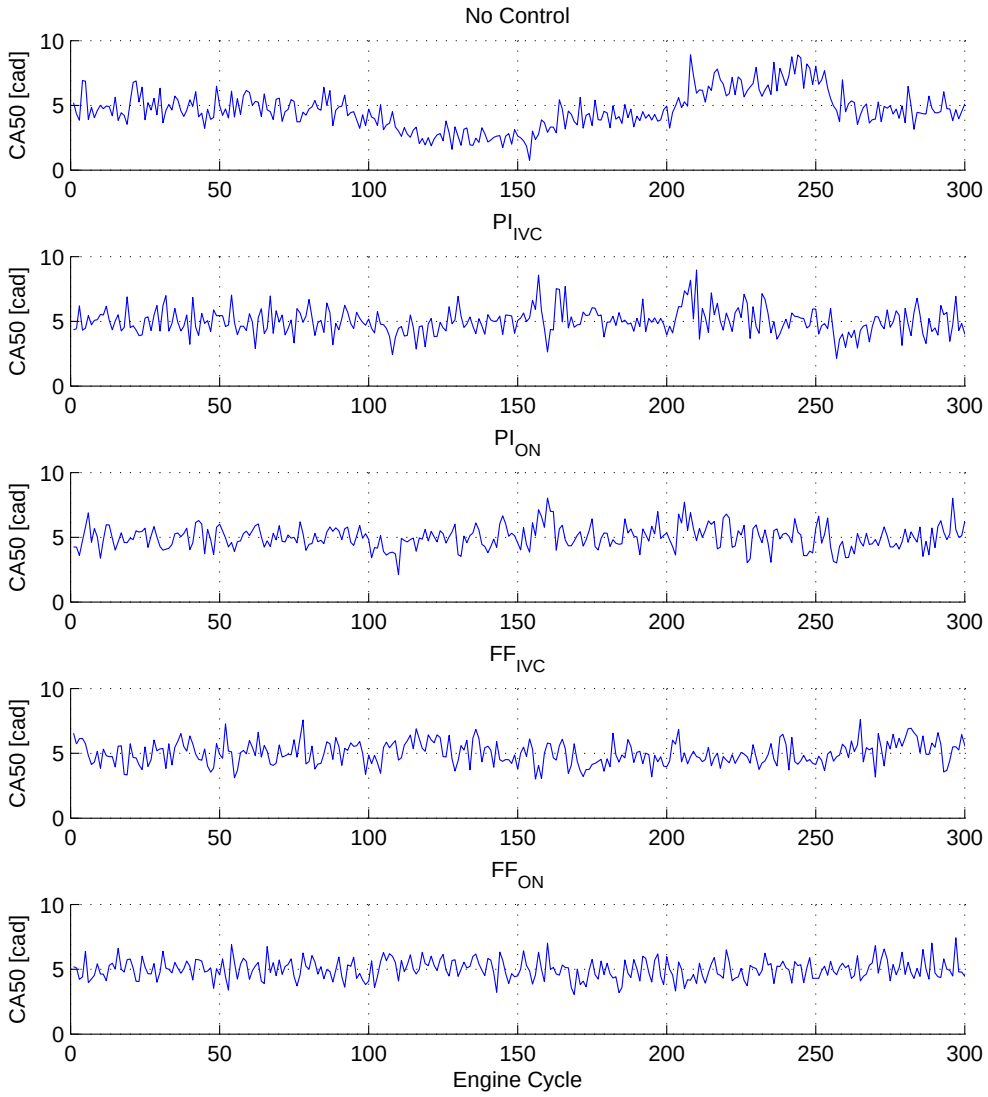

Figure 5.40: Injected fuel energy disturbance rejection - CA50 plotted for a disturbance of 50J at engine cycle 100. Time sequence of no control; PI control using IVC timing; PI control using fuel octane number; feedforward control using IVC timing; and feedforward control using fuel octane number. (test points $FF4E_{OL}$, $FF4E_{PIivc}$, $FF4E_{PIon}$ $FF4E_{FFivc}$, and $FF4E_{FFon}$)

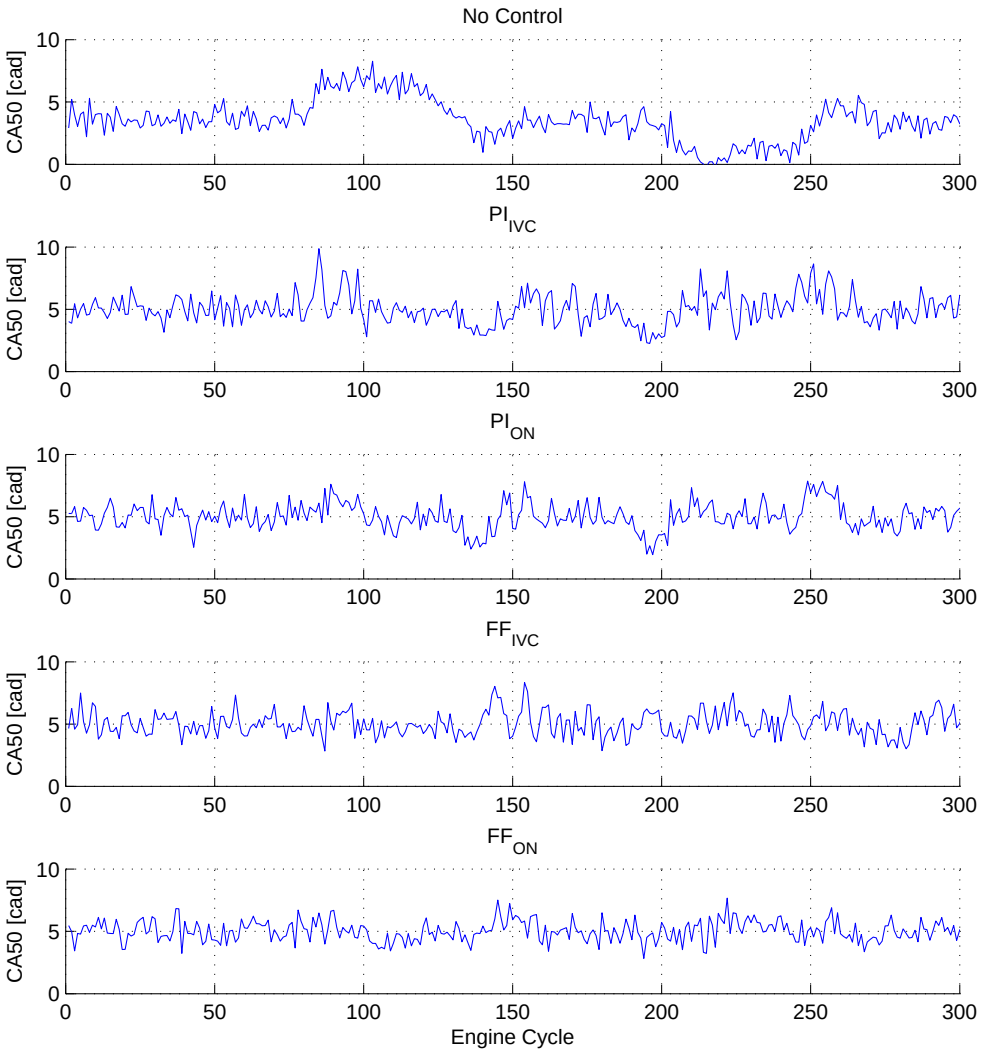

Figure 5.41: Engine speed disturbance rejection - CA50 plotted for a disturbance of 100RPM at engine cycle 100. Time sequence of no control; PI control using IVC timing; PI control using fuel octane number; feedforward control using IVC timing; and feedforward control using fuel octane number. (test points $FF4RPM_{OL}$, $FF4RPM_{PIivc}$, $FF4RPM_{PIon}$ $FF4RPM_{FFivc}$, and $FF4RPM_{FFon}$)

The controllers are also tested for their ability to reject multiple disturbances. For these tests the injected fuel energy is stepped 50J at the 100th engine cycle, and the engine speed is simultaneously increased by 100RPM. At the 150th engine cycle

the inputs are stepped back to their original values. At the 200th engine cycle these inputs are stepped in the other direction for a similar duration of 50 engine cycles. The results of this test for BasePoint2 engine conditions can be seen in Figure 5.42. For this test the variance in CA50 is 2.66, 1.38, 1.22, 0.88, and 0.85 for no control, PI control with IVC timing, PI control with fuel octane, feedforward control with IVC timing, and feedforward control with fuel octane. A definite improvement is seen between using the PI control and feedforward control, and both control methods shown substantial improvement over the uncompensated case.

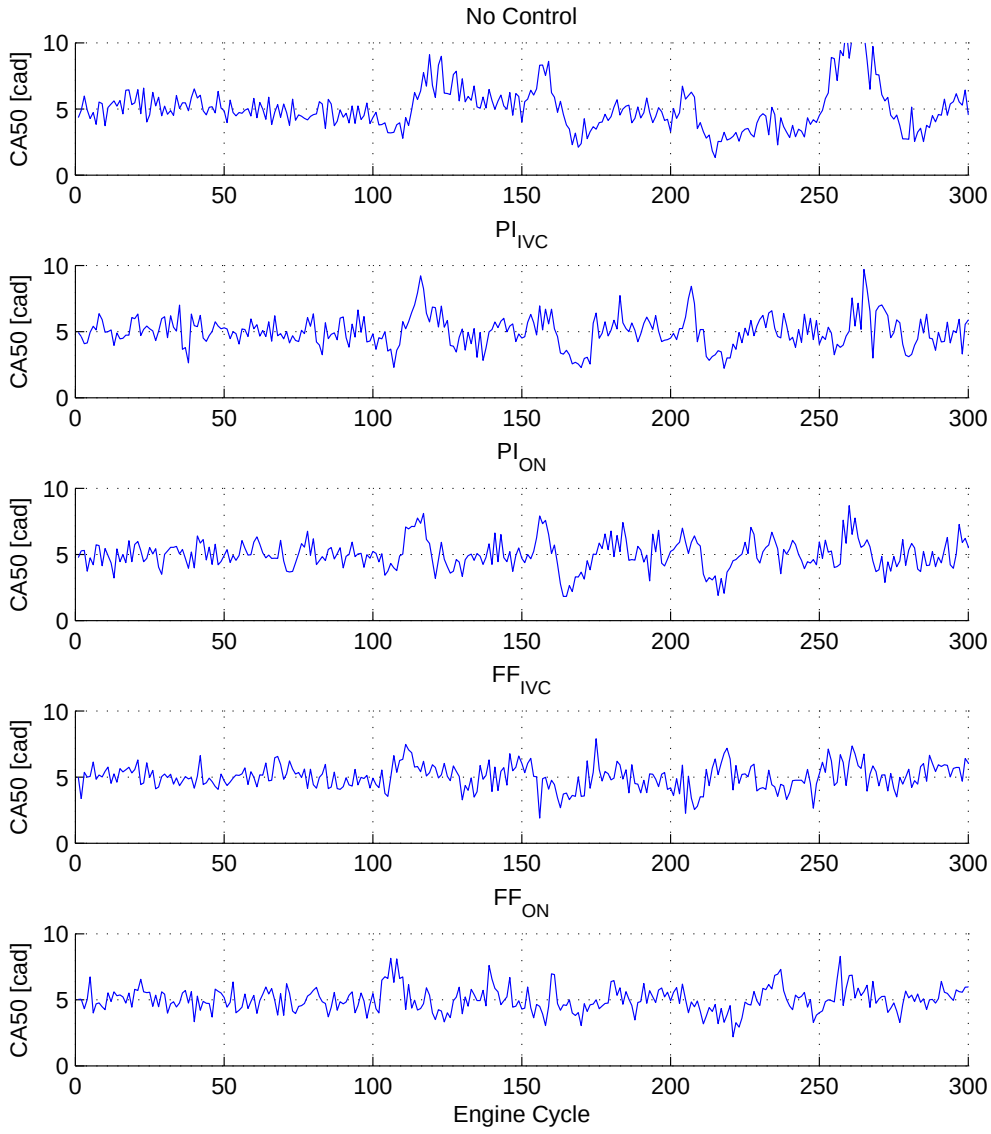

Figure 5.42: Multiple disturbance rejection - CA50 plotted for a disturbance of 1000RPM at engine cycle 100. Time sequence of no control; PI control using IVC timing; PI control using fuel octane number; feedforward control using IVC timing; and feedforward control using fuel octane number. (test points $FF2MULT_{OL}$, $FF2MULT_{PIivc}$, $FF2MULT_{PIon}$ $FF2MULT_{FFivc}$, $FF2MULT_{FFon}$)

5.3 Summary

In this chapter system identification techniques are used to identify process models. IVC timing, fuel octane, injected fuel energy and engine speed, are the four different inputs used, and their effects on the HCCI combustion timing, CA50, is found. Figure 5.43 shows a diagram of the four separate models that are identified. It is seen that ARMAX models give similar results to Box-Jenkins models. Residual analysis is done to show how well each model predicts the combustion timing. Most models are found have more than a 50% fit percent. Different sizes of inputs excitation are used to evaluate the input-output relationship linearity and it is found that the model can be assumed to be linear in the range tested. Models are identified at each of the five different engine conditions outlined in Table 3.3. The models from the different conditions are found to be very similar in their dynamic performance and their steady state gain. A model is also made from the combination of the data from all five test points, and the fit of this model is found to be quite good.

The identified models are used to derive feedforward controllers. This is done to try to eliminate the transient error in combustion timing seen in Chapter 4 when the engine was subject to known load and speed disturbances. The feedforward controllers are first simulated to ensure that they are stable and function as expected. A transient error is present in the simulations despite model inversion due to the time delays of the system. The controllers are experimentally tested against PI controllers and a case where no control is used. These controllers are tested for both engine speed and injected fuel energy disturbances at the five engine conditions outlined in Table 3.3. The combustion timing variance is computed for all these tests and the results show that feedforward controllers have lower CA50 variation than the PI controllers. No significant difference in the error variance is seen between using IVC timing and fuel octane controllers.

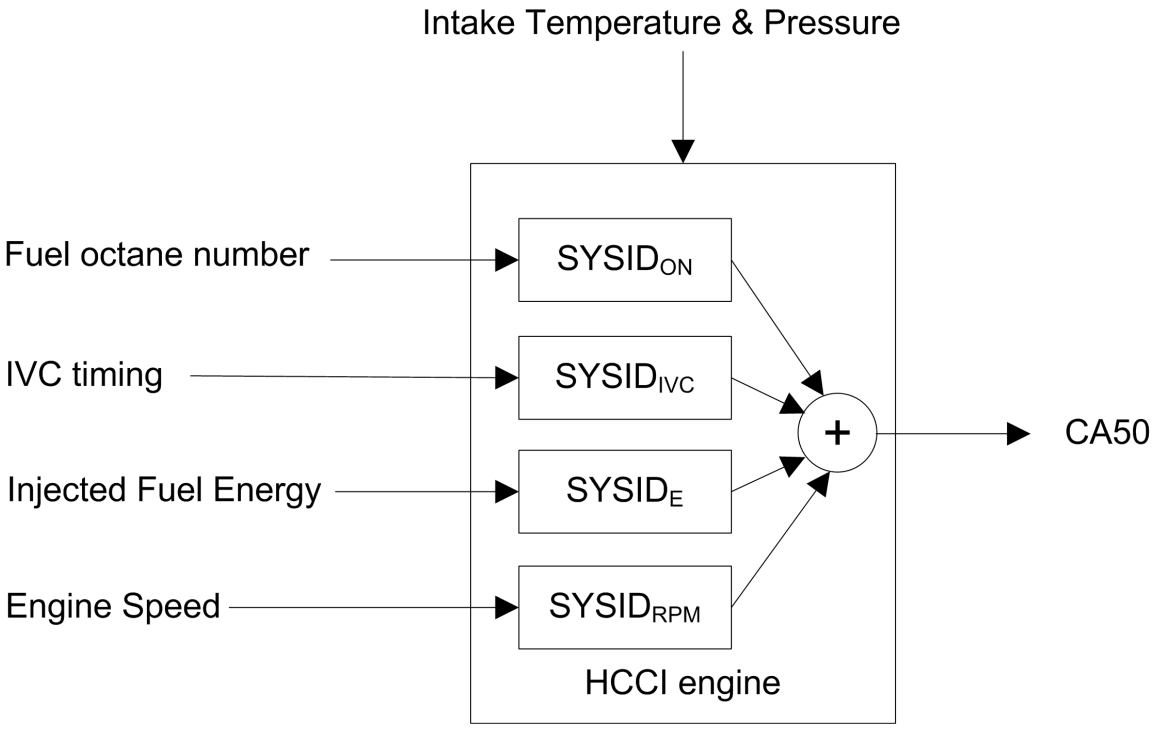

Figure 5.43: Summary block diagram of the process models that are found using system identification techniques.

Chapter 6

Conclusion

This chapter summarizes the important results obtained in this study and conclusions are listed. Alternate algorithms for HCCI control are suggested. Different actuators are discussed and suggestions are made for modifications to the experimental setup.

6.1 Conclusions

In this study a single cylinder research engine is equipped with a cylinder head incorporating a variable camshaft phasing. Using 0.1 ° crank angle based cylinder pressure measurements and a combustion analysis system to compute the real-time combustion timing (CA50) as an output feedback control is implemented. Two different input actuation methods are implemented: one uses the camshaft phasing to modulate the effective compression ratio; and the other adjusts the fuel octane using two independent fuel injection systems. PI feedback control and feedforward control using model inversion is tested. The models are identified using system identification methods.

Major results and conclusions:

- Proportional Integral (PI) controllers are found to provide satisfactory results in regulating HCCI combustion timing for the cases tested. The controllers using two different actuation methods of IVC timing and fuel octane are able

to compensate for disturbances in both engine speed and injected fuel energy. However, large errors are present in some cases, and these are sometimes seen to cause engine misfire, which is undesirable. Similar variances during regulatory control are found for the two controllers using each independent method of actuation; IVC timing and fuel octane.

- Although the combustion timing (CA50) is regulated to 5 °aTDC poor combustion occurred in low dilution level cases due to the increase level of knock intensity.

- Regulatory PI control is tested over a range of injected fuel energy. It is found that the load range using fuel octane control is larger than the range obtained with IVC timing control. This is due to the effect the IVC timing has on the dilution of the air fuel mixture.

- The indicated efficiency is found to change for different load levels even when the CA50 timing is regulated. This suggests that an engine speed/engine load defined valued of a CA50 setpoint is required for optimal engine efficiency.

- System identification techniques are used to identify process models at five different engine conditions. The models are found to be quite similar for the different engine conditions. A single model is made using data from all five engine conditions. This model is found to simulate the dynamics quite well.

- The average process models are inverted to form feedforward controllers to improve the measured disturbance rejection. The feedforward controllers are found to perform better than the PI controllers.

6.2 Future Work

There are many avenues that could be further pursued to improved the control of HCCI as well as improve it's limited operating range.

- It was seen that the burn duration of the HCCI combustion event changes at different engine conditions. This parameter was noted to affect the optimum timing of CA50, so it is suggested that the setpoint of CA50 should be a function of the burn duration, or a modeled estimate of the burn duration.

- It was noted that poor combustion resulted in some cases due to the increased knock intensity. This poor combustion is characterized by increased NVH as well as potentially higher levels of NO_x. This increased knock could be avoided if a measure of the knock intensity is used as a feedback parameter for a multi-input controller.

- For this study only single input/single output controllers are investigated. It is possible that a more optimal controller scheme could be made by using both the IVC timing control and fuel octane control.

- The experimental setup used in this study is also equipped with variable phasing on the exhaust camshaft. This actuator could be used to adjust the internal EGR which has been shown to be very influential on the HCCI combustion [Zhao, 2007a].

Bibliography

[NOm, 1994] (1994). *HORIBA CLA-510SS Instruction Manual*.

[THC, 1999] (1999). *HORIBA FIA-510 Instruction Manual*.

[O2m, 1999] (1999). *Siemens ULTRAMAT 6E/F, OXYMAT 6E/F Instruction Manual*. Siemens.

[mat, 2006] (2006). *Matlab: System Identificaiton Toolbox*. The MathWorks, Inc., v6.1.3 edition.

[e55, 2007] (2007). *"Mercedes-Benz Internal Service Manual for Engine Models 272 and 273"*.

[A&D Technologies, 2001] A&D Technologies (2001). *BASELINE CAS Manual*.

[A&D Technologies, 2003] A&D Technologies (2003). *ADAPT 4.6 User Manual*.

[AG, 2007] AG, D. (2007). Mercedes-Benz Presents the Future of the Gasoline Engine: DiesOtto Gasoline Engine with Diesel Genes. 2007.

[Agrell et al., 2003a] Agrell, F., Angstrom, H.-E., Eriksson, B., Wikander, J., and Linderyd, J. (2003a). Transient Control of HCCI Through Combined Intake and Exhaust Valve Actuation. *SAE 2003-01-3172*.

[Agrell et al., 2005a] Agrell, F., Angstrom, H.-E., Eriksson, B., Wikander, J., and Linderyd, J. (2005a). Control of HCCI During Engine Transients by Aid of Variable

Valve Timings Through the Use of Model Based Non-Linear Compensation. *SAE 2005-01-0131.*

[Agrell et al., 2005b] Agrell, F., Angstrom, H.-E., Eriksson, B., Wikander, J., and Linderyd, J. (2005b). Transient Control of HCCI Combustion by aid of Variable Valve Timing Through the use of a Engine State Corrected CA50- Controller Combined with an In-Cylinder State Estimator Estimating Lambda. *SAE 2005-01-2128.*

[Agrell et al., 2003b] Agrell, F., Eriksson, B., Angstrom, H.-E., and amd Johan Linderyd, J. W. (2003b). Integrated Simulation and Engine Test of Closed-Loop HCCI Control By Aid of Variable Valve Timings. *SAE 2003-01-0748.* Collection.

[Atkins, 2004] Atkins, M. (2004). Experiemntal Examination of the Effects of Fuel Octane and Dilutent on HCCI Combustion. Master's thesis, University of Alberta.

[Atkins and Koch, 2003] Atkins, M. A. and Koch, C. R. (2003). A Well-to-Wheel Comparison of Several Powertrain Technologies. *SAE Paper 2003-01-0081.*

[Atkins and Koch, 2005] Atkins, M. J. and Koch, C. R. (2005). The Effect of Fuel Octane and Diluent on HCCI Combustion. *Proc. IMechE, Part D*, 219:665 – 675.

[Bengtsson, 2004] Bengtsson, J. (2004). *Closed-Loop Control of HCCI Engine Dynamics.* PhD thesis, Lund University.

[Bengtsson et al., 2004] Bengtsson, J., Strandh, P., Johansson, R., Tunestal, P., and Johansson, B. (2004). Cycle-To-Cycle Control of a Dual-Fuel HCCI Engine. *SAE 2004-01-0941.* Collection.

[Bengtsson et al., 2006a] Bengtsson, J., Strandh, P., Johansson, R., Tunestal, P., and Johansson, B. (2006a). Hybrid control of homogeneous charge compression ignition (HCCI) engine dynamics. *International Journal of Control*, 79(5):422 – 48.

[Bengtsson et al., 2006b] Bengtsson, J., Strandh, P., Johansson, R., Tunestal, P., and Johansson, B. (2006b). Model predictive control of homogeneous charge compression ignition (HCCI) engine dynamics. Munich, Germany.

[Bengtsson et al., 2006c] Bengtsson, J., Strandh, P., Johansson, R., Tunestal, P., and Johansson, B. (2006c). Multi-Output Control of a Heavy Duty HCCI Engine Using Variable Valve Actuation and Model Predictive Control. *SAE 2006-01-0873*.

[Bengtsson et al., 2007] Bengtsson, J., Strandh, P., Johansson, R., Tunestal, P., and Johansson, B. (2007). Hybrid modelling of homogeneous charge compression ignition (HCCI) engine dynamics - A survey. *International Journal of Control*, 80(11):1814 – 1848.

[Borg, 2003] Borg, J. (2003). Hitachi North America. Personal Communication.

[Borg et al., 2006] Borg, J. M., Saikalis, G., Oho, S., and Cheok, K. C. (2006). Knock Signal Analysis Using the Discrete Wavelet Transform. *SAE 2006-01-0226*.

[Chang et al., 2007] Chang, K., Lavoie, G. A., Babajimopoulos, A., Filipi, Z. S., and Assanis, D. N. (2007). Control of a Multi-Cylinder HCCI Engine During Transient Operation by Modulating Resiudal Gas Fraction to Compensate for Wall Temperature Effects. *SAE 2007-01-0204*.

[Checkel and Dale, 1986] Checkel, D. and Dale, D. (1986). Computerized Knock Detection From Engine Pressure Records. *SAE 860028*.

[Chiang and Stefanopoulou, 2007] Chiang, C.-J. and Stefanopoulou, A. (2007). Stability analysis in homogeneous charge compression ignition (HCCI) engines with high dilution. *IEEE Transactions on Control Systems Technology*, 15(2):209 – 19.

[Chiang et al., 2007] Chiang, C.-J., Stefanopoulou, A. G., and Jankovic, M. (2007). Nonlinear observer-based control of load transitions in homogeneous charge com-

pression ignition engines. *IEEE Transactions on Control Systems Technology*, 15(3):438 – 448.

[Department of Energy, 2007] Department of Energy, U. G. (2007). Energy Consumption by Sector, Selected Years, 1949-2007. Technical report.

[Draper, 1933] Draper, C. S. (1933). The Physical Effects of Detonation in a Closed Cylindrical Chamber. Technical Report 493, National Advisory Committee for Aeronautics.

[dSPACE GmbH, 2004] dSPACE GmbH (2004). *MicroAutoBox: Hardware Installation and Configuration*.

[Eng, 2002] Eng, J. A. (2002). Characterization of Pressure Waves in HCCI Combustion. *SAE 2002-01-2859*.

[Franklin et al., 1998] Franklin, G., Powell, D., and Workman, M. (1998). *Digital Control of Dynamic Systems*. Addison Wesley Longman, Inc.

[Garcia and Morari, 1982] Garcia, C. E. and Morari, M. (1982). Internal Model Control - 1. Unifying review and some new results. *Industrial & Engineering Chemistry, Process Design and Development*, 21(2):308 – 323.

[Haraldsson et al., 2004] Haraldsson, G., Hyvonen, J., Tunestal, P., and Johansson, B. (2004). HCCI Closed-Loop Combustion Control Using Fast Thermal Management. *SAE 2004-01-0943*. Collection.

[Heywood, 1988] Heywood, J. B. (1988). *Internal Combustion Engine Fundamentals*. McGraw-Hill, Inc.

[Hildingsson et al., 2005] Hildingsson, L., Persson, H., Johansson, B., Collin, R., Nygran, J., Richter, M., Alden, M., Hasegawa, R., and Yanagihara, H. (2005). Optical

Diagnostics of HCCI and UNIBUS Using 2-D PLIF of OH and Formaldehyde. *SAE 2005-01-0175*.

[Hyvonen et al., 2003] Hyvonen, J., Haraldsson, G., and Johansson, B. (2003). Operating Range in a Multi Cylinder HCCI Engine Using Variable Compression Ratio. *SAE 2003-01-1829*.

[Johnson and Moradi, 2005] Johnson, M. A. and Moradi, M. H. (2005). *PID Control: New Identificatioin and Design Methods*. Springer.

[Kalghatgi, 2007] Kalghatgi, G. T. (2007). Fuel Effects in CAI gasoline engines. In Zhao, H., editor, *Homogeneous Charge Compression Ignition (HCCI) and Controlled Auto Ignition (CAI) Engines for the Automotive Industry*, chapter 9. Woodhead Publishing Limited, Brunel University UK.

[Kiencke and Nielsen, 2000] Kiencke, U. and Nielsen, L. (2000). *Automotive Control Systems: For Engine, Driveline, and Vehicle*. Society of Automotive Engineers.

[Kirchen et al., 2007] Kirchen, P. N., Shahbahkti, M., and Koch, C. R. (2007). A Skeletal Kinetic Mechanism for PRF Combustion in HCCI Engines. *Combustion Science and Technology*, 179:1059–1083.

[Kongsereeparp and Checkel, 2008] Kongsereeparp, P. and Checkel, D. (2008). Study of Reformer Gas Effects on n-Heptane HCCI Combustion Using a Chemical Kinetic Mechanism Optimized by Genetic Algorithm. *SAE 2008-01-0039*.

[Kongsereeparp and Checkel, 2007] Kongsereeparp, P. and Checkel, M. D. (2007). Novel Method of Setting Initial Conditions for Multi-Zone HCCI Combustion Modelling. *SAE 2007-01-0674*.

[Kulzer et al., 2007] Kulzer, A., Hathout, J.-P., Sauer, C., Karrelmeyer, R., Fischer, W., and Christ, A. (2007). Multi-Mode Combustion Strategies with CAI for a GDI Engine. *SAE 2007-01-0214*.

[Kusakak et al., 2002] Kusakak, J., ichiro Tsuzuki, K., Daisho, Y., and Saito, T. (2002). A numerical study oncombustion and exhaust gas emissions characteristics of a dual-fuel natural gas engine using a multi-dimensional model combined with detailed kinetics. *SAE 2002-01-1750*.

[Lavy et al., 2000] Lavy, J., Dabadie, J.-C., Angelberger, C., Duret, P., Willand, J., Juretzka, A., Schalfein, J., Ma, T., Lendresse, Y., Satre, A., Schulz, C., Kramer, H., Zhao, H., and Damiano, L. (2000). Innovative Ultra-low NOx Controlled Auto-Ignition Combustion Process for Gasoline Engines: the 4-Space Project. *SAE 2000-01-1837*.

[Levine, 1996] Levine, W. S., editor (1996). *The Control Handbook*. CRC Press LLC.

[Livengood and Wu, 1955] Livengood, J. C. and Wu, P. C. (1955). Corrleation of Autoignition of Hydrocarbon Fuels at High Temperature and Pressures-Fitting of a Mathematical Model. *Proceedings of Fifth International Symposium on Combustion*, page 347.

[Ljung, 1987] Ljung, L. (1987). *System Identification: Theory for the user*. Prentice-Hall, Inc.

[Lupul, 2008] Lupul, R. (2008). Steady State and Transient Characterization of a HCCI Engine with Varying Octane Fuel. Master's thesis, University of Alberta.

[Matthews et al., 2005] Matthews, J., Santoso, H., and Cheng, W. K. (2005). Load Control for an HCCI Engine. *SAE 2005-01-0150*.

[Mayr, 1970] Mayr, O. (1970). *The Origins of Feedback Control*. Cambridge, MA: MIT Press.

[Milovanovic et al., 2005] Milovanovic, N., Blundell, D., Pearson, R., Turner, J., and Chen, R. (2005). Enlarging the Operational Range of a Gasoline HCCI Engine by Controlling the Coolant Temperature. *SAE 2005-01-0157*.

[Montgomery and Runger, 2003] Montgomery, D. C. and Runger, G. C. (2003). *Applied Statistics and Probablility for Engineers*. John Wiley & Sons, Inc.

[Motors, 2007] Motors, G. (2007). GM Takes New Combustion Technology Out of the Lab and Onto the Road. 2007.

[Najt and Foster, 1983] Najt, P. M. and Foster, D. E. (1983). Compression-Ignited Homogeneous Charge Combustion. *SAE 830264*.

[Olsson et al., 2004] Olsson, J.-O., Tunestal, P., and Johansson, B. (2004). Boosting for High Load HCCI. *SAE 2004-01-0940*.

[Olsson et al., 2001] Olsson, J.-O., Tunestl, P., and Johansson, B. (2001). Closed-Loop Control of an HCCI Engine. *SAE 2001-01-1031*.

[Onishi et al., 1979] Onishi, S., Jo, S. H., Shoda, K., Jo, P. D., and Kato, S. (1979). Active Thermo-Atmosphere Combustion (ATAC)- A New Combustion Process for Internal Combustion Engines. *SAE 790501*.

[Pfeiffer et al., 2004] Pfeiffer, R., Haraldsson, G., Olsson, J.-O., Tunestal, P., Johansson, R., and Johansson, B. (2004). System identification and LQG control of variable-compression HCCI engine dynamics. In *International Conference on Control Applications*, volume 2, pages 1442 – 1447, Taipei, Taiwan.

[Rassweiler and Withrow, 1938] Rassweiler, G. M. and Withrow, L. (1938). Motion Pictures of Engine Flames Correlated with Pressure Cards. *SAW Trans.*, 83:185–204.

[R.Turns, 2000] R.Turns, S. (2000). *An Introduction To Combustion*. McGraw-Hill.

[Santoso et al., 2005] Santoso, H., Matthews, J., and Cheng, W. K. (2005). Managing SIHCCI Dual-Mode Operation. *SAE 2005-01-0162*.

[Shahbakhti and Koch, 2008] Shahbakhti, M. and Koch, C. R. (2008). Characterizing the Cyclic Variability of Ignition Timing in an HCCI Engine Fueled with n-Heptane/iso-Octane Blend Fuels. *International Journal of Engine Research*.

[Shahbakhti et al., 2007a] Shahbakhti, M., Lupul, R., Audet, A., and Koch, C. R. (2007a). Experimental Study of HCCI Cyclic Variations for Low-Octane PRF Fuel Blends. In *Combustion Institute/Canadian Section (CI/CS) Spring Technical Meeting*.

[Shahbakhti et al., 2007b] Shahbakhti, M., Lupul, R., and Koch, C. (2007b). Sensitivity Analysis & Modeling of HCCI Auto-Ignition Timing. In *Fifth IFAC Symposium on Advances in Automotive Control*, pages 303–310.

[Shahbakhti et al., 2007c] Shahbakhti, M., Lupul, R., and Koch, C. R. (2007c). Predicting HCCI Auto-Ignition Timing by Extending a Modified Knock-Integral Method. *SAE 2007-01-0222*.

[Shaver et al., 2005] Shaver, G., Roelle, M., and Gerdes, J. (2005). Decoupled control of combustion timing and work output in residual-affected HCCI engines. In *American Control Conference*, volume vol. 6, pages 3871 – 6, Portland, OR, USA.

[Shaver et al., 2006a] Shaver, G. M., Roelle, M., and Gerdes, J. C. (2006a). A two-input two-output control model of HCCI engines. In *American Control Conference*, volume 2006, pages 472 – 477, Minneapolis, MN, United States.

[Shaver et al., 2006b] Shaver, G. M., Roelle, M. J., and Gerdes, J. C. (2006b). Modeling cycle-to-cycle dynamics and mode transition in HCCI engines with variable valve actuation. *Control Engineering Practice*, 14(3 SPEC ISS):213 – 222.

[Sheppard et al., 2002] Sheppard, C., Tolgane, S., and Woolley, R. (2002). On the Nature of Autoignition Leading to Knock in HCCI Engines. *SAE 2002-01-2831.*

[Skogestad and Postlethwaite, 2005] Skogestad, S. and Postlethwaite, I. (2005). *Multivariable Feedback Control.* John Wiley & Sons Ltd.

[Souder et al., 2004] Souder, J. S., Mack, J. H., Hedrick, J. K., and Dibble, R. W. (2004). Microphones and knock sensors for feedback control of HCCI engines. In *ASME Internal Combustion Engine Division*, Long Beach, CA, United States.

[Stone, 1999] Stone, R. (1999). *Introduction to Internal Combustion Engines.* Society of Automotive Engineers, Inc.

[Strandh et al., 2005] Strandh, P., Bengtsson, J., Johansson, R., Tunestl, P., and Johansson, B. (2005). Variable Valve Actuation for Timing Control of a Homogeneous Charge Compression Ignition Engine. *SAE 2005-01-0147.*

[Swan et al., 2007] Swan, K., Shahbakhti, M., and Koch, C. R. (2007). Predicting Start of Combustion Using a Modified Knock Integral Method for an HCCI Engine. In *SAE 2006 Transactions Journal of Engines*, number ISBN 978-0-7680-1835-6, pages 611–620. Society of Automotve Engineers. SAE 2006 Transactions.

[Taylor, 1977] Taylor, C. F. (1977). *The Internal Combustion Engine in Theory and Practice Volume 2: Combustion, Fuels, Materials, Design.* MIT Press.

[Tetsuo Ohmura and Iida, 2006] Tetsuo Ohmura, M. I. and Iida, N. (2006). A Study on Combustion Control by Using Internal and External EGR for HCCI Engines Fuelled with DME. *SAE 2006-35-0045*.

[Tunestal and Johansson, 2007] Tunestal, P. and Johansson, B. (2007). HCCI Control. In Zhao, H., editor, *Homogeneous Charge Compression Ignition (HCCI) and Controlled Auto Ignition (CAI) Engines for the Automotive Industry*, chapter 7. Woodhead Publishing Limited, Brunel University UK.

[Vernhaegen and Verdult, 2007] Vernhaegen, M. and Verdult, V. (2007). *Filtering and System Identification*. Cambridge University Press.

[Vressner et al., 2003] Vressner, A., Lundin, A., Christensen, M., Tunestal, P., and Johnasson, B. (2003). Pressure Oscillations During Rapid HCCI Combustion. *SAE 2003-01-3217*.

[Westbrook et al., 2002] Westbrook, C. K., Pitz, W. J., Boercker, J. E., Curran, H. J., Griffiths, J. F., Mohamed, C., and Ribaucor, M. (2002). Detailed chemical kinetic reaction mechanisms for autoignition of isomers of heptane under rapid compression. In *Proceedings of the Combustion Institute*, pages 1311–1318.

[Zhao, 2007a] Zhao, H. (2007a). Four-Stroke CAI engines with residual gas trapping. In Zhao, H., editor, *Homogeneous Charge Compression Ignition (HCCI) and Controlled Auto Ignition (CAI) Engines for the Automotive Industry*, chapter 5. Woodhead Publishing Limited, Brunel University UK.

[Zhao, 2007b] Zhao, H. (2007b). Motivation, Defenition, and History of HCCI/CAI. In Zhao, H., editor, *Homogeneous Charge Compression Ignition (HCCI) and Controlled Auto Ignition (CAI) Engines for the Automotive Industry*, chapter 1. Woodhead Publishing Limited, Brunel University UK.

[Zhao, 2007c] Zhao, H. (2007c). Overview of CAI/HCCIgasoline Engines. In Zhao, H., editor, *Homogeneous Charge Compression Ignition (HCCI) and Controlled Auto Ignition (CAI) Engines for the Automotive Industry*, chapter 2. Woodhead Publishing Limited, Brunel University UK.

Appendix A

Experimental Data Summary

A.1 Repeatability Analysis

To quantify the repeatability of the experiential apparatus the IVC timing sweep for BasePoint1 is repeated on 5 different occasions. The IVC timing range perturbs most of the important measured parameters of the engine. A plot of the CA50 timing as function of the IVC timing for the five different sweeps is shown in Figure A.1. Here it is seen that all five sweeps show a similar trends but that each sweep is not identical. Error bars are also shown in this figure. Part of the error in the resulting combustion timing results in the inability to recreate identical experimental conditions, and part of the error is due to the uncertainty of the measurements, sensor accuracy, resolution, repeatability and time variability of the engine.

The mean and average values of the engine operating conditions are shown in Table A.1. These values are calculated for three different points along the IVC timing sweep; one at the center of the range ($IVC = 215^oaTDC$) and the other two at the limits of combustion ($IVC = 205$ and 215^oATDC). In this table the mean and standard deviation of the intake manifold temperature is shown, T_{man}. It is seen that the mean value of this parameter does not change appreciably over the timing sweep and that the standard deviation of this parameter is below 1^oC for the whole

range. This is important since HCCI is very sensitive to the intake temperature. The coolant temperature, T_{cool} is also shown in this table. The mean value of the coolant temperature does not change more than 0.5^oC over the timing sweep and the standard deviation does not get higher than 1.2^oC. HCCI combustion is also very sensitive to the temperature of the coolant, so the stability and consistency of this parameter is also very important. The manifold pressure, P_{man}, does not change substantially over the timing sweep range and its standard deviation is below 0.3kPa. The mean engine speed is nearly identical for the three different valve timings seen in the table, and the standard deviations are very low. Also shown are the mean values and standard deviations for the intake and exhaust timings. The standard deviations of these values are below 0.5^o's.

The mean and standard deviations of the measured engine parameters are shown in Table A.2. These values are calculated for three different points along the IVC timing sweep; one at the center of the range ($IVC = 215^oaTDC$) and the other two at the limits of combustion ($IVC = 205and215^oATDC$). In the first row of this table the mean and standard deviation of CA50 are shown. The maximum standard deviation of the CA50 is almost 1 °at the latest IVC timing. It is noticed that as the mean value of CA50 gets later in the cycle, that the standard deviation of this value increases. The standard deviations of the measured $IMEP$ values are seen to be quite low, with the maximum of $0.06bar$, or 1.5% of the mean value. A similar magnitude of deviation is also seen in the measurement of torque, where the maximum standard deviation is $0.42Nm$, or 0.2% of the mean value. The $IMEP$ measurement is calculated with the in-cylinder pressure transducer while the torque measurement uses a load cell located where the engine load is applied; the torque includes the internal friction of the engine. This internal friction is mainly a function engine speed which is constant for these tests shown here [Heywood, 1988], so a similar magnitude of deviation is expected between IMEP and torque, which is verified here. A maximum of 5% coefficient of

variation of the knock intensity, P_{rms}, is seen in this range of data. Large deviations of the CO, uHC, and CO_2 are seen in this table. In some cases the coefficient of variation of these parameters is as high as 25%. All three of these parameters are measured using the emissions bench. Low variation of the air fuel ratio is seen, the maximum coefficient of variation is 1.7%. A similar error in the measurement of the air flow ratio is seen.

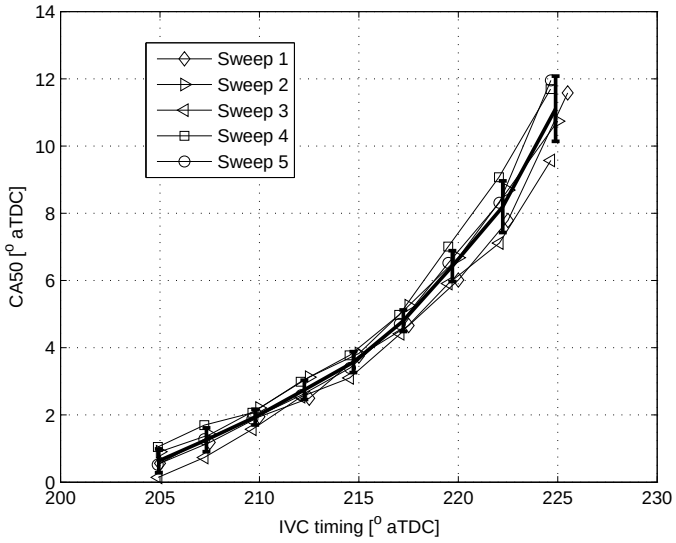

Figure A.1: Repeatability of IVC timing sweep for BasePoint1. Error bars are also shown in the figure.

Table A.1: Repeatability of engine conditions.

	$IVC = 205^oaTDC$		$IVC = 215^oaTDC$		$IVC = 225^oaTDC$	
Input	Mean	Standard Deviation	Mean	Standard Deviation	Mean	Standard Deviation
$T_{man}[^oC]$	59.70	0.89	59.87	0.50	59.99	0.74
$T_{coolant}[^oC]$	69.90	1.02	70.09	1.12	69.55	0.78
$P_{man}[kpa]$	109.00	0.29	109.86	0.21	110.86	0.25
$w_{engine}[RPM]$	1022.67	1.54	1022.50	1.61	1022.45	1.34
$IVC[^oaTDC]$	204.94	0.06	214.73	0.25	224.89	0.37
$EVC[^oaTDC]$	-31.55	0.41	-31.52	0.44	-31.51	0.44

Table A.2: Uncertainty of measured engine parameters.

	$IVC = 205^oaTDC$		$IVC = 215^oaTDC$		$IVC = 225^oaTDC$	
Parameter	Mean	Standard Deviation	Mean	Standard Deviation	Mean	Standard Deviation
$CA50[^oaTDC]$	0.64	0.35	3.57	0.31	11.11	0.97
$IMEP[bar]$	3.77	0.04	3.93	0.02	3.96	0.06
$Torque[Nm]$	16.89	0.27	17.72	0.20	17.67	0.42
$P_{rms}[kPa]$	5.88	0.22	4.61	0.23	2.54	0.13
$CO[\%]$	0.15	0.03	0.16	0.02	0.24	0.05
$uHC[ppm]$	2335.00	182.65	2506.28	171.55	3445.59	387.81
$CO_2[\%]$	5.15	0.05	5.28	0.04	5.33	0.08
$\lambda[-]$	2.51	0.04	2.42	0.04	2.31	0.03
$\dot{m}_{air}[\frac{g}{s}]$	5.27	0.10	5.08	0.08	4.86	0.08

The system identification procedure with data from a different day is done to find out how repeatable the whole analysis is. System identification data was retaken for the $SYSID2$ test point. All the inputs were excited at the same levels using the same PRBS. The models were identified using the same scaling values and pure time delays. To compare the two models, the original models and the repeated ones, the step response of the models was analyzed. The step response of the ARMAX models for excitation of IVC timing, fuel octane, injected fuel energy and engine speed can be seen in Figure A.2, A.3, A.4, and A.5 respectively. From these figures it is seen that the step response of the model from the different days are all very similar, with the exception of the models identified between injected fuel energy and CA50. This experiment is seen to be not very repeatable. The identified models are shown in Table A.3.

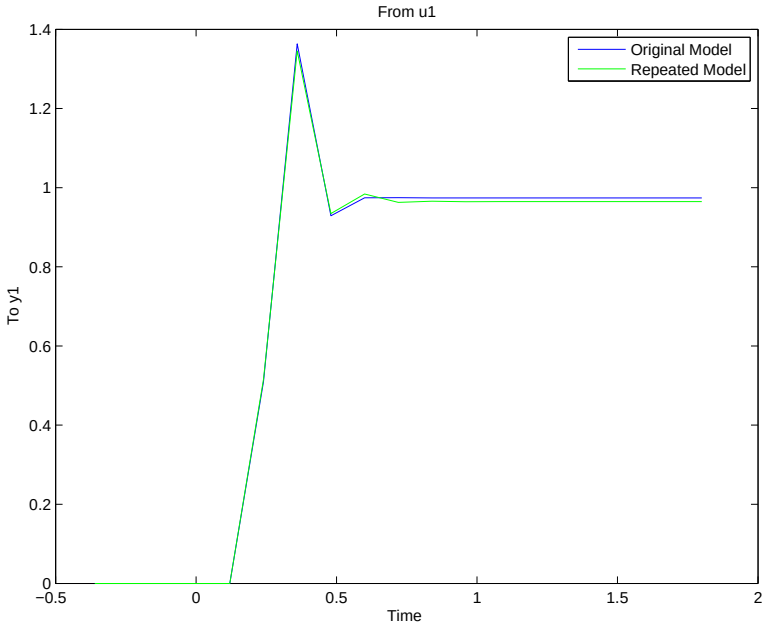

Figure A.2: Repeated SYSID2 test for IVC timing

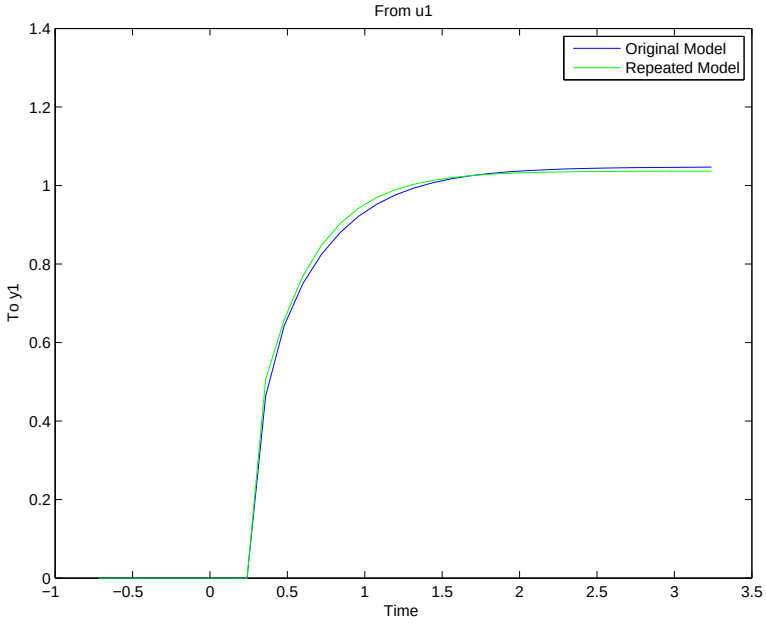

Figure A.3: Repeated SYSID2 test for fuel octane

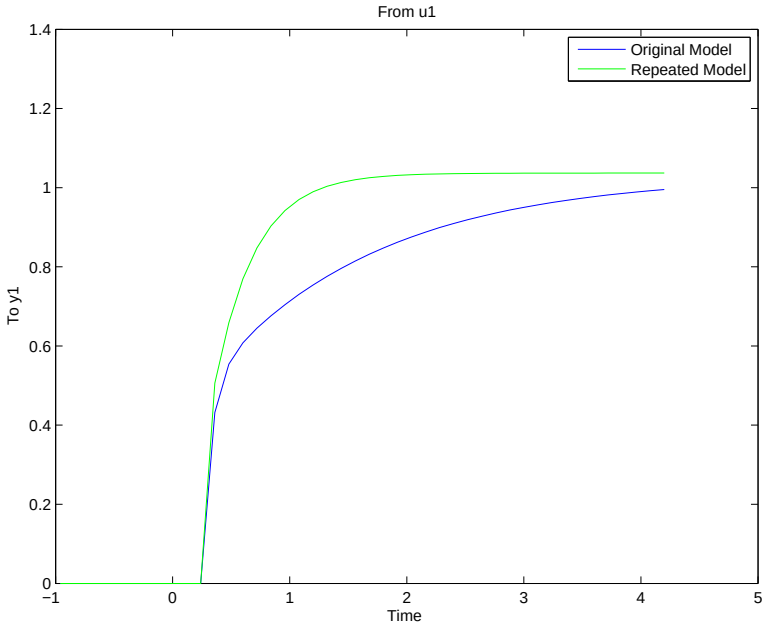

Figure A.4: Repeated SYSID2 test for fuel energy

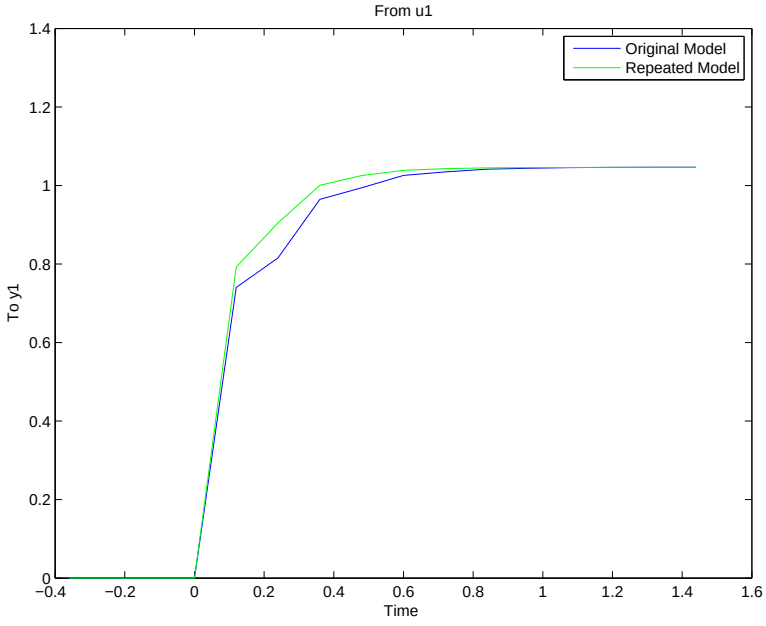

Figure A.5: Repeated SYSID2 test for engine speed

Table A.3: Table of repeated $SYSID2$ Models

Input	Original	Repeated
IVC Timing	$\frac{0.50977(z+2.101)(z-0.2921)}{z^2(z^2+0.1337z+0.01492)}$	$\frac{0.51563(z+2.03)(z-0.3998)}{z^2(z+0.2319)(z-0.2108)}$
Fuel Octane	$\frac{0.46386(z-0.5369)}{z^2(z-0.7521)(z-0.1726)}$	$\frac{0.50611(z-0.3935)}{z^2(z-0.7074)(z+0.01165)}$
Fuel Energy	$\frac{0.43198(z-0.8512)}{z^2(z-0.9206)(z-0.2137)}$	$\frac{0.67369(z-0.7659)}{z^2(z-0.8487)(z-0.05215)}$
Engine Speed	$\frac{0.74z}{(z-0.4909)(z+0.3891)}$	$\frac{0.79z}{(z-0.3961)(z+0.2543)}$

A.2 Description of Data Logs

Data is recorded by three different processors, the baseline CAS system, the ADAPT DAC system and the dSPACE MicroAutobox. Data logging is first initiated on the MicroAutobox which saves for either for 45 seconds at 100Hz, for 300 engine cycles or for 3000 engine cycles. After the dSPACE data log is started the ADAPT data log is initiated, which saves for 45 seconds at 10Hz, then the data save operation for the CAS system is initiated which is currently set up to save for 300 engine cycles (approximately 36 seconds at 1000RPM) or for 3000 engine cycle for system identification data. All these data log operations are started within 3 or 4 seconds of each other.

All the data logging operations are started manually, so they are not in time with each other. All three data loggers save the same trace of CA50 as computed by the CAS computer. If the data logs need to be synchronized it can be done off line using the CA50 measurements of each data logger. Each test must be synchronized individually since the time delays are different for every test.

Once recorded all the data is then transferred to the shared folder HCCI DATA on KOCH-GRAD09. The folders are labeled with the date that the data was taken, and each test is numbered sequentially. Errors occur when taking the data and some tests are deleted or not ever recorded, so some test numbers will not appear. The subfolders contain files recorded by the CAS computer; these folders are labeled with

the test number. The CAS data is initially stored as .001 file type. These files are then post processed by the CAS program into .P01 files which can be read by MatLab. A MatLab script then changes these files to a .mat file. The dSPACE system stores the data as a MatLab structure, while the ADAPT data log is stored as a .csv file.

A MatLab function has been written that takes all the files from the three different data loggers and compiles then into one .mat file. This file is named 'CombinedTest(i)', with i being the test number. Each parameter is renamed to avoid confusion when analysis is done. Tables A.4-A.8 show the parameter names, description, etc. for this .mat file. All the analysis and plotting is done with these combined data files.

Inside the same folder as the combined data logs is also an Excel file that has a summary of the tests that were taken on that date. This spreadsheet contains rounded average values of the main engine parameters, reason each test was taken and important notes on the quality of the data point.

The rest of this Appendix chapter describes the different data sets used in the analysis for this thesis. Some basic parameters of the data points are displayed in the tables, as well as the date and test number of the data set so that further analysis can be done if needed.

Table A.4: Parameter Descriptions - 1

Parameter	Description	Data Logger	Units	Save Rate	Sensor or Actuator
A_Tci	coolant inlet temp	Adapt DAC	deg C	10Hz	$\frac{1}{16}$" JType Thermocouple
A_Tco	coolant outlet temp	Adapt DAC	deg C	10Hz	$\frac{1}{16}$" J-Type Thermocouple
A_Tcr	coolant reservior temp	Adapt DAC	deg C	10Hz	$\frac{1}{8}$" K-Type Thermocouple
A_Te	exhaust temp	Adapt DAC	deg C	10Hz	$\frac{1}{16}$" J-Type Thermocouple
A_To	oil temp	Adapt DAC	deg C	10Hz	$\frac{1}{8}$" K-Type Thermocouple
A_Tcond	condenser tank temp	Adapt DAC	deg C	10Hz	$\frac{1}{8}$" K-Type Thermocouple
A_Tfuel	n-heptane temp	Adapt DAC	deg C	10Hz	$\frac{1}{8}$" K-Type Thermocouple
A_Tor	oil reservoir temp	Adapt DAC	deg C	10Hz	$\frac{1}{8}$" K-Type Thermocouple
A_Txducer	pressure transducer coolant temp	Adapt DAC	deg C	10Hz	$\frac{1}{8}$" K-Type Thermocouple
A_Trunner	intake runner temperature	Adapt DAC	deg C	10Hz	$\frac{1}{16}$" J-Type Thermocouple
A_Tman	intake manifold temperature	Adapt DAC	deg C	10Hz	$\frac{1}{16}$" J-Type Thermocouple
A_Tamb	ambient temperature	Adapt DAC	deg C	10Hz	$\frac{1}{8}$" K-Type Thermocouple
A_Tsuperout	supercharger exit temperature	Adapt DAC	deg C	10Hz	$\frac{1}{8}$" K-Type Thermocouple
A_CO2	carbon dioxide in exhaust	Adapt DAC	%	10Hz	emissions bench

Table A.5: Parameter Descriptions - 2

Parameter	Description	Data Logger	Units	Save Rate	Sensor or Actuator
A_CO	carbon monoxide in exhaust	Adapt DAC	%	10Hz	emissions bench
A_NOx	nitrous oxides in exhaust	Adapt DAC	ppm	10Hz	emissions bench
A_O2	oxygen in exhuast	Adapt DAC	%	10Hz	emissions bench
A_THC	unburned hydrocarbons in exhuast	Adapt DAC	ppm	10Hz	emissions bench
A_AF	air flow rate	Adapt DAC	g/sec	10Hz	laminar air flow meter
A_MF	fuel flow rate, n-heptane	Adapt DAC	kg/hr	10Hz	peirburg PLU4000
A_OP	oil pressure	Adapt DAC	PSI	10Hz	Setra Pressure Transducer
A_EP	exhaust pressure	Adapt DAC	kPa	10Hz	Valadyne Pressure Transducer
A_FP1	n-heptane fuel pressure	Adapt DAC	PSI	10Hz	Setra Pressure Transducer
A_FP2	iso-octane fuel pressure	Adapt DAC	PSI	10Hz	Valadyne Pressure Transducer
A_PBARO	barometric pressure	Adapt DAC	kPa	10Hz	Mercury barometer
A_PMAN	manifold pressure	Adapt DAC	PSI	10Hz	Setra Pressure Transducer
A_PRUN	intake runner pressure	Adapt DAC	kPa	10Hz	Valadyne Pressure Transducer
A_Torque	torque on dynomometer	Adapt DAC	Nm	10Hz	load cell
A_Speed	engine speed	Adapt DAC	RPM	10Hz	proximity sensor
A_SuperSpeed	supercharger speed	Adapt DAC	RPM	10Hz	tachometerr
A_Lambda	wideband o2	Adapt DAC	lambda	10Hz	AFR-1200
A_CA50	ca50 computer by CAS	Adapt DAC	CAD	10Hz	piezoelectric pressure transducer

Table A.6: Parameter Descriptions - 3

Parameter	Description	Data Logger	Units	Save Rate	Sensor or Actuator
D_PWISO	iso-octane total pulse width	dSPACE	ms	2engine revolutions	fuel injector
D_PWHEP	n-heptane pulse width	dSPACE	ms	2engine revolutions	fuel injector
D_FANG	injector pulse end angle	dSPACE	CAD	2engine revolutions	fuel injector
D_RPM	engine speed	dSPACE	RPM	2engine revolutions	hall effect sensor on 36-1 wheel
D_ON	injected PRF value	dSPACE	PRF	2engine revolutions	fuel injector
D_MF	injected fuel mass	dSPACE	g	2engine revolutions	fuel injector
D_E	injected fuel energy	dSPACE	kJ	2engine revolutions	fuel injector
D_NOx	nitrous oxides in exhuast	dSPACE	ppm	2engine revolutions	nox sensor
D_O2	oxygen in exhaust	dSPACE	%	2engine revolutions	wideband O2
D_LAMBDA	air fuel ratio	dSPACE	lambda	2engine revolutions	wideband O2
D_CA50	ca50 computed by CAS	dSPACE	CAD	2engine revolutions	piezoelectric pressure transducer
D_IANGLE	calculated intake phase	dSPACE	CAD	2engine revolutions	intake phaser
D_IVC	calculated IVC	dSPACE	CAD	2engine revolutions	intake phaser
D_EANGLE	calculated exhaust phase	dSPACE	CAD	2engine revolutions	exhaust phaser
D_EVC	calculated EVC	dSPACE	CAD	2engine revolutions	exhaust phaser

Table A.7: Parameter Descriptions - 4

Parameter	Description	Data Logger	Units	Save Rate	Sensor or Actuator
C_rawpress	cylinder pressure trace	CAS	kPa	0.1CAD	piezoelectric pressure transducer
C_rawknock	knock sensor trace	CAS	V	0.1CAD	piezoelectric pressure transducer
C_rawtime	time corresponding to pressure trace	CAS	s	0.1CAD	3600 pulse per rev encoder
C_rawca50	ca50 computed by CAS	CAS	CAD	2engine revolutions	piezoelectric pressure transducer
C_rawimep	imep computed by CAS	CAS	bar	2engine revolutions	piezoelectric pressure transducer
C_rawnmep	net mep computed by CAS	CAS	bar	2engine revolutions	piezoelectric pressure transducer
C_timeca50	time corresponding to ca50 trace	CAS	s	2engine revolutions	3600 pulse per rev encoder
C_rawki	knock intensity from pressure trace	CAS		2engine revolutions	piezoelectric pressure transducer
C_rawknockki	knock intensity from knock trace	CAS		2engine revolutions	knock sensor
C_rawmap	manifold pressure	CAS		1 CAD	Setra Pressure Transducer
C_rawmaptime	time signal from manifold pressure	CAS	s	1CAD	3600 pulse per rev encoder
C_rawvolume	volume trace	CAS		0.1 CAD	3600 pulse per rev encoder

Table A.8: Parameter Descriptions - 5

Parameter	Description	Data Logger	Units	Save Rate	Sensor or Actuator
M_KI	knock intensity	CAS		2engine revolutions	piezoelectric pressure transducer
M_MassFlow	air and fuel flow into engine	post processed	g/s	test average	/
M_Power	power seen at dyno	post processed	W	test average	/
M_arms	Arms	post processed	V	2engine revolutions	/
M_bmep	brake mep	post processed	bar	test average	/
M_bsco	brake specific carbon monoxide	post processed	g/kWhr	test average	/
M_bsco2	brake specific carbon dioxide	post processed	g/kWhr	test average	/
M_bsfc	brake specific fuel consumption	post processed	g/kWhr	test average	/
M_bsnox	brake specific nitrous oxides	post processed	g/kWhr	test average	/
M_bsuhc	brake specific unburned fuel	post processed	g/kWhr	test average	/
M_covimep	coefficient of variation of IMEP	post processed	%	test average	/
M_etaI	indicated efficiency	post processed	%	test average	/
M_fmep	friction mean effective pressure	post processed	bar	test average	/
M_prms	Prms	post processed	bar	2engine revolutions	/
M_stdpman	variation in manifold pressure	post processed	kPa	test average	/
M_stdcool	variation in coolant temperature	post processed	C	test average	/
M_stdint	variation in intake temperature	post processed	C	test average	/

A.3 Data for Chapter 2

Table A.9: Chapter 2 Data

Test Code	Date & Test Number	Speed [RPM]	Engine Load [IMEP]	Timing [CA50]	Exhaust O_2 [%]	fuel octane [PRF]	IVC [°aTDC]	T_{int} [°C]	P_{int} [psi]
$HCCI1$	apr7 08, test36	1029	4.2	4.8	2.23	0	200	40	14.9
$HCCI2$	apr26 08, test7	1025	3.5	11.3	11.1	18	220	60	110
$HCCI3$	apr7 08, test38	1027	4	2.6	2.22	0	200	41	15
$HCCI4$	apr7 08, test39	1023	3.7	5.1	1.88	0	224	41	15.3
$SI1$	jun20 08, test1	1025	4.1	5.1	0.17	100	219	42	62
$MOT1$	apr7 08, test37	1029	3.1	0.8	2.99	0	200	40	14.9
$IEGR1$	apr7 08, test20	1026	3.4	-1.1	2.53	0	200	90	17.2
$IEGR2$	apr7 08, test21	1026	3.4	-0.3	2.57	0	200	88	17.2
$IEGR3$	apr7 08, test22	1026	3.3	0.7	2.62	0	200	87	17.2
$IEGR4$	apr7 08, test23	1026	3.2	0.9	2.65	0	200	87	17.2
$IEGR5$	apr7 08, test24	1026	3.1	1.9	2.71	0	200	86	17.2
$IEGR6$	apr7 08, test25	1025	3.1	1.9	2.74	0	200	87	17.2
$IEGR7$	apr7 08, test26	1025	2.9	3	2.79	0	200	87	17.2
$IEGR8$	apr7 08, test27	1025	2.8	3.2	2.83	0	200	87	17.2
$IEGR9$	apr7 08, test28	1025	2.6	3.7	2.87	0	200	86	17.2
$IEGR10$	apr7 08, test29	1025	3.3	0.1	2.62	0	200	86	17.2
$IEGR11$	apr7 08, test30	1025	3.3	-0.6	2.58	0	200	86	17.4
$IEGR12$	apr7 08, test31	1025	3.3	-1.5	2.52	0	200	87	17.5
$IEGR13$	apr7 08, test32	1025	3.3	1.1	2.67	0	200	86	17.2

A.4 Data for Chapter 3

Table A.10: Knock Intensity Calibration for Chapter 3

Test Code	Date & Test Number	Speed [RPM]	Engine Load [IMEP]	Timing [CA50]	Exhaust O_2 [%]	fuel octane [PRF]	IVC [°aTDC]	T_{int} [°C]	P_{int} [psi]
$KI11$	mar12 08, test1	1026	3.2	-1.2	2.51	0	200	63	16.1
$KI2$	mar12 08, test2	1023	1.6	3.9	3.09	0	204	64	16.2
$KI3$	mar12 08, test3	1023	2.7	3.7	2.83	0	204	64	16.1
$KI4$	mar12 08, test4	1022	3.1	0.9	2.62	0	204	64	16.1
$KI5$	mar12 08, test5	1022	3.2	-0.3	2.53	0	204	64	16.1
$KI6$	mar12 08, test6	1022	3.2	-1.5	2.45	0	204	64	16.1
$KI7$	mar12 08, test7	1022	3.1	-2.6	2.36	0	204	64	16.1
$KI8$	mar12 08, test8	1022	3.1	-3.2	2.29	0	204	64	16.1
$KI9$	mar12 08, test9	1025	3.1	11.5	2.44	0	204	59	12.9
$KI10$	mar12 08, test10	1023	3	7	2.2	0	204	57	13
$KI11$	mar12 08, test11	1023	3.1	5.4	2.13	0	204	55	13
$KI12$	mar12 08, test12	1023	3.2	3.8	2.05	0	204	54	13
$KI13$	mar12 08, test13	1023	3.1	2.2	2	0	204	55	13
$KI14$	mar12 08, test14	1023	3	1.4	1.96	0	204	56	13

Table A.11: Chapter 3 data

Test Code	Date & Test Number	Speed [RPM]	Engine Load [IMEP]	Timing [CA50]	Exhaust O_2 [%]	fuel octane [PRF]	IVC [°aTDC]	T_{int} [°C]	P_{int} [psi]
$IVC11$	Jan 11 08, test50	1200	na	na	na	na	na	na	na
$EVC1$	Jan 11 08, test51	1200	na	na	na	na	na	na	na
$CA50_{cal}$	Jul 8 08, test1	1200	4.6	7.4	0	100	220	22	62.7

Table A.12: Experimental BasePoints for Chapter 3

Test Code	Date & Test Number	Speed [RPM]	Engine Load [IMEP]	Timing [CA50]	Exhaust O_2 [%]	fuel octane [PRF]	IVC [°aTDC]	T_{int} [°C]	P_{int} [psi]
*BasePoint*1	jul22 08, test2	1025	3.9	5.8	10.71	10	220	62	110
*BasePoint*2	jul22 08, test3	1025	4.1	6.6	11.4	28	220	80	126
*BasePoint*3	jul22 08, test4	1025	4.1	6.6	12.11	43	219	101	141
*BasePoint*4	jul22 08, test5	1266	4.1	4.5	11.43	11	220	82	125
*BasePoint*5	jul22 08, test6	1506	3.7	8.4	12.07	6	220	84	125

A.5 Data for Chapter 4

Table A.13: IVC timing sweeps - 1

Test Code	Date & Test Number	Speed [RPM]	Engine Load [IMEP]	Timing [CA50]	Exhaust O_2 [%]	fuel octane [PRF]	IVC [°aTDC]	T_{int} [°C]	P_{int} [kPa]
$BasePoint1_{IVCss}$	April 26, Test 36	1021	3.8	1.2	11.62	10	208	58	109
$BasePoint1_{IVCss}$	April 26, Test 35	1021	3.8	1.9	11.55	10	210	59	110
$BasePoint1_{IVCss}$	April 26, Test 34	1021	3.9	2.5	11.45	10	213	59	110
$BasePoint1_{IVCss}$	April 26, Test 33	1021	3.9	3.8	11.38	10	215	59	110
$BasePoint1_{IVCss}$	April 26, Test 32	1021	4	4.7	11.28	10	218	59	110
$BasePoint1_{IVCss}$	April 26, Test 31	1021	4	5.9	11.19	10	220	59	111
$BasePoint1_{IVCss}$	April 26, Test 28	1021	4	6	11.17	10	220	59	111
$BasePoint1_{IVCss}$	April 26, Test 29	1021	4	7.8	11.07	10	222	59	111
$BasePoint1_{IVCss}$	April 26, Test 30	1021	3.9	11.6	11.01	10	226	59	111
$BasePoint2_{IVCss}$	April 26, Test 79	1024	4	-0.7	12.3	28	200	82	123
$BasePoint2_{IVCss}$	April 26, Test 78	1021	4.1	0.1	12.16	28	205	83	124
$BasePoint2_{IVCss}$	April 26, Test 77	1021	4.2	1.1	12.03	28	210	82	125
$BasePoint2_{IVCss}$	April 26, Test 76	1022	4.3	2.8	11.89	28	215	83	125
$BasePoint2_{IVCss}$	April 26, Test 75	1022	4.3	5.9	11.73	28	220	81	126
$BasePoint2_{IVCss}$	April 26, Test 80	1022	4.3	5.9	11.72	28	220	82	125
$BasePoint2_{IVCss}$	April 26, Test 81	1022	4.3	9.3	11.54	28	225	82	126
$BasePoint3_{IVCss}$	April 27, Test 35	1024	4.1	-0.2	12.61	43	205	105	137
$BasePoint3_{IVCss}$	April 27, Test 34	1024	4.2	0.4	12.57	43	207	105	137
$BasePoint3_{IVCss}$	April 27, Test 33	1024	4.2	1	12.51	43	210	104	137
$BasePoint3_{IVCss}$	April 27, Test 32	1024	4.3	1.8	12.46	43	212	104	138
$BasePoint3_{IVCss}$	April 27, Test 31	1024	4.3	3.2	12.41	43	215	103	138
$BasePoint3_{IVCss}$	April 27, Test 29	1024	4.4	5.5	12.26	43	220	105	139
$BasePoint3_{IVCss}$	April 27, Test 38	1024	4.4	5.7	12.27	43	220	104	139
$BasePoint3_{IVCss}$	April 27, Test 39	1024	4.4	6.8	12.19	43	223	104	139
$BasePoint3_{IVCss}$	April 27, Test 40	1024	4.3	8.9	12.11	43	225	105	140

Table A.14: IVC timing sweeps - 2

Test Code	Date & Test Number	Speed [RPM]	Engine Load [IMEP]	Timing [CA50]	Exhaust O_2 [%]	fuel octane [PRF]	IVC [°aTDC]	T_{int} [°C]	P_{int} [kPa]
$BasePoint4_{IVCss}$	April 27, Test 79	1265	4.3	2.8	11.89	11	218	82	126
$BasePoint4_{IVCss}$	April 27, Test 78	1265	4.3	4.1	11.84	11	220	81	127
$BasePoint4_{IVCss}$	April 27, Test 82	1265	4.3	4.1	11.81	11	220	81	126
$BasePoint4_{IVCss}$	April 27, Test 83	1264	4.3	5.7	11.74	11	223	81	127
$BasePoint4_{IVCss}$	April 27, Test 84	1264	4.3	6.8	11.64	11	225	81	127
$BasePoint4_{IVCss}$	April 27, Test 85	1264	4.3	9.5	11.57	11	228	81	127
$BasePoint5_{IVCss}$	April 30, Test 32	1503	4	2.8	12.32	6	208	84	123
$BasePoint5_{IVCss}$	April 30, Test 31	1503	4	3.2	12.27	6	210	85	123
$BasePoint5_{IVCss}$	April 30, Test 30	1503	4.1	3.4	12.21	6	212	85	123
$BasePoint5_{IVCss}$	April 30, Test 29	1503	4.1	4.4	12.17	6	214	85	123
$BasePoint5_{IVCss}$	April 30, Test 28	1504	4.1	5.1	12.11	6	216	85	124
$BasePoint5_{IVCss}$	April 30, Test 27	1504	4.1	6.2	12.06	6	218	85	124
$BasePoint5_{IVCss}$	April 30, Test 26	1504	4.1	8.3	12	6	221	85	124
$BasePoint5_{IVCss}$	April 30, Test 24	1504	4.1	7.2	12	6	220	85	124
$BasePoint5_{IVCss}$	April 30, Test 25	1504	4	9	11.97	6	222	84	124

Table A.15: Fuel octane sweeps - 1

Test Code	Date & Test Number	Speed [RPM]	Engine Load [IMEP]	Timing [CA50]	Exhaust O_2 [%]	fuel octane [PRF]	IVC [°aTDC]	T_{int} [°C]	P_{int} [kPa]
$BasePoint1_{ONss}$	April 26, Test 11	1025	3.8	3.4	11.27	4	220	60	110
$BasePoint1_{ONss}$	April 26, Test 10	1025	3.8	4.4	11.4	6	220	60	110
$BasePoint1_{ONss}$	April 26, Test 9	1025	4	4.5	11.09	8	220	59	110
$BasePoint1_{ONss}$	April 26, Test 8	1025	4	5.6	11.02	10	220	59	110
$BasePoint1_{ONss}$	April 26, Test 2	1025	4.1	5.1	10.97	10	220	59	111
$BasePoint1_{ONss}$	April 26, Test 3	1025	4.1	5.8	10.9	12	220	60	111
$BasePoint1_{ONss}$	April 26, Test 4	1025	4.1	6.9	10.89	14	220	60	111
$BasePoint1_{ONss}$	April 26, Test 5	1025	4.2	8.7	10.85	16	220	60	111
$BasePoint1_{ONsweep}$	April 26, Test 6	1025	4.2	10	10.88	18	220	61	110
$BasePoint2_{ONss}$	April 26, Test 58	1021	4.1	0.2	11.7	15	220	81	126
$BasePoint2_{ONss}$	April 26, Test 59	1021	4.2	1.9	11.68	20	220	82	126
$BasePoint2_{ONss}$	April 26, Test 60	1021	4.3	4	11.7	25	220	82	126
$BasePoint2_{ONss}$	April 26, Test 61	1021	4.3	7	11.75	30	220	82	125
$BasePoint2_{ONss}$	April 26, Test 10	1025	4.2	-0.7	12.23	28	220	102	139
$BasePoint3_{ONss}$	April 27, Test 9	1025	4.2	0.2	12.27	30	220	101	139
$BasePoint3_{ONss}$	April 27, Test 8	1025	4.2	1	12.27	32	220	101	139
$BasePoint3_{ONss}$	April 27, Test 7	1025	4.3	2.3	12.29	34	220	100	139
$BasePoint3_{ONss}$	April 27, Test 5	1025	4.3	2.5	12.31	36	220	101	139
$BasePoint3_{ONss}$	April 27, Test 4	1025	4.3	3.7	12.33	38	220	101	139
$BasePoint3_{ONss}$	April 27, Test 3	1025	4.4	4.7	12.35	40	220	101	139
$BasePoint3_{ONss}$	April 27, Test 13	1025	4.4	6.4	12.29	44	220	103	139
$BasePoint3_{ONss}$	April 27, Test 14	1025	4.3	7.7	12.32	46	220	104	139
$BasePoint3_{ONss}$	April 27, Test 15	1025	4.2	9.5	12.37	48	220	104	139

Table A.16: Fuel octane sweeps - 2

Test Code	Date & Test Number	Speed [RPM]	Engine Load [IMEP]	Timing [CA50]	Exhaust O_2 [%]	fuel octane [PRF]	IVC [°aTDC]	T_{int} [°C]	P_{int} [kPa]
$BasePoint4_{ONss}$	April 27, Test 60	1265	4.3	2.8	11.87	7	220	80	126
$BasePoint4_{ONss}$	April 27, Test 59	1265	4.3	4.1	11.98	9	220	80	126
$BasePoint4_{ONss}$	April 27, Test 58	1265	4.3	4.8	11.94	11	220	80	127
$BasePoint4_{ONss}$	April 27, Test 61	1265	4.3	4.5	11.87	11	220	80	126
$BasePoint4_{ONsweep}$	April 27, Test 62	1265	4.4	5.1	11.78	13	220	81	126
$BasePoint4_{ONss}$	April 27, Test 63	1265	4.4	6.3	11.79	15	220	81	126
$BasePoint4_{ONss}$	April 27, Test 64	1265	4.4	7.3	11.79	17	220	81	126
$BasePoint4_{ONss}$	April 27, Test 65	1265	4.4	9.4	11.8	19	220	81	126
$BasePoint5_{ONss}$	April 30, Test 2	1506	4.3	4.2	11.64	2	220	86	125
$BasePoint5_{ONss}$	April 30, Test 12	1505	4.3	4.9	11.67	3	220	85	124
$BasePoint5_{ONss}$	April 30, Test 3	1506	4.2	5.5	11.81	4	220	85	125
$BasePoint5_{ONss}$	April 30, Test 11	1505	4.2	6.7	11.94	5	220	85	125
$BasePoint5_{ONss}$	April 30, Test 4	1505	4.2	7.3	11.96	6	220	85	125
$BasePoint5_{ONss}$	April 30, Test 10	1505	4.4	7.4	11.6	7	220	85	125
$BasePoint5_{ONss}$	April 30, Test 5	1505	4.3	9.4	11.75	8	220	83	124
$BasePoint5_{ONss}$	April 30, Test 9	1505	4.3	8.9	11.72	9	220	85	124
$BasePoint5_{ONss}$	April 30, Test 6	1505	4.3	9.8	11.67	10	220	85	124
$BasePoint5_{ONss}$	April 30, Test 8	1505	4.3	9.8	11.6	11	220	86	125
$BasePoint5_{ONss}$	April 30, Test 7	1505	4.3	10.9	11.6	12	220	85	124

Table A.17: IVC step inputs

Test Code	Date & Test Number	Speed [RPM]	Engine Load [IMEP]	Timing [CA50]	Exhaust O_2 [%]	fuel octane [PRF]	IVC [°aTDC]	T_{int} [°C]	P_{int} [kPa]
$BP1_{IVCstep}$	apr26 08, test38	1021	3.9	5.1	11.31	10	217	58	110
$BP2_{IVCstep}$	apr26 08, test82	1022	4.3	5.6	11.7	28	220	83	126
$BP3_{IVCstep}$	apr27 08, test41	1024	4.3	4	12.26	43	219	107	139
$BP4_{IVCstep}$	apr27 08, test86	1264	4.3	3.1	11.84	11	219	83	126
$BP5_{IVCstep}$	apr30 08, test34	1503	4.1	5.8	12.15	6	216	84	124

Table A.18: Fuel octane step inputs

Test Code	Date & Test Number	Speed [RPM]	Engine Load [IMEP]	Timing [CA50]	Exhaust O_2 [%]	fuel octane [PRF]	IVC [°aTDC]	T_{int} [°C]	P_{int} [kPa]
$BP1_{ONstep}$	apr26 08, test13	1024	4	6.2	11.01	11	220	60	110
$BP2_{ONstep}$	apr26 08, test63	1021	4.3	4.7	11.69	27	220	82	126
$BP3_{ONstep}$	apr27 08, test17	1025	4.3	4	12.27	41	220	105	139
$BP4_{ONstep}$	apr27 08, test66	1265	4.3	3.9	11.83	10	220	82	126
$BP5_{ONstep}$	apr30 08, test14	1505	4.2	7.6	11.91	6	220	85	124

Table A.19: Injected fuel energy disturbance - IVC control

Test Code	Date & Test Number	Speed [RPM]	Engine Load [IMEP]	Timing [CA50]	Exhaust O_2 [%]	fuel octane [PRF]	IVC [°aTDC]	T_{int} [°C]	P_{int} [kPa]
$BP1_{IVCtransient1}$	apr26 08, test47	1021	3.9	5.1	11.19	10	219	60	111
$BP2_{IVCtransient1}$	apr26 08, test91	1021	4.3	5.1	11.72	28	219	82	125
$BP3_{IVCtransient1}$	apr27 08, test49	1024	4.4	5.1	12.23	43	220	106	139
$BP4_{IVCtransient1}$	apr27 08, test94	1264	4.3	5.1	11.63	11	224	84	127
$BP5_{IVCtransient1}$	apr30 08, test40	1503	3.9	7.1	NaN	6	220	86	17.9

Table A.20: Engine speed disturbance - IVC control

Test Code	Date & Test Number	Speed [RPM]	Engine Load [IMEP]	Timing [CA50]	Exhaust O_2 [%]	fuel octane [PRF]	IVC [°aTDC]	T_{int} [°C]	P_{int} [kPa]
$BP1_{IVCtransient2}$	apr26 08, test49	1019	3.9	5.1	11.24	10	219	60	111
$BP2_{IVCtransient2}$	apr26 08, test92	1020	4.3	5.1	11.73	28	219	82	125
$BP3_{IVCtransient2}$	apr27 08, test51	1023	4.3	5.1	12.22	43	221	106	139
$BP4_{IVCtransient2}$	apr27 08, test96	1268	4.3	5.1	11.66	11	224	84	127
$BP5_{IVCtransient2}$	apr30 08, test43	1502	3.9	7.1	NaN	6	220	87	18

Table A.21: Injected fuel energy disturbance - fuel octane control

Test Code	Date & Test Number	Speed [RPM]	Engine Load [IMEP]	Timing [CA50]	Exhaust O_2 [%]	fuel octane [PRF]	IVC [°aTDC]	T_{int} [°C]	P_{int} [kPa]
$BP1_{ONtransient1}$	apr26 08, test23	1022	3.9	5.1	11.15	8	220	59	110
$BP2_{ONtransient1}$	apr26 08, test71	1021	4.3	5.1	11.63	30	220	86	125
$BP3_{ONtransient1}$	apr27 08, test25	1024	4.3	5.1	12.26	44	220	107	139
$BP4_{ONtransient1}$	apr27 08, test74	1264	4.3	5.1	11.77	14	220	83	126
$BP5_{ONtransient1}$	apr30 08, test20	1504	4.3	7.1	11.64	8	220	87	125

Table A.22: Injected fuel energy disturbance - fuel octane control

Test Code	Date & Test Number	Speed [RPM]	Engine Load [IMEP]	Timing [CA50]	Exhaust O_2 [%]	fuel octane [PRF]	IVC [°aTDC]	T_{int} [°C]	P_{int} [kPa]
$BP1_{ONtransient2}$	apr26 08, test26	1020	3.9	5.1	11.18	7	220	58	111
$BP2_{ONtransient2}$	apr26 08, test73	1023	4.3	5.1	11.63	30	220	86	126
$BP3_{ONtransient2}$	apr27 08, test27	1024	4.4	5	12.25	44	220	107	139
$BP4_{ONtransient2}$	apr27 08, test77	1264	4.4	5.1	11.77	14	220	83	126
$BP5_{ONtransient2}$	apr30 08, test22	1504	4.3	7.1	11.64	8	220	87	124

Table A.23: Load range sweep at BasePoint1 - IVC control

Test Code	Date & Test Number	Speed [RPM]	Engine Load [IMEP]	Timing [CA50]	Exhaust O_2 [%]	fuel octane [PRF]	IVC [°aTDC]	T_{int} [°C]	P_{int} [kPa]
$BP1_{IVCloadsweep}$	jun20 08, test19	1024	4	5.1	10.79	10	218	60	111
$BP1_{IVCloadsweep}$	jun20 08, test20	1024	4.1	5.1	10.3	10	223	60	111
$BP1_{IVCloadsweep}$	jun20 08, test21	1023	3.9	5.1	11.3	10	214	59	110
$BP1_{IVCloadsweep}$	jun20 08, test22	1023	3.8	5.1	11.67	10	210	59	110
$BP1_{IVCloadsweep}$	jun20 08, test23	1023	3.6	5.1	12	10	206	58	110
$BP1_{IVCloadsweep}$	jun20 08, test24	1027	3.3	5.4	12.46	10	200	58	109

Table A.24: Load range sweep at BasePoint2 - IVC control

Test Code	Date & Test Number	Speed [RPM]	Engine Load [IMEP]	Timing [CA50]	Exhaust O_2 [%]	fuel octane [PRF]	IVC [°aTDC]	T_{int} [°C]	P_{int} [kPa]
$BP2_{IVCloadsweep}$	jun20 08, test2	1025	4.2	5.1	11.52	28	215	81	124
$BP2_{IVCloadsweep}$	jun20 08, test3	1025	4.4	5.1	11.03	28	220	82	124
$BP2_{IVCloadsweep}$	jun20 08, test4	1025	4.4	5.1	10.17	28	227	81	126
$BP2_{IVCloadsweep}$	jun20 08, test5	1025	4	5.1	11.86	28	212	81	123
$BP2_{IVCloadsweep}$	jun20 08, test6	1025	3.9	5.1	12.21	28	208	81	122
$BP2_{IVCloadsweep}$	jun20 08, test7	1024	3.7	5.1	12.58	28	202	81	121

Table A.25: Load range sweep at BasePoint3 - IVC control

Test Code	Date & Test Number	Speed [RPM]	Engine Load [IMEP]	Timing [CA50]	Exhaust O_2 [%]	fuel octane [PRF]	IVC [°aTDC]	T_{int} [°C]	P_{int} [kPa]
$BP3_{IVCloadsweep}$	jun20 08, test51	1022	4.3	5.1	11.96	43	219	103	138
$BP3_{IVCloadsweep}$	jun20 08, test52	1022	4.4	5.1	11.6	43	222	103	139
$BP3_{IVCloadsweep}$	jun20 08, test53	1022	4.5	5	11.3	43	225	104	140
$BP3_{IVCloadsweep}$	jun20 08, test54	1022	4.6	5.1	10.98	43	227	105	141
$BP3_{IVCloadsweep}$	jun20 08, test55	1022	4.6	5.1	10.48	43	231	105	142
$BP3_{IVCloadsweep}$	jun20 08, test56	1021	4.1	5.1	12.35	43	214	102	137
$BP3_{IVCloadsweep}$	jun20 08, test57	1021	4	5.1	12.63	43	211	103	137
$BP3_{IVCloadsweep}$	jun20 08, test58	1022	3.8	5.1	12.91	43	208	103	137
$BP3_{IVCloadsweep}$	jun20 08, test59	1022	3.5	5.1	13.22	43	204	104	136
$BP3_{IVCloadsweep}$	jun20 08, test60	1026	3	5.5	13.5	43	200	103	136

Table A.26: Load range sweep at BasePoint4 - IVC control

Test Code	Date & Test Number	Speed [RPM]	Engine Load [IMEP]	Timing [CA50]	Exhaust O_2 [%]	fuel octane [PRF]	IVC [°aTDC]	T_{int} [°C]	P_{int} [kPa]
$BP4_{IVCloadsweep}$	jun20 08, test70	1265	4.2	5.1	11.48	11	222	81	126
$BP4_{IVCloadsweep}$	jun20 08, test71	1265	4.4	5.1	11.07	11	225	81	127
$BP4_{IVCloadsweep}$	jun20 08, test72	1265	4.4	5	10.54	11	229	81	128
$BP4_{IVCloadsweep}$	jun20 08, test73	1265	4.1	5.1	11.81	11	219	82	126
$BP4_{IVCloadsweep}$	jun20 08, test74	1265	3.9	5.1	12.16	11	215	82	125
$BP4_{IVCloadsweep}$	jun20 08, test75	1265	3.7	5.1	12.59	11	210	82	124
$BP4_{IVCloadsweep}$	jun20 08, test76	1265	3.3	5.1	13.02	11	203	81	123

Table A.27: Load range sweep at BasePoint5 - IVC control

Test Code	Date & Test Number	Speed [RPM]	Engine Load [IMEP]	Timing [CA50]	Exhaust O_2 [%]	fuel octane [PRF]	IVC [°aTDC]	T_{int} [°C]	P_{int} [kPa]
$BP5_{IVCloadsweep}$	jun20 08, test84	1505	3.5	5.1	12.98	6	205	84	124
$BP5_{IVCloadsweep}$	jun20 08, test85	1505	3.7	5.1	12.68	6	210	84	124
$BP5_{IVCloadsweep}$	jun20 08, test86	1505	3.9	5.1	12.34	6	214	84	124
$BP5_{IVCloadsweep}$	jun20 08, test87	1505	4.2	5.1	11.9	6	218	84	126
$BP5_{IVCloadsweep}$	jun20 08, test88	1505	4.3	5.1	11.55	6	222	84	126

Table A.28: Load range sweep at BasePoint1 - fuel octane control

Test Code	Date & Test Number	Speed [RPM]	Engine Load [IMEP]	Timing [CA50]	Exhaust O_2 [%]	fuel octane [PRF]	IVC [°aTDC]	T_{int} [°C]	P_{int} [kPa]
$BP1_{ONloadsweep}$	jun20 08, test15	1024	4	5.1	10.82	9	220	60	111
$BP1_{ONloadsweep}$	jun20 08, test16	1024	4.2	5.1	10.19	17	220	60	111
$BP1_{ONloadsweep}$	jun20 08, test17	1024	3.8	5.1	11.24	3	220	60	111
$BP1_{ONloadsweep}$	jun20 08, test18	1024	3.8	6.3	11.43	0	219	60	111

Table A.29: Load range sweep at BasePoint2 - fuel octane control

Test Code	Date & Test Number	Speed [RPM]	Engine Load [IMEP]	Timing [CA50]	Exhaust O_2 [%]	fuel octane [PRF]	IVC [°aTDC]	T_{int} [°C]	P_{int} [kPa]
$BP2_{ONloadsweep}$	jun20 08, test8	1024	4.2	5.1	11.34	26	220	81	125
$BP2_{ONloadsweep}$	jun20 08, test9	1024	4.4	5.1	11.12	28	220	80	125
$BP2_{ONloadsweep}$	jun20 08, test10	1024	4.5	5.1	10.64	34	220	81	125
$BP2_{ONloadsweep}$	jun20 08, test11	1024	4.1	5.1	11.7	22	220	82	125
$BP2_{ONloadsweep}$	jun20 08, test12	1024	3.8	5.1	12.1	16	219	81	124
$BP2_{ONloadsweep}$	jun20 08, test13	1024	3.6	5.1	12.44	12	219	81	124
$BP2_{ONloadsweep}$	jun20 08, test14	1024	3.4	5.1	12.66	9	219	81	124

Table A.30: Load range sweep at BasePoint3 - fuel octane control

Test Code	Date & Test Number	Speed [RPM]	Engine Load [IMEP]	Timing [CA50]	Exhaust O_2 [%]	fuel octane [PRF]	IVC [°aTDC]	T_{int} [°C]	P_{int} [kPa]
$BP3_{ONloadsweep}$	jun20 08, test40	1023	4.3	5.1	12.12	41	220	104	140
$BP3_{ONloadsweep}$	jun20 08, test41	1023	4.4	5.1	11.7	45	220	104	138
$BP3_{ONloadsweep}$	jun20 08, test42	1023	4.5	5.1	11.49	47	220	104	138
$BP3_{ONloadsweep}$	jun20 08, test43	1023	4.6	5.1	11.27	50	220	104	139
$BP3_{ONloadsweep}$	jun20 08, test44	1023	4.7	5	11.05	52	220	105	139
$BP3_{ONloadsweep}$	jun20 08, test45	1023	4.7	5	10.82	54	220	105	139
$BP3_{ONloadsweep}$	jun20 08, test46	1023	4.2	5.1	12.15	38	220	102	138
$BP3_{ONloadsweep}$	jun20 08, test47	1023	4	5.1	12.39	36	220	103	138
$BP3_{ONloadsweep}$	jun20 08, test48	1023	3.9	5.1	12.59	34	220	104	138
$BP3_{ONloadsweep}$	jun20 08, test49	1023	3.7	5.1	12.8	31	219	104	139
$BP3_{ONloadsweep}$	jun20 08, test50	1022	3.5	5.1	13	29	219	105	138

Table A.31: Load range sweep at BasePoint4 - fuel octane control

Test Code	Date & Test Number	Speed [RPM]	Engine Load [IMEP]	Timing [CA50]	Exhaust O_2 [%]	fuel octane [PRF]	IVC [°aTDC]	T_{int} [°C]	P_{int} [kPa]
$BP4_{ONloadsweep}$	jun20 08, test65	1265	4.3	5.1	11.48	13	220	81	126
$BP4_{ONloadsweep}$	jun20 08, test66	1265	4.4	5.1	11.2	16	220	81	126
$BP4_{ONloadsweep}$	jun20 08, test67	1265	4.5	5.1	10.95	19	220	80	126
$BP4_{ONloadsweep}$	jun20 08, test68	1265	4	5.1	11.91	8	220	81	126
$BP4_{ONloadsweep}$	jun20 08, test69	1265	3.8	5.1	12.31	4	220	81	126

Table A.32: Load range sweep at BasePoint5 - fuel octane control

Test Code	Date & Test Number	Speed [RPM]	Engine Load [IMEP]	Timing [CA50]	Exhaust O_2 [%]	fuel octane [PRF]	IVC [°aTDC]	T_{int} [°C]	P_{int} [kPa]
$BP5_{ONloadsweep}$	jun20 08, test80	1505	4.1	5	11.98	1	220	85	126
$BP5_{ONloadsweep}$	jun20 08, test81	1505	4.1	5	11.96	3	220	85	126
$BP5_{ONloadsweep}$	jun20 08, test82	1505	4.2	5.1	11.71	7	220	85	126
$BP5_{ONloadsweep}$	jun20 08, test83	1505	4.4	5	11.21	12	220	85	126

Table A.33: Load range sweep at BasePoint1 - no control

Test Code	Date & Test Number	Speed [RPM]	Engine Load [IMEP]	Timing [CA50]	Exhaust O_2 [%]	fuel octane [PRF]	IVC [°aTDC]	T_{int} [°C]	P_{int} [kPa]
$BP1_{OLloadsweep}$	jun20 08, test25	1023	4	6	10.76	10	220	59	110
$BP1_{OLloadsweep}$	jun20 08, test26	1023	3.9	2.8	10.38	10	220	60	111
$BP1_{OLloadsweep}$	jun20 08, test27	1023	3.9	7.6	11.07	10	220	59	110
$BP1_{OLloadsweep}$	jun20 08, test28	1023	3.8	9.2	11.21	10	219	60	110

Table A.34: Load range sweep at BasePoint2 - no control

Test Code	Date & Test Number	Speed [RPM]	Engine Load [IMEP]	Timing [CA50]	Exhaust O_2 [%]	fuel octane [PRF]	IVC [°aTDC]	T_{int} [°C]	P_{int} [kPa]
$BP2_{OLloadsweep}$	jun20 08, test29	1023	4.2	5.9	11.48	28	220	81	126
$BP2_{OLloadsweep}$	jun20 08, test30	1023	4.3	4.2	11.22	28	220	81	126
$BP2_{OLloadsweep}$	jun20 08, test31	1023	4.3	2.3	10.93	28	220	81	126
$BP2_{OLloadsweep}$	jun20 08, test32	1023	4.1	7.3	11.68	28	219	82	126
$BP2_{OLloadsweep}$	jun20 08, test33	1023	3.8	9.9	11.93	28	219	82	125

Table A.35: Load range sweep at BasePoint3 - no control

Test Code	Date & Test Number	Speed [RPM]	Engine Load [IMEP]	Timing [CA50]	Exhaust O_2 [%]	fuel octane [PRF]	IVC [°aTDC]	T_{int} [°C]	P_{int} [kPa]
$BP3_{OLloadsweep}$	jun20 08, test34	1023	4.3	5.9	12.12	43	220	103	139
$BP3_{OLloadsweep}$	jun20 08, test35	1023	4.3	3.4	11.81	43	220	105	139
$BP3_{OLloadsweep}$	jun20 08, test36	1023	4.4	2.5	11.59	43	220	103	139
$BP3_{OLloadsweep}$	jun20 08, test37	1023	4.4	1.9	11.41	43	220	103	139
$BP3_{OLloadsweep}$	jun20 08, test38	1023	4.1	7.2	12.28	43	219	104	139
$BP3_{OLloadsweep}$	jun20 08, test39	1023	3.9	8.1	12.39	43	219	105	139

Table A.36: Load range sweep at BasePoint4 - no control

Test Code	Date & Test Number	Speed [RPM]	Engine Load [IMEP]	Timing [CA50]	Exhaust O_2 [%]	fuel octane [PRF]	IVC [°aTDC]	T_{int} [°C]	P_{int} [kPa]
$BP4_{OLloadsweep}$	jun20 08, test61	1265	4.2	5	11.62	11	220	80	126
$BP4_{OLloadsweep}$	jun20 08, test62	1265	4.3	3	11.34	11	220	81	126
$BP4_{OLloadsweep}$	jun20 08, test63	1265	4.1	6.3	11.81	11	220	81	126
$BP4_{OLloadsweep}$	jun20 08, test64	1265	3.8	8.4	12.08	11	220	80	126

Table A.37: Load range sweep at BasePoint5 - no control

Test Code	Date & Test Number	Speed [RPM]	Engine Load [IMEP]	Timing [CA50]	Exhaust O_2 [%]	fuel octane [PRF]	IVC [°aTDC]	T_{int} [°C]	P_{int} [kPa]
$BP5_{OLloadsweep}$	jun20 08, test77	1505	3.9	7.9	12.22	6	220	84	125
$BP5_{OLloadsweep}$	jun20 08, test78	1505	4.2	4.8	11.86	6	220	85	126
$BP5_{OLloadsweep}$	jun20 08, test79	1505	4.2	3.9	11.73	6	220	85	126

A.6 Data for Chapter 5

Table A.38: System identification data points.

Test Code	Date & Test Number	Speed [RPM]	Engine Load [IMEP]	Timing [CA50]	Exhaust O_2 [%]	fuel octane [PRF]	IVC [°aTDC]	T_{int} [°C]	P_{int} [kPa]
$SYSID1_{IVC}$	June 12, Test 2	1024	4	4.9	10.96	10	213	59	110
$SYSID1_{ON}$	June 12 , Test 3	1024	4.1	5.4	10.55	8	220	61	111
$SYSID1_{E}$	June 12 , Test 6	1023	3.9	7.4	10.85	10	220	61	111
$SYSID1_{RPM}$	June 12, Test 5	1004	4	5.7	10.79	10	220	61	111
$SYSID2_{IVC}$	June 6, Test 5	1022	4.2	4.4	11.3	28	214	83	125
$SYSID2_{ON}$	June 6, Test 2	1022	4.2	4.9	11.19	24	220	82	125
$SYSID2_{E}$	June 12, Test 6	1004	4	5.7	10.79	10	220	61	111
$SYSID2_{RPM}$	June 12, Test 7	1024	4	4.9	10.96	10	213	59	110
$SYSID3_{IVC}$	June 16, Test 9	1024	4.2	3.2	12.17	40	211	100	138
$SYSID3_{ON}$	June 16, Test 10	1022	4.2	3.1	11.94	35	220	101	138
$SYSID3_{E}1$	June 16, Test 11	1022	4.1	5.9	11.99	40	220	101	138
$SYSID3_{RPM}$	June 16, Test 12	981	4.2	4.7	12.02	40	220	101	139
$SYSID4_{IVC}$	June 16, Test 1	1267	4.2	5.8	11.55	11	219	80	1258
$SYSID4_{ON}$	June 16, Test 2	1266	4.3	4.8	11.41	10	220	81	125
$SYSID4_{E}$	June 16, Test 3	1266	4.2	5.5	11.52	11	220	81	125
$SYSID4_{RPM}$	June 16, Test 4	1261	4.2	5.6	11.53	11	220	80	125
$SYSID5_{IVC}$	June 16, Test 5	1506	4	5.8	12.12	6	216	85	125
$SYSID5_{ON}$	June 16, Test 6	1506	4.3	5.7	11.6	5	220	85	126
$SYSID5_{E}$	June 16, Test 7	1505	4	7.3	12.02	6	220	85	125
$SYSID5_{RPM}$	June 16, Test 8	1468	3.9	6.6	12.06	6	220	86	126

Table A.39: System identification data points - linearity test.

Test Code	Date & Test Number	Speed [RPM]	Engine Load [IMEP]	Timing [CA50]	Exhaust O_2 [%]	fuel octane [PRF]	IVC [°aTDC]	T_{int} [°C]	P_{int} [kPa]
$SYSID2_{ONl}$	jun6 08, test2	1022	4.2	4.9	11.19	24	220	82	125
$SYSID2_{ONm}$	jun6 08, test3	1022	4.3	4.7	11.15	25	220	82	125
$SYSID2_{ONs}$	jun6 08, test4	1022	4.3	4.4	11.12	25	220	83	125
$SYSID2_{IVCl}$	jun6 08, test5	1022	4.2	4.4	11.3	28	214	83	125
$SYSID2_{IVCm}$	jun6 08, test6	1022	4.2	3.7	11.32	28	213	83	124
$SYSID2_{IVCs}$	jun6 08, test7	1021	4.2	3.5	11.31	28	213	83	124

Table A.40: Injected fuel energy disturbance - various controllers

Test Code	Date & Test Number	Speed [RPM]	Engine Load [IMEP]	Timing [CA50]	Exhaust O_2 [%]	fuel octane [PRF]	IVC [°aTDC]	T_{int} [°C]	P_{int} [kPa]
$FF1_{OL}$	June 24, Test 10	1024	4	7	10.69	10	220	60	110
$FF1_{PIivc}$	June 24, Test 13	1024	3.9	5.1	10.8	6	219	59	110
$FF1_{PIon}$	June 24, Test 14	1024	4	5.1	10.84	10	216	60	110
$FF1_{FFivc}$	June 24, Test 15	1024	4	5.1	10.76	10	217	59	110
$FF1_{FFon}$	June 24, Test 16	1024	3.9	5	10.83	5	220	59	110
$FF2_{OL}$	June 24, Test 21	1023	4.2	5.2	11.31	28	220	86	126
$FF2_{PIivc}$	June 24, Test 17	1023	4.2	5.1	11.41	28	218	83	125
$FF2_{PIon}$	June 24, Test 18	1023	4.2	5.1	11.32	27	219	84	126
$FF2_{FFivc}$	June 24, Test 19	1023	4.2	5.1	11.36	28	218	84	125
$FF2_{FFon}$	June 24, Test 20	1023	4.2	5.1	11.31	28	219	85	126
$FF3_{OL}$	June 24, Test 23	1022	4.2	5.2	12.06	41	219	103	139
$FF3_{PIivc}$	June 24, Test 31	1022	4.2	5	11.67	41	223	109	138
$FF3_{PIon}$	June 24, Test 29	1022	4.2	5.1	11.83	44	219	109	137
$FF3_{FFivc}$	June 24, Test 25	1022	4.2	5.1	11.75	41	223	107	138
$FF3_{FFon}$	June 24, Test 27	1022	4.2	5.1	11.85	44	220	108	138
$FF4_{OL}$	June 24, Test 33	1263	4.1	4.6	11.55	11	220	84	126
$FF4_{PIivc}$	June 24, Test 35	1263	4.2	5.1	11.39	11	224	86	128
$FF4_{PIon}$	June 24, Test 37	1263	4.2	5.1	11.35	16	220	88	125
$FF4_{FFivc}$	June 24, Test 39	1263	4.2	5.1	11.18	11	224	87	126
$FF4_{FFon}$	June 24, Test 41	1263	4.3	5.1	11.3	17	220	88	126
$FF5_{OL}$	June 24, Test 43	1502	3.9	6	11.92	6	220	87	125
$FF5_{PIivc}$	June 24, Test 49	1502	4	5	12.02	6	217	86	125
$FF5_{PIon}$	June 24, Test 51	1502	4.1	5	11.65	4	220	86	126
$FF5_{FFivc}$	June 24, Test 45	1502	4	5.1	12.05	6	216	87	125
$FF5_{FFon}$	June 24, Test 47	1502	4.1	5	11.69	4	220	86	126

Table A.41: Engine speed disturbance - various controllers

Test Code	Date & Test Number	Speed [RPM]	Engine Load [IMEP]	Timing [CA50]	Exhaust O_2 [%]	fuel octane [PRF]	IVC [°aTDC]	T_{int} [°C]	P_{int} [kPa]
$FF1RPM_{OL}$	June 24, Test 100	1018	4	6.3	10.86	10	220	59	111
$FF1RPM_{PIivc}$	June 24, Test 107	1021	4	5.1	10.84	10	218	60	111
$FF1RPM_{PIon}$	June 24, Test 104	1021	4	5	10.81	8	220	60	111
$FF1RPM_{FFivc}$	June 24, Test 105	1019	4	5.1	10.81	10	219	60	111
$FF1RPM_{FFon}$	June 24, Test 104	1021	4	5	10.81	8	220	60	111
$FF2RPM_{OL}$	June 24, Test 111	1022	4.2	6	11.48	28	220	83	126
$FF2RPM_{PIivc}$	June 24, Test 113	1022	4.2	5.1	11.52	28	218	82	126
$FF2RPM_{PION}$	June 24, Test 115	1021	4.2	5.1	11.47	27	220	83	126
$FF2RPM_{FFivc}$	June 24, Test 119	1021	4.2	5.1	11.39	28	220	84	126
$FF2RPM_{FFon}$	June 24, Test 117	1021	4.2	5.1	11.4	28	220	84	126
$FF3RPM_{OL}$	June 24, Test 24	1017	4.2	5	12.09	41	220	105	140
$FF3RPM_{PIivc}$	June 24, Test 32	1019	4.2	5.1	11.7	41	223	109	138
$FF3RPM_{PIon}$	June 24, Test 30	1021	4.2	5.1	11.84	44	220	109	137
$FF3RPM_{FFivc}$	June 24, Test 26	1020	4.2	5	11.78	41	222	107	138
$FF3RPM_{FFon}$	June 24, Test 28	1019	4.2	5.1	11.86	44	220	108	137
$FF4RPM_{OL}$	June 24, Test 34	1262	4.1	3.6	11.55	11	220	85	128
$FF4RPM_{PPivc}$	June 24, Test 36	1260	4.2	5.1	11.36	11	225	87	129
$FF4RPM_{PIon}$	June 24, Test 38	1259	4.3	5.1	11.32	17	220	88	126
$FF4RPM_{FFivc}$	June 24, Test 40	1262	4.2	5.1	11.19	11	224	87	126
$FF4RPM_{FFon}$	June 24, Test 42	1261	4.3	5.1	11.29	17	220	87	125
$FF5RPM_{OL}$	June 24, Test 44	1501	4	6.6	11.95	6	220	87	125
$FF5RPM_{PIivc}$	June 24, Test 50	1502	4	5	12.09	6	215	86	125
$FF5RPM_{PIon}$	June 24, Test 52	1497	4.2	5	11.63	3	220	86	126
$FF5RPM_{FFivc}$	June 24, Test 46	1501	4	5.1	12.05	6	217	87	125
$FF5RPM_{FFon}$	June 24, Test 48	1501	4.1	5.1	11.71	4	220	86	126

Table A.42: Injected fuel energy disturbance - various controllers

Test Code	Date & Test Number	Speed [RPM]	Engine Load [IMEP]	Timing [CA50]	Exhaust O_2 [%]	fuel octane [PRF]	IVC [°aTDC]	T_{int} [°C]	P_{int} [kPa]
$FF2MULT_{FFivc}$	jul22 08, test24	1020	4	5.1	11.43	28	217	82	125
$FF2MULT_{FFon}$	jul22 08, test25	1025	4	5.1	11.34	26	220	83	125
$FF2MULT_{PIon}$	jul22 08, test26	1021	4	5.1	11.32	27	220	85	125
$FF2MULT_{PIivc}$	jul22 08, test27	1020	4	5.1	11.33	28	219	85	125
$FF2MULT_{OL}$	jul22 08, test28	1023	4	5.2	11.3	28	220	86	125

Appendix B

Camshaft Phaser Control System

B.1 Description of the System Hardware

B.1.1 Vane-type Camshaft Phasers

The vane-type camshaft phasers are taken from a Mercedes E550 production engine [e55, 2007]. The phase of each camshaft is independently controlled and is changed a maximum of 20 °, which gives a valve timing adjustment of 40 °of crankshaft rotation. Phasing of the camshafts is accomplished by moving oil in and out of cavities inside the phaser, which then moves the camshaft relative to the outside of the phaser, which is fixed to the crankshaft through the timing chain. The oil is regulated in and out of these cavities with a hydraulic valve. Feedback control is necessary for the operation of this system. A schematic of the phaser can be seen in Figure B.1

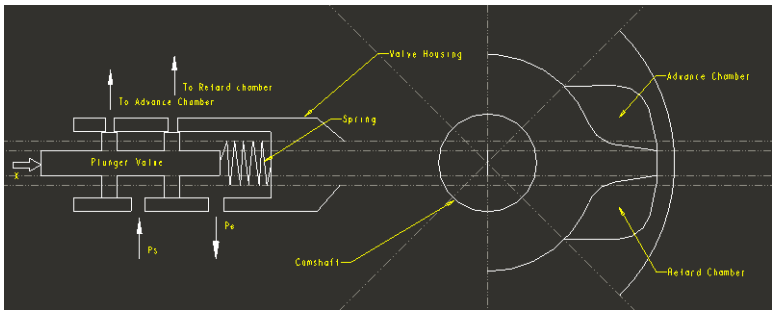

Figure B.1: Schematic of the oil system for the camshaft phaser.

A simple model of the vane phaser and valve shows that the system is an integration between the input x, position of the valve, and the output θ, the angular position of the phaser. It is similar to that of Example 2.17 of [Franklin et al., 1998]. To derive a mathematical model of the system it is first assumed that the oil flow through the valve is proportional to the position of the valve. The oil flow into the phaser is:

$$Q_1 = \frac{1}{\rho R_1}(p_s - p_1)^{1/2}x \tag{B.1}$$

Where:R_1 = flow resistance and ρ = oil density.

A similar equation is derived for the oil flow out of the phaser:

$$Q_2 = \frac{1}{\rho R_2}(p_2 - p_e)^{1/2}x \tag{B.2}$$

Applying conservation of mass to the vane portion of the phaser gives an equation for the angular speed of vane:

$$\dot{\theta}Al = Q_1 = Q_2 \tag{B.3}$$

Where A is the effective pressure area and l is the centroid to effective area.

A moment balance on the vane gives:

$$Al(p_1 - p_2) - T = J\dot{\dot{\theta}} \tag{B.4}$$

It is assumed that the valve exposes the oil passageways equally, so the flow resistances are equal:

$$R_1 = R_2 \tag{B.5}$$

Also, it is assumed that the angular rotation is constant, so there is no angular acceleration of the phaser, and the assumption that there is no applied torque, T, to

the phaser. Equation B.4 and Equation B.5 gives:

$$p_1 = p_2 = \frac{p_s + p_e}{2} \tag{B.6}$$

From Equation B.3 and Equation B.6 the relationship between x and θ is:

$$\dot{\theta} = \frac{\sqrt{p_s - p_e}}{\sqrt{2}A\rho Rl}x \tag{B.7}$$

Taking the Laplace transform of Equation B.7, in the s-domain the simplified model of the plant is:

$$G(s) = \frac{K}{s} \tag{B.8}$$

$$K = \frac{\sqrt{p_s - p_e}}{\sqrt{2}A\rho Rl}$$

Equation B.8 shows that the system is a simple integration between the input and the output. Figure B.2 shows the model open loop impulse response of the system. The change in θ is proportional to the constant K, which relies on the oil pressure and the fixed properties of the phaser.

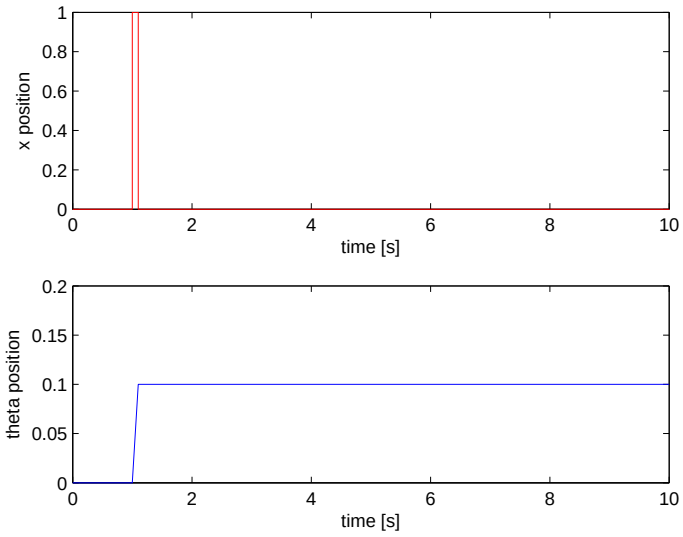

Figure B.2: This show the simulated open loop response of the phaser to a impulse input.

B.1.2 Physical Camshaft System

The camshafts are driven by a chain from the crankshaft. This assembly is custom built, as the production system drove 2 cylinder heads from the crankshaft sprocket. The two camshafts are tied together with a set of gears on the outside of each phaser, and this gear set is connected to the camshaft sprocket. A illustration of this setup can be seen in Figure B.3.

A 36-1 toothed wheel is placed on the crankshaft. A hall effect sensor detects the movement of the toothed wheel. This information is fed into the MicroAutoBox. On each phaser element is another hall effect wheel which gives 4 pulses per revolution. The signals from these hall effect sensors are also fed into the MicroAutobox. The impulse wheels on the camshafts can be seen in Figure B.3.

Figure B.3: The timing chain and gear set that drive that camshafts. This figure also shows the impulse wheel for the hall effect sensor.

B.1.3 Oil System

Oil pressure is regulated with a standard oil pressure regulator. The oil pump is driven externally by a electric motor, not driven off the crankshaft like traditional automotive systems. The benefit of the externally controlled oil pump is that oil pressure will not fluctuate as much as engine speed is increased or decreased. The oil temperature is also monitored and controlled. It is cooled with an oil to water heat exchanger and heated with electric heaters placed in the oil reservoir. The oil temperature and pressure are both measured as they enter the cylinder head.

B.1.4 Electrical System

Figure B.4 shows a schematic of the electrical system for the camshaft phasing control. While this system uses the hall effect sensors and actuators from the Mercedes engine,

all the wiring is custom made in order to interface with the MicroAutobox.

The solenoid actuators used to move the oil valve are stock components from the Mercedes engine. Their displacement is controlled by Pulse Width Modulation (PWM) at a carrier frequency of 200Hz. They have a displacement of 4.25mm and a maximum current draw of 1.1A a their maximum displacement.

The controller used is the dSPACE MicroAutoBox 1401 [dSPACE GmbH, 2004]. This ECU has a processor that run at 300MHz. It also contain the necessary hardware for analog I/O digital I/O as well as serial and CAN communication. This controller has been specifically designed by dSPACE for engine applications, and has PWM drivers.

The MicroAutoBox contains no power electronics to drive components such as the fuel injectors, camshaft phasers, or spark plugs. The power electronics to interface between the MicroAutoBox and the engine have been built by Bill Bizuk. These electronics are used to power the solenoid actuators and were designed by Hitachi [Borg, 2003].

While the MicroAutobox is running it communicates with a host PC using the dSPACE program ControlDesk. This connection enables users to monitor the system as well as tune the control parameters and change set points. The system communicates over a fiber optic line to a dSPACE card in the host PC.

All the power for the system is delivered by a power supply set a 13.8 volts. This power supply provides a constant voltage supply. It is used instead of a 12 volt automotive battery and charger because as this system charges and discharges the voltage fluctuates between 11 and 14 volts.

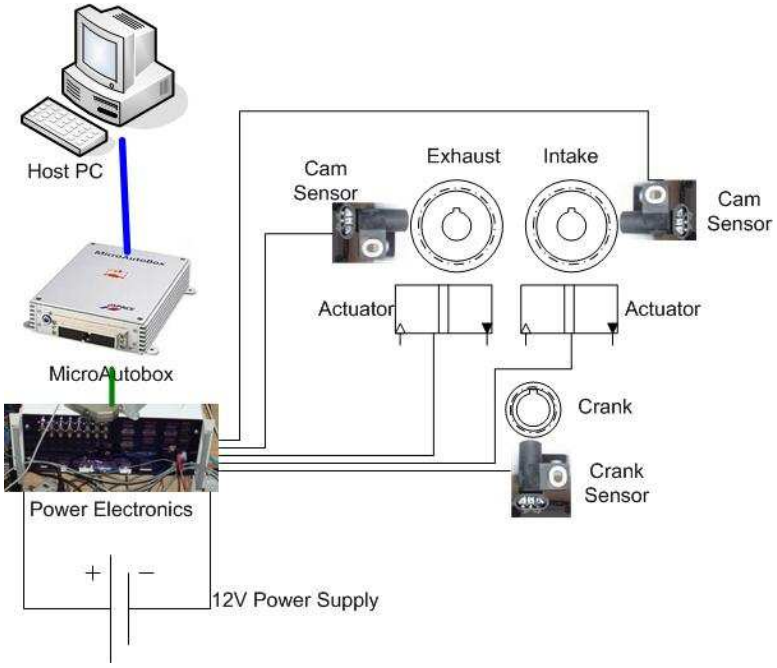

Figure B.4: Wiring schematic of the camshaft phasing system.

B.2 Software and Control Loop Definition

All the software for the MicroAutobox is done in MatLab Simulink. dSPACE provides pre-written blocks for all the I/O and setup on the MicroAutobox. The control algorithms and other computations are written using the standard blocks in Simulink. Once the model is written in Simulink the necessary C-code is complied and uploaded onto the MicroAutoBox.

Figure B.5 shows the model for the phaser control.

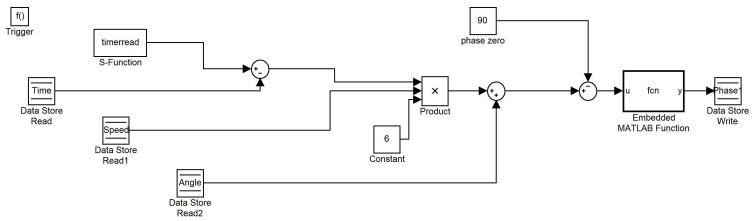

Figure B.5: Simulink model designed to compute the phase angle of the camshafts.

The hall effect signals from the two camshafts are wired into the MicroAutoBox as external hardware interrupts. As soon as a rising edge is detected, which happens four times a revolution, a timer is immediately read. The crankshaft signal is also used as an interrupt source, and each time a crank tooth is detected the same timer is also read. These two time values are subtracted, and using the last computed value of engine speed the angular distance between camshaft signal and the last crankshaft tooth is estimated. This code provides an accurate measurement of the camshaft phase 4 times an engine cycle, 2 times per crank revolution.

The control loop of the camshaft is time based. Figure 3.4 shows the Simulink model for the controller of the phaser. The system is a PI controller. The controller runs a 1KHz.

B.3 Open Loop and Closed Loop Results

The sensitivity of the phaser is first tested. The duty cycle for the solenoid actuator is set to certain points and the resulting phase change of the valves is measured. Figure B.6 shows the result phase velocity as a function of the duty cycle, which directly controls the solenoid displacement. As derived earlier there should be a linear relationship between the phase velocity and the solenoid plunger displacement, yet it is apparent in the figure that this is not the case. The discrepancy between the model and the real world can be attributed to the simplifying assumptions made in the model derivation.

The PI controllers are manually tuned for minimum overshoot and quick response. The proportional and integral gains are 0.015 and 0.000006 respectively. Closed loop step response results can be seen in Figure B.7 and B.8 for the intake and exhaust camshafts. As seen in the figures the responses to negative and positive steps are different. This is attributed to nonlinearities in the phasers, and the effect of the

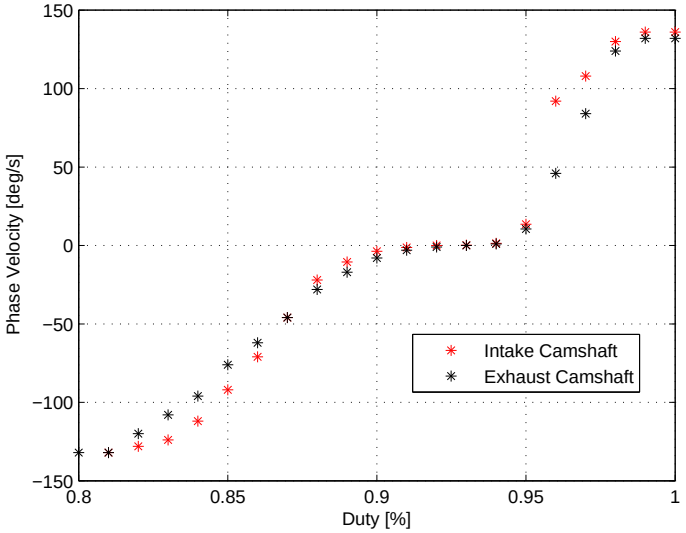

Figure B.6: Phase velocity as a function of the duty cycle of the actuator.

torque on the camshaft.

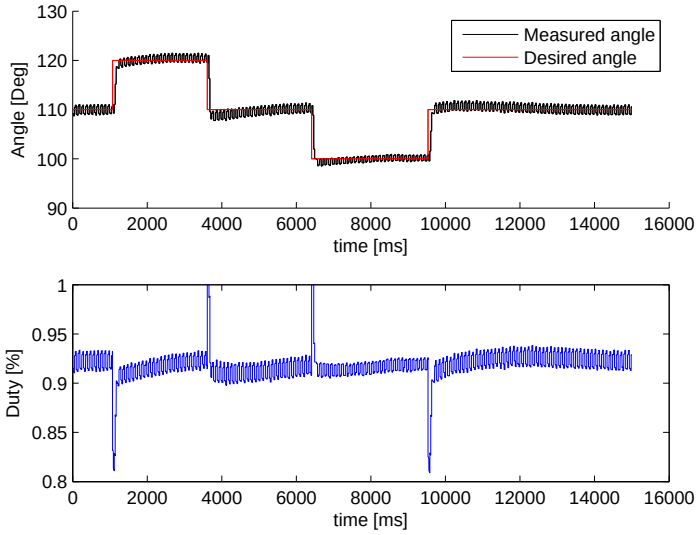

Figure B.7: The change of intake camshaft phase as a result of an step input with P I control.

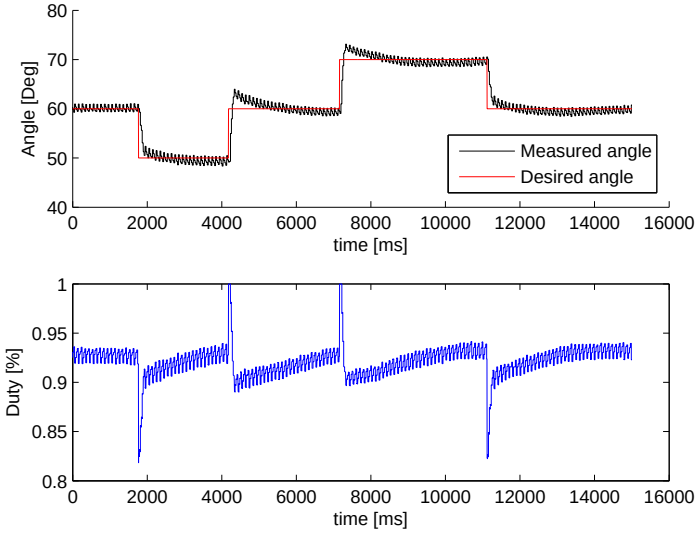

Figure B.8: The change of exhaust camshaft phase as a result of an step input with P I control.

Appendix C

Mercedes E550 Cylinder Head

C.1 Head Modifications

To fit the cylinder head on the one-cylinder setup the production cylinder head required modifications. The cylinder head was first cut in half with a band-saw as seen in Figure C.1. The coolant and oil channels that were exposed were welded shut. On this new cut face the hole for the in-cylinder pressure transducer is drilled.

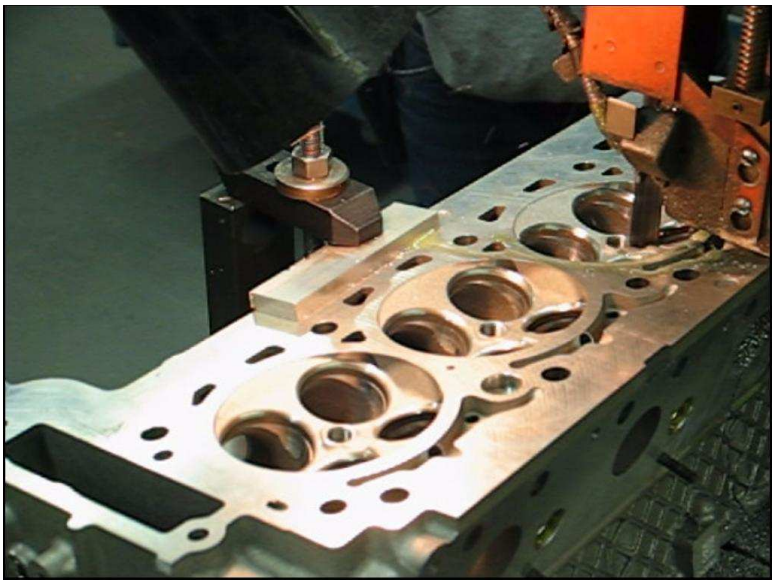

Figure C.1: Cylinder head as it gets resized by the band-saw.

C.2 Valve Lift Profile

The valve lift profile is required for determining the maximum valve lift and the valve duration. Also, to accurately model the gas dynamics of the engine an accurately measured profile is needed.

Before the valve profiles could be measured the cylinder head had to be slightly modified. Since the engine is equipped with hydraulic lifters, if the camshafts are turned without any oil pressure in the head a different valve lift profile would be measured. To correct this one lifter element is modified to be solid (by tack welding it), and then a shim is made to fit under the lifter so that there is no clearance between the roller and the cam when the valves are closed. The shim is sized iteratively with a feeler gauge. There is approximately 0.05mm (0.002") error in this. An extender shaft is also added to the camshaft so that it could be mounted in a chuck. All the bearing surfaces are greased prior to doing the measurements.

A dial gage is mounted to the cylinder head. The gauge had 0.025mm (0.001") resolution. It is visually aligned to be perpendicular to the valve face, it is within 5 °'s of perpendicular . The stroke of the dial gauge is 0.5". The camshaft is attached to the chuck in a Tinius Olsen torsion testing machine using a solid steel shaft. There is zero backlash between the chuck of the machine and the camshaft. Mounted on the chuck of the torsion testing machine is a degree wheel with 1 °increments. The torsion testing machine is then hand cranked through the 360 °'s of the camshaft rotation. The lift is measured at 2.5 °intervals. Two measurement sets are taken for each camshaft (intake and exhaust). A plot of the profile can be seen in Figure C.2. It is important to note that the camshafts are turned in the direction they turn in actual operation, the intake is turned clockwise when looking at the from of the engine and the exhaust was turned anti-clockwise when looking at the front of the engine.

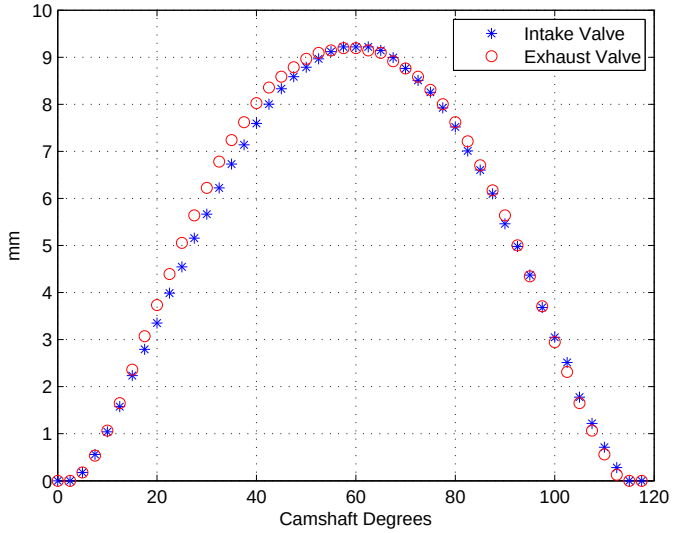

Figure C.2: The measured valve lift profiles. The reference in degree's is arbitrary.

C.3 Combustion Chamber Volume

To accurately determine the compression ratio of the engine it is required that the volume of the combustion chamber inside the cylinder head is known. To measure this, the valves are installed in the head, and the springs maintained a tight seal in the valves seats. The spark plug hole is filled with plasticine. A sheet of Lexan is then sealed to the deck surface with vacuum grease. Using a 5cc syringe machine oil is injected into a hole in the sheet of Lexan into the combustion chamber. Oil is used since it seals easier than water. Oil is added to the combustion chamber until it was seen to be full (no air pockets visible through the Lexan sheet). This process is repeated three times. The results of these three measurements can be seen in Table C.1. The combustion chamber volume is approximately 66ml. These measurements are done on combustion chamber that had not been modified for the installation of a pressure transducer, but since the transducer is flush mounted, its effect is assumed to be negligible. The effect of using plasticine instead of an actual spark plug is also assumed to be negligible.

Table C.1: Measurement of the combustion chamber volume. The resolution of the 5ml syringe used was 0.1ml.

Test Run	Measured Volume
1	66ml
2	66ml
3	65ml

C.4 Combustion Chamber Geometry

Molds of the combustion chamber of the cylinder head are made with Automotive Body Filler ("Bondo"). One mold is made with valves in their closed position, while another mold is made with disks place on the valves to simulate their open position. These molds are used to design the piston so that maximum compression ratio can be achieved.

C.5 Valve Discharge Coefficients

The transient motion of fluid flow can be readily predicted using computer simulation codes, such as GT-Power. Yet, in order to properly model the fluid flow the effects of all flow restrictions, such as the throttle, any bends, any expansions or contractions, and the effects of the valves themselves need to be known in advance. In the engine the valves move in a predefined path determined by the camshaft. The pressures inside the cylinder, and in the intake or exhaust manifold are constantly changing. There is never a steady state flow situation that exists inside the engine. However, if the the steady state discharge coefficients are measured for the valves at discrete lift values this can be used in simulations.

The discharge coefficients for the Mercedes e5.5 head are measured. They are measured in both forward and reverse directions for both the intake and exhaust valves.

C.5.1 Measurement Apparatus

Using ASME standard MFC-3M-2004 an orifice flow meter is designed that is capable of measuring the mass flow rate. A 1.5" orifice plate is placed inside of a 2" smooth steel pipe. Using the Reader-Harris/Gallagher equation, which gives the discharge coefficient of the orifice plate, the pressure drop across the plate can be used to predict the mass flow rate:

$$q_m = \frac{C}{\sqrt{1-\beta^4}}\epsilon\frac{\pi}{4}d^2\sqrt{2\delta p\rho_1} \tag{C.1}$$

where:

$\beta = d/D$

ϵ = Expansibility factor

C = discharge coefficient

δp = differential pressure

The differential pressure is measured using D and D/2 pressure taps above and below the orifice plate. A temperature measurement is also taken above the plate to calculate the actual density. Since the fluid is air expansion effects are accounted for with the expansibility factor.

As discussed in Heywood, the mass flow rate through a poppet valve is similar to that of isentropic compressible flow through a restriction:

$$m = \frac{C_D A_T p_0}{\sqrt{RT_0}}\left(\frac{p_T}{p_0}\right)^{1/\gamma}\left\{\frac{2\gamma}{\gamma-1}\left[1-\frac{p_t}{po}^{(\gamma-1)/\gamma}\right]\right\}^{1/2} \tag{C.2}$$

Once the mass flow rate has been determined from the orifice flow meter, only the pressure drop across the restriction, the fluid properties, and a value of the reference area are required for the calculation of the valve discharge coefficient. Since the valve geometry is somewhat complex many authors differ from their choice of reference

area. The reference area used in the is analysis is the one given by Heywood:

$$A_C = \pi D_v L_v \tag{C.3}$$

This area varies linearly with valve lift, which is not true for other definitions of reference area. The discharge coefficient is then given by:

$$C_d = \frac{m_a}{A_r P_1 (RT_v)^{0.5}} \frac{P_1}{P_2}^{1/\gamma} \left[\frac{2\gamma}{\gamma - 1} (1 - (P_2/P_1)^{(}(\gamma - 1)/\gamma)) \right]^{-0.5}; \tag{C.4}$$

For the flow tests done on the Mercedes cylinder head the air is supplied using building compressed air. A first attempt was made to flow the head using air supplied with a supercharger, but the maximum air supplied by the supercharger was not enough to test the valve to their peak flow capacity. The pressure drop across the valves is measured using a Validyne pressure transducer that is calibrated before and after the experiment. A temperature measurement at the upstream side of the flow through the valve is made with a J-Type thermocouple with an ice bath reference junction. The valve lift is set using a threaded rod position with a custom built plate.

Valve position is incremented by 1.1mm. At each valve position five flow measurements were made, from just over a pressure ratio of 1 to as close to 2 as could be achieved by the apparatus. Measurements for both valves (since it is a 4 valve head) are made for the exhaust valves in the forward and reverse direction, and for the intake valves in the reverse direction. It is found that for the forward direction a large pressure drop could not be created over the valves. The two valves are tested to the limit of the apparatus, and then the test is repeated using only one valve.

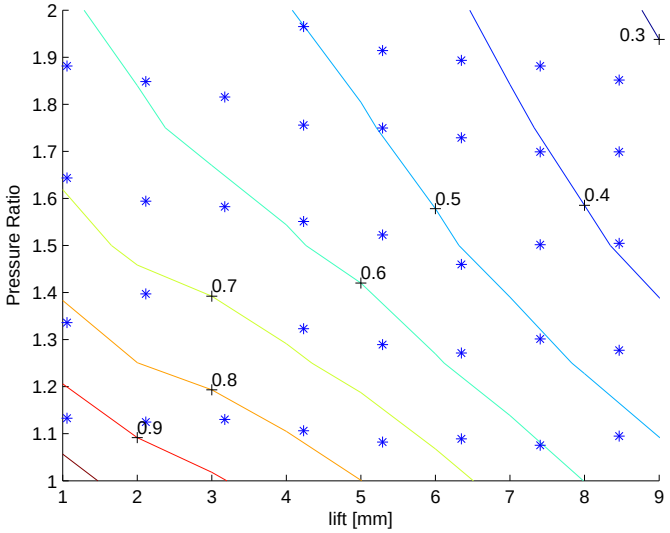

Figure C.3: Two exhaust valves flown in the forward direction.

C.5.2 Results

Due to noise considerations the tests had to be ran on a Saturday so as not to disturb the rest on the MecE building. Some example contour plots of the discharge coefficients for the exhaust valves can be seen in Figures C.3 and C.4.

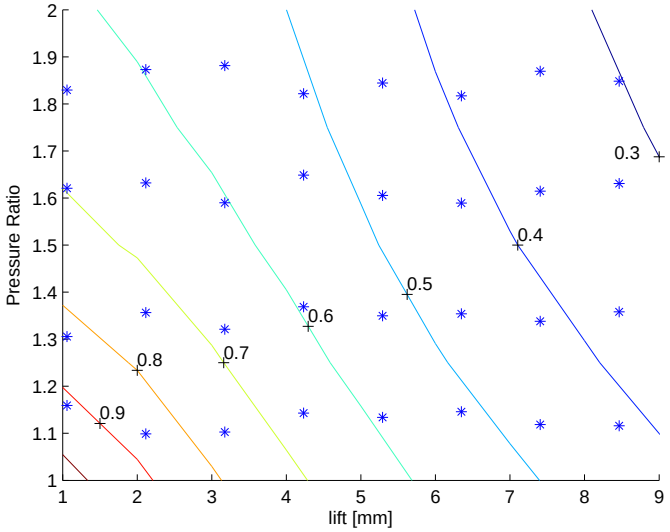

Figure C.4: Two exhaust valves flown in the reverse direction.

Appendix D

Experimental Setup and Calibrations

D.1 Programs Used

Table D.1: Programs used for this thesis.

Filename	Description
ricardo.mdl	Simulink model file that is compiled and loaded onto the dSPACE MicroAutoBox.
Ricardo_Experiment.cdx	ControlDesk file used to control the MicroAutoBox.
phaser_sep28.tst	ADAPT configuration file.
SingleCylinder5.ini	ADAPT screen layout file.
Mercedes_phaser. CASConfiguration.xml	CAS configuration file.
THESIS_cas2mat.m	MatLab file to convert CAS .p01 file to .mat files.
THESIS_DATAANALYSIS.m	MatLab file to assemble data from three different data logs and save as one smaller .mat file. Also computes performance metrics and produces an Excel sheet that summarizes the points.
THESIS_SYSID.m	MatLab file used to identify models from the experimental data.

D.2 Injector Flow Rate Calibration

For the study performed accurate knowledge of the mass flow rate of fuel into the engine is required. While PLU4000 performs fast accurate fuel flow measurements,

the system only has one fuel measurement system yet two separate fuel systems are used for the experimental engine, as seen in Figure 3.8. To estimate the fuel flowing through the second fuel system, which is the iso-Octane fuel system, a calibration is performed.

The fuel flow through the injector is a function of the pressure drop across the injector, the time the injector is open and the voltage applied to the injector. As seen in Figure 3.8 the pressure of the fuel system is referenced to the intake manifold. The differential pressure between the fuel and manifold is set to $3bar$ and is assumed to be constant for all tests. The battery voltage effects the flow rate through the injector by changing how fast he injector opens and closes. For this experiment a HP 6033A power supply is used to supply the injector with a constant voltage of 13.8V.

Running the engine in spark ignition mode the pulse width of the injector being tested is incremented from 0 to 8.5ms in 0.5ms steps. At each step the system is allowed 30 seconds to stabilize, and then the flow measurement from the PLU4000 was read. This flow measurement is for the last 20 seconds through the system, so it incorporates approximately 41 injection events. This test is performed multiple times. Table D.2 shows the results of the fuel injection calibration for both fuel systems. The average fuel flow rate is converted to an injector flow volume using Equation D.1. Injector pulse width and the calculated injector flow volume is shown in Figures D.1 and D.2 for the iso-Octane and n-Heptane fuel systems. The correlation between the injector flow volume and the pulse width is very linear, $R^2 = 0.99$. There is an offset in the pulse width which is a result of the opening and closing time of the injector. Using linear correlation the fuel flow rate for any injection width within the calibrated range can be calculated and these calibration coefficients are shown in Table D.2.

$$V[dm^3] = \dot{V}[\frac{dm^3}{hr}]/3600 * (1/(RPM/60)) * 2; \tag{D.1}$$

Table D.2: Calibration data for fuel injector calibration at 1000RPM

	iso-Octane			n-Heptane		
PW [s]	$\dot{V}$ $[\frac{dm^3}{hr}]$	Volume $[m^3]$	Mass [g]	$\dot{V}$ $[\frac{dm^3}{hr}]$	Volume $[m^3]$	Mass [g]
0.0015	0.0525	0.0025	0.0017	0.0000	0.0000	0.0000
0.0020	0.0926	0.0044	0.0030	0.0828	0.0039	0.0027
0.0025	0.1195	0.0056	0.0039	0.1204	0.0057	0.0039
0.0030	0.1699	0.0080	0.0055	0.1553	0.0074	0.0050
0.0035	0.1927	0.0091	0.0063	0.1751	0.0083	0.0057
0.0040	0.2279	0.0107	0.0074	0.1997	0.0095	0.0065
0.0045	0.2645	0.0125	0.0086	0.2373	0.0113	0.0077
0.0050	0.2880	0.0136	0.0094	0.2859	0.0136	0.0093
0.0055	0.3322	0.0156	0.0108	0.3297	0.0157	0.0107
0.0060	0.3695	0.0174	0.0120	0.3659	0.0174	0.0119
0.0065	0.3965	0.0187	0.0129	0.3995	0.0190	0.0130
0.0070	0.4379	0.0206	0.0142	0.4330	0.0206	0.0141
0.0075	0.4752	0.0224	0.0155	0.4692	0.0223	0.0153
0.0080	0.5049	0.0238	0.0164	0.5055	0.0240	0.0164
0.0085	0.5374	0.0253	0.0175	0.5383	0.0256	0.0175

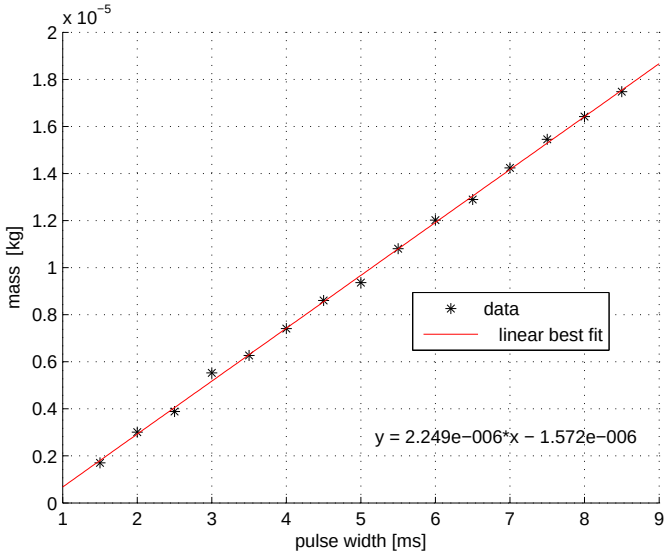

Figure D.1: Linear best fit between the injector pulse width and the calculate fuel volume for the iso-Octane fuel system. $R^2 = 0.99$

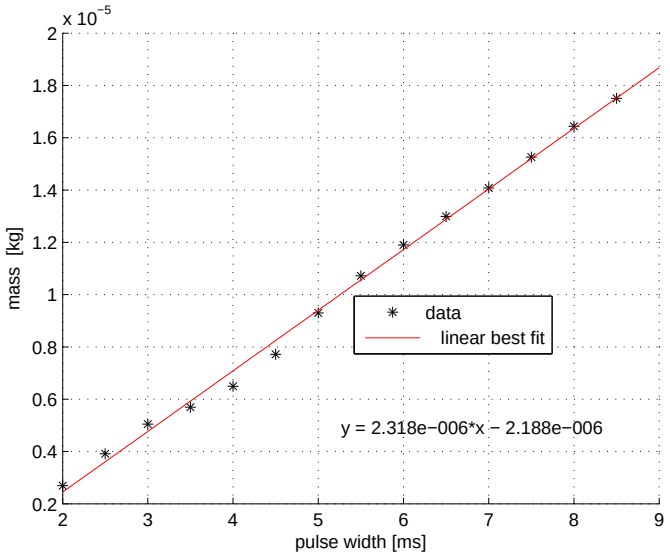

Figure D.2: Linear best fit between the injector pulse width and the calculate fuel volume for the n-Heptane fuel system. $R^2 = 0.99$

Table D.3: Calculated pulse width offsets and injector flow rate used in the study.

	iso-Octane	n-Heptane
Injector Flow rate $[\frac{g}{s}]$	2.25	2.32
Pulse Width Offset [ms]	0.70	0.94

D.3 Oil and Coolant Temperature Control

Both the oil and coolant temperatures are controlled by a water-to-water heat exchanger and a electric-pneumatic valve. The oil and coolants system schematics can be seen in Figures D.3 and D.4 respectively. The cold water is supplied from the building. The heaters in the system are only necessary for during warm-up, and after the engine reaches operating temperatures the heaters are turned off.

The ADAPT system controls the set-point for the water flow valves. A proportional integral control loop is set up so that the temperature can be regulated at certain set-points. For the coolant temperature loop the controlled temperature is measured as the coolant enters the cylinder head. For the oil temperature control loop

the temperature is measured as the oil enters the cylinder head. The gains of the PI controllers are manually tuned. The controllers are able to regulate the temperature to within 2 °C of the desired temperature.

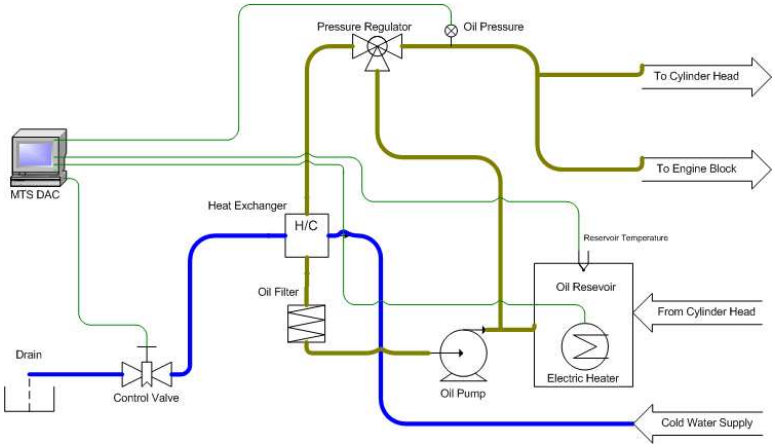

Figure D.3: Schematic of the oil system.

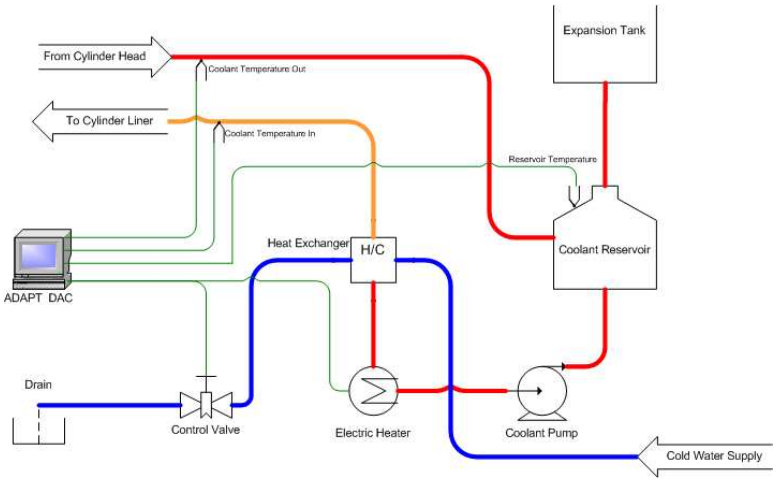

Figure D.4: Schematic of the coolant system.

D.4 Pressure Sensor

The in-cylinder pressure is measured with a piezo-electric pressure sensor, Kistler 6043A60. The output of this sensor is proportional to the change in pressure so a charge amplifier, $MTS1108$, is used to produce an absolute value of pressure. This

type of pressure sensor is subsequent to substantial drift during operation, which is due the fact that the output is integrated to produce a pressure reading. Each engine cycle the valve of the piezo-electric pressure sensor is pegged to the value of a diaphragm pressure sensor that produces an absolute reading. This pegging operation is done with the Baseline CAS system. A schematic of this system is shown in Figure D.5. The piezo-electric sensor is calibrated before any data is taken. Although the system is factory calibrated the manufactured suggest calibrating the whole measurement system to ensure the system is properly installed. The calibration is done with a dead weight calibrator, and a single calibration is seen in Figure D.6. The results of multiple calibrations are shown in Figure D.7. The determined sensitivity is 0.1988 $\frac{pC}{bar}$, which is very close to the factory calibration of 0.197 $\frac{pC}{bar}$. The factory calibration is used since there is a large uncertainty in the calibration that is done here.

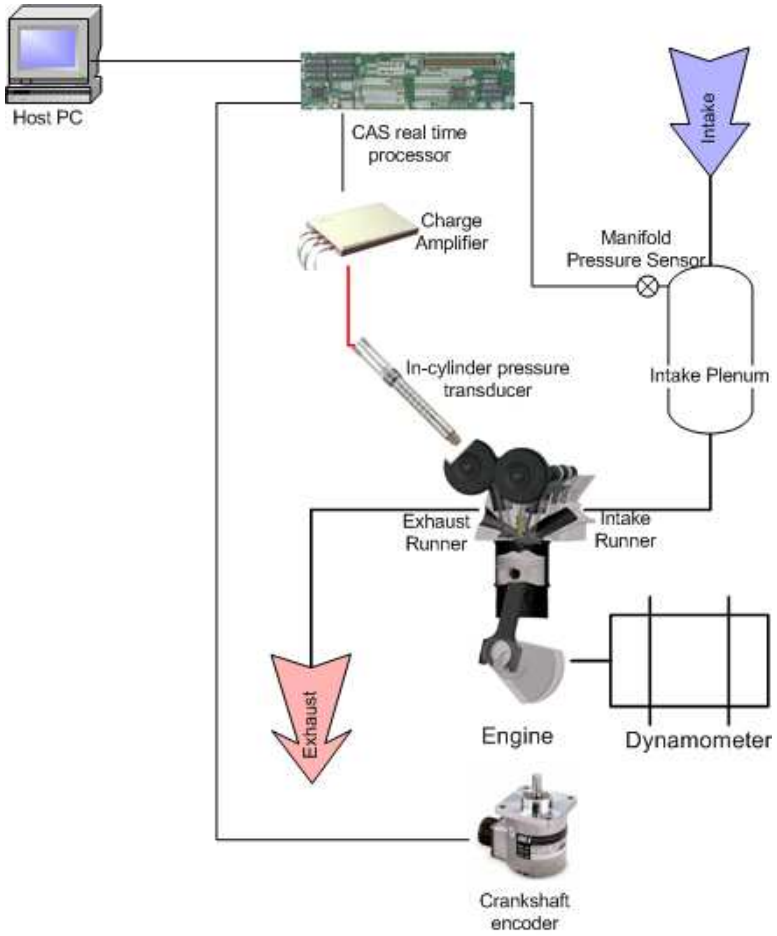

Figure D.5: Schematic of the in-cylinder pressure measurement and the absolute pressure pegging.

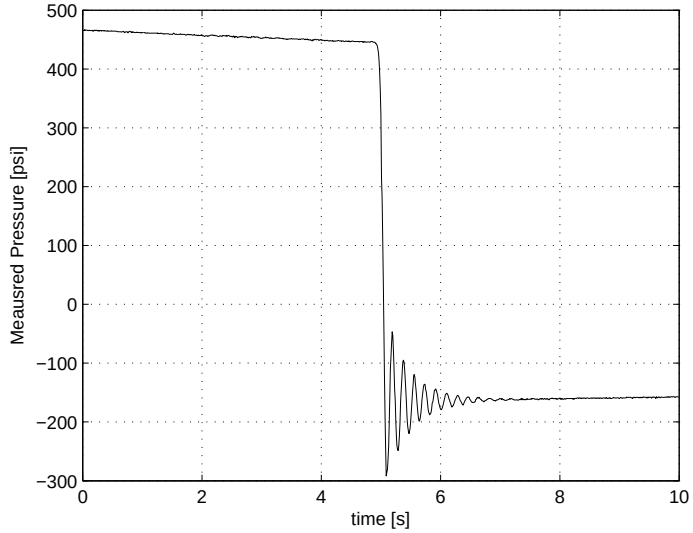

Figure D.6: Example of the step in pressure applied by the deadweight calibrator.

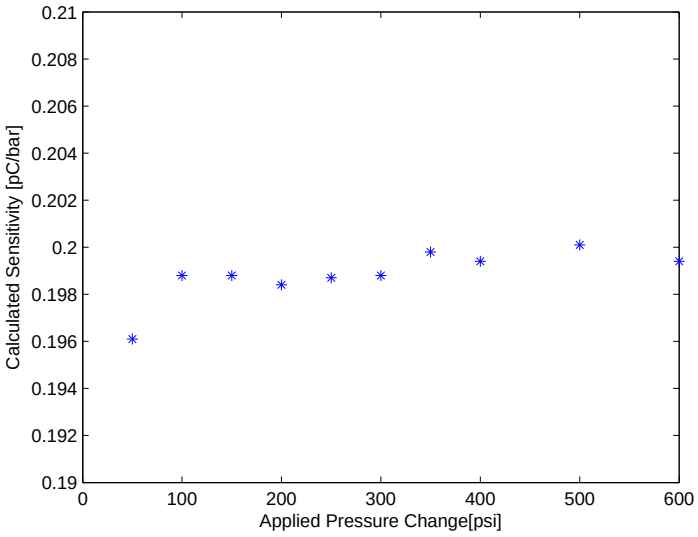

Figure D.7: Results of a multiple calibrations done of the piezoelectric pressure transducer. The calculated mean sensitivity is 0.1988 pC/bar.

D.5 Emission Bench

The emissions were sampled 5cm downstream of the exhaust ports. The emission sample was then cooled to room temperature in a heat exchanger. All the soot

particles were filter out with a 0.1 micron particulate filter, and then the sample was routed to the emissions bench where uHC, NOx, O2, CO2 and CO were measured. The output of each meter gave the volumetric concentration of each chemical species, either in ppm or %. The data was converted to a mass flow rate so that brake specific emissions data could be calculated. This was done by assuming that the exhaust gas behaves ideally. Assuming the molar mass of the exhaust is 29.12 the mass fraction of each chemical species can be found similar to Equation D.2. The mass flow rate of the exhaust is assumed to be the same as the sum of the intake air and fuel, this neglects any blowby which is usually less than 1% [Heywood, 1988]. Using Equation D.4 the mass flow rate of the chemical species can be calculated. The brake specific emissions are calculated according to Equation D.5.

$$x_{CO} = \frac{M_{CO}}{M_{total}} \tilde{x_{CO}} \tag{D.2}$$

$$\dot{m_{total}} = \dot{m_{air}} + \dot{m_{fuel}} \tag{D.3}$$

$$\dot{m_{CO}} = x_{CO} \dot{m_{total}} \tag{D.4}$$

$$bsco = \frac{\dot{m_{CO}}}{BrakePower} \tag{D.5}$$

The unburned hydrocarbons were measured using a *Horiba FIA-510* [THC, 1999]. Inside this device a hydrogen flame is maintained, and the sample gas is combined with the unburned hydrogen. The flame is placed between two electrodes, and a DC voltage is applied these electrode. There is an ion current that flows between these electrodes that is affected by the number of carbon atoms in the flame. When there are hydrocarbons in the sample they are burned in the flame and change the

ion current accordingly. The ion current is amplified and measured, and gives a volumetric amount of unburned hydrocarbons in the sample gas. The unit requires a constant supply of hydrogen gas for operation.

The nitrous oxide (NO) concentration was measured with a *Horiba CLA-510SS*. This device uses the chemiluminescent method [NOm, 1994]. When NO and ozone (O_3) are mixed they react to form oxygen (O_2) and nitrogen dioxide (NO_2). The NO_2 is initially in an excited state, and when it returns to the ground state it emits light. The light is measured inside the meter and gives an measure of the volumetric concentration of the NO in the sample gas. The unit generates the ozone, so it requires no operation gas.

The oxygen (O_2) sensor uses the paramagnetic property of the oxygen to determine the volumetric oxygen concentration [O2m, 1999]. The *Siemens OXYMAT-6E* uses a reference gas in the measurement (N_2 in our case). The reference gas is mixed with the sample gas inside a magnetic field. Oxygen's paramagnetism causes a flow, and this flow is proportional to the oxygen's concentration. This flow is measured and interpreted as the oxygen concentration. This unit requires a constant supply of N_2 for operation.

The carbon monoxide (CO) and carbon dioxide (CO_2) detectors are housed in the same device, a *Siemens ULTRAMAT-6E*. Both gases are measured using that same techniques that uses the gas specific infrared wave absorbtion [O2m, 1999]. Both these meter do not rely on any reference gas for operation.

Table D.4: Emissions Bench

Purpose	**Manufacturer & Model**	**Specifications**
uHC Meter	Horiba FIA-510	Range: 0-10000 ppmC Linearity:+-1.0% of full scale Reproducibility: +-0.5% of full scale
NO_x meter	Horiba CLA-510SS	Range: 0 - 5000ppmNO Repeatability: +-0.5% of full scale
O_2 Meter	Siemens OXYMAT6	Range: 0-25% Linearity: 1% Repeatability: 1%
CO Meter	Siemens ULTRAMAT6	Range: 0-10% Linearity: 0.5% Repeatability: 1%
CO_2 Meter	Siemens ULTRAMAT6	Range: 0-25% Linearity: 0.5% Repeatability: 1%

D.6 dSPACE CA50 calibration

The recorded CA50 values from both systems are shown in Figure D.8.

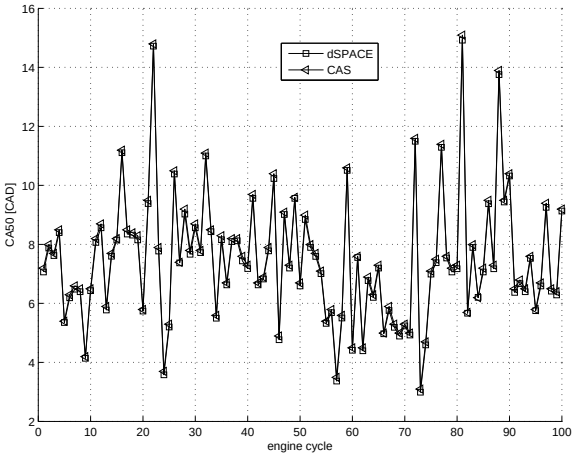

Figure D.8: CA50 calculated by CAS and the CA50 interpreted by the MicroAutobox. (test point $CA50_{cal}$)

D.7 CAS Time Delay

For control purposes is important to know the time delay between the change in engine conditions and the actual output of this change by the CAS computer, the computation delay of the CAS system. In this thesis only CA50 is used in the controller but a similar delay is expected for other metrics such as knock intensity and IMEP. To determine the delay the engine is run normal operating conditions under spark ignition mode. The spark is turned off, which will change the CA50 from a normal value, around 5 °, to the misfire value of 20 °. The output of the CAS computer is read by the dSPACE computer, which is controlling the spark. The number of cycles between the spark cut and the change seen in the CA50 is the computation delay of CAS. From Figure D.9 it is seen that the delay is 2 cycles.

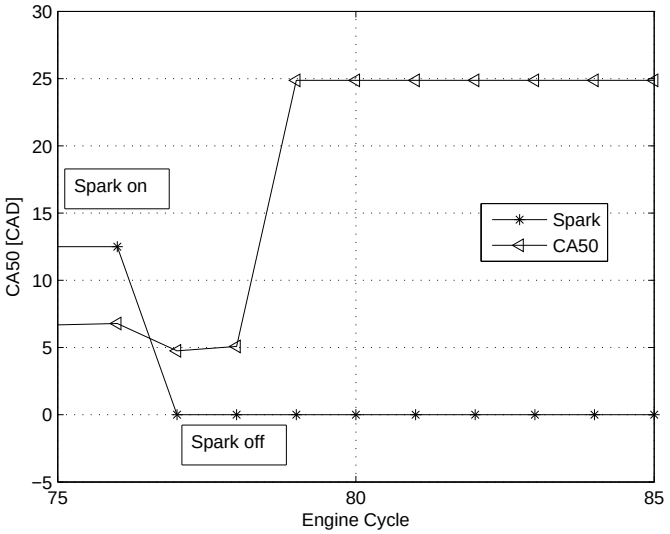

Figure D.9: Determination of CAS calculation delay. After the spark is turned of the change in the CA50 timing is not seen until 2 cycles later.

D.8 Load Cell Calibration

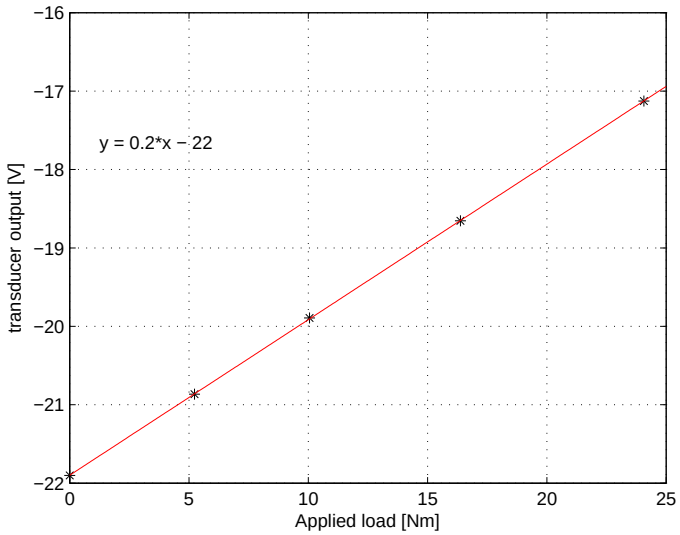

Figure D.10: Sample calibration of the dynamometer load cell. The linear fit has an r^2 value of 0.9999, and a maximum full scale error of 0.23%

D.9 Pressure Transducer Calibrations

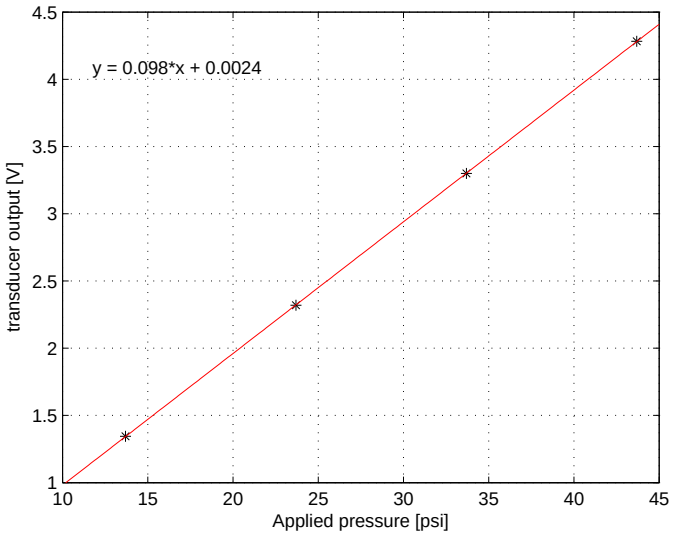

Figure D.11: Sample calibration of the absolute pressure transducer for the intake manifold. The linear fit has an r^2 value of 0.9999, and a maximum full scale error of 0.06%

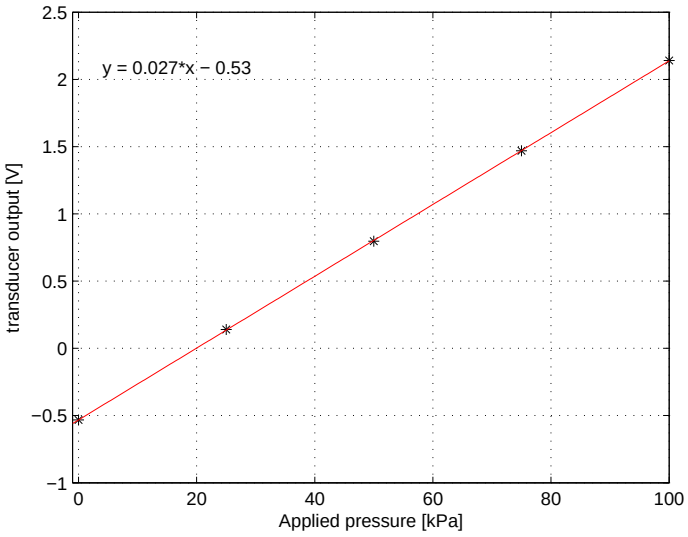

Figure D.12: Sample calibration of the relative pressure transducer for the intake manifold. The linear fit has an r^2 value of 0.9999, and a maximum full scale error of 0.22%

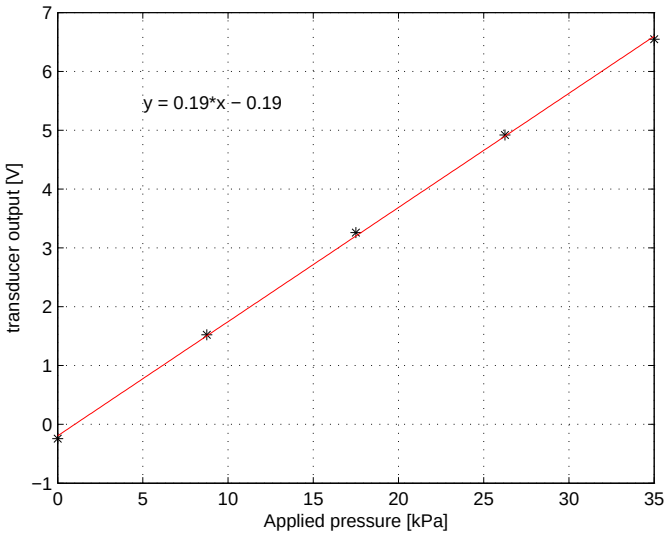

Figure D.13: Sample calibration of the pressure transducer for the exhaust manifold. The linear fit has an r^2 value of 0.9996, and a maximum full scale error of 0.88%

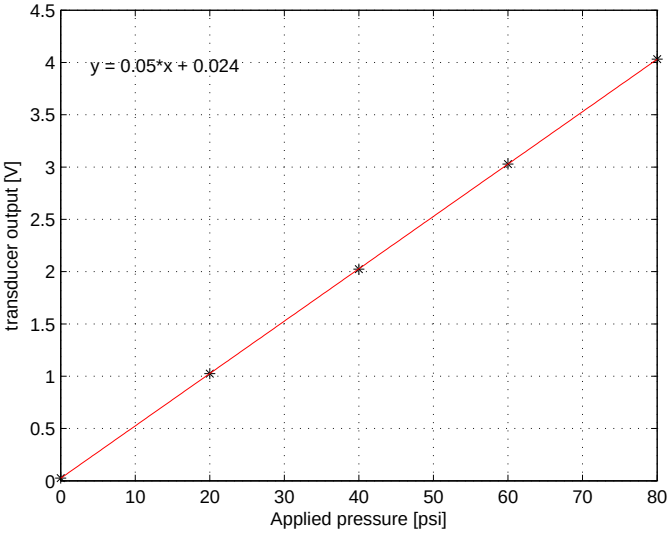

Figure D.14: Sample calibration of the pressure transducer for the iso-Octane fuel system. The linear fit has an r^2 value of 0.9999, and a maximum full scale error of 0.07%

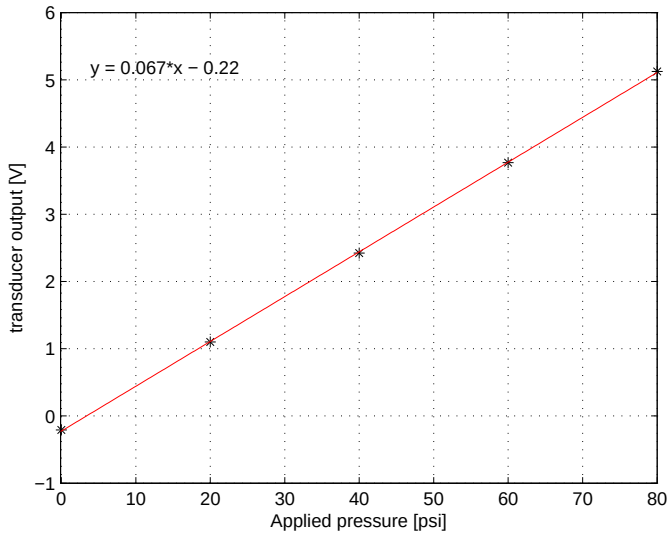

Figure D.15: Sample calibration of the pressure transducer for the n-Heptane fuel system. The linear fit has an r^2 value of 0.9999, and a maximum full scale error of 0.38%

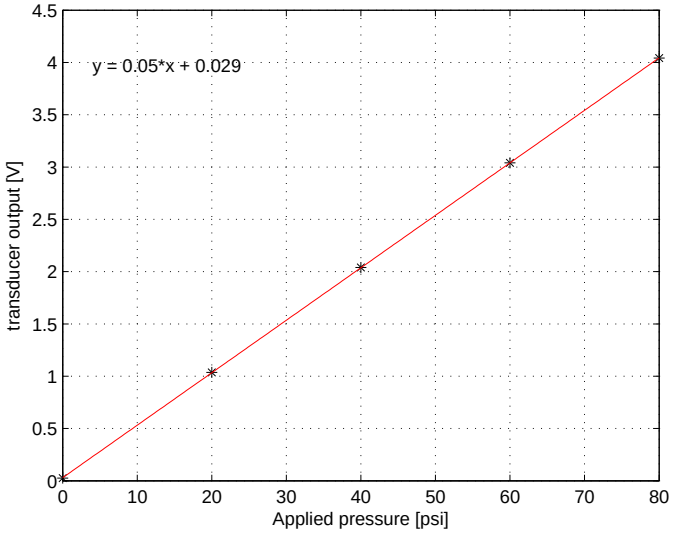

Figure D.16: Sample calibration of the pressure transducer for the oil system. The linear fit has an r^2 value of 0.9999, and a maximum full scale error of 0.09%

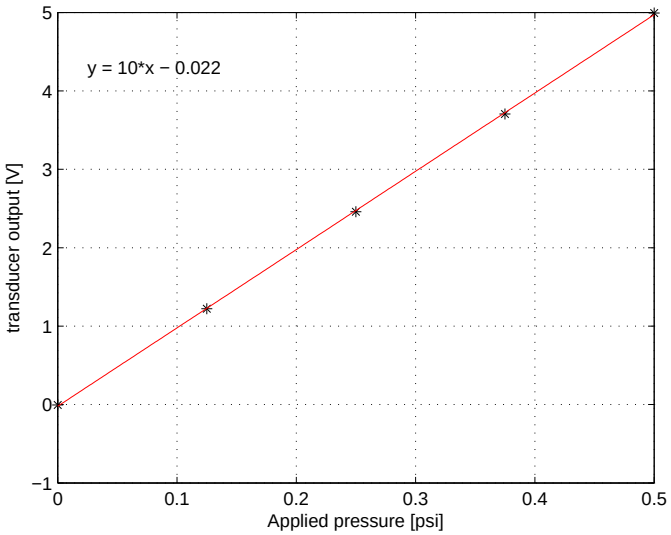

Figure D.17: Sample calibration of the pressure transducer for the laminar air flow meter. The linear fit has an r^2 value of 0.9999, and a maximum full scale error of 0.46%

D.10 Laminar Air Flow Calibration

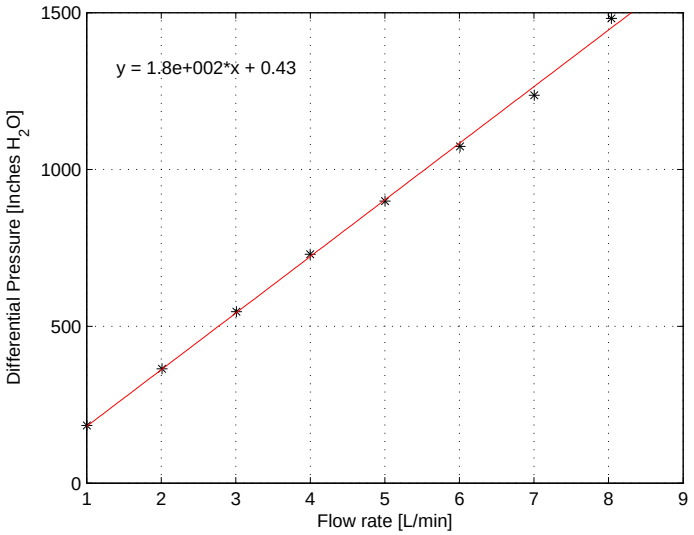

Figure D.18: Calibration of the laminar air flow meter, performed by Labcal Ltd.

Appendix E

Feedforward Controller Design

E.1 IVC Feedforward Controller

The identified model between IVC timing and CA50 is determined as:

$$G = \frac{0.392z + 0.970}{z^3 + 0.315z^2 + 0.171z} \tag{E.1}$$

$$= \frac{z^{-2}(0.392 + .970z^{-1})}{1 + 0.315z^{-1} + 0.171z^{-2}} \tag{E.2}$$

$$= 0.392z^{-2}\frac{(1 + 2.474z^{-1})}{(1 + 0.315z^{-1} + 0.171^{z-2})} \tag{E.3}$$

This model has both a time delay of two samples and a non-minimum phase zero at -2.474. Both of these portions are non-invertible. The model is separated into invertible, G_{m-} and non-invertible portions G_{m+}:

$$G = G_{m+}G_{m-} \tag{E.4}$$

The factorization of a non-minimum phase zero plus a time delay is given by [Garcia and Morari, 1982]:

$$G_{m+} = z^{-d} * \left[\frac{1 - \zeta z^{-1}}{1 - \frac{1}{\zeta} z^{-1}} * \frac{1 - \frac{1}{\zeta}}{1 - \zeta} \right] \tag{E.5}$$

When $d = 2$ and $\zeta = -2.474$, this becomes:

$$G_{m+} = 0.404 z^{-2} \frac{1 + 2.474 z^{-1}}{1 + .404 z^{-1}} \tag{E.6}$$

The invertible portion of the model can now be derived:

$$G_{m-} = G / G_{m+} \tag{E.7}$$

$$= \frac{0.392 z^{-2} \frac{(1+2.474 z^{-1}}{(1+0.315 z^{-1} + 0.171 z^{-2}}}{.404 z^{-2} \frac{1+2.474 z^{-1}}{1+0.404 z^{-1}}} \tag{E.8}$$

$$= 0.9703 \frac{1 + 0.404 z^{-1}}{1 + .315 z^{-1} + 0.171 z^{-2}} \tag{E.9}$$

This transfer function can now be inverted to design the feedforward controller via:

$$FF = \frac{G_{E-CA50}}{G_{m-}} \tag{E.10}$$

and

$$FF = \frac{G_{RPM-CA50}}{G_{m-}} \tag{E.11}$$

The feedforward controller will compensate for the measured disturbances of both

injected fuel energy and engine speed. The models are given by:

$$G_{E-CA50} = \frac{0.562z - 0.493}{z^4 - 1.04z^3 + 0.100z^2} \quad \text{(E.12)}$$

$$= 0.562z^{-3}\frac{(1 - 0.8772z^{-1})}{(1 - 0.9328z^{-1})(1 - 0.1072z^{-1})} \quad \text{(E.13)}$$

for the injected fuel energy and:

$$G_{RPM-CA50} = \frac{0.657z}{z^2 - 0.148z - 0.165} \quad \text{(E.14)}$$

$$= 0.657z^{-1}\frac{1}{(1 - 0.4869z^{-1})(1 - 0.3389z^{-1})} \quad \text{(E.15)}$$

for the engine speed. A two cycle time delay has been removed from the model of IVC timing to CA50 so that it can be inverted. In order for the models to temporally line up a two cycle delay needs to be removed from the disturbance models. This can be done for G_{E-CA50} but not for $G_{RPM-CA50}$ since this model only has a delay of one cycle.

The resulting feedforward controllers are:

$$FF_{E-IVC} = \frac{0.562z^{-1}\frac{(1-0.8772z^{-1})}{(1-0.9328z^{-1})(1-0.1072z^{-1})}}{0.9703\frac{(1+1.404z^{-1})}{1+.305z^{-1}+0.171z^{-2}}} \quad \text{(E.16)}$$

$$= z^{-1}0.579\frac{(1 - 0.8772z^{-1})(1 + .305z^{-1} + 0.171z^{-2})}{(1 - 0.9328z^{-1})(1 - 0.1072z^{-1})(1 + 1.404z^{-1})} \quad \text{(E.17)}$$

$$= \frac{0.5806z^3 - 0.3264z^2 - 0.06116z - 0.0871}{z^4 - 0.635z^3 - 0.3212z^2 + 0.0405z^1} \quad \text{(E.18)}$$

for compensation of the injected fuel energy disturbance by IVC timing and:

$$FF_{RPM-IVC} = \frac{0.657\frac{1}{(1-0.4869z^{-1})(1-0.3389z^{-1})}}{0.9703\frac{(1+1.404z^{-1})}{1+.305z^{-1}+0.171z^{-2}}} \quad \text{(E.19)}$$

$$= 0.677\frac{1+.305z^{-1}+0.171z^{-2}}{(1-0.4869z^{-1})(1-0.3389z^{-1})(1+1.404z^{-1})} \quad \text{(E.20)}$$

$$= \frac{0.6788z^3+0.2138z^2+0.1161z^1}{z^3+0.257z^2-0.2249z^1-0.06683} \quad \text{(E.21)}$$

for compensation of the engine speed disturbance by IVC timing.

E.2 Fuel Octane Feedforward Controller

The identified model between fuel octane and CA50 is determined as:

$$G = \frac{0.464z-0.213}{z^4-0.738z^3-0.002z^2} \quad \text{(E.22)}$$

$$= \frac{z^{-3}(0.464-0.213z^{-1}}{1-0.738z^{-1}-0.002z^{-2}} \quad \text{(E.23)}$$

$$= 0.464z^{-3}\frac{(1-0.4591z^{-1})}{(1-0.7407z^{-1})(1+0.0027z^{-1})} \quad \text{(E.24)}$$

This model has no non-minimum phase zeros, but it has a time delay of 3 samples. The invertible portion of the model is:

$$G_{m-} = 0.464\frac{(1-0.4591z^{-1})}{(1-0.7407z^{-1})(1+0.0027z^{-1})} \quad \text{(E.25)}$$

which is merely the original model without the time delay. The same models of G_{E-CA50} and $G_{RPM-CA50}$ are used for the design feedforward controls using fuel octane number. So that both models are temporally aligned a 3 cycle delay is removed from these models. This is accomplished with the G_{E-CA50} model but not for the $G_{RPM-CA50}$ model. The resulting feedforward controllers are:

$$FF_{E-ON} = \frac{0.562z^{-1}\frac{(1-0.8772z^{-1})}{(1-0.9328z^{-1})(1-0.1072z^{-1})}}{0.464\frac{(1-0.4591z^{-1})}{(1-0.7407z^{-1})(1+0.0027z^{-1})}} \quad \text{(E.26)}$$

$$= \frac{0.562z^3 - 0.9078z^2 + 0.3627z + 0.000986}{0.464z^3 - 0.6956z^2 + 0.2679z - 0.0213} \quad \text{(E.27)}$$

for the compensation of the injected fuel energy disturbance by the fuel octane number and:

$$FF_{RPM-ON} = \frac{0.657\frac{1}{(1-0.4869z^{-1})(1-0.3389z^{-1})}}{0.464\frac{(1-0.RPM4591z^{-1})}{(1-0.7407z^{-1})(1+0.0027z^{-1})}} \quad \text{(E.28)}$$

$$= \frac{0.657z^3 - 0.4849z^2 - 0.001314z}{0.464z^3 - 0.2817z^2 - 0.04504z + 0.03515} \quad \text{(E.29)}$$

for the compensation of engine speed disturbances by fuel octane number.

E.3 Simulink Models

Simulink models used to evaluate the functionality of the feedforward controllers.

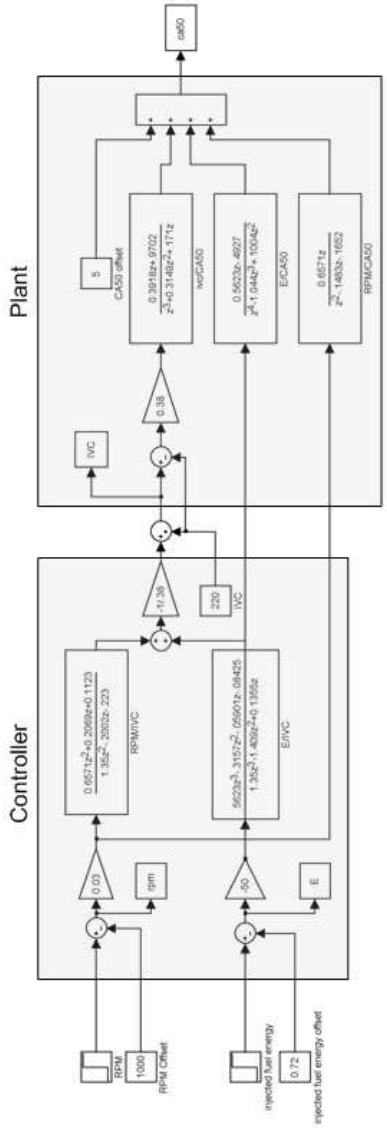

Figure E.1: Simulink model for the simulation of the feedforward controller using IVC timing to regulation the HCCI combustion timing.

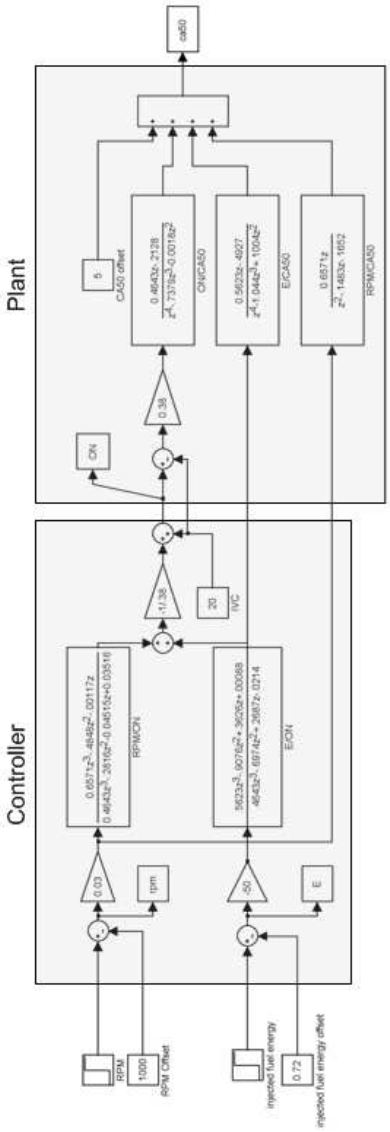

Figure E.2: Simulink model for the simulation of the feedforward controller using fuel octane number to regulation the HCCI combustion timing.